Investigating the therapeutic potential of

targeting the calcium-sensing receptor in asthma

Jiayin Diao

Bachelor of Science (Honours)

A thesis submitted for the degree of Doctor of Philosophy

at Monash University in 2021

Copyright notice

Table of Contents

Abstract

Asthma is a heterogeneous chronic airway disease, characterised by airway inflammation and remodelling leading to airway hyperresponsiveness (AHR). Asthma affects ~340 million patients worldwide (World Health Organization, 2017b). In severe asthma, symptoms may remain uncontrolled with current treatments. Moreover, current drug therapies do not treat all aspects of asthma. Therefore, new therapeutics are required. The aim of this study was to investigate the therapeutic potential of targeting the calcium-sensing receptor (CaSR) in asthma.

The CaSR is a G-protein coupled receptor that detects changes in extracellular calcium (Ca^{2+}_o) to maintain Ca^{2+}_o homeostasis, but it also responds to other positively charged ligands such as polyamines. The CaSR is upregulated in asthma, and allosteric CaSR agonists, such as polyamines, induce bronchoconstriction (Yarova et al., 2015). CaSR negative allosteric modulators (NAMs) have proven therapeutic effects in opposing different pathobiologies in mouse asthma models (Thompson et al., 2016; Yarova et al., 2021; Yarova et al., 2015). For example, the CaSR NAM, NPS2143, reduced airway inflammation, remodelling and AHR in mouse models of chronic allergic airway disease or acute lung injury (Lee et al., 2017; Thompson et al., 2016; Yarova et al., 2015). However, current knowledge gaps remain, including: **i**) how do CaSR NAMs compare to standard-of-care treatments; **ii**) how effective are different NAM classes at inhibiting CaSR signalling in response to asthma-relevant agonists such as polyamines; and **iii**) how do polyamines bind to and activate the CaSR.

In this thesis, we characterised the ability of different CaSR NAMs (NPS2143, Pfizer compound 1, BMS compound 1, ATF936 and ronacaleret) to inhibit polyamine-mediated CaSR signalling, and compared the bronchodilatory effects of three NAMs to standard-of-care treatments. We showed that CaSR NAMs engender biased modulation, with preferential inhibition of spermine-induced intracellular calcium (Ca^{2+}_i) mobilisation versus IP_1 accumulation in HEK293 cells transfected with the CaSR. Biased CaSR NAMs had differential effects on methacholine (MCh)-induced airway contraction in mouse airways. Of note, CaSR NAMs maintained bronchodilator effects under β_2-AR desensitisation when standard treatment, salbutamol had no bronchodilator effects. Furthermore, we proved that overnight incubation with CaSR NAMs prevent MCh-induced airway contraction.

Further, we characterised CaSR mRNA expression and Ca^{2+}_i mobilisation responses to contractile mediators (MCh, spermine and Ca^{2+}_o) in human airway smooth muscle (ASM) cells. We detected minimal CaSR mRNA expression and variable Ca^{2+}_i mobilisation responses to

these contractile mediators that were not related to the asthma status of the donors from which ASM cells were collected.

Finally, we probed the binding and function of polyamines at the CaSR. We applied site-directed mutagenesis and Ca^{2+}_i mobilisation assays combined with a cooperative agonist operational model of agonism to quantify changes in the affinity and efficacy of polyamines upon mutations of amino acids. We proved that polyamines bind to multiple binding sites located both in the CaSR extracellular and seven transmembrane or extracellular loop domains, but binding sites and activation residues likely differ between agonists.

The results of this thesis validate the CaSR as a putative novel drug target in asthma, and provide important structure-function data that will facilitate the design of novel NAMs that oppose polyamine signalling via the CaSR.

Declaration

This thesis is an original work of my research and contains no material which has been accepted for the award of any other degree or diploma at any university or equivalent institution and that, to the best of my knowledge and belief, this thesis contains no material previously published or written by another person, except where due reference is made in the text of the thesis.

Signature: …….....

Print Name: Jiayin Diao

Date: 19.05.2021

Publications during enrolment

Peer-reviewed articles

Diao J., DeBono A., Josephs T.M., Bourke J.E., Capuano B., Gregory K.J., Leach K. 2021. Therapeutic opportunities of targeting allosteric binding sites on the calcium-sensing receptor. *ACS Pharmacol. Transl. Sci*. 4, 2, 666–679.

Keller A., Kufareva I., Josephs T.M., **Diao J.**, Mai V.T., Conigrave A.D., Christopoulos A., Gregory K.J., Leach K. 2018. Identification of global and ligand-specific calcium-sensing receptor activation mechanisms. *Mol Pharm*. 93, 6, 619-630

Gregory K.J., Giraldo J., **Diao J.**, Christopoulos A., Leach K. 2020. Evaluation of operational models of agonism and allosterism at receptors with multiple orthosteric binding sites. *Mol Pharm.* 97, 1, 35-45

Presentations

Diao J., Keller A., Bourke J.E., Gregory K.J., Leach K. Probing the binding and function of polyamines at the calcium-sensing receptor. Australasian Society of Clinical and Experimental Pharmacologists and Toxicologists 2018. Adelaide, Australia (Oral & Poster)

Diao J., Keller A., Bourke J.E., Gregory K.J., Leach K. Probing the binding and function of polyamines at the calcium-sensing receptor. Molecular Pharmacology of G protein-coupled receptors 2018. Melbourne, Australia (Poster)

Diao J., Gregory K.J., Leach K., Bourke J.E. Investigating the role of the calcium-sensing receptor in airway contraction using mouse precision cut lung slices. Australasian Society of Clinical and Experimental Pharmacologists and Toxicologists 2019. Queenstown, New Zealand (Oral & Poster)

Diao J., Maksdi C., Lam M., Gregory K.J., Leach K., Bourke J.E. Exploring the potential role of the calcium-sensing receptor in a house dust mite model of allergic airway disease. Thoracic Society of Australia and New Zealand 2019. Melbourne, Australia (Oral)

Bourke J.E., **Diao J.**, Lam M., Maksdi C., Gregory K.J., Leach K. The calcium-sensing receptor CaSR mediates airway contraction in a house dust mite model of allergic airway disease. European Respiratory Society 2019. Madrid, Spain (oral)

Diao J., Lam M., Gregory K.J., Leach K., Bourke J.E. Investigating the role of the calcium-sensing receptor in airway contraction using mouse precision cut lung slices. Young Investigator Meeting on Airway Smooth Muscle 2019. Sydney, Australia (oral)

Bourke J.E., **Diao J.**, Gregory K.J., Leach K. The calcium-sensing receptor mediates airway contraction in mouse precision cut lung slices. American Thoracic Society 2020. Philadelphia, United States of America (Poster)

Diao J., Gregory K.J, Leach K., Bourke J.E. Investigating the role of the calcium-sensing receptor in airway contraction using mouse precision cut lung slices. Lorne Conference on Protein Structure and Function 2020. Lorne, Australia (poster) (cannot attend due to COVID19)

Diao J., Lam M., Gregory K.J., Leach K. Bourke J.E. Investigating the role of the calcium-sensing receptor in airway contraction using mouse precision cut lung slices. Thoracic Society of Australia and New Zealand 2020. Melbourne, Australia (Oral) (conference postponed to 2021 due to COVID19).

Diao J., Lam M., Gregory K.J., Leach K., Bourke J.E. Biased negative allosteric modulators for the calcium-sensing receptor have differential bronchodilator and bronchoprotective effects in mouse precision cut lung slices. Australasian Society of Clinical and Experimental Pharmacologists and Toxicologists 2020. Virtual (Oral & Poster)

Thesis including published works declaration

I hereby declare that this thesis contains no material which has been accepted for the award of any other degree or diploma at any university or equivalent institution and that, to the best of my knowledge and belief, this thesis contains no material previously published or written by another person, except where due reference is made in the text of the thesis.

This thesis includes one review published in peer reviewed journals. The ideas, development and writing up of all the papers in the thesis were the principal responsibility of myself, the student, working within the Drug Discovery Biology theme within the Monash Institute of Pharmaceutical Sciences and Department of Pharmacology, Biomedicine Discovery Institute, under the supervision of

Thesis chapter	Publication title	Status (published, in press, accepted or returned for revision, submitted	Nature and % of student contribution	Co-author name(s) Nature and % of co-author's contribution*	Co-author(s). Monash student Y/N*
Appendix 1 & sections 1.4.5. & 1.8 of Chapter 1	Therapeutic opportunities of targeting allosteric binding sites on the calcium-sensing receptor	Published	50% wrote and edited the manuscript	1) A.D. (wrote and edited the manuscript, 30%) 2) T.M.J., J.E.B, B.C., K.J.G (edit the manuscript, combined, 10%) 3) K.L (wrote and edited the manuscript, 10%)	No

I have not renumbered sections of submitted or published papers in order to generate a consistent presentation within the thesis.

Student name: Jiayin Diao

Student Signature: Date: 19.05.2021

I hereby certify that the above declaration correctly reflects the nature and extent of the student's and co-authors' contributions to this work. In instances where I am not the responsible author I have consulted with the responsible author to agree on the respective contributions of the authors.

Main supervisor name: Katie Leach

Main supervisor signature: Date: 19.05.2021

Acknowledgements

First and foremost, I would like to express my sincere gratitude to my supervisors, Dr Katie Leach, Dr Karen Gregory and A/Prof Jane Bourke for their invaluable guidance and encouragement over the past four years. To Katie, thank you for your immense amount of effort, invaluable advice and constructictive criticism during my PhD. Your insight and knowledge into this project steered me through this research from the beginning to its end. The incredible support and guidance from you inspire me to work harder and achieve more. To Jane, thank you for your professional guidane in asthma and animal work which allowed me to go through this research more smoothly. To Karen, thank you for all of your invaluable suggestion and critisism about molecular pharmacology.

I would like to say thank you to every present and past member in endocrine, neuropharmacology & cardiovascular lab and respiratory pharmacology lab, especially to Dr Andrew Keller, Dr Tracy Josephs, Dr Maggie Lam and Dr. Emma Lamanna. Andrew and Tracy have provided invaluable suggestions and guidance about biochemistiry and structure-function biology, which helped me identify and troubleshoot lots of problems throughout these four years. Maggie and Emma supported me with setting up immense animal experiments. Thank you to everyone else in these two labs who have assisted me to complete my PhD. Thank you to my PhD panel members: Dr Sab Ventura, Dr Celine Valant and Dr Simona Carbone. Thank you all for your thoughtful insignts and suggestions on this project.

Thank you to all 2017 DDB PhD cohorts, Samantha McNeill, Nichun Chung, Winnie Gao, Bui San Thai, Phuc Trinh and Cindy Zhang. I will never forget all the support from these six amazing girls. The past four years have been hard for all of us but we have made it! I would never make it through my PhD degree without the support from them and their friendship. Thank you to Sam for all the warm huddles, immense support and late-night tissue culture clubs throughout past four years. Thank you to all PhD cohorts in Department of Pharmacology, May Zhu, Tommy Huynh, Vivien Mao and many others. I will always remember the bright and inspiring talks in the student room and your company during my long day animal works. I do not know where our future will lead us to but we will always be together in spirit.

Thank you to all my family members, epecailly to my parents, grandparents and uncle. Thank you all for your understanding and unconditioned support to not only my PhD study, but also everything in my life. Thank you to all my friends for the comfort and encouragement during all these years.

This research was supported by an Australian Government Research Training Program (RTP) scholarship.

致谢

光阴如水，岁月如禅，在即将迈入而立之年的时候，我的全职学生生涯即将结束。博士生涯持续了整整 4 年零二个月，2017.3.19-2021.5.19。在即将交论文的此刻，回忆起这段时间的经历都觉得像恍如隔世，朦朦胧胧。想表达的情感有很多，想感谢的人也太多。这一路有很多很多美丽的风景，也有很多很多挫折。这一路有很多很多很多一直在帮助我鼓励着我的老师、同学和亲朋好友，没有你们无私的陪伴和帮助，我不可能坚持到今天这一步。

感谢导师凯蒂、简和凯伦在我博士期间的悉心教导和无穷的心血。是你们的教导和帮助让这个课题成为了可能。感谢凯蒂，在我论文的选题、执行到最终论文的定稿都耗费了无数心血。感谢简和凯伦在每个实验阶段对我的帮助。你们对科研的独到见解和专注让我受益良多，特此表达我衷心的感谢。感谢安德鲁、特雷西、麦琪和艾玛还有其他所有同一个实验室的同僚们的帮助，每一次的学术谈话聊天都让我受益匪浅，实验过程也都得到了实验室大家的帮助和支持。

感谢我的至亲，父母、外婆、爷爷奶奶、舅舅舅妈和远在天堂的外公，是你们一直以来的支持让我能安心于学业，替我承担了大部分的家庭责任。我一直期盼学业完成后可以报答长辈，却发现我能回报的其实是微乎其微的。逝者如斯夫，不舍昼夜，“子欲养而亲不待”的无奈，我想要去做到的弥补是如此的苍白无力。

感谢 2017 届的同窗，萨曼莎、妮钧、佩珊、高絜，张新和福。我们 7 人来自于世界各地，经历不同，性格不同，却产生了很奇妙的化学反应。这四年来我们一起经历了很多，有很多美好的团建的回忆，也有在实验室爆肝做实验和在巨大的压力下完成各项任务的崩溃，但事后想想每一个片段都是美好的。无论我们人生的火车最终会开往何方，我都会铭记这段与你们共度的岁月，能够认识你们和与你们为友是博士期间除了学识我最大的收获！愿友谊地久天长！

感谢所有国内国外的好友这一路的陪伴，因为出国且读博的关系和早已进入社会的同龄伙伴在生活经历和想法上都有一定的脱节，但是只要一聚在一起吃饭聊天，就马上能建立起联系。是和你们的联系，让我能够保持初心，

难寻少年时，总有少年来。不敢说自己在人生的每一个阶段都做到全力以赴了，但想想还是没有太辜负自己和他人吧。期盼未来，但愿你我都能在世间走出一条属于自己的路，不枉此生。

衷心祝愿我爱的人和爱我的人在今后的道路上平平安安，身体健康，一切顺遂！

Abbreviations

7TM	seven transmembrane
A2B	adenosine 2B
AC	adenylyl cyclase
AHR	airway hyperresponsiveness
ASM	airway smooth muscle
BMD	bone mineral density
Ca^{2+}_i	intracellular calcium ion
Ca^{2+}_o	extracellular calcium ion
cAMP	cyclic adenosine monophosphate
CaSR	calcium sensing receptor
CHO	Chinese hamster ovary
DAG	1,2-diacylglycerol
DMEM	Dulbecco's Modified Eagle's medium
DNA	deoxyribonucleic acid
ECD	extracellular domain
ECL	extracellular loop
ECM	extracellular matrix
ECP	eosinophil cationic protein
EDTA	ethylenediaminetetraacetic acid
EGFR	epidermal growth factor receptor
EMBP	eosinophil major basic protein
EPX	eosinophil peroxidase
ER	endoplasmic reticulum
ERK	extracellular signal-regulated kinase
FBS	fetal bovine serum
FHH	familial hypocalciuric hypercalcaemia
GABA	gamma-aminobutyric acid
GDP	guanosine-5'-diphosphate
GM-CSF	granulocyte-macrophage colony-stimulating factor
GPCR	G protein-coupled receptor

GRE	glucocorticoid response element
GRK	G protein kinase
GTP	guanosine-5'-triphosphate
HDAC	histone deacetylase
HEK293	human embryonic kidney 293
HEPES	N-2-hydroxyethylpiperazine-N'-2-ethanesulfonic acid
i.v.	intravenous
ICS	inhaled corticosteroid
IP1/IP3	inositol phosphate/inositol-1,4,5-triphosphate
JNK	Jun N-terminal kinase
LABA	long acting β_2-agonist
LB	Luria Bertani
mAChR	muscarinic acetylcholine receptor
MARK	mitogen-activated protein kinase
MBP	major basic protein
MCh	methacholine
MCP	monocyte chemotactic protein
MDCK	Madin-Darby canine kidney
mGluR	metabotropic glutamate receptor
NAL	neutral allosteric ligand
NAM	negative allosteric modulator
NF- κB	nuclear factor- κB
nH	Hill slope
NO	nitric oxide
NSTP	neonatal severe primary hyperparathyroidism
PAM	positive allosteric modulator
PBS	phosphate buffered solution
PCR	polymerase chain reaction
PHPT	primary hyperparathyroidism
PIP_2	phosphatidylinositol 4,5-biphosphate
PKC	protein kinase C
PLA2	phospholipase A2

PLC	phospholipase C
PLD	phospholipase D
PO_3^{4-}	phosphate ion
PP2A	protein phosphate 2A
PTH	parathyroid hormone
PTHrP	parathyroid hormone-related protein
RANKL	receptor activator of nuclear factor κB ligand
RFU	relative fluorescent units
RNA	ribonucleic acid
RT	room temperature
SABA	short acting β_2-agonist
SHPT	secondary hyperparathyroidism
SNP	single nucleotide polymorphism
SO_4^{2-}	sulphate ion
SR	sarcoplasmic reticulum
SRE	serum response element
TAL	thick ascending limb
tet	tetracycline
TM	transmembrane
TNCA	tryptophan derivative, L-1,2,3,4-tetrahydronorharman-3-carboxylic acid
TNF	tumor necrosis factor
TRPV5	transient receptor potential cation channel subfamily V member 5
VFT	venus flytrap
WT	wild type

Chapter 1

General introduction

Sections adapted from published works:

Chapter section	Published work
1.4.5. exogenous allosteric ligands	**Diao J.,** DeBono A., Josephs T.M., Bourke J.E., Capuano B., Gregory K.J., Leach K. 2021. Therapeutic opportunities of targeting allosteric binding sites on the calcium-sensing receptor. *ACS Pharmacol. Transl. Sci*. 4, 2, 666–679.
1.8. Clinical utility of CaSR allosteric modulators	

1.1. G protein-coupled receptors

Guanine nucleotide-binding protein (G protein)-coupled receptors (GPCRs) comprise the largest protein superfamily of transmembrane receptors, encoded by approximately 4% of the human genome (reviewed in Foord, 2002). Over 800 human GPCR genes have been identified, in which approximately 400 are predicted to be olfactory receptors (Fredriksson et al., 2003). GPCRs are ubiquitously expressed not only on the cell surface, but also in the endoplasmic reticulum, Golgi apparatus, nuclear membrane and inside the nucleus (Boivin et al., 2008; Calebiro et al., 2010; Re et al., 2010). They respond to a diverse range of ligands that include neurotransmitters, ions, amino acids and large proteins (Lagerström & Schiöth, 2008; Marinissen & Gutkind, 2001), as well as unidentified ligands that bind to orphan GPCRs (Tang et al., 2012). GPCRs couple to signalling effectors, such as heterotrimeric G proteins ($G_{i/o}$, $G_{q/11}$, G_s, $G_{12/13}$), kinases and arrestins (Wess et al., 2008). Coupling to G proteins leads to the exchange of guanosine-5'-diphosphate (GDP) for guanosine-5'-triphosphate (GTP) on the G protein α subunit, and separation of Gα from the βγ heterodimer, initiating downstream signalling events (Marinissen & Gutkind, 2001).

GPCRs are characterised by conserved seven transmembrane spanning α-helical domains (7TMs), which connect an extracellular amino and intracellular carboxyl terminal domain (Fredrujssib et al., 2003). GPCRs represent the most important class of pharmacological targets (Lagerström & Schiöth, 2008). The physiological and pathophysiological functions of GPCRs are very diverse, including thermoregulation, memory, immunity, sleep, and anxiety (Bert et al., 2008; Blier et al., 1997; Ghanemi, 2015; LeDoux, 2000; Savitz et al., 2009). GPCRs also represent important druggable targets for treating diseases, accounting for ~30% of all currently marketed medicines (George et al., 2002). However, their full potential as drug targets remains to be discovered. First, currently marketed drugs target only approximately 50 GPCRs, with more than 700 GPCRs untargeted (Lagerström & Schiöth, 2008). Second, the majority of GPCR-targeting drugs bind to the orthosteric binding site to either mimic or block the effects of the endogenous agonist. The disadvantages of using competitive agonists or antagonists include: **i**) lack of subtype selectivity, because orthosteric binding sites between receptor subtypes share high amino acid sequence and structural similarity; and **ii**) risk of toxicity, because overdosing leads to hyper- or hypo-activation of receptors (reviewed in May et al., 2007). As a result, during the past few decades, the focus on drug discovery has moved from targeting orthosteric sites to allosteric sites.

1.1.1. Allosterism: a new phenomenon in GPCR drug discovery

Allosteric binding sites are topographically distinct from, but conformationally linked to, the orthosteric binding site. Orthosteric and allosteric ligands can therefore bind simultaneously to the same receptor. Allosteric ligands stabilise conformational changes in a GPCR, acting cooperatively with orthosteric ligands to modify orthosteric ligand binding affinity (denoted by the cooperativity factor, α) or efficacy (denoted by the cooperativity factor, β). Cooperativity is a measure of the strength and direction of the allosteric change in affinity or efficacy.

Allosteric ligands that enhance affinity or efficacy are termed positive allosteric modulators (PAMs) and those that reduce orthosteric ligand affinity or efficacy are termed negative allosteric modulators (Christopoulos et al., 2014). Allosteric modulators may also bind to the receptor without modulating orthosteric ligand binding affinity or efficacy, and are termed neutral allosteric ligands (NALs). Thus, $\alpha\beta < 1$ denotes a NAM, $\alpha\beta = 1$ denotes a NAL and $\alpha\beta > 1$ denotes a PAM. However, the same allosteric ligands may modulate orthosteric affinity and efficacy in opposite directions. Further, allosteric modulation is ligand-specific (probe dependent) and pathway-specific (biased allosteric modulation) (reviewed in Wootten et al., 2013). Probe dependence and biased modulation will be further discussed in section 1.1.2.).

Allosteric ligands can also activate or inactivate receptor signalling in the absence of orthosteric ligands (Langmead & Christopoulos, 2006; Schwartz et al., 2006). Such ligands are termed allosteric agonists and categorised into full or partial agonists, and inverse agonists, depending on their pharmacological properties (Langmead & Christopoulos, 2006; Schwartz et al., 2006). There are three key advantages to allosteric ligands as drugs compared to orthosteric drugs: **i**) allosteric binding sites are typically less conserved therefore allosteric ligands have greater subtype selectivity; **ii**) allosteric ligands may demonstrate different cooperativities at different receptor subtypes, thus further improving subtype selectivity. For example, thiochrome binds to all five mAChRs, and is a PAM at the M_4 mAChR but a NAL at the other mAChR subtypes (Langmead & Christopoulos, 2006); **iii**) cooperativity is saturable, which means there is a maximum effect of the modulator even at concentrations that saturate receptor occupancy. Therefore, allosteric modulators are less likely to cause overdose; and **iv**) pure allosteric modulators have no intrinsic efficacy, therefore they only enhance or inhibit receptor activity when the endogenous ligand is present. This maintains both temporal and spatial profiles of receptor activation.

1.1.2. Biased agonism

In addition to allosterism, another important phenomenon with relevance to GPCR drug discovery is biased agonism. GPCRs are dynamic proteins that shift between different conformations that may be stabilised by distinct ligands (Kenakin & Christopoulos, 2013). Upon binding to distinct ligands, GPCRs couple to various signalling effectors, including different G proteins and kinases, to activate divergent signalling pathways (Kenakin & Christopoulos, 2013). Biased agonism refers to the phenomenon whereby different ligands stimulate divergent signalling pathways to the exclusion of others by stabilising distinct conformations. Biased agonism provides opportunities to design superior therapeutics because biased ligands have the potential to specifically activate beneficial signalling pathways while avoiding adverse effect-related pathways. However, biased agonism also provides challenges for designing therapeutics. The current challenges include: **i**) an often limited understanding of the individual signalling pathways related to therapeutic efficacy and adverse side effects (Kenakin & Christopoulos, 2013); and **ii**) the dependence of biased agonism on the ligand, cellular background, and cellular context. Therefore *in vitro* pharmacological profiles might not reflect biased profiles *in vivo*. Furthermore, any changes in cellular context, such as membrane compositions and signalling partners in disease conditions, have the potential to alter biased agonism profiles compared to those in healthy conditions. These challenges complicate discovery of biased therapeutics.

1.2. Class C GPCRs

The GPCR superfamily is classified into six classes, A-F, based on sequence homology within the transmembrane helices, whilst four main families are accepted and termed class A (rhodopsin-like), class B (adhesion and secretin), class C (metabotropic glutamate) and class F (frizzled) (Fredriksson et al., 2003). Between different families, very little common sequence identity (<20%) occurs in the 7TM, and little similarity is observed in the extracellular N-terminal domains (which are relatively short at 10-50 amino acids in monoamine and peptide receptors, and much larger at 350-600 amino acids for glycoprotein hormone and other non-hormone receptors) (Katritch et al., 2013).

The focus of this thesis is on an important class C GPCR called the calcium-sensing receptor (CaSR). Class C GPCRs also include the metabotropic glutamate receptors (mGluRs), the gamma-aminobutyric acid (GABA) type B receptor, the taste 1 receptors ($T1R_1$-$T1R_3$), the pheromone receptors and seven orphan receptors. Class C GPCRs are characterised by two unique structural features: **i**) a large bi-lobed N terminal Venus flytrap (VFT) domain, which contains the orthosteric binding site and is the main contact point at which the receptors form constitutive dimers (either hetero or homo) (Foord et al., 2005); and **ii**) a region composed of nine highly conserved cysteine residues, named the cysteine-rich domain (although this is absent in $GABA_B$ receptors).

1.2.1 CaSR

The human *CASR* gene has 8 exons and is located on chromosome 3q12.3-21(Hendy & Canaff, 2016). It has long been known that increases in extracellular calcium ($Ca^{2+}{}_o$) concentrations activate the CaSR, inhibiting parathyroid hormone (PTH) synthesis and secretion from the parathyroid glands. Immunoblotting of the CaSR shows that the mature CaSR under reducing conditions exists as a fully glycosylated and cell surface-expressed form at ~150 kDa. Glycosylation is crucial for CaSR folding, trafficking and cell surface expression (reviewed in Tfelt-Hansen & Brown, 2005). The CaSR is expressed and functionally active in various vertebrates, including tetrapods, bony fish and humans (Herberger & Loretz, 2013). The CaSR is ubiquitously expressed in various tissues in the human body, such as the parathyroid glands, kidney, airway, heart, and bone, and is responsible for a diverse range of calcitropic and non-calcitropic functions (which will be further discussed in section 1.6.). The main calcitropic function of the CaSR is to regulate the plasma Ca^{2+} concentration in the human body by regulating PTH secretion, urinary Ca^{2+} excretion, Ca^{2+} storage in the bone, and $Ca^{2+}{}_o$ re-absorption in the small intestine or stomach (Brown et al., 1993; Brown & Macleod, 2001). Non-calcitropic functions of the CaSR include vascular calcification, bronchoconstriction, and others (Hannan et al., 2019).

1.3. Structure of the CaSR

The CaSR is expressed as a 1078 amino-acid polypeptide, consisting of a large extracellular domain (ECD) containing a bi-lobed venus flytrap (VFT), cysteine rich domain (CRD), followed by 7TMs connected with three extracellular loops (ECLs; ECL1-3) and three intracellular loops (ICLs; ICL1-3), and a C-terminal. The CaSR can form homodimers or heterodimers with other class C GPCRs, $mGluR_{1/5}$ or the $GABA_B$ receptors, by covalent and noncovalent interactions between the amino-terminal VFT lobe of each monomer (Chang et al., 2007; Gama et al., 2001; Geng et al., 2016; Jiang et al., 2004). Dimerisation is important for the pharmacological function of the CaSR.

1.3.1. ECD

Recent X-ray crystallography studies have demonstrated the structures of both active and inactive states of the CaSR ECD, thereby revealing ECD activation mechanisms, which are similar to those in other class C GPCRs (Geng et al., 2016). Structural studies demonstrate that the CaSR ECD consists of two protomers, which sit side-by-side and face opposite directions (**Figure 1.1**). Each protomer consists of two lobe-shaped domains, lobe 1 (LB1) and lobe 2 (LB2), as well as CRDs (**Figure 1.1**) (Geng et al., 2016; Zhang et al., 2016) (**Figure 1.1**). LB1 and LB2 form an interdomain cleft, which in all other class C GPCRs is the orthosteric agonist binding site for L-amino acids or similar entities (Geng et al., 2012; Koehl et al., 2019). The CaSR ECD undergoes large conformational changes upon activation (Geng et al., 2016; Zhang et al., 2016). In the presence of activators, movement of LB1 and LB2 closes the cleft ("closed" conformation) with an increased buried surface area compared to that observed in the inactive state, when the lobes adopt an "open" conformation and the interdomain cleft is empty. Closure of the cleft causes the LB2 and CRDs of the two protomers to approach one another, causing a reduction in the distance between the C-termini of the two ECD protomers from 83 A^o to 23 A^o upon activation (**Figure 1.1**).

The CaSR VFT contains eight experimentally-validated N-linked glycosylation sites (N90, N130, N261, N287, N446, N468, N488 and N541). The importance of these sites is demonstrated by mutations at these residues, which significantly reduce receptor expression and, consequently, signal transduction (Ray et al., 1998). The physiological importance of the CaSR VFT is

demonstrated by findings that: **i**) multiple naturally occurring ligand binding sites exist in this region (the details will be discussed in section 1.4.); and **ii**) mutations in this region affect the cell surface expression and biological activity of the receptor.

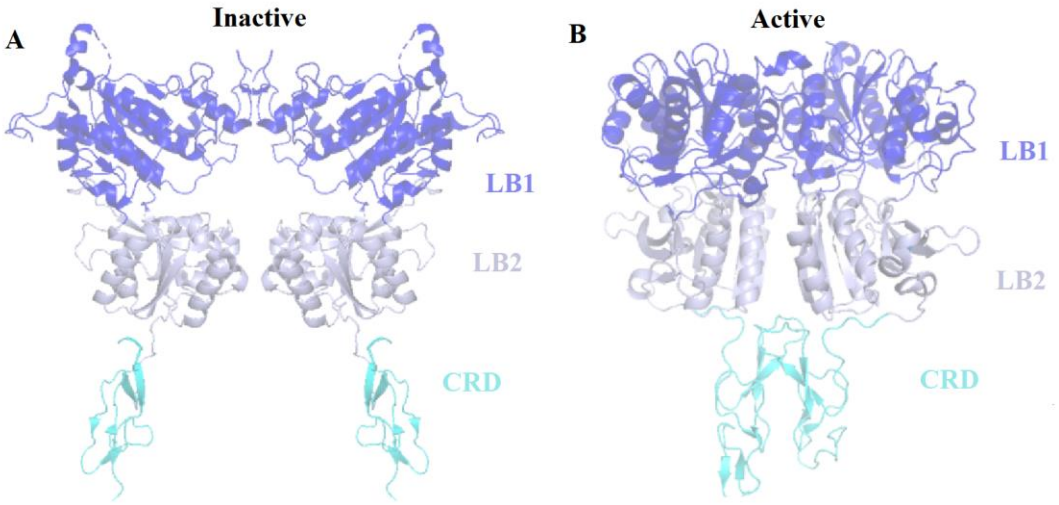

Figure 1.1. Structures of the CaSR ECD determined using x-ray crystallography (Geng et al., 2016). **A**) CaSR ECD inactive-state structure following ECD purification in the presence of 2 mM Ca^{2+}_o (PDB ID: 5k5t); **B**) CaSR ECD active-state structure following ECD purification in the presence of 10 mM Ca^{2+}_o and 10 mM L-Trp (PDB ID: 5k5s). Structures are shown in cartoon form (ligands not shown). The CaSR ECD is composed of two protomers that each consist of three domains: LB1 (blue), LB2 (grey) and a CRD (cyan).

1.3.2. 7TM, ECLs and ICLs

The CaSR 7TM spans residues 613-862 (termed TM1-TM7), connected by three ECLs and three ICLs, which are a common feature of all GPCRs (Garrett et al., 1995). Extensive mutagenesis studies demonstrate that the 7TM region is largely involved in receptor dimerisation through non-covalent interactions and is crucial for initiating downstream G protein-mediated signalling (Chang et al., 2000; Kos et al., 2003; Zhao et al., 1999). Further, mutation of $C677^{ECL1}$ and $C765^{ECL2}$ (where the superscript denotes the ECL number in which the residue is located), disrupts a disulphide bond that is important for maintaining the structural stability of the CaSR (Ray et al., 2004). Residues in ICLs and ECLs are also important for receptor activation and biased signalling (Goolam et al., 2014; Leach et al., 2012).

1.3.3. C-terminal tail

The CaSR 7TM is preceded by a large C-terminal tail comprised of 216 amino acids (Heath et al., 1996; Ray et al., 1997). The C-tail of the CaSR is generally more variable than the VFT and 7TM among different species (Pin et al., 2003), although residues 863-925 (responsible for maintaining cell surface expression and biological activity) and residues 960-984 (responsible for binding to accessory proteins) are highly conserved among different species (Awata et al., 2001; Hjälm et al., 2001; Pin et al., 2003; Ray et al., 1997). The membrane proximal region of the CaSR contains residues responsible for both initiation of signalling cascades and receptor cell surface expression (Chang et al., 2001; Gama & Breitwieser, 1998; Ray et al., 1997). For instance, H880A and F882A mutants, located in a region of the C-tail predicted to form a helix, show reduced biological activity compared to the wild type (WT) receptor (Gama & Breitwieser, 1998). Also, while protein kinase C (PKC) has an inhibitory effect on CaSR-mediated Ca^{2+}_i mobilisation, this is largely decreased in HEK293 cells expressing CaSR mutated at T888A, S895A or S915A, suggesting these three residues are PKC phosphorylation sites (Bai et al., 1998). Furthermore, CaSR activators enhance the phosphorylation of T888, suggesting that CaSR activates PKC, which in turn phosphorylates the CaSR at T888 to inhibit CaSR activity (Davies et al., 2006).

1.4. Ligands of the CaSR and their binding sites

1.4.1 Cations and anions

In addition to the primary physiological agonist Ca^{2+}_o, the CaSR responds to a large variety of divalent cations including Sr^{2+} Ba^{2+}, Co^{2+}, Fe^{2+}, Ni^{2+}, Mg^{2+} and Pb^{2+}, as well as trivalent cations including Gd^{3+}, Al^{3+}, Y^{3+}, Eu^{3+} and Tb^{3+} (Chen et al., 1989; Katsuyuki et al., 2010; McGehee et al., 1997). Four binding sites for Ca^{2+}_o within the VFT domain have been revealed, which are, surprisingly, topographically distinct from the conserved orthosteric sites in all other class C GPCR members. Ca^{2+}_o forms interactions with: 1) backbone carbonyl oxygen atoms of I81, S84, L87 and L88; 2) hydroxyl group of T100 and carbonyl atom of N102; 3) hydroxyl groups of S302 and S303 4) carboxylate group of D234 and carbonyl oxygen of E231 and G557 (**Figure 1.2**). At least one binding site for Ca^{2+}_o also exists in the 7TM because Ca^{2+}_o stimulates Ca^{2+}_i mobilisation at an N-terminally truncated CaSR (Leach et al., 2016). In a separate experimentally-determined

ECD structure, two Mg^{2+} binding sites were identified, one of which was very close to Ca^{2+}_o binding site 1 (Mg^{2+} is coordinated with the backbone of I81, L87 and L88) (site 5;) and the other binding site is mediated through E231, S240 and E241 (Zhang et al., 2016) (site 6; **Figure 1.2**). Compared to cations, which activate the CaSR, anions such as phosphate (PO_4^{3-}) and sulphate (SO_4^{2-}) are important for stabilising the inactive VFT conformation. Binding sites for these two anions have been revealed (Geng et al., 2016). Sulphate binds to the CaSR via coordination with R62 and Y63 (site 7), R66, T412 and H413 (site 8) as well as R69, W70, R415 and S417 (site 9). Two PO_4^{3-} binding sites were identified, site 10 (in coordination with R66, R69, W70, R415 and S417) and site 11 (E191, H192, R520 and K517) (**Figure 1.2**)**.** However, experimental data is required to validate these anion binding sites. A Gd^{3+} binding site was also identified and mediated through E228, E229 and E232 (site 12). Notably, effects of mutations in the ligand binding sites on agonist affinity or efficacy (and mutant cell surface expression) have not been quantified and these binding sites have therefore not been validated experimentally (Geng et al., 2016; Zhang et al., 2016).

1.4.2 L-Amino acids

L-amino acids are allosteric modulators of CaSR activity, as they enhance Ca^{2+}-elicited CaSR activation but have no activity on their own (Conigrave et al., 2000; Zhang et al., 2002). Furthermore, Ca^{2+}_o only acts as a full agonist when L-amino acids are present, as the fully active VFT conformation only occurs when the cleft is bound to an L-amino acid or similar entity (Geng et al., 2016; Zhang et al., 2016). In general, the CaSR shows greater affinity for larger aliphatic and aromatic L-amino acids and their rank order of effectiveness to left-shift the concentration-response curve to Ca^{2+} (from the lowest to the highest) is: L-Leu = L-Arg < L-Glu< L-Ala < L-His < L-Trp = L-Phe (Brown & Macleod, 2001; Conigrave et al., 2000). L-amino acids positively modulate the actions of Ca^{2+}_o as measured by Ca^{2+}_i mobilisation, IP_3 formation and MAPK activity (Conigrave et al., 2000; Kifor et al., 2001) and also in native tissues, as measured by PTH release (Conigrave et al., 2004). Intriguingly, compared with cations, L-amino acids have a biased effect towards CaSR-mediated Ca^{2+}_i mobilisation versus phosphorylation of $ERK_{1/2}$ (Lee et al., 2007).

CaSR ECD crystal structures reveal that L-Trp forms hydrogen bonds with S147, A168, S170, E297, in addition to hydrophobic contacts with W70, T145, Y218 and A298 (site 13; **Figure 1.2.**)

(Geng et al., 2016). Furthermore, the tryptophan derivative, L-1,2,3,4-tetrahydronorharman-3-carboxylic acid (TNCA) binds to the CaSR at S147, E297 and A298 (site 14; Figure **1.2**) Interestingly, the L-amino acid binding site is in the conserved cleft that is the orthosteric binding site in other class C GPCRs (Broadhead et al., 2011; Geng et al., 2016; Mun et al., 2005; Mun et al., 2004; Zhang et al., 2016; Zhang et al., 2002).

1.4.3 Polyamines

Endogenous polyamines can also activate the CaSR, with spermine (with four positive charges), spermidine (with three positive charges) and putrescine (with two positive charges) as the most potent (Quinn et al., 1997). The rank order of polyamine potency at the CaSR is as follows (from the lowest to the highest): putrescine < spermidine < spermine, the same as their positive charges (Quinn et al., 1997). Current studies suggest that polyamines bind to the CaSR 7TMs but further investigation is required (Ray & Northup, 2002).

1.4.4 Polypeptides and proteins

Before the CaSR was identified, poly-arginine and poly-lysine were known to activate similar cellular responses to Ca^{2+}_o in bovine parathyroid cells (Brown et al., 1991). Later, these polypeptides were shown to exert such cellular effects through the CaSR (Ruat et al., 1996). Similarly, amyloid peptide, which is also positively charged, stimulates the CaSR (Brown & Macleod, 2001). Other polypeptides, such as eosinophil cationic protein (ECP), activate the CaSR to elicit pathophysiological functions (Yarova et al., 2015). However, the binding sites of polypeptides have not been elucidated.

Etelcalcetide is the only approved peptide therapeutic that targets the CaSR, used as a treatment for secondary hyperparathyroidism in haemodialysis patients (Walter et al., 2013). Etelcalcetide is comprised of seven D-amino acids and has been classified as a PAM-agonist because it can both potentiate Ca^{2+}_o-mediated receptor activity and activate the receptor in the absence of Ca^{2+}_o *in vitro* (Walter et al., 2013). However, 0.5 mM $MgCl_2$ was present in the assay buffer when discerning etelcalcetide had efficacy in IP_1 accumulation assays. Therefore, it is not well-validated whether etelcalcetide activates IP_1 accumulation due to its own agonism or potentiation of Mg^{2+} in the

buffer (Walter et al., 2013). *In vivo,* etelcalcetide reduces PTH and serum Ca^{2+} in both normal and renally comprised rats (Walter et al., 2013). In two parallel phase III, randomised studies, more than 70% of haemodialysis patients who received etelcalcetide, achieved >30 % PTH reduction from baseline (Block et al., 2017b).

Etelcalcetide is the only peptide CaSR PAM discovered so far. Etelcalcetide has a distinct binding site in the CaSR VFT compared with small molecule CaSR PAMs (the binding sites of small molecule PAMs will be further discussed in section 1.4.5.). Etelcalcetide coordinates with C482 via a disulphide bond (Alexander et al., 2015) (Site 15; **Figure 1.2**). However, the affinity and cooperativity of etelcalcetide at the CaSR has not been quantified.

1.4.5 Exogenous allosteric ligands

1.4.5.1 Small molecule PAMs

For the first generation of CaSR PAMs, several structurally related arylalkylamine CaSR PAMs were developed, including NPS R-467, NPS R-568 and cinacalcet (reviewed in Nemeth et al., 2018). Arylalkylamine PAMs are PAM-agonists. That is, arylalkylamine PAMs enhance $Ca^{2+}{}_o$-mediated $Ca^{2+}{}_i$ mobilisation in recombinant cells or reduce PTH secretion from parathyroid cells *in vitro* and activate the CaSR in the absence of cations (i.e. $Ca^{2+}{}_o$, Mg^{2+}) (Cook et al., 2015; Keller et al., 2018; Nemeth et al., 2004). Due to the absence of a high resolution full CaSR structure, mutagenesis studies and computational docking have been applied to determine the binding site(s) of arylalkylamine PAMs (Bu et al., 2008; Keller et al., 2018; Leach et al., 2016; Miedlich et al., 2004; Petrel et al., 2004; Petrel et al., 2003). More recent studies have quantified the effect of amino acid substitutions on PAM affinity, cooperativity and agonism using an operational model of allosterism (Gregory et al., 2020; Leach et al., 2007). Key amino acid residues that contribute to the affinity of arylalkylamine PAMs are located in TMs 2, 3, 5, 6 and 7, as well as ECLs 2 and 3; $F668^{2.56}$ (numbering in superscript refers to that assigned in Pin et al. (2003) to denote the residue position relative to the most highly conserved residue in each TM domain across the class C GPCRs), $F684^{3.36}$, $F688^{3.40}$, $A772^{5.39}$, $W818^{6.50}$, $F821^{6.53}$, $Y825^{6.57}$, $E837^{7.32}$, $A840^{7.35}$, $I841^{7.36}$, $E767^{ECL2}$ and $V833^{ECL3}$ (Keller et al., 2018). Mapping these residues onto a homology model of the CaSR based on the $mGlu_1$ and $mGlu_5$ receptor crystal structures revealed a large small

molecule binding cavity that spans from the top to the middle of the 7TMs (Figure 1.2). PAM binding in this cavity is predicted to be facilitated by a hydrogen bond interaction between E837$^{7.32}$ and the secondary amine of the arylalkylamines (Bu et al., 2008; Keller et al., 2018; Leach et al., 2016; Miedlich et al., 2004; Petrel et al., 2004; Petrel et al., 2003). The predicted 7TM binding pocket of CaSR arylalkylamine PAMs is commensurate with that observed for the binding site of a NAM co-crystallised with $mGlu_1$ (Wu et al., 2014), and common across the class C GPCR family. Sample arylalkylamine PAMs of the CaSR are listed in **Figure 1.3**.

In 2010, ACADIA pharmaceuticals discovered benzothiazole-containing CaSR PAMs that were structurally and chemically distinct from the arylalkylamine PAMs, leading to the identification of AC265347 (Gustafsson et al., 2010; Ma et al., 2011). Like the arylalkylamines, AC265347 demonstrates agonist activity in the absence of cations, but it is a more potent and efficacious agonist (Cook et al., 2015). AC265347 is also a biased CaSR allosteric modulator that preferentially enhances CaSR-mediated phosphorylation of ERK1/2 versus $Ca^{2+}{}_i$ mobilisation. In contrast, phenylalklyamine PAMs show the reverse biased modulatory profile (Cook et al., 2015). While AC265347 is predicted to bind within the 7TM cavity, it is unaffected by many of the mutations that reduce cinacalcet affinity (Leach et al., 2016). Importantly, AC265347 lacks an ionisable nitrogen and is therefore not predicted to form an ionic interaction with E837$^{7.32}$. Computational docking studies supported by mutagenesis suggest that AC265347 sits deeper in the 7TM bundle in comparison to the arylalkylamine PAMs (Leach et al., 2016) (**Figure 1.2**). By binding deeper within the 7TM bundle, AC265347 may stabilise distinct receptor states relative to arylalkylamine PAMs, engendering biased CaSR signalling.

1.4.5.2 Small molecule NAMs

A high throughput screen and subsequent medicinal chemistry effort at SmithKline Beecham led to the discovery of the first CaSR NAM, NPS2143, which has an arylalkylamine scaffold (Marquis et al., 2009). Subsequent efforts to progress arylalkylamine NAMs clinically led to the development of several NAMs with structural and chemical similarity to NPS2143, including ronacaleret (Marquis et al., 2010; Marquis et al., 2009), JTT305 (otherwise known as MK3552) (Shinagawa et al., 2011), and NPSP795 (Lago et al., 2006). Arylalkylamine NAMs are predicted to bind within the same 7TM cavity as arylalkylamine PAMs and form a hydrogen bond with

E837$^{7.32}$ via their secondary amine (Josephs et al., 2020; Leach et al., 2016). In fact, the predicted binding pose for the arylalkylamine NAMs is very similar to the predicted pose for arylalkylamine PAMs, making it difficult to discern from computational modelling how these structurally similar PAMs and NAMs have opposing effects on CaSR signalling. Future structural elucidation of the CaSR 7TM bound to PAMs and NAMs is needed to fully appreciate how these small molecules alter CaSR structure and function.

In addition to the arylalkylamine NAMs, a screening program at Novartis identified quinazolinone-containing compounds as CaSR NAMs, which were advanced to yield ATF936 and AXT914 (Widler, 2011; Widler et al., 2010). ATF936 has greater negative cooperativity in comparison to NPS2143, meaning that it is better at blocking CaSR activity (Josephs et al., 2020). Mutagenesis and docking studies predict the quinazolinone-containing NAMs bind in the 7TM allosteric cavity, but in a distinct manner to the arylalkylamine PAMs and NAMs (Bu et al., 2008; Josephs et al., 2020; Miedlich et al., 2004). For instance, some mutations that reduce NPS2143 affinity have no effect on the affinity of ATF936 affinity (Josephs et al., 2020; Widler et al., 2010). A more detailed structural understanding of the binding of quinazolinone-containing NAMs may afford the opportunity to design NAMs with even greater affinity or cooperativity.

Intriguingly, a structurally and chemically distinct CaSR NAM, known as BMS compound 1, is predicted to bind to a second as yet unidentified allosteric site in the CaSR's 7TM or ECLs (Josephs et al., 2020). Multiple allosteric binding sites within the 7TM of class C GPCRs is not unprecedented. For $mGlu_5$, several PAM chemotypes are thought to bind outside the common allosteric pocket as evidenced by non-competitive interactions with a radiolabelled NAM (Hammond et al., 2010; Noetzel et al., 2013). Once again, structural resolution of the BMS compound 1 binding site would provide further opportunities for drug discovery efforts at the CaSR to identify novel allosteric modulators that target this site and may give rise to NAMs with biased modulatory properties. Sample arylalkylamine NAMs of the CaSR are listed in **Figure 1.4**.

1.4.5.3 Mode-switching allosteric modulator

Calhex231 is structurally and chemically related to cinacalcet and the other arylalkylamine PAMs, and indeed it was discovered from an SAR study based on the PAM calindol. Surprisingly,

calhex231 was reported to be a NAM because it inhibited a maximally effective concentration of Ca^{2+}_o in an IP accumulation assay (Kessler et al., 2006). Recent work, however, has revealed that calhex231 is both a PAM and a NAM depending on whether it occupies a single protomer in the CaSR dimer or both protomers (Gregory et al., 2018). The binding of calhex231 to one protomer inhibits the binding of calhex231 to the second protomer. Using an allosteric quaternary complex model, it was shown that calhex231 switches to a NAM because its negative cooperativity with itself is greater in the presence of an agonist (Gregory et al., 2018). The calhex231 binding site overlaps with the binding site for cinacalcet, NPS2143 and other arylalkylamine PAMs and NAMs (Gregory et al., 2018). The ability of calhex231, but not other PAMs and NAMs, to mode-switch is predicted to be due to a cyclohexane ring in calhex231, which may offer more flexibility when bound to the CaSR and thus allow calhex231 to adopt at least two distinct binding poses (Gregory et al., 2018).

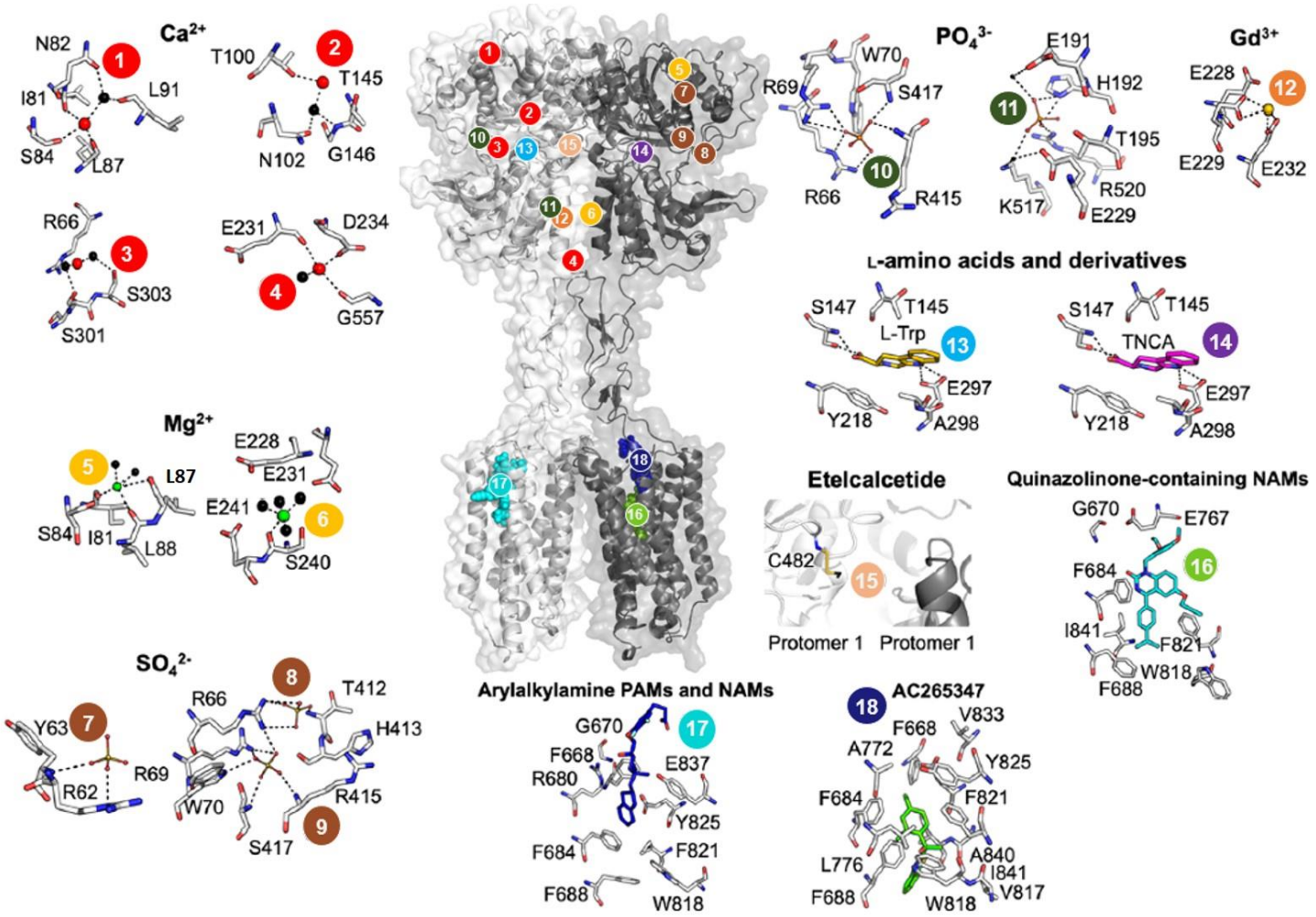

Figure 1.2. CaSR model and predicted ligand binding sites. The published crystal structure of the CaSR ECD (PDB) was superimposed onto a published model of the CaSR's 7TM (Josephs et al., 2020). ECLs and ICLs based on homology with the metabotropic glutamate receptor 5 crystal structure (PDB 4OO9). Numbers correspond to ligand binding sites predicted as follows: Ca^{2+} (sites 1-4), Mg^{2+} (5-6), SO_4^{2-} (7-9), PO_4^{3-} (10-11), Gd^{3+} (12), L-Trp (13), TNCA (14), etelcalcetide (15), AC265347 (16), quinazolinone-containing NAMs (17) and arylalkylamine PAMs and NAMs (18). Figure adapted from Diao et al. (2021)

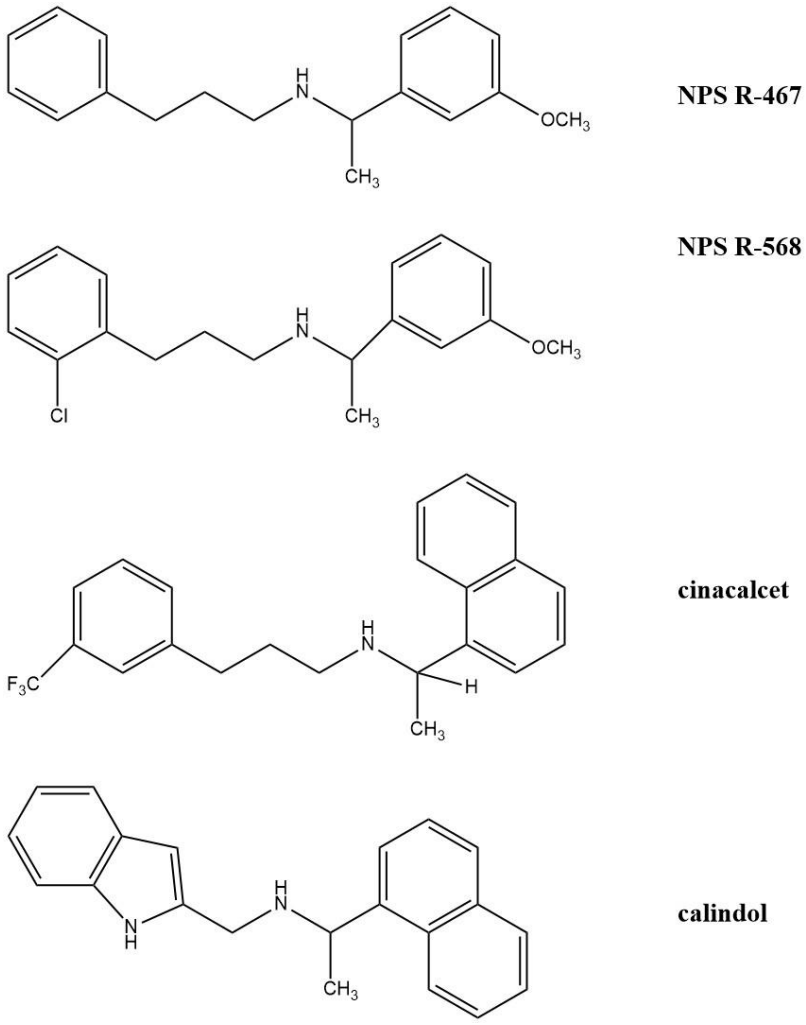

Figure 1.3. Chemical structures of arylalkylamine PAMs of the CaSR

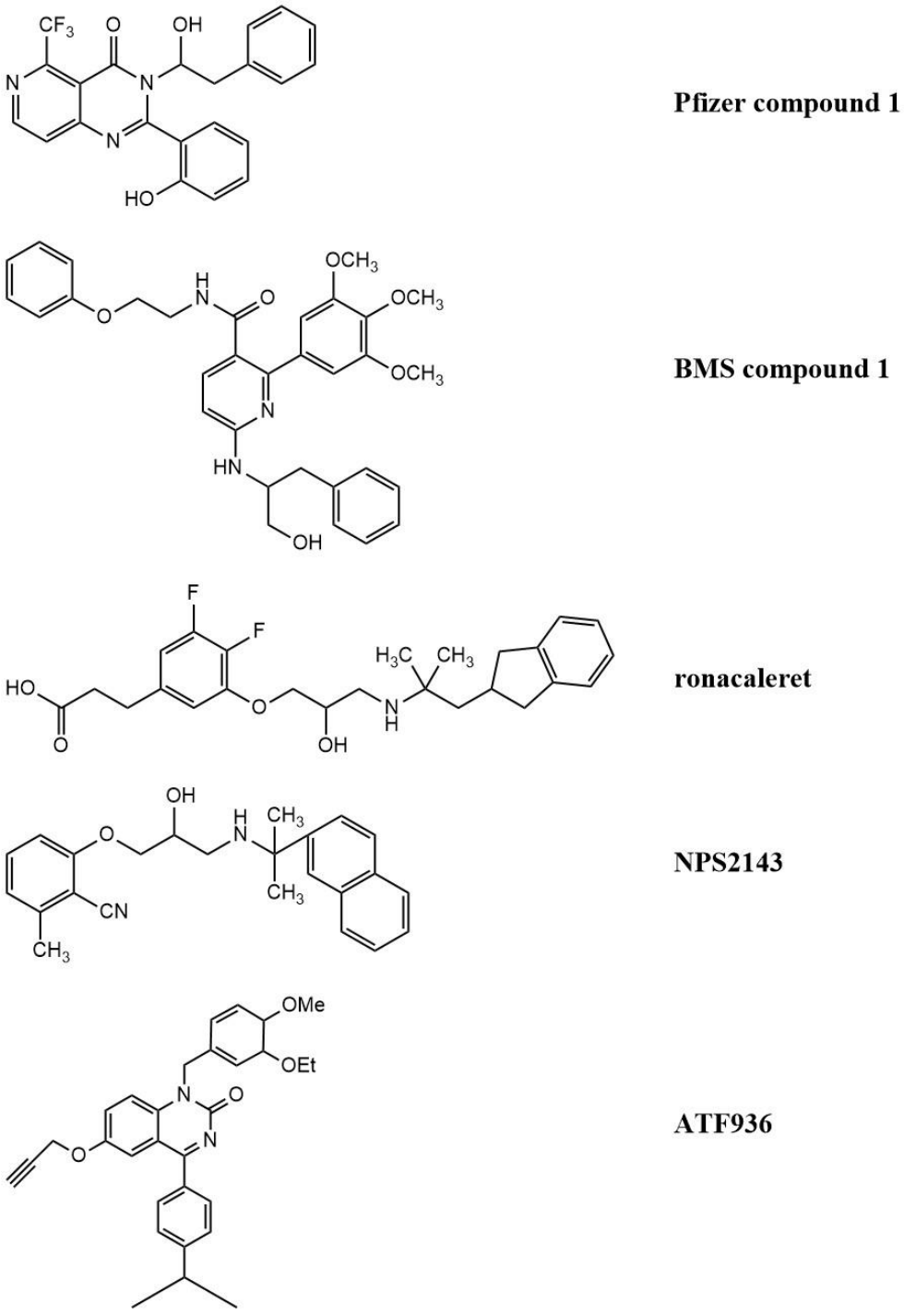

Figure 1.4. Chemical structures of chemically distinct NAMs of the CaSR.

1.5. CaSR signalling mechanisms

The CaSR couples to $G_{q/11}$, $G_{i/o}$, G_s (under certain conditions) and potentially $G_{12/13}$ (Conigrave & Hampson, 2010; Leach et al., 2020; Mamillapalli & Wysolmerski, 2010). Furthermore, activation of the CaSR can also increase intracellular calcium (Ca^{2+}_i) concentrations by stimulating L-type voltage-gated and transient receptor potential ion channels on the plasma membrane, probably via a PKC-dependent mechanism (McGehee et al., 1997; Thomsen et al., 2012b). The underlying reasons for CaSR coupling to multiple different heterotrimeric G proteins still remain to be investigated (Conigrave & Hampson, 2010). However, binding of different ligands to the CaSR leads to stabilisation of distinct conformational receptor states and consequent coupling to different G proteins, suggesting that the CaSR's promiscuous coupling to different transducers is important for its function. The principal downstream signalling pathways to the CaSR are summarised in **Figure 1.5.**

1.5.1. $G_{q/11}$

Coupling of the CaSR to $G_{q/11}$ leads to activation of phosphatidylinositol-specific phospholipase C (PI-PLC), which results in the production of inositol triphosphate (IP_3) and diacylglycerol (DAG) (Conigrave & Hampson, 2010). The subsequent binding of IP_3 to IP_3 receptors on the endoplasmic reticulum releases Ca^{2+}_i (Nemeth & Scarpa, 1986; Nemeth & Scarpa, 1987). Increased Ca^{2+}_i leads to activation of phospholipase A2 (PLA_2) and PKC (Hofer & Brown, 2003; Kifor et al., 2001). CaSR-$G_{q/11}$ pathways are observed in various cell types, including parathyroid cells and osteoblasts (Godwin & Soltoff, 2002; Wettschureck et al., 2007). In the parathyroid gland, double knockout of G_q and G_{11} α-subunits depleted Ca^{2+}_o-dependent negative control of parathyroid hormone secretion (Wettschureck et al., 2007). The migration of pre-osteoblasts to sites of bone resorption also involves a PLC-dependent pathway (Godwin & Soltoff, 2002). $ERK_{1/2}$ may also contribute to the activation of PLA_2 in HEK293-CaSR downstream from $G_{q/11}$ (Handlogten et al., 2001) although in another study, activation of PLA_2 was independent of the ERK pathway in bovine parathyroid and HEK293-CaSR (Kifor et al., 2001). Similarly, while pre-treatment of parathyroid cells or HEK293-CaSR cells with 2 mM Ca^{2+}_o resulted in down-regulation of PKC and abolishment of phospholipase D (PLD) activity in one study (Kifor et al., 1997), another study demonstrated that exposure of Madin-Darby canine kidney (MDCK)-CaSR cells to 5 mM Ca^{2+}_o

did not lead to a reduction in PLD activity (Huang et al., 2004). Such inconsistent results may be due to the different cell types or concentrations of Ca^{2+}_o used in different studies (Hjälm et al., 2001; Huang et al., 2004), demonstrating the importance of using relevant cell types and agonist concentrations to investigate CaSR-$G_{q/11}$ pathways.

1.5.2. $G_{12/13}$

It is still not fully validated whether CaSR directly couples to $G_{12/13}$ due to a lack of specific $G_{12/13}$ inhibitors and overlapping effectors downstream from $G_{12/13}$ and $G_{q/11}$. Activation of the CaSR leads to phosphorylation of Rho and PLD, probably via $G_{12/13}$ (Kelly et al., 2007; Siehler, 2009). Besides Rho family kinases, $G_{12/13}$ also modulates tyrosine kinases, protein phosphatases including protein phosphatase 2A (PP2A) and Wnt3a-Frizzled signalling, supporting various CaSR-mediated effects on cell fate (Kelly et al., 2007). In MDCK cells, activation of the CaSR by Ca^{2+}_o resulted in the translocation of Rho to the cell membrane as well as activation of serum response element (SRE)-mediated gene transcription (Huang et al., 2004; Pi et al., 2002). Treatment with the Rho family inhibitor, C3 exoenzyme, lead to inhibition of SRE activity in HEK293-CaSR cells, while activation of Rho involved the recruitment of the Rho-guanine nucleotide exchange factor, Lbc and filamin (Pi et al., 2002). However, these studies do not confirm whether CaSR-mediated Rho activity is directly linked to $G_{12/13}$.

1.5.3. $G_{i/o}$

The CaSR couples to $G_{i/o}$, resulting in inhibition of adenylyl cyclase (AC) thereby reducing cyclic adenosine monophosphate (cAMP) levels. CaSR-mediated $G_{i/o}$ activation also stimulates extracellular signal-regulated kinase 1/2 ($ERK_{1/2}$), c-Jun N-terminal kinase (JNK) and p38 MAPK (Ogata et al., 2006). Src kinases induce a signalling cascade that leads to phosphorylation of ERK, via the Raf-MEK-ERK pathway (Kifor et al., 2001; McNeil et al., 1998). Furthermore, CaSR-mediated PLC and PKC also activate $ERK_{1/2}$, probably via coupling to $G_{q/11}$ and $G_{i/o}$ subunits (Kifor et al., 2001). Multiple studies have revealed different cascades downstream from CaSR-mediated $G_{i/o}$ activation in different cell types, such as PI3K in HEK-CaSR cells and ovarian surface epithelial cells (Hobson et al., 2003), JNK in NIH/3T3 cells (a fibroblast cell line) and p38

MAPK in mouse osteoblastic cells and rat H-500 Leydig cancer cell lines (Hoff et al., 1999; Tfelt-Hansen et al., 2003). Similar to the $G_{q/11}$ coupling pathway, different specific cascades that are involved with CaSR-$G_{i/o}$ are observed in different cell backgrounds.

1.5.4. G_s

In some cell types, the CaSR couples to G_s proteins, leading to increased intracellular cAMP levels and activation of PKA. CaSR-G_s coupling was identified in immortalised and malignant breast cells and in an AtT-20 pituitary-derived cell line (Mamillapalli et al., 2008; Mamillapalli & Wysolmerski, 2010; Thomsen et al., 2012b). However, cAMP production is not observed in HEK293-CaSR cells (Thomsen et al., 2012a). Compared to CaSR-activated $G_{i/o}$ and $G_{q/11}$ pathways, the detailed signalling cascades downstream from CaSR-mediated G_s coupling remain to be investigated.

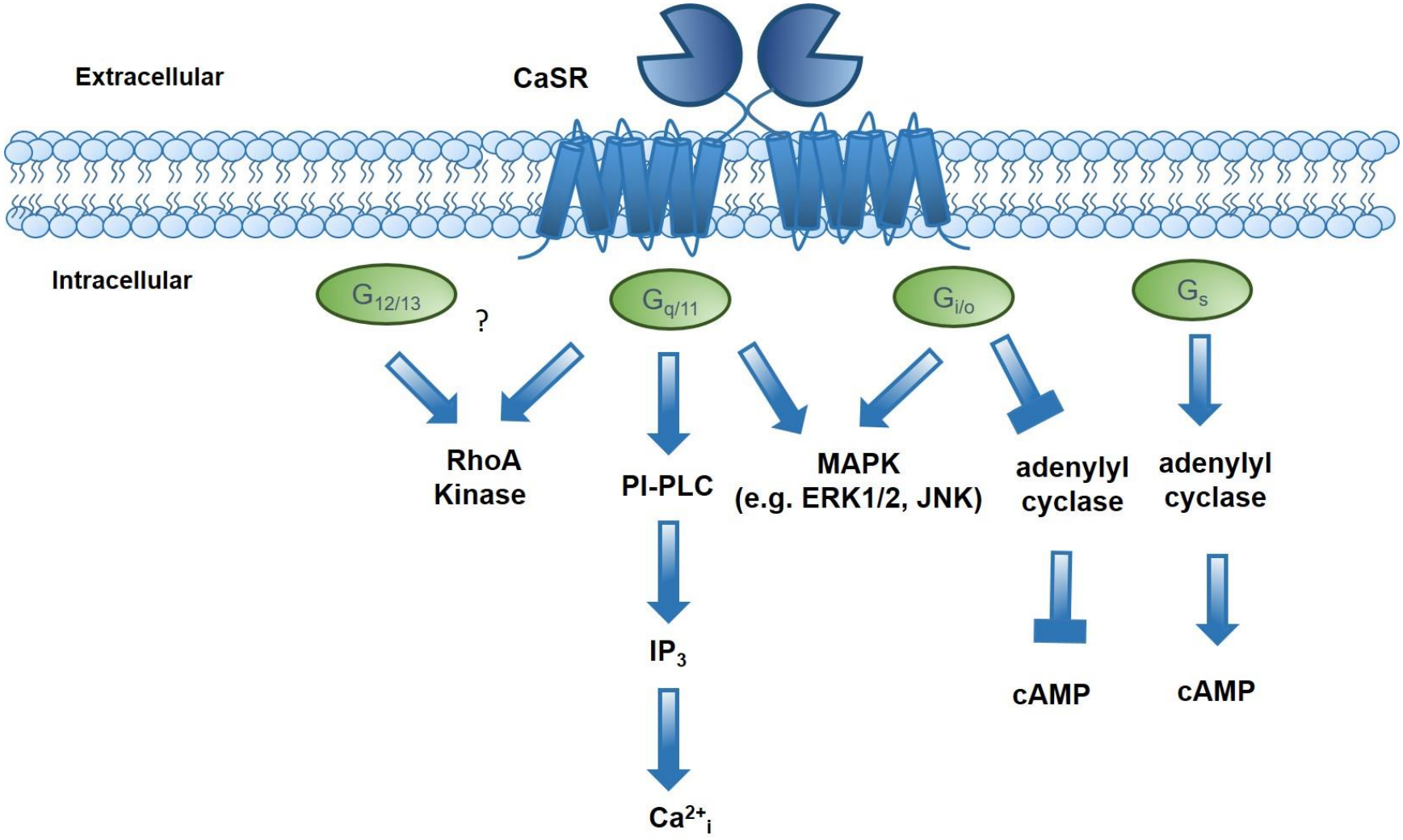

Figure 1.5. The principal downstream signalling pathways of the CaSR. The CaSR couples to heterotrimeric G proteins, G_q, $G_{i/o}$, G_s and possibly $G_{12/13}$. CaSR coupling to $G_{q/11}$ results in PI-PLC-IP_3-mediated Ca^{2+}_i mobilisation. Activation of G_q and possibly $G_{12/13}$ leads to RhoA kinase activity. CaSR coupling to $G_{i/o}$ leads to activation of MARK (including ERK1/2 and JNK) and inhibition of AC and cAMP. CaSR coupling to G_s stimulates AC and cAMP.

1.6 The (patho) physiological roles of the CaSR in various organs

1.6.1 Parathyroid glands

The CaSR is a key mediator of the negative feedback loop regulating PTH secretion and parathyroid cell proliferation in response to changes in blood Ca^{2+}_o concentrations (Fan et al., 2018; LeBoff et al., 1985; Nemeth & Scarpa, 1986). The normal Ca^{2+}_o concentration range is between 1.1-1.3 mM). Under hypercalcaemia condition, PTH secretion activates PTH1 receptor on the bone and kidneys to enhance bone resorption and CaSR in the renal cortical thick ascending limbs (TALs) of Henle's loop is activated to increase Ca^{2+}_o excretion (Loupy et al., 2012). Expression of the CaSR in the parathyroid glands is regulated by the active form of vitamin D, 1, 25$(OH)_2$D, which influences vitamin D response elements on the *CASR* gene promotor. Under normal physiological conditions, activation of the CaSR leads to AC inhibition, PKC activation and Ca^{2+}_i mobilisation from intracellular stores, which collectively decrease PTH gene transcription and PTH secretion (Kifor et al., 1997). Under pathophysiological conditions, such as hypocalcaemia, low concentrations of Ca^{2+}_o lead to parathyroid cell proliferation to maintain high levels of PTH release (Corbetta et al., 2002). The physiological importance of the CaSR in PTH secretion is demonstrated by mice with parathyroid-specific CaSR ablation, which have hyperparathyroidism and hypercalcaemia (Chang et al., 2008).

1.6.1 Kidney

The CaSR is highly expressed and plays specific roles at each distinct section in the kidney. The CaSR in the kidneys responds to increased concentrations of serum Ca^{2+} by decreasing Ca^{2+} reabsorption via both PTH-dependent and independent pathways (Kos et al., 2003; Riccardi et al., 1998; Riccardi D, 1995). The kidney CaSR plays roles in regulating ion homeostasis in the proximal tubule, ascending limb, distal convoluted tubule amongst other regions of the kidneys (Ba et al., 2003; Douglas et al., 2010; Loupy et al., 2012; Renkema et al., 2009; Riccardi & Valenti, 2016; Topala et al., 2008). In the thick ascending limb (TAL), CaSR detects Ca^{2+}_o concentrations and regulates renal Ca^{2+} excretion, probably via the claudin 14 tight junction protein (Kantham et al., 2009; Tadatoshi et al., 2017; Toka, 2014; Toka et al., 2012). In the proximal TAL, CaSR activation inhibits Na-K-Cl co-transporters and inwardly rectifying K^+ channels, resulting in decreased Na^+, Cl^-, and K^+ reabsorption (Cha et al., 2011; Watanabe Sumiyo, 2002). In the medullary TAL and cortical TAL, CaSR activation inhibits

NaCl and Ca^{2+} and Mg^{2+} reabsorption, respectively (Sands et al., 1997). In the inner medullary collecting duct, CaSR activation inhibits vasopressin-elicited water reabsorption (Sands et al., 1997). In the juxtaglomerular apparatus, activation of the CaSR by the calcimimetic, cinacalcet, inhibits renin secretion in rats (Atchison et al., 2010). In the distal convoluted tubule, activation of the CaSR stimulates the epithelial transient receptor potential cation channel subfamily V member 5 (TRPV5) channel to regulate Ca^{2+} reabsorption (Topala et al., 2009). Overall, the CaSR in the kidney balances ion homeostasis by adjusting ion excretion and reabsorption.

1.6.3 Bone

The CaSR is expressed in osteoblasts and osteoclasts as well as chondrocytes, with distinct functions in each cell type (Chang et al., 2008; Yamaguchi et al., 1998). The CaSR promotes osteoblast proliferation, likely via JNK signalling (Chattopadhyay et al., 2004; Dvorak et al., 2004), and participates in both differentiation and apoptosis of osteoclasts through the PLC pathway (Mentaverri et al., 2006). In preclinical studies, activation of the CaSR in osteoblasts by strontium activated bone anabolic pathways including Wnt signalling and Akt phosphorylation, suggesting the therapeutic potential of the CaSR to treat osteoporosis (Fromigué et al., 2009). The CaSR is also highly expressed in cartilage chondrocytes in the growth plate of long bones. Osteoblast-or chondrocyte specific-CaSR knockout mice demonstrated bone undermineralisation, spontaneous bone fractures, growth plate chondrogenesis and other bone-related symptoms, highlighting the physiological importance of the CaSR in osteoblasts and chondrocytes (Chang et al., 2008; Dvorak-Ewell et al., 2011). Therefore, the CaSR has been regarded as a drug target of interest to treat bone anabolic diseases.

1.6.4 Digestive system

The CaSR is widely distributed in the digestive system, from the oesophagus to the stomach, small intestine and colon (Chattopadhyay et al., 1998; Riccardi et al., 1995). The CaSR senses nutrients and regulates enteroendocrine hormone secretion, fluid balance, and cell proliferation and differentiation (Alamshah et al., 2017; MacLeod, 2013; Tang et al., 2016). The CaSR in the digestive system functions likely via phosphorylation of ERK and stimulation of Ca^{2+}_i mobilisation (Buchan et al., 2001; Busque et al., 2005; Chakrabarty et al., 2003; Justinich et

al., 2008). CaSR activation induces gastrin secretion from D and G cells and also acid secretion from parietal cells (Bevilacqua et al., 2005). Its stimulation in G cells induces cellular proliferation (Feng et al., 2010; Rey et al., 2012). CaSR activation by L-amino acids promotes anti-inflammatory effects in intestinal epithelial cells (Mine & Zhang, 2015). Treatment with 5 mM L-Trp inhibited tumour necrosis factor (TNF)-α-induced interleukin (IL)-8 secretion in HT-29 (human colorectal adenocarcinoma cell line) or Caco-2 cells (human colorectal adenocarcinoma cell line) as well as enhancing phosphorylation of JNK or IκBα (Mine & Zhang, 2015). The fact that these inhibitory effects were opposed by NPS2143 suggests CaSR activation mediates anti-inflammatory effects in the digestive system.

1.6.5 Nervous system

The CaSR is expressed in both the central and peripheral nervous systems, including on nerve terminals, astrocytes, and microglial cells (Ruat et al., 1995; Yano et al., 2004). The CaSR in the nervous system senses various stimuli, including Ca^{2+}, Na^{+} and spermine (Chattopadhyay et al., 2007; Tharmalingam et al., 2016). The CaSR regulates neuronal excitability by regulating ion currents that mediate the initiation of action potentials and associated neuronal depolarization, regulating Ca^{2+}-activated K^{+} channels (Vassilev et al., 1997; Yano S, 2004; Ye et al., 1997). Furthermore, the CaSR promotes dendritic growth within the hippocampus (Vizard et al., 2008). The pathophysiological functions of the CaSR are implicated in brain disorders, such as Alzheimer disease and ischaemic brain injury (Conley et al., 2009). The CaSR is activated by amyloid-β1–42 peptide fragment (Aβ1-42), which is implicated in Alzheimer's disease (Conley et al., 2009). Further, the treatment with NPS2143 inhibited Aβ1-42 and p-tau secretion in mouse model (Chiarini et al., 2017), suggesting that CaSR NAMs have the potential to oppose progression of this neurodegenerative disease.

1.6.6 Breast

The CaSR is expressed in breast epithelial cells and CaSR expression and activity are increased during lactation (Cheng et al., 1998; VanHouten et al., 2004). The main role of the CaSR in breast epithelial cells is to regulate Ca^{2+} transportation into milk. During maternal hypocalcaemia, parathyroid hormone-related protein (PTHrP) produced from breast cells is

increased as a result of reduced activity of the CaSR. PTHrP stimulates bone reabsorption of Ca^{2+} to restore Ca^{2+} in the body (Kim & Wysolmerski, 2016) to protect from hypocalcaemia.

1.6.7 Cardiovascular system

The CaSR is also found in cardiac tissues, including arterial vessels, vascular smooth muscle cells and endothelial cells (Guerman et al., 2007; Schepelmann et al., 2016; Schreckenberg & Schlüter, 2018; Wang et al., 2003). In general, activation of the CaSR stimulates vascular smooth muscle cell proliferation and calcification, and regulates blood pressure. Ablation of CaSRs in vascular smooth muscle cells caused loss of contractility of the aorta and mesenteric arteries and decreases diastolic and mean arterial blood pressure. Intracisternal injection of the PAM, NPS R-467, reduced blood pressure associated with sympathoinhibition in a dose-dependent manner *in vivo* (Kobayashi-Torii et al., 2011). Further, CaSR levels were negatively correlated with the levels of cAMP and angiotensin II, but positively correlated with renin, which promotes increased vascular modelling and vascular smooth muscle cell proliferation (Qu et al., 2016; Smajilovic et al., 2011). These data suggest that the CaSR plays a role in the renin-angiotensin system and regulates blood pressure.

1.6.8 Respiratory system

The CaSR is expressed in both human fetal and adult lungs. The main roles of the CaSR in human fetal lungs include regulation of fluid secretion, lung growth and development (Brennan et al., 2016; Roesler et al., 2019). Furthermore, activation of the CaSR by NPS R-568 inhibited branching morphogenesis (Finney et al., 2008). The fetal CaSR modulates the intrinsic lung developmental programme (Roesler et al., 2019).

In adult lungs, the CaSR is expressed on airway smooth muscle (ASM) and its expression is increased in ASM cells from human with asthma and in pulmonary arterial smooth muscle cells from patients with idiopathic pulmonary artery hypertension, as measured by quantitative reverse transcription polymerase chain reaction (qRT-PCR) and western blot analysis CaSR protein expression (Yamamura et al., 2012; Yarova et al., 2015). In allergen-sensitised mice, CaSR mRNA expression was increased in ASM cell exposure to the asthma-associated pro-inflammatory cytokines TNF-α and IL-13 in comparison to unsensitised mice (Yarova et al., 2015). Furthermore, polyamines induce airway contraction and inflammation by activating the

CaSR. Treatment with nebulized CaSR NAMs of BALB/c mice showed a trend of decreased polyamine-induced airway contraction and decreased airway inflammation to the same degree as ICSs (especially macrophages, eosinophil and lymphocytes) without unwanted systemic effects (Yarova et al., 2021; Yarova et al., 2015). Consistent with this, NPS2143 decreased 65% of immune cells in bronchoalveolar fluid and reduced ASM thickness and fibrosis in a mixed allergen treated mouse model of asthma or lipopolysaccharide-induced lung injury (Lee et al., 2017; Thompson et al., 2016), suggesting the potential of CaSR NAMs to treat asthma (discussed in greater detail in section 1.10).

1.7 Clinical utility of CaSR allosteric modulators

1.7.1 CaSR PAMs for hyperparathyroidism

Given the CaSR's pivotal role in negatively regulating PTH secretion, three CaSR PAMs are currently on the market to treat hyperparathyroidism. Most commonly, hyperparathyroidism is caused by parathyroid adenoma or carcinoma resulting in primary hyperparathyroidism (PHPT). It can also occur secondary to chronic kidney disease, where impaired phosphate excretion and renal 1,25-dihydroxyvitamin D3 synthesis lead to decreased Ca^{2+}_o and a consequent increase in PTH synthesis and secretion, as well as parathyroid hyperplasia.

Cinacalcet (Sensipar™) was the first CaSR-targeting drug to gain FDA approval in 2004 for haemodialysis patients with secondary hyperparathyroidism (SHPT) caused by chronic kidney disease (Lindberg et al., 2003; Quarles et al., 2003). Cinacalcet was also the first FDA-approved GPCR allosteric modulator to reach the market. Cinacalcet has since been FDA-approved to treat hypercalcemia in adults with parathyroid carcinoma or who cannot undergo parathyroidectomy. Cinacalcet is generally safe and well tolerated, although gastrointestinal (GI) adverse events, including nausea, vomiting or loss of appetite, occur in approximately 30% of patients (Bover et al., 2016; Fukagawa et al., 2018). Cinacalcet can also cause transient episodes of hypocalcaemia in some patients. Further, there is some variability in the degree to which patients respond to cinacalcet (Rottembourg et al., 2019). While cinacalcet responsiveness can depend on the severity of SHPT, CaSR single nucleotide polymorphisms (SNP) may influence cinacalcet efficacy. For instance, SHPT patients with an R990G SNP demonstrate higher sensitivity to cinacalcet, with a larger proportion of G990 carriers experiencing a cinacalcet-mediated suppression in PTH compared to patients with the predominant R990 allele (Jeong et al., 2016; Rothe et al., 2008; Rothe et al., 2005). These

findings suggest that a personalised medicines approach may need to be considered when treating patients with CaSR-targeting therapies.

In 2017, etelcalcetide (Parsabiv) was approved by the FDA as an intravenous CaSR PAM for the treatment of SHPT in adults. Etelcalcetide's intravenous (i.v.) route of administration is advantageous because it can be delivered at the end of a haemodialysis session, thus ensuring patient compliance. While etelcalcetide was expected to induce fewer GI adverse events compared to cinacalcet because it is not ingested orally, self-reported symptoms of nausea and vomiting were not significantly different between SHPT patients given i.v. etelcalcetide or oral cinacalcet (Block et al., 2017a). Nonetheless, a one-year safety and efficacy trial of i.v. etelcalcetide revealed no major safety concerns (Bushinsky et al., 2019), although like cinacalcet, etelcalcetide can cause hypocalcaemia (Palmer et al., 2020).

Recently, evocalcet (alternative names MT-4580 and KHK7580) was approved for the management of SHPT in Japanese patients that remain refractory to SHPT with cinacalcet (Akizawa et al., 2018; Fukagawa et al., 2018; Kawata et al., 2018; Shigematsu et al., 2018). For these patients, the cinacalcet dose cannot be sufficiently increased due to adverse gastrointestinal events (Block et al., 2009; Gincherman et al., 2010). Evocalcet has higher bioavailability in comparison to cinacalcet, and lower doses are therefore required to suppress serum PTH levels (Kawata et al., 2018). In rats, evocalcet suppresses PTH secretion while having no significant effect on gastric emptying, unlike cinacalcet treated rats and patients where emptying is delayed (Kawata et al., 2018). Evocalcet also had a reduced incidence of vomiting compared to cinacalcet in marmosets (Fukumoto et al., 2010; Kawata et al., 2018). In humans, evocalcet offers good short-term tolerability in terms of upper gastrointestinal symptoms while still providing therapeutic efficacy similar to cinacalcet (Shigematsu et al., 2018). However, while the severity of these side effects is reduced compared to cinacalcet (Palmer et al., 2020), approximately 19% of evocalcet-treated patients still experience nausea and vomiting, compared to 33% of patients treated with cinacalcet (Fukagawa et al., 2018).

1.7.2 PAMs for hypercalcaemia

The importance of the CaSR in Ca^{2+}_o homeostasis is highlighted by the many naturally occurring mutations in the *CASR* gene itself, or in genes encoding $G\alpha_{11}$ (*GNA11*; located on chromosome 19p13.3), which mediates CaSR signal transduction, or adapter protein 2 sigma subunit 1 (*AP2S1*; located on chromosome 19q13.3), which regulates CaSR cell surface

expression (Nesbit et al., 2013). Inactivating mutations in these proteins cause familial hypocalciuric hypercalcaemia (FHH) or neonatal severe primary hyperparathyroidism (NSHPT).

FHH type 1 (FHH1; the most common form of FHH) and NSHPT are caused by inactivating *CASR* mutations (Hannan et al., 2019) that reduce CaSR sensitivity to Ca^{2+}_o, or impair the biosynthesis and post-translational processing of the CaSR within the endoplasmic reticulum or Golgi apparatus, leading to CaSR mis-folding and impaired cell surface expression (Huang & Breitwieser, 2007; White et al., 2009). Furthermore, some *CASR* mutations engender biased agonism by altering the preference of the CaSR for coupling to particular signalling pathways (Leach et al., 2012). The prevalence of FHH1 is up to 1 per 1350 (Dershem et al., 2020). FHH1 is characterised by mild or moderate elevations of serum calcium and magnesium, with mildly elevated or normal PTH levels. While FHH1 patients are often asymptomatic, up to 30% of patients experience symptomatic hypercalcaemia, whereas others develop chondrocalcinosis, acute pancreatitis and gallstones (Thakker, 2004). Importantly, FHH1-causing mutations increase the risk of cardiovascular disease, heart failure, dementia, major depression, alcohol abuse, neck and leg fractures, osteoarthritis, kidney stones, pancreatitis, asthma and other diseases (Dershem et al., 2020; Eller-Vainicher et al., 2014; Gorvin, 2019; Grzegorzewska et al., 2018; Marz et al., 2007; Vezzoli et al., 2011; Vezzoli et al., 2013; Wang et al., 2016). These findings suggest that it may be appropriate to treat FHH1 even in asymptomatic patients. Further, the much rarer but more severe disorder, NSHPT, is characterised by life threatening hypercalcaemia, skeletal under-mineralisation and deformities, and death if left untreated (Hannan et al., 2016), therefore it is essential that infants diagnosed with NSHPT are treated.

Increasingly cinacalcet is being recognised as a viable therapeutic for the treatment of NSHPT and symptomatic FHH1, and cinacalcet has shown some success in treating NHSPT in addition to complications related to FHH1 in patients harbouring loss-of-function or loss-of-expression CaSR mutations (Alon & VanDeVoorde, 2010; Fisher et al., 2015; Gannon et al., 2014; Gunganah et al., 2014; Mastromatteo et al., 2014; Timmers et al., 2006; Wilhelm-Bals et al., 2012). There are, however, increasing reports of NSHPT patients who do not respond adequately to cinacalcet, in some cases due to homozygous mutations that result in truncation of the CaSR before the 7TM cinacalcet binding site (Atay et al., 2014; Savas-Erdeve et al., 2016). Cinacalcet-unresponsive patients may also harbour missense mutations or in-frame deletions that result in expression of a full-length CaSR with single amino acid mutations, or a

CaSR in which exon 5, encoding amino acids 476-536 in the ECD is deleted (Capozza et al., 2018; García Soblechero et al., 2013; Murphy et al., 2016). In these instances, cinacalcet may be ineffective because the mutation may reduce cinacalcet affinity or its ability to potentiate Ca^{2+}_o by decreasing allosteric cooperativity. In cases of severe mutation-induced receptor impairment, the mutation may render cinacalcet unable to sufficiently restore receptor function even if affinity or cooperativity are unaffected (Leach et al., 2013). Interestingly, compared to cinacalcet, AC265347 was more effective a potentiating Ca^{2+}_o-mediated signalling responses at four FHH1/NSHPT-causing CaSR mutants, suggesting that alternative PAMs may be better than cinacalcet at rescuing inactivating CaSR mutants (Ma et al., 2011). However, as AC265347 is not approved clinically, total parathyroidectomy is currently required to normalise serum PTH levels in patients who do not respond to current therapeutic interventions.

Four *GNA11* mutations have been identified in FHH2-affected individuals (FHH2 is the least common form of FHH), which are predicted to impair guanine nucleotide binding or disrupt G protein activation of intracellular signalling proteins such as PLC (Hannan et al., 2016; Nesbit et al., 2013). FHH2 patients typically have mild hypercalcaemia and normal serum concentrations of PTH (Nesbit et al., 2013). In recombinant cells expressing FHH2-causing *GNA11* mutations, cinacalcet restored impaired CaSR signalling (Babinsky et al., 2016). Similarly, in mice with a germline loss-of-function *GNA11* mutation, cinacalcet corrected hypercalcaemia and reduced elevated serum PTH concentrations (Howles et al., 2017). Importantly, cinacalcet also normalised serum calcium concentrations in a FHH2 patient with hypercalcaemia (Gorvin et al., 2018a). However, given the typically asymptomatic nature of FHH2, there is no clear benefit in treating most FHH2 patients with pharmacological interventions.

Four missense *AP2S1* mutations that cause FHH3 have been identified (Fujisawa et al., 2013; Hendy et al., 2014; Vargas-Poussou et al., 2016). FHH3-causing mutations disrupt AP2σ-mediated CaSR endocytosis, and consequently impair CaSR signalling from endosomes (Gorvin et al., 2018b; Nesbit et al., 2013). FHH3 is the most severe form of FHH, and is more commonly characterised by symptomatic hypercalcaemia (Hannan et al., 2015a; Vargas-Poussou et al., 2016). FHH3 may also be associated with recurrent pancreatitis and cognitive dysfunction (McMurtry et al., 1992). Cinacalcet corrected impaired CaSR signalling resulting from FHH3-causing *AP2S1* mutations, and rectified symptomatic hypercalcaemia in three FHH3 patients (Howles et al., 2016). These findings demonstrate that CaSR PAMs such as cinacalcet may be useful in the management of FHH3.

1.7.3 NAMs for osteoporosis

The first manifestation of osteoporosis is typically a fracture (Sözen et al., 2017). Therefore, treatments are aimed at preventing further bone loss, such as with the use of bisphosphonates (e.g. alendronate), or restoring bone mass and density with recombinant human PTH (1-34) (rhPTH (1-34)) or rhPTH (1-84), which have anabolic actions by increasing the number of bone-forming osteoblasts (Brixen et al., 2004). However, rhPTH (1-34) has received a black box warning label in the USA because high doses induced osteosarcoma in long-term carcinogenicity studies in rats (Tashjian & Goltzman, 2008). Further, rhPTH requires daily subcutaneous administration, and an orally active anabolic compound therefore continues to be of interest. Small molecule CaSR NAMs have been consequently developed as potential orally available therapeutics for osteoporosis because they stimulate the release of endogenous PTH by mimicking a drop in Ca^{2+}_o levels.

NPS2143 was the first CaSR NAM to be evaluated in an ovariectomised rat model of postmenopausal osteoporosis. However, following 5 weeks of daily NPS2143 administration, no net increase in bone mass and density was observed (Gowen et al., 2000b; Marquis et al., 2009; Nemeth, 2002). The high volume of NPS2143 distribution resulted in prolonged NPS2143 exposure and sustained elevations in PTH levels, in contrast to plasma levels of rhPTH (1-34), which reached a comparable maximum concentration but returned to baseline much more rapidly. It was soon realised that CaSR NAMs would best exert an anabolic effect if they had a short half-life to ensure transient stimulation of PTH release that promptly returned to basal levels. This is because prolonged exposure to PTH mimics hyperparathyroidism, thus stimulating bone resorption at the expense of bone formation (Dobnig & Turner, 1997).

Ronacaleret was the second CaSR NAM to be evaluated in osteoporosis. While ronacaleret is structurally similar to NPS2143, it is more metabolically labile (Balan et al., 2009; Kumar et al., 2010). However, a clinical trial in postmenopausal women given ronacaleret for 12 months demonstrated only a modest increase in bone mass and density of the lumbar spine compared to large increases seen in patients receiving rhPTH(1-34) or alendronate, while hip, femoral neck and trochanter bone mass and density were decreased in the ronacaleret-treated group (Fitzpatrick et al., 2012). Similarly, in a phase 2 clinical trial in postmenopausal women treated with JTT305/MK-5442 for 6 months, no significant increases in bone mass and density were observed over placebo, despite evidence of an increase in markers of bone formation (Halse et al., 2014b). A clinical trial of AXT914 was also terminated early due to a lack of effect of

AXT914 on bone formation markers and a dose-limiting increase in serum calcium after 4-weeks of treatment (John et al., 2014).

The reasons why CaSR NAMs do not stimulate bone formation are not fully understood, but may be linked to on-target CaSR effects in cells and tissues outside the parathyroid gland. For instance, CaSR NAMs may inhibit the important function of the CaSR in bone-forming osteoblasts, thus counteracting the effects of transient PTH release. Further, while the pharmacokinetic profiles of ronacaleret, JTT305/MK3552 and AXT914 were more favourable than NPS2143, NAM-mediated elevations in serum PTH concentrations remained above baseline in humans for more than 3.5 hours (Fitzpatrick et al., 2012; Halse et al., 2014b; John et al., 2014), whereas levels of rhPTH return to baseline rapidly following rhPTH injection (Caltabiano et al., 2013). Prolonged PTH release was more apparent at higher NAM doses that were cleared less rapidly, therefore the design of NAMs that can be administered at lower doses, such as those with greater affinity or cooperativity, could help to overcome this issue. Regardless of the reasons for CaSR NAM failures in the clinic, the development of NAMs for osteoporosis has been discontinued, and efforts have instead focussed on repurposing CaSR NAMs for alternative disorders.

1.7 NAMs for ADH and Bartter syndrome V

Recent interest has been garnered in repurposing CaSR NAMs for heterozygous activating mutations in the *CASR* or *GNA11* genes, which cause autosomal dominant hypocalcaemia type 1 (ADH1) or Bartter syndrome V (*CASR*), or ADH2 (*GNA11*). ADH is characterised by a mild or moderate decrease in serum calcium and PTH concentrations (Hannan et al., 2016; Hannan et al., 2012; Li et al., 2014; Nesbit et al., 2013). Many ADH sufferers experience symptomatic hypocalcaemia, which may include tingling and painful muscular spasms in the hands and feet, as well as seizures. Some ADH1 patients also suffer from calcifications in the kidneys and basal ganglia or elevated bone mineral density (Hannan et al., 2016). In more severe cases, gain-of-function *CASR* mutations promote renal loss of sodium, potassium, magnesium and chloride ions, and consequent hypokalaemic alkalosis and hyperreninaemic hyperaldosteronism, a condition called Bartter syndrome V (Hannan et al., 2016). The prevalence of ADH1 is approximately 1 per 25,000 (Dershem et al., 2020). Currently, over 90 different CaSR mutations have been linked to ADH1. Among them, over 95% are missense mutations, with the remaining 5% represented by frame-shift or in-frame insertion and deletion

mutations (Li et al., 2014). ADH2 is rarer than ADH1 and has been associated with six different activating missense *GNA11* mutations, located at the interface between the helical and GTPase domains of the $G\alpha_{11}$ protein (Mannstadt et al., 2013; Piret et al.). This region is involved in GDP-GTP exchange, and located at the $G_{\alpha 11}$ carboxyl terminal, which is involved with coupling to downstream G proteins. CaSR NAMs are a viable therapeutic strategy for caused by gain-of-function mutations in both the CaSR and $G\alpha_{11}$.

Promisingly, NPS2143 can normalise signalling responses associated with ADH-causing *CASR* and *GNA11* mutations *in vitro* (Babinsky et al., 2016; Hannan et al., 2015b; Leach et al., 2013; Letz et al., 2010). NPS2143 can also increase $Ca^{2+}{}_o$ and PTH concentrations in ADH1 and ADH2 mouse models (Gorvin et al., 2017; Hannan et al., 2015b; Roszko et al., 2017), and prevent nephrocalcinosis in an ADH1 mouse model (Dong et al., 2015). However, NPS2143 is less effective, at least *in vitro*, at gain-of-function *CASR* mutations that cause Bartter syndrome type V (Leach et al., 2013; Letz et al., 2010). In contrast, quinazolinone-derived NAMs (such as ATF936) can better rectify Bartter syndrome type V mutations *in vitro* (Letz et al., 2014) and may represent a class of NAMs with lower propensity to be affected by pharmacogenetic effects compared to arylalkylamine-derived NAMs like NPS2143.

Although originally developed for osteoporosis, the arylalkylamine-derived NAM, NPSP795, entered phase II clinical trials for the treatment of ADH1. NPSP795 robustly increased PTH in 3 out of 5 ADH1 trial patients and caused a small reduction in renal Ca^{2+} excretion. However, NPSP795 had no significant effect on serum $Ca^{2+}{}_o$ levels, and had variable effects on PTH (Roberts et al., 2019). The high variability in NPSP795 efficacy may in part be attributable to the underlying disease-causing mutations. Some ADH1 mutations are in close proximity to the common 7TM allosteric binding site, or NPSP795 may not have sufficient affinity or cooperativity to overcome some mutation-induced enhancement in CaSR signalling (Leach et al., 2016; Leach et al., 2013). However, pharmacogenetic effects do not completely explain interpatient variation in the efficacy of NPSP795. For instance, two patients in the study carried the same mutation (A840V). A840V faces into the 7TM binding cavity and contributes to the binding of the arylalkylamine NAM, NPS2143 (Leach et al., 2016). However, while serum PTH levels were robustly increased in one A840V-harbouring patient, NPSP795 had only a modest effect on PTH levels in the other, despite similar NPSP795 concentrations being reached in both patients. It therefore remains to be determined why some ADH patients may respond to CaSR NAMs, while others do not.

1.8 Asthma

Asthma is a chronic airway disorder, characterised by recurrent attacks of breathlessness, wheezing, coughing and chest tightness (Holgate et al., 2015). It comprises chronic progression and acute exacerbation, involving long-term disordered narrowing of the airway with a further narrowing during an acute attack. The latter is usually triggered by a stimulus, such as pollen, smoke, air pollution or viral infection (Subbarao et al., 2009). During an asthmatic attack, the hypersensitive airways become sore, swollen, allergic and irritated, with the affected individual developing breathing difficulties (Martinez & Verceli, 2013). This shortness of breath can be lethal if treated improperly but its mortality rate is relatively low compared to other chronic airway diseases (World Health Organization, 2017b).

There are three major pathophysiological components of asthma: **i**) airway inflammation, **ii**) airway remodelling, and **iii**) airway hyperresponsiveness (AHR) (Holgate, 2012). Although previously classified as either atopic (allergic) or non-atopic, it is clear that asthma has multiple phenotypes, differentiated by the age of onset, the type of inflammation and/or comorbidities (Holgate et al., 2015). The most common type of asthma is early-onset allergic asthma, driven by a Th2-mediated response to allergens, with other asthma types including exercise- and aspirin-induced bronchoconstriction, neutrophilic asthma and asthma either worsened or associated with obesity.

1.8.1 The socio-economic impact of asthma

Asthma is one of the most common airway diseases. Despite numerous approaches to treat asthma, its prevalence, mortality and economic burden have increased over the past two decades. Globally, there are >300 million patients currently suffering from asthma and it caused ~383,000 deaths in 2015, accounting for 1% of the global disease-related deaths (World Health Organization, 2017b). The World Health Organization (2017a) also estimates that the number of asthma deaths will continue to increase without appropriate treatments or diagnoses. Besides its lethality, asthma can also reduce life quality. Depending on the severity, asthma patients are generally limited from active physical exercise and have significantly higher risk of psychiatric disorders (Bateman et al., 2008; Kuehn, 2008).

Among all ages of patients, children (aged from 3 to 15 years old) and the elderly (over 65 years old) are most severely affected by asthma and have the highest mortality rate (Gong et

al., 2014). The prevalence of asthma is higher in developed versus developing countries (Akinbami et al., 2012). Australia has one of the highest prevalences of asthma in the world (10.8%) and the underlying reasons are still controversial (Australian Bureau of Statistics, 2015; Masoli et al., 2004). In terms of economic burden, the Australian Bureau of Statistics (2015) reported that the Australian government spent $655 million dollars on asthma in 2008-2009, with half spent on prescription pharmaceuticals. Although the number of asthma-related deaths in Australia is lower than other countries (e.g. 455 asthma-related deaths in 2015 reported by National Asthma Council Australia), deaths have been at the same level for many years, suggesting that better treatment strategies are still required (Australian Centre for Asthma Monitoring, 2007; Australian Centre for Asthma Monitoring, 2008).

1.8.2 Pathogenesis of asthma

1.8.2.1 Excessive contraction of the airway

The ASM cell is the main effector cell responsible for the excessive contraction of the airways in asthma, termed AHR. ASM is one of the structural components of airway walls, present from the large trachea to the smallest respiratory bronchioles (reviewed in Gunst, 2012; Ouedraogo & Roux, 2014). In the lung trachea, ASM is only found within the trachealis membrane, which extends along the dorsal side of the trachea. In the main bronchi, ASM is arranged circumferentially and helically within the airway wall, surrounded by rings of cartilage. However, once the main bronchi divide into smaller bronchioles, extending into the lungs, the cartilage diminishes and ASM forms a continuous layer, representing the major structural component of the intralobular airways.

The precise physiological function of ASM remains controversial but its pathophysiological role in asthma has been well established (Bara et al., 2010; Ouedraogo & Roux, 2014). One of the most accepted hypotheses for the physiological function of ASM is that it regulates the distribution of lung ventilation (Gunst, 2012). Since ASM is the major structural component in the intralobular airway, its contraction in this part of the lung could largely affect the distensibility of the lungs via modulating lung compliance (Oti, 1983).

The contractile status of ASM is under the control of both neurotransmitters and mediators released from resident and inflammatory cells in the airway (Ouedraogo & Roux, 2014). Unlike skeletal, cardiac or other types of muscle, the source of Ca^{2+} required for initiating smooth

muscle contraction is mainly released from intracellular stores (Amrani & Panettieri, 2003). For example, histamine and acetylcholine induce ASM contraction via this pathway (Ouedraogo & Roux, 2014). The pro-contractile response of ASM is primarily regulated by GPCRs that are G_q and $G_{12/13}$-coupled. G_q promotes activation of phospholipase C-β (PLCβ), which hydrolyses phosphatidylinositol 4,5-biphosphate (PIP_2) leading to production of IP_3 and DAG (Hall, 2000). IP_3 binds to its receptor, IP_3R, on the sarcoplasmic reticulum (SR) and results in release of Ca^{2+} into the cytosol (Berridge, 1993). Intracellular Ca^{2+} binds to calmodulin and forms a Ca^{2+}-calmodulin complex, which promotes Ca^{2+}-calmodulin complex-dependent myosin light chain kinase (MLCK). MLCK phosphorylates regulatory MLCs forming phosphorylated-MLC (pMLC), which is responsible for regulating actin-myosin cross-bridge cycling and ASM contraction. To terminate ASM contraction, pMLC is usually dephosphorylated by myosin light chain phosphatase (MLCP). Both MLCK and MLCP activity are regulated by protein kinase A and protein kinase C (which is activated by DAG) (Morgan et al., 2014; Mukherjee et al., 2013). PKA phosphorylates IP_3 receptors and MLCK to reduce their affinity for IP_3 and calmodulin, respectively (Morgan et al., 2014). Both mechanisms limit the release of $Ca^{2+}{}_i$ and thereby inhibit ASM contraction.

Compared to G_q-coupled receptors, G_s-coupled receptors promote relaxation of ASM. The β_2-adrenoceptor (β_2-AR) is the predominant G_s-coupled receptor on ASM (Billington & Penn, 2003), although other G_s-coupled receptors such as adenosine 2B (A_2B), also contribute to ASM relaxation (Brown et al., 2008). G_s activates adenylyl cyclase (AC), which catalyses the formation of cyclic AMP (cAMP) from cytoplasmic ATP. The production of cAMP leads to the activation of PKA, which reduces ASM contraction via the previously described mechanisms.

Under normal physiological conditions, ASM contraction is well-regulated, which allows continuous and sufficient gas exchange in the lung. However, in asthma, pro-contractile G_q-coupled receptor agonists, such as histamine, leukotrienes, prostaglandins and polyamines, are upregulated and released, in some instances by exaggerated infiltration of inflammatory cells (the details will be discussed in 2.4.3.) (Deshpande & Penn, 2006). Overall, this leads to increased constriction of ASM leading to potential airway closure and obstruction in asthma.

1.8.2.2 Airway inflammation

Airway inflammation in asthma results from an exaggerated immune response to certain external stimuli, such as toxins and microbes (Ganesan et al., 2013; Heijink et al., 2014). In the asthmatic airway, tyrosine kinase-linked receptors or GPCRs on epithelial and ASM cells are hyperreactive and this leads to release of excessive proinflammatory cytokines and chemokines. Epithelial cells release proinflammatory cytokines (e.g. thymic stromal lymphopoietin (TSLP), IL-25 and IL-33) and chemokines (Siracusa et al., 2012) whereas ASM cells release cytokines (e.g. IL-1, IL-5, IL-6, IL-8) and chemokines (e.g. eotaxin and RANTES) to recruit immune cells to the airway (Amrani & Panettieri, 2002; Freyer et al., 2001; Lazaar & Panettieri, 2001). In allergic T-helper (Th) asthma, eosinophils are the predominant immune cells recruited. Th2 cytokines, IL-4 and IL-13, induce the endothelial cells to express vascular cell adhesion molecule (VCAM)-1 (Bochner et al., 1995; Schleimer et al., 1992), which promotes eosinophil adherence to endothelial cells (Nagata et al., 1995; Nagata et al., 1999). Eosinophils then cross the endothelium via chemoattractants such as normal T cell expressed and secreted (RANTES), eotaxin, monocyte chemotactic protein (MCP)-3 and MCP-4 (Nagata et al., 2001). Eosinophils are activated and degranulated by granulocyte-macrophage colony-stimulating factor (GM-CSF) (Nagata et al., 1998), releasing a variety of inflammatory mediators, including cysteinyl leukotrienes, reactive oxygen species, ECP, eosinophil peroxidase (EPX), major basic proteins (MBP) and cytokines (Gleich, 2000; Kita, 2013; Weller, 2000) (the details will be discussed in section 2). Neutrophils, recruited by IL-8, are typically increased in more severe asthma and acute asthma exacerbations (Fahy et al., 1995; Kikuchi et al., 2006; Nakagome et al., 2012; Shannon et al., 2007). Neutrophils contribute to asthma severity via neutrophil-mediated oxidative stress or neutrophil protease-mediated goblet cell degranulation (Innes et al., 2009). Basophils secrete circulating granulocytes and contain cytoplasmic granules with histamine, which is a bronchoconstrictor agent (Nadif et al., 2013; Schwartz & Voehringer, 2011). A wide variety of inflammatory cells are recruited in different types of asthma.

1.8.2.3 Airway remodelling

Airway remodelling refers to the structural changes in the airway, including epithelial proliferation, hyperplasia and hypertrophy of ASM and deposition of extracellular matrix (ECM) (Martin & Verma, 2012). During an asthma attack, ASM function is dysregulated and

overreacts to contractile agonists such as acetylcholine (ACh) and spermine, leading to increased airway contraction (airway hyperresponsiveness; AHR) and resultant breathlessness. In asthma, airway remodeling and inflammation are closely correlated and affect each other by positive feedback, but airway remodeling can occur in the absence of airway inflammation (Tang et al., 2006). Proinflammatory mediators, such as epidermal growth factor receptor ligands, IL-9 and IL-13, also promote epithelial proliferation and goblet differentiation whereas the structural cells of the airways induce airway inflammatory responses (Cohn et al., 2004).

In both human asthma and animal models of allergic airways disease, epithelial cells differentiate into mucus secreting goblet cells and both the number and size of mucus glands increase (Li & Wilson, 1997). The presence of excessive mucus, protein, and inflammatory cells contributes to obstruction of the airways and the disruption of surfactant functions. Furthermore, resident fibroblasts can differentiate to myofibroblasts and contribute to subepithelial collagen deposition, which results in thickening of the airway wall (Jeffery, 2001). This increase in airway wall thickness exacerbates airway narrowing (James et al., 1989). Collagen deposition also has important but controversial effects on airway responsiveness. During tidal breathing (air into or out of the lungs during quiet breathing), the parenchyma exerts forces on the airway wall, which results in bronchodilation but this effect is largely abolished by the increased thickness of the asthmatic airway wall (Gunst & Stropp, 1988). On the other hand, collagen deposition reduces buckling of the epithelium due to bronchoconstriction to a greater extent than under normal physiological conditions (Lambert et al., 1994). Therefore, the overall effects of collagen on AHR are unclear.

1.8.3 Polycations in asthma

Polyamines are aliphatic cations found ubiquitously in the body. Polyamines are implicated in a wide variety of cellular functions, such as cell growth and differentiation (Agostinelli et al., 2010). Polyamines can be ingested in food or synthesized by human cells (Soda, 2010). Polyamine synthesis and metabolism are tightly regulated (**Figure 1.7**). Concentrations of polyamines in organs are relatively higher than in the peripheral circulation (Pegg, 2016). The levels of polyamines are low in non-proliferating cells, but their levels increase once mitogenic stimulation begins (Pegg, 2016). Although full details of their actions remain to be investigated, polyamines have been shown in multiple studies to contribute to inflammation and cell

proliferation (Jain, 2018), and polyamines may play a role in exacerbating asthma (Yarova et al., 2015).

The effects of polyamines on inflammation have been well established. Polyamines prolong the eosinophil life span by inhibiting apoptosis and they regulate eosinophil migration by enhancing the cell-surface levels of the adhesion molecule integrin CD11b (Ilmarinen et al., 2015; Ilmarinen et al., 2012). Furthermore, polyamines induce the release of histamine from mast cells, which can exacerbate inflammation and potentially cause acute bronchoconstriction in asthma (García-Faroldi et al., 2010). In terms of neutrophils and macrophages, polyamines induce the respiratory burst (exogenous superoxide) generated by neutrophils or increase macrophage differentiation by inducing IL-4 and polarizing monocytes into M_2 macrophage subtypes, both exacerbating asthma severity (Guarnieri et al., 1987; Van den Bossche et al., 2012). The depletion of polyamines via induction of polyamine catabolism reduced the gene expression level of M_2 macrophages, which are the main subtypes in asthma (Van den Bossche et al., 2012). All of these inflammatory cells play an important role in airway inflammation as described in section 1.8.2.2.

Previous studies have demonstrated that arginase activity is increased in murine asthma models, and results in increased production of polyamines and consequent AHR (Kurosawa et al., 1992; North et al., 2013). The polyamine spermine increases ACh-mediated contraction of ASM cells *ex vivo* (Grasemann et al., 2012). A possible explanation for this potentiation is that the level of the endogenous bronchodilator nitric oxide (NO) is reduced because L-arginine is a common precursor for the synthesis of both polyamines and NO. Alternatively, polyamines may directly activate the CaSR expressed on ASM cells, inducing the release of $Ca^{2+}{}_i$ and amplifying ACh-mediated contraction (discussed in 1.8.2.1) (Yarova et al., 2015).

As discussed in section 1.8.2.2., the release of polycations by eosinophils may increase asthma severity. MBP disrupts the integrity of lipid bilayers via cytotoxic effects whereas EPX is a peroxidase that produces reactive oxidants and radical species (Blanchard & Rothenberg, 2009). However, recently, Yarova et al. (2015) provided evidence that polycations mediate ASM contraction via the CaSR. Polyamines induce $Ca^{2+}{}_i$ mobilisation, p38 MARK phosphorylation and cAMP breakdown in ASM cells via the CaSR (Yarova et al., 2015). All of these effects were abolished once CaSR on the ASM was knocked out, suggesting that the CaSR plays an important role in mediating the effect of polycations in asthma.

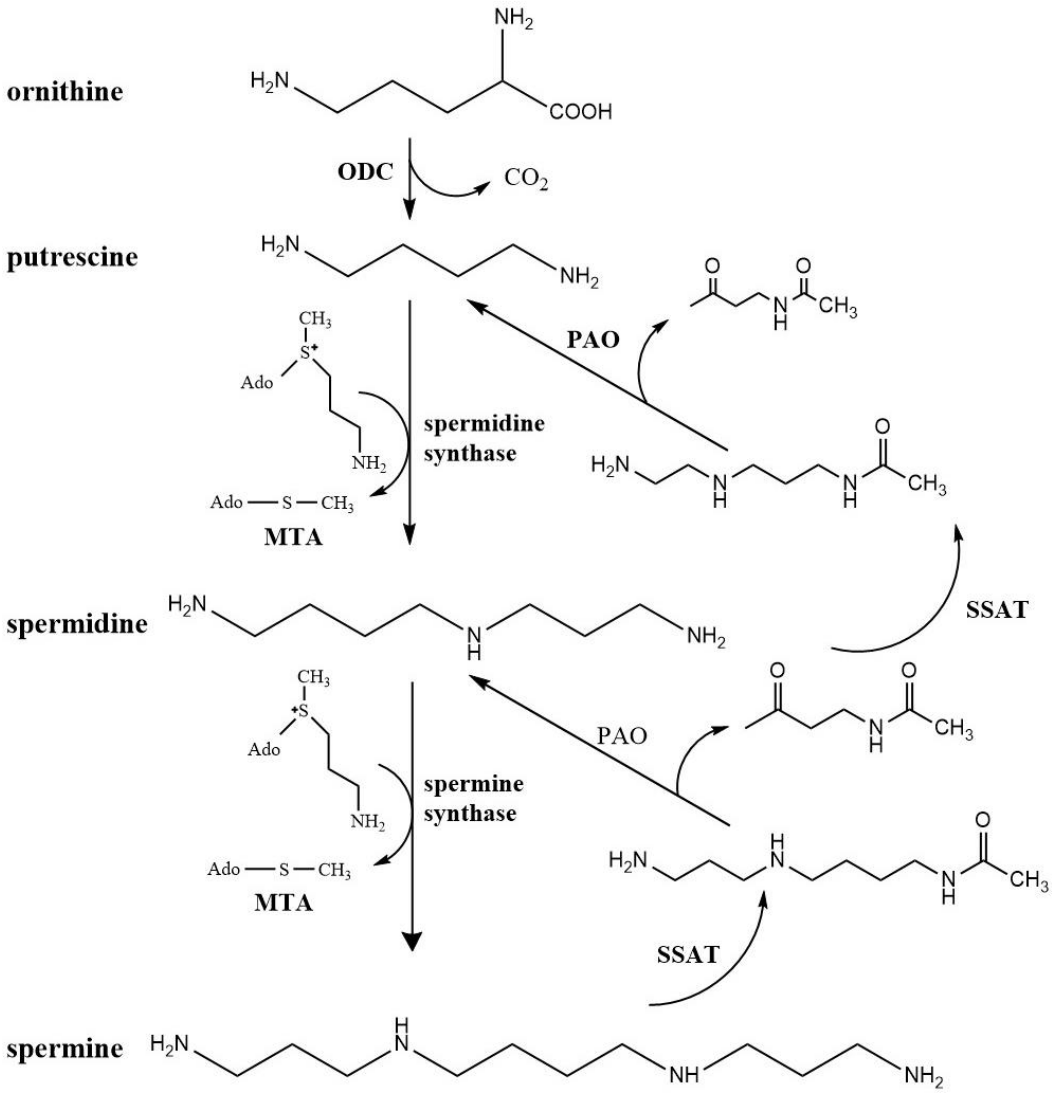

Figure 1.7. The polyamine metabolic pathway. The first precursor for polyamine synthesis is arginine, which is converted into L-ornithine by arginase (Raina A, 1984). Putrescine is then synthesised from L-ornithine by ornithine decarboxylase (ODC) and further converted into spermidine and spermine by two distinct aminopropyl transferase synthases (Agostinelli et al., 2010; Iacomino et al., 2012; Maarsingh et al., 2008). MTA, 5'-methylthioadenosine; ODC, ornithine decarboxylase; SSAT, spermidine/spermine-N1 acetyl-transferase; PAO, acetylpolyamine oxidase.

1.8.4 Current treatments for asthma and their limitations

Mainstream treatments for asthma include inhaled anti-inflammatory corticosteroids (ICSs) and bronchodilator β_2-AR agonists, either alone or as combination therapy, and leukotriene receptor antagonists (Fergeson et al., 2017). ICSs and β_2-AR agonists have been used to treat asthma since the 1950s and they significantly reduce asthmatic symptoms and mortality rates (Tattersfield, 1997). On the basis of potential dual bronchoprotective and anti-inflammatory effects, leukotriene antagonists were predicted to have significant benefits in asthma, but

clinical outcomes have been disappointing, and ICSs and β_2-AR agonists remain the preferred treatments (Ducharme et al., 2006; Nelson et al., 2000). Countless efforts have been made to discover new treatments for asthma over the past two decades. The introduction of omalizumab targeting IgE in allergic asthma, or mepolizumab and dupilimab targeting IL-5 or IL-4/IL-13 has led to improved outcomes in selected patients who are not well-controlled despite optimised doses of standard therapy.

Despite this progress, there remains an unmet need for more effective asthma treatments. Notably, the frequent use of β_2-AR agonists is associated with receptor desensitization and loss of efficacy, while steroid resistance can result in uncontrolled inflammation. No current drug effectively prevents AHR or reverses established airway remodelling. Targeting of GPCRs holds the most potential for drug discovery to overcome these limitations, Identification of a therapy that targets more than one pathophysiological aspect of asthma would be potentially more powerful than any current treatments.

1.9.1 ICSs

ICSs have been used as the first line therapy for patients with persistent asthma for decades (reviewed in Alangari, 2014; Barnes, 2006b). They can be used for mild and moderate levels of asthma, and in both chronic progression and acute exacerbation (Dahl et al., 1993; Juniper et al., 1990a; Juniper et al., 1990b). Pulmonary function, relapse rate and rate of hospital admission or length of stay are improved with ICSs (Rowe et al., 1999). However, ICSs have no effect on peak expiratory flow rate (maximum speed of expiration, used to define a person's ability to breath out air), even at the highest dosage (Brenner et al., 2000).

ICSs reduce the frequency and severity of asthma attacks via their anti-inflammatory effects. ICSs bind to cytoplasmic glucocorticoid receptors (GRs), thus stimulating GR translocation to the nucleus, where they homodimerise (Barnes, 2006a). The GR homodimer consequently binds to a glucocorticoid response element (GRE) in the promoter region of steroid responsive genes, thereby enhancing transcription of anti-inflammatory genes, including those that encode cytokines and chemokines (e.g. IL-10, IL-12 and IL-1), mitogen-activated protein kinase phosphatase-1 (an inhibitor of the MAPK inflammatory pathway), and β_2-ARs (which will be further discussed in section 1.9.2.) (Barnes, 2006a; Clark et al., 2008; Hart et al., 2000). On the other hand, GRs also decrease inflammatory cytokines by suppressing gene transcription of chemotactic mediators and adhesion molecules mediated by transcription factors such as

nuclear factor-κB (NF-κB) and activator protein-1 and inhibiting the survival of inflammatory cells in the airways, especially eosinophils, T-lymphocytes and mast cells (Barnes, 2006b). Besides its interaction with GR element (GRE), GRs can also regulate gene transcription by working with CREB-binding protein and thus enhancing recruitment of histone deacetylase (HADAC2) (Barnes, 2006a). HADAC2 induced by administration of ICSs reverses histone acetylation, therefore reducing airway inflammation in asthma (Barnes, 2006a).

Some asthmatic patients do not benefit from corticosteroid treatments because they are intolerant or resistant. Ten percent of asthmatic patients need maximal dosages of ICSs to control their asthma symptoms and symptoms in ~1% of asthmatic patients cannot be treated by ICSs at all (Barnes et al., 1995). Resistance to ICSs may result from ICS-induced reduced expression or activity of GRs (Barnes, 2004a) although many other mechanisms have been implicated (Wadhwa et al., 2019).

1.9.2 β_2-AR agonist treatment

β_2-AR agonists are effective bronchodilators, opposing ASM contraction irrespective of the contractile stimulus (Kume et al., 1994). β_2-AR agonists couple to G_s and adenylate cyclase, leading to increased cAMP to oppose calcium signalling resulting in airway relaxation. Both short-acting β_2-agonists (SABAs) and long-acting β_2-agonists (LABAs) are used in asthma, with the latter only used in combination with ICS as preventer medication. β_2-agonists have several limitations, as excessive use can result in tolerance due to β_2-AR desensitisation, which in turn predisposes to increased risk of life-threatening attacks (Bush, 2019). Desensitisation of β_2-ARs is mediated by several mechanisms: phosphorylation and uncoupling from G proteins, internalisation and down-regulation (Shore & Moore, 2003). PKA directly phosphorylates β_2-AR itself whereas G protein receptor kinases (GRK) bind to β_2-AR and the GRK-phosphorylated receptors then bind to arrestins, ultimately leading to uncoupling of G proteins from β_2-AR and termination of receptor signalling (Bouvier et al., 1989; Krupnick & Benovic, 1998). Internalisation of β_2-AR is also induced by arrestins, which act as scaffolding proteins, connecting β_2-AR with clathrin. The β_2-AR is subsequently endocytosed into endosomes (Goodman et al., 1997). Although β_2-AR agonists are the most commonly used treatment for excessive bronchoconstriction in asthma, the potential for receptor desensitisation identifies a need for alternative or adjunct dilator therapies.

1.10 Novel therapeutics for asthma

Previous studies have demonstrated that CaSR NAMs have various therapeutic effects in different disease models, including models of acute lung injury induced by lipopolysaccharide, allergic airways disease induced by ovalbumin or mixed allergen challenge (Lee et al., 2017; Yarova et al., 2015). CaSR NAM NPS89636 treatment reduced airway inflammatory cells and pro-inflammatory cytokines in the airway (Lee et al., 2017; Yarova et al., 2015). NPS2143 inhibited ASM thickening and airway fibrosis but could not reverse airway inflammation, following mixed allergen challenge (Lee et al., 2017; Thompson et al., 2016). Furthermore, NPSP-795 had better ant-inflammatory efficacy than the steroid fluticasone propionate when daily treatment commenced after ovalbumin sensitisation and challenge (Yarova et al., 2021). In terms of bronchodilator effects, NPS89636 prevented *in vitro* contraction to spermine in small mouse airways (Yarova et al., 2015) whereas NPSP-795 and ronacaleret, reversed contraction of mouse trachea to acetylcholine (Yarova et al., 2021; Yarova et al., 2015). These results suggest it is important to screen different CaSR NAM chemotypes against different asthma aspects. The multiple effects of NAMs may arise from inhibition of CaSR coupling to multiple heterotrimeric G proteins, including $G_{q/11}$, $G_{12/13}$ and $G_{i/o}$, which are all involved in pathophysiological pathways in asthma (Conigrave & Ward, 2013).

1.11 Aims

Despite growing evidence for the CaSR being a putative therapeutic target in asthma, there is still a lack of understanding of: i) the signalling pathways relevant to asthma that are activated by polyamines via the CaSR; ii) the efficacy profile of biased and probe-dependent NAMs to reverse airway contraction, and; iii) the structural basis for polyamine binding to and activation of the CaSR.

In this project, we sought to validate the CaSR as a therapeutic target for treating asthma by determining whether CaSR NAMs can reverse or prevent mouse airway contraction (**Aim 1**) or increased CaSR expression and signalling activated by polyamines in primary healthy and asthmatic ASM cells (**Aim 2**). Finally, we sought to determine the binding sites and efficacy residues of polycations in the CaSR (**Aim 3**).

Chapter 2

Characterising CaSR NAM-mediated bronchodilation in mouse airways

2.1 Introduction

Asthma is a heterogeneous chronic airway disease, characterised by airway inflammation and airway remodelling leading to AHR (Holgate, 2012). SABAs, such as salbutamol, relieve symptoms of breathlessness, while anti-inflammatory ICS alone or in combination with LABAs reduce inflammation and the frequency and severity of asthma attacks (Fergeson et al., 2017). With increasing disease severity, the frequent use of higher doses of salbutamol can lead to potential receptor desensitization and loss of dilator efficacy. Novel therapies that overcome these limitations are required to improve symptom control and reduce mortality when current dilator treatments are ineffective (Cazzola et al., 2012).

The ASM cell is the main effector cell responsible for AHR in asthma. In asthma, chronic airway inflammation promotes ASM cell sensitivity to elevations in intracellular calcium (Ca^{2+}_i), as well as airway remodelling that increases the bulk of ASM. These changes enhance contractile responses to non-specific stimuli (reviewed in Lam et al., 2019). The contractile status of ASM is under the control of neurotransmitters and inflammatory mediators acting via GPCRs (Billington & Penn, 2003). $G_{q/11}$-coupled GPCRs, including the M_3 muscarinic acetylcholine receptor (mAChR), stimulate IP_3 production and consequent release of Ca^{2+}_i to promote ASM contraction. In contrast, G_s-coupled GPCRs, such as the β_2 AR, increase signalling via cAMP and PKA pathways to oppose Ca^{2+}-mediated contraction and elicit airway relaxation.

The CaSR is expressed in ASM (Roesler et al., 2019; Yarova et al., 2015) and has a well-established role in Ca^{2+}_o homeostasis (Brown et al., 1993). However, activation of the CaSR increases Ca^{2+}_i mobilisation and can therefore also drive ASM contraction (Yarova et al., 2015). Of note, CaSR expression is upregulated in ASM from human asthmatic subjects and from mice sensitised with mixed allergens (ovalbumin, Aspergillus sp, Alternaria sp and HDM) (Yarova et al., 2015). Furthermore, endogenous CaSR agonists, such as the polyamine spermine, are increased in blood and sputum from asthmatics (Kurosawa et al., 1992) and induce contraction of isolated airways (Yarova et al., 2015), suggesting that the CaSR may be a novel target for asthma treatment.

Synthetic small molecule CaSR NAMs have been discovered. These include amino alcohol NAMs such as NPS2143, NPS89636 and ronacaleret (Gowen et al., 2000a; Yang et al., 2009), quinazolinone NAMs such as ATF936, as well as structurally distinct NAMs such as BMS compound 1 and Pfizer compound 1 (**Figure 1.4**). Mutagenesis studies have shown that CaSR

NAMs bind to sites that are topographically distinct from the endogenous CaSR agonist, Ca^{2+}_o, and inhibit Ca^{2+}_o-mediated Ca^{2+}_i mobilisation in HEK293 cells (Josephs et al., 2019). However, different NAMs display distinct pharmacological profiles at the CaSR in terms of their ability to inhibit Ca^{2+}_o-mediated signalling. These differences are due to their distinct affinities and cooperativities (magnitude and direction of allosteric effects) at the receptor. Little is known about how CaSR NAMs inhibit polyamine activity at the CaSR.

The effects of *in vivo* treatment with CaSR NAMs has previously been assessed in a model of acute lung injury induced by lipopolysaccharide (Lee et al., 2017), models of allergic airways disease induced by ovalbumin or mixed allergen challenge (Lee et al., 2017; Yarova et al., 2015). Preventative treatment with NPS89636 reduced inflammatory cell influx and levels of pro-inflammatory cytokines in the lung (Lee et al., 2017; Yarova et al., 2015) while NPS2143 also inhibited allergen-induced ASM thickening and airway fibrosis (Lee et al., 2017; Thompson et al., 2016). Chronic treatment with either NAM prevented the development of AHR to MCh following allergen challenge (Lee et al., 2017; Yarova et al., 2015). Although NPS2143 failed to reverse inflammation when administered after mixed allergen challenge (Lee et al., 2017; Thompson et al., 2016), a recent study showed that NPSP-795, a CaSR NAM previously tested in clinical trials for osteoporosis, had greater ant-inflammatory efficacy than the steroid fluticasone propionate when daily treatment commenced after ovalbumin sensitisation and challenge (Yarova et al., 2021).

Of note, CaSR NAMs have also shown efficacy as acute bronchodilators. NPS89636 prevented *in vitro* contraction to spermine in mouse intrapulmonary airways in PCLS (Yarova et al., 2015), while a series of CaSR NAMs, including NPSP-795 and ronacaleret, reversed contraction of mouse trachea to acetylcholine (Yarova et al., 2021). Further investigation of the mechanisms whereby different NAMs inhibit the activity of polyamines such as spermine at the CaSR is required. It is also important to establish whether all different CaSR NAM chemotypes reverse ASM contraction, and to compare their acute effects with salbutamol to support their therapeutic potential for the treatment of asthma.

In this study, we have assessed the ability of different CaSR NAMs to inhibit polyamine-mediated cellular Ca^{2+}_i mobilisation and IP_1 accumulation in recombinant HEK293 cells. Mouse PCLS were then used to compare the relative dilator efficacy of selected NAMs to β_2 AR agonists. We demonstrate differential bronchodilator effects of CaSR NAMs, maintained

under conditions of β_2 AR desensitization, supporting their use as novel alternative or adjunct agents to oppose airway contraction.

2.2 Methods

2.2.1 Materials

The following materials were synthesized: Pfizer compound 1, ATF936 and ronacaleret (Institut de Recherches Servier, France) as described previously (Li et al., 2013; Widler et al., 2010); BMS compound 1 (SYNthesis Med Chem Research PTY, Parkville, Australia) as described (Yang et al., 2009). The following materials were purchased: Flp-In™ TREX™ Human Embryonic Kidney (HEK) 293 cells and ultra-pure low melting point agarose (Invitrogen, Carlsbad, USA); Fluo-4-AM (Molecular Devices, San Jose, USA); Fluo-8-AM (acetoxymethyl ester) (Abcam, Cambridge, USA); Methacholine (MCh), ionomycin, salbutamol (Sigma Aldrich, St Louis, USA), USA); Hank's balanced salt solution (HBSS; Thermo Fisher, USA); Dulbecco's Modified Eagle's Medium (high glucose), poly-D-lysine (PDL) and blasticidin HCl (Invitrogen, Carlsbad, USA), hygromycin B (Roche, Mannheim, Germany), tetracycline (dissolved in 100% ethanol, stored at 3 mg/mL at -20°C); 1M N-2-hydroxyethylpiperazine-N-2-ethane sulfonic acid (HEPES) (Gibco Life Technologies, AU).

2.2.2 Generation and Maintenance of FlpIn HEK TRex Cells stably expressing the CaSR

The generation of DNA and FlpIn HEK TREx cells stably expressing c-myc-tagged WT CaSR in pcDNA5/frt/TO has been described previously (Davey et al., 2012; Leach et al., 2016). FlpIn HEK TREx CaSR cells were maintained in DMEM containing 5% FBS, 200 μg/mL hygromycin B and 5 μg/mL blasticidin S HCl.

2.2.3 Ca^{2+}_i mobilisation assay

FlpIn HEK293 TRex-expressing CaSR cells were seeded in clear 96-well plates coated with PDL (50 μg mL^{-1}) at 80,000 cells/well and incubated overnight in the presence of 5 or 100 ng mL^{-1} tetracycline to induce low or high CaSR expression. On the following day, cells were washed with assay buffer (150 mM NaCl, 2.6 mM KCl, 1.18 mM $MgCl_2$, 10 mM D-Glucose,

10 mM HEPES, 1.2 mM $CaCl_2$, 0.5 % BSA and 4 mM probenecid at pH 7.4) and loaded with Fluo-8 AM (1 μM in assay buffer) for 1 hr at 37 ºC. CaSR NAMs were added to cells and pre-incubated for 20 min prior to the addition of spermine using a Flexstation 1 or 3 (Molecular Devices; Sunnyvale, California). Alternatively, for NAM interaction experiments, cells were washed, loaded with Fluo-8 AM and pre-incubated with CaSR NAMs as described before but using assay buffer with 1.2mM $CaCl_2$. The effects of NAMs on release of $Ca^{2+}{}_i$ in response to spermine were measured at 37°C using a Flexstation. Fluorescence was detected for 60 sec at 490 nm excitation and 520 nm emission and the peak $Ca^{2+}{}_i$ mobilisation response (approximately 12 sec after agonist addition) was used for the subsequent determination of the agonist response. Relative peak fluorescence units were normalised to the fluorescence stimulated by 1 μM ionomycin to account for differences in cell number and loading efficiency.

2.2.4 IP_1 accumulation assay

Following overnight induction of CaSR receptor expression with 100 ng/mL tetracycline, cells were harvested and re-suspended in assay buffer (150 mM NaCl, 2.6 mM KCl, 1.18 mM $MgCl_2$, 10 mM D-glucose, 10 mM HEPES, 0.1 mM $CaCl_2$, 50 mM LiCl, pH 7.4) at 1.43 $x10^6$ cells per mL. Spermine was added with either vehicle (assay buffer) or NAM along with $1x10^4$ cells in a total volume of 14 μL to each well of 384-well white proxiplates (PerkinElmer). Plates were then centrifuged for 1 min at 350 *x g* and incubated at 37 ºC for 45 min. The IP- One Tb™ assay kit (CisBio Bioassays, Codolet, France) was used to detect myo-IP1, based on FRET between d2-conjugated IP1 and Lumi4™-Tb cryptate conjugated anti-IP1 antibody. These reagents were diluted 1:30 with lysis buffer and 3 μL of each was added to wells following agonist stimulation. Lysates were incubated for 1 hr and FRET was detected using an Envision plate reader (PerkinElmer) where emission of Lumi4-Tb cryptate was detected at 620 nm and emission of d2-conjugated IP_1 at 665 nm. Results were calculated from the 665 nm/620 nm ratio.

2.2.5 Animals

All animal experimental procedures were approved by Monash University Animal Ethics Research Committee (approval MARP-2, #7135 and #15151) and complied with the Guidelines of the National Health and Medical Research Council (NHMRC) of Australia on

Animal Experimentation. Male C57/BL6 mice (6-8 weeks old) were obtained from the Animal Research Platform, Monash University. Mice were caged at 22ºC and given free access to food and water.

2.2.6 PCLS

PCLS were prepared as previously described (Bourke et al., 2014). After euthanasia, mouse lungs were inflated with warm 2% w/v ultra-pure low melting point agarose in HBSS supplemented with 40 mM HEPES (sHBSS) via a tracheal cannula, followed by a small bolus of air to push the agarose into alveolar spaces. The agarose was solidified at 4ºC for 20 min, before a single lung lobe was dissected and mounted in a vibratome (VT 1000S, Leica Microsystems) in cold sHBSS to prepare serially sectioned into 150-220 μm thick PCLS. Slices were cultured in 24 well plates for up to 48 hr in high-glucose DMEM supplemented with 1% penicillin-streptomycin solution, at 37ºC and 5% CO_2. Slices were cultured for 16-24 hr before assessment of airway reactivity, with some slices also treated with CaSR NAMs (10 μM) or salbutamol (100 μM) to assess potential bronchoprotection and/or desensitisation (Donovan et al., 2014).

2.2.7 Acquisition of small airway images.

Phase contrast microscopy was conducted using an inverted microscope (Eclipse Ti-U; Nikon). Individual slices were placed in a custom-made perfusion chamber between 2 cover glasses (approximately 100 μL volume) and covered in fine wire mesh (Small Parts Inc.) with a small hole cut over the airway under examination. A single airway (150–400 μm diameter) was selected for experimentation based on the presence of an intact layer of epithelial cells displaying ciliary activity. PCLS were perfused with sHBSS or drugs (spermine, MCh, salbutamol, NPS2143, Pfizer compound 1 or BMS compound 1), delivered using a gravity fed system, for assessment of airway responses.

Some slices were treated with 20 mM caffeine and 50 μM ryanodine as a model to examine the relative contributions of inhibition of Ca^{2+} oscillations and Ca^{2+} sensitivity to dilator responses (Bai & Sanderson, 2006; Bourke et al., 2014). Treatment with caffeine and ryanodine has been shown to empty internal Ca^{2+} stores, clamp Ca^{2+}_i at a sustained high level and abolish subsequent contractile agonist-induced Ca^{2+} oscillations. Under these conditions, subsequent

airway contraction is due to increases in Ca^{2+} sensitivity alone, mediated by activation of RhoA/Rho kinase and/or PKC/CPI-17 pathways to decrease the activity of myosin light chain phosphatase and oppose relaxation (Bai & Sanderson, 2006; Bourke et al., 2014).

2.2.8 Image analysis.

Digital images were recorded in time lapse (0.5 Hz) using image acquisition software (Video Savant; IO industries, Inc.), converted to TIFF files and analysed using PC software NIH/Scion (Scion Corporation). An appropriate grey scale threshold was chosen to distinguish between the airway lumen and surrounding tissue, with lumen area in each image calculated by pixel summation. Responses were averaged over the last minute or measured as the maximal relaxation/contraction during each perfusion condition.

For PCLS experiments, airway contraction to spermine or MCh was measured as the decrease in lumen area, normalised as a percentage of the initial area. Airway relaxation to salbutamol or NAMs was expressed as a percentage of the MCh-induced pre-contraction.

2.2.9 Data and Statistical analysis

All non-linear regression analysis was performed using GraphPad Prism® 8.0.2 (GraphPad Software, San Diego, Cam USA). All parameters were derived as logarithms.

The following four-parameter equation was fitted to concentration-response data for spermine in mouse PCLS, and MCh and salbutamol in PCLS:

$$\text{Response} = \text{Bottom} + \frac{(\text{Top} - \text{Bottom}) \text{ X } (A^{nH})}{A^{nH} + EC_{50}^{nH}}$$

Eq. 1

Where Bottom and Top represent the bottom and top asymptotes of the curve, respectively; A denotes the agonist concentration; nH (hill slope) describes the steepness of the curve, constrained to unity for PCLS; and EC_{50} is the concentration of agonist that gives the mid-point response between Bottom and Top.

The following operational model of agonism was fitted to data describing spermine at the CaSR in HEK293 cells:

$$\text{Response}=\frac{Em\ \tau A^{nT}[A]^{nBnT}}{\tau A^{nT}[A]^{nBnT}+([A]^{nB}+KA^{nB})^{nT}}$$

Eq. 2

Where [A] is agonist concentration, K_A is the agonist equilibrium dissociation constant; τ_A is the agonist efficacy; E_m is the maximal system response and was determined from the response to $Ca^{2+}{}_o$ at the CaSR; *nT* is the logistic transducer function linking agonist concentration to response and was constrained to unity; *nB* is the slope of agonist binding linking agonist concentration to occupancy.

The following operational model of allosterism was fitted to data describing the interaction between spermine and the NAMs in HEK293 cells:

$$\text{Response}=\frac{E_m\ (\tau_A[A]^{nB}(K_B+\alpha\beta\ [B]+\ \tau_B\ [B][K_A]^{nB})^{nT}}{([A]^{nB}K_B+\ K_A{}^{nB}K_B+\ K_A^{nB}\ [B]+\ \alpha\beta\ [B]+\tau_B[B][K_A]^{nB})^{nT}}$$

Eq. 3

Where K_A, τ_A, [A], *nB*, *nT* and E_m are the same as in Eq 2; K_B is the affinity of the NAM; τ_B is the operational efficacy of the NAM; α and β are the allosteric effects on orthosteric agonist affinity and efficacy, respectively; and [B] is the NAM concentration

The following biphasic equation was fitted to concentration-response curves for NAM-mediated bronchorelaxation in PCLS:

$$\text{Response}=Bottom+\frac{(Top-Bottom)\times Frac}{10^{(EC_{50}\_1-A)\times nH1}}+\frac{(Top-Bottom)\times(1-Frac)}{10^{(EC_{50}\_2-A)\times nH2}}$$

Eq 4.

Where Top and bottom are the same as in the Equation 1, nH1 and nH2 are unitless slope factors and were constrained to unity in this study, Frac is the fraction of the concentration-response curve derived from the more potent phase, EC_{50}_1 and EC_{50}_2 are the agonist

concentrations that give half-maximal responses in the first and second phases of the concentration-response curves.

2.3 Results

2.3.1 Spermine causes transient contraction and potentiates MCh-induced contraction in mouse airways

As previously reported, the CaSR agonist spermine induces airway contraction (Yarova et al., 2015). In the present study, in mouse PCLS, spermine elicited contraction in a concentration-dependent manner, but each response was transient, lasting less than one minute (**Figure 2.1A, B**). All airways responded to 300 μM spermine, with variability in lower threshold concentrations evident between preparations (**Figure 2.1C**). From individually fitted curves (dotted lines), the estimated maximal reduction in airway area to spermine was 54±9%, with a pEC_{50} of 5.1±0.6 **(Table 2.1**). By comparison, MCh caused similar maximal reduction in airway area (**Figure 2.1D, Table 2.1**) but was 20-fold more potent than spermine (*P<0.05; unpaired t test; **Table 2.1**).

We next investigated whether spermine potentiated MCh-induced contraction consistent with a previous report (Yarova et al., 2015). Contraction to MCh was increased in the presence of 300 μM spermine (EC_{80}) (**Figure 2.1A**), with spermine causing a leftward shift in the MCh concentration-response curve (**Figure 2.1D**). There was a trend towards an increased maximal MCh response, and a significant 7.9-fold increase in MCh potency in the presence of spermine ($^{\#}$P<0.01; paired t test; **Table 2.1).**

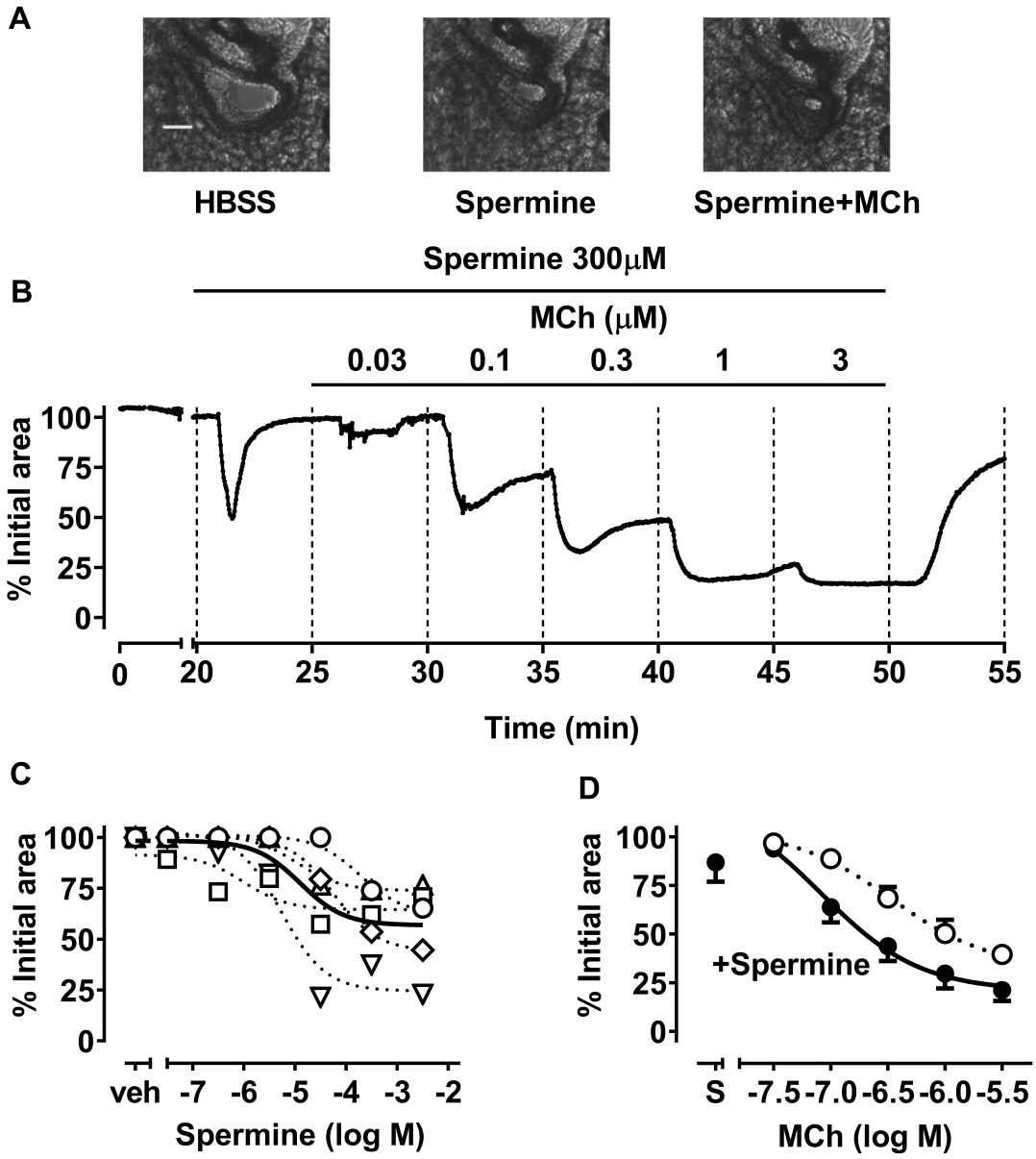

Figure 2.1. The CaSR agonist spermine causes transient airway contraction and increases contraction to MCh in mouse PCLS. PCLS were prepared from naïve male C57/Bl6J mice for concentration-response curves to spermine and MCh. **A.** Representative images of airways during perfusion with HBSS buffer, 300 μM spermine or 3 μM MCh with spermine. Scale bar = 50 μm. **B.** Representative trace showing transient contraction to 300 μM spermine followed by stable contractions to increasing concentrations of MCh, perfused at 5-minute intervals in the presence of spermine. **C.** Contraction to spermine, shown as grouped data (solid line) and individual fitted curves (n=5). **D.** Contraction to MCh alone (n=4) and MCh in the presence of 300 μM spermine (n=4). S = spermine alone before MCh. Data are expressed as % initial airway lumen area, mean ± s.e.m. Curves through the data points are the best fit of equation 2 to the data.

Table 2.1. Comparison of potency and maximum contraction of spermine or MCh in the absence and presence of 300 μM spermine in mouse small airways *in vitro*. Airway reactivity was assessed in PCLS, with potency and maximum (% reduction in initial area) obtained from individual log concentration-response curves. Data are expressed as mean ± s.e.m. *P<0.05, unpaired t test compared with spermine; #P<0.01, paired t test compared with MCh.

	(n)	pEC_{50}	Maximum contraction (%)
Spermine	5	5.1±0.6	54±9
MCh	4	6.4±0.2*	70±4
MCh + spermine	4	7.3±0.3#	83±4

2.3.2 CaSR NAMs differentially inhibit spermine-induced Ca^{2+}_i mobilisation and IP_1 accumulation in FlpIn HEK293 TRex cells via the CaSR.

The following NAMs were investigated in this study: **i**) NPS2143 and ronacaleret are amino alcohol NAMs and two of the first CaSR NAMs to be discovered and evaluated for osteoporosis in preclinical (NPS2143) or human clinical (ronacaleret) trials (Fitzpatrick et al., 2011; Gowen et al., 2000a); **ii**) ATF936 is a quinazolinone NAM that failed in clinical trials for osteoporosis due to limited efficacy (Cosman et al., 2016; Halse et al., 2014a); **iii**) BMS compound 1 and Pfizer compound 1 are chemically distinct NAMs that did not progress to clinical trials for osteoporosis.

We characterised how CaSR NAMs inhibit spermine-induced IP_1 accumulation and Ca^{2+}_i-mobilisation via the CaSR in HEK293 cells because these two pathways contribute to ASM contraction. We initially characterised the interactions of spermine with the CaSR in Ca^{2+}_i mobilisation assays (**Figure 2.2A**). Using 100 ng/mL tetracycline to induce maximum CaSR expression, spermine potency was 4.40±0.02, the maximum spermine response approached 100% of the 1 μM ionomycin response, and the binding slope and hill slope was 1.8±0.2 and 2.3±0.12, respectively (**Figure 2.2A**). The steep spermine hill slope is consistent with the steep Ca^{2+}_o hill slope driven by Ca^{2+}_o binding to multiple binding sites in a positively cooperative manner (Gregory et al., 2020). Spermine concentration-response assays were additionally performed in cells where CaSR expression was submaximally induced using 5 ng/mL tetracycline. Under these low CaSR expression conditions, receptor reserve was decreased, causing the spermine concentration-response curve to shift to the right, as well as a reduction in the spermine maximum response (to approximately 70% of the ionomycin response) (**Figure 2.2A**). Equation 2 was fitted to spermine concentration-response data generated under high and low CaSR expression conditions to derive the spermine affinity (pK_A), efficacy ($log\tau_A$) and binding slope (nB) at the CaSR (**Figure 2.2A & Table 2.2**). These data confirmed that the

spermine binding slope was greater than unity, suggesting that spermine binds to more than one site on the CaSR. In this study, we assume binding slope of spermine-mediated Ca^{2+}_i and IP_1 accumulation is equal to1.8 for simplicity (Gregory et al., 2020).

Next, spermine-mediated IP_1 accumulation was assessed. In the IP_1 accumulation assay, the maximum spermine-induced response was only 70% that of Ca^{2+}_o (**Figure 2.2B**), meaning spermine was a partial agonist compared to Ca^{2+}_o. Therefore, spermine affinity and efficacy in the IP_1 accumulation assay were derived using the response to Ca^{2+}_o as the maximum system response. For this analysis, we assumed the simplest scenario where nB did not differ between signalling pathways, and nB was therefore constrained to the value derived from analysis of spermine-mediated Ca^{2+}_i mobilisation data. Spermine affinity was 10-fold higher for Ca^{2+}_i mobilisation than IP_1 accumulation. (pK_A: 3.5±0.05 vs 2.5±0.09), while efficacy was more than 10-fold higher for the Ca^{2+}_i mobilisation pathway ($log\tau_A$: 1.70±0.04 vs -0.0523) (**Table 2.2**).

Next, we assessed the ability of five CaSR NAMs (NPS2143, Pfizer compound, BMS compound 1, ATF936 and ronacaleret) to inhibit spermine-mediated signalling. All CaSR NAMs investigated in this study inhibited spermine-induced Ca^{2+}_i mobilisation but to varying extents (**Figure 2.2C, E, G, I, K**). Pfizer compound 1 and ATF936 almost completely abolished the spermine response (**Figure 2.2E & I**). In comparison, NPS2143 reduced spermine potency but only partially attenuated the spermine maximum response, while BMS compound 1 reduced spermine potency but had no effect on the spermine maximum response (**Figure 2.2G**). NAMs were also assessed for their ability to inhibit spermine-mediated IP_1 accumulation. While NPS2143, Pfizer compound 1, ATF936 and ronacaleret inhibited IP_1 accumulation stimulated by spermine, BMS compound 1 was without effect (**Figure 2.2D, F, H, J & L**).

The interactions between the CaSR NAMs and spermine at the CaSR were analysed using an operational model of allosterism to quantify NAM functional affinities (referred to herein as pK_B) and cooperativities ($\alpha\beta$) (Eq 3). Since CaSR NAMs alone did not mediate any responses in Ca^{2+}_i mobilisation or IP_1 accumulation assays, τ was constrained to 0 for this analysis. The affinities of NAMs for the CaSR varied by up to 100-fold in Ca^{2+}_i mobilisation assays (one-way ANOVA with Tukey's multiple comparisons test). The rank NAM pK_B order was NPS2143 = Pfizer compound 1 > ATF936 > Ronacaleret > BMS compound 1(**Table 2.2**). The rank order of the NAMs was Pfizer compound 1 = ATF936 > NPS2143 > ronacaleret > BMS compound 1 (**Table 2.2**). As observed in Ca^{2+}_i mobilisation assays, CaSR NAMs also

showed differential modulation in IP_1 accumulation assays. The rank NAM pK_B order in IP_1 assays was NPS2143 = Pfizer compound 1 > ATF936 > ronacaleret > BMS compound 1. The rank NAM logαβ order in IP_1 assays was Pfizer compound 1 = ATF936 = ronacaleret = NPS2143 > BMS compound 1 (**Table 2.2**). BMS compound 1 was without effect in IP_1 assays (**Figure 2.2 G, H**).

Based on the results of NAM interaction studies with spermine in Ca^{2+}_i mobilisation and IP1 accumulation assays, we selected Pfizer compound 1 with the highest cooperativity and affinity in opposing spermine in Ca^{2+}_i and IP_1 assays, NPS2143 as a prototypical CaSR NAM, and BMS compound 1 with the lowest cooperativity and biased effects towards opposing Ca^{2+}_i mobilisation versus IP_1 accumulation, to assess their potential bronchorelaxant effects in mouse airways.

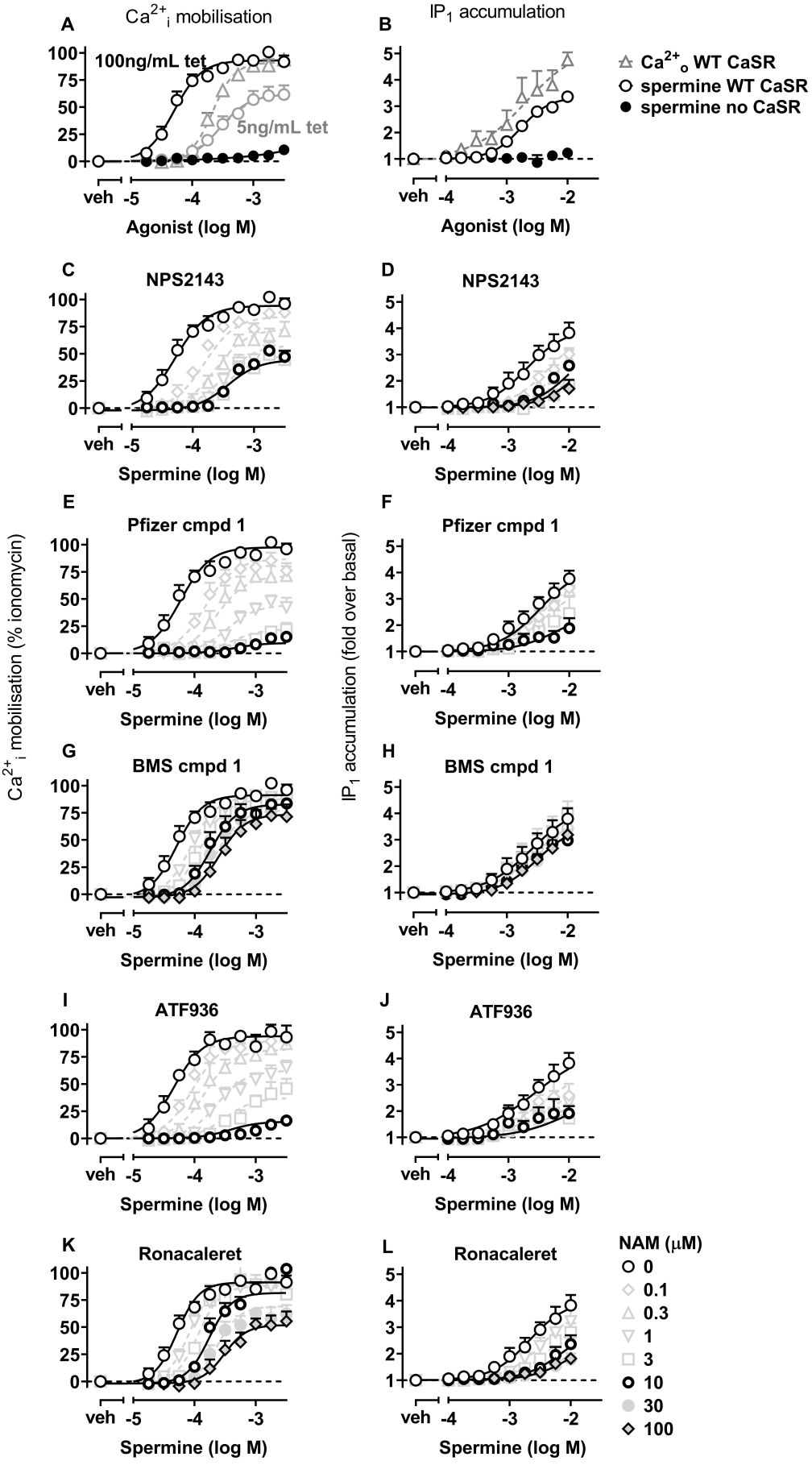
A
Ca2+i mobilisation
100ng/mL tet
5ng/mL tet
Agonist (log M)
B
IP1 accumulation
Ca2+o WT CaSR
spermine WT CaSR
spermine no CaSR
C
NPS2143
Spermine (log M)
D
NPS2143
E
Pfizer cmpd 1
F
Pfizer cmpd 1
G
BMS cmpd 1
H
BMS cmpd 1
I
ATF936
J
ATF936
K
Ronacaleret
L
Ronacaleret
Ca2+i mobilisation (% ionomycin)
IP1 accumulation (fold over basal)
NAM (μM)
0
0.1
0.3
1
3
10
30
100

Figure 2.2. CaSR NAMs differentially inhibit spermine-induced Ca^{2+}_i mobilisation and IP_1 accumulation in FlpIn HEK293 TRex cells stably expressing the CaSR. Spermine induces **A.** Ca^{2+}_i mobilisation and **B.** IP_1 accumulation in FlpIn HEK293 TRex cells stably transfected with the CaSR induced by 5ng/mL or 100ng/mL tetracycline overnight. The effects of **C.** NPS2143 **E.** Pfizer compound 1 **G.** BMS compound 1, **I.** ATF936, **K.** ronacaleret on the peak Ca^{2+}_i mobilisation responses to spermine were determined and corrected to the baseline response prior to the addition of agonist or vehicle and normalised to 1μM ionomycin. The effects of **D.** NPS2143 **F.** Pfizer compound 1, **H.** BMS compound 1, **J.** ATF936, **I.** ronacaleret on the IP_1 accumulation response to spermine were measured and normalized as fold over basal (vehicle). Data are mean ± s.e.m. determined in 4-5 separate experiments performed in duplicate. Curves through the data points are the best fit of equation 2 to the data in **A**&**B** and equation 2 in **C-L**.

Table 2.2. Spermine affinity (pK_A), efficacy ($log\tau_A$) and NAM affinity (pK_B) and cooperativity ($log\alpha\beta$) estimates derived from Ca^{2+}_i mobilisation and IP_1 accumulation assays measuring NAM inhibition of spermine responses. Data are mean ±s.e.m from the indicated number of independent experiments (n) performed in duplicate, analysed using equation 3. NR denotes to no response. ND denotes to not determined

	Ca^{2+}_i mobilisation				IP_1 accumulation			
	pK_A (n)	$log\tau_A$	pK_B	$Log\alpha\beta$ ($\alpha\beta$)	pK_A (n)	$Log\tau_A$	pK_B	$Log\alpha\beta$ ($\alpha\beta$)
NPS2143	3.32±0.01 (5)	1.69±0.09	7.94±0.13	-1.89±0.10	2.67±0.22 (4)	0.25±0.19	6.49±0.33	-0.90±0.33
Pfizer compound 1	3.39±0.04 (5)	1.38±0.08	7.66±0.13	-2.27±0.17	2.53±0.15 (3)	0.30±0.19	7.02±0.13	-1.2±0.17
BMS compound 1	3.32±0.06 (4)	1.49±0.17	6.13±0.22	-1.26±0.26	NR (4)			
ATF936	3.50±0.01 (4)	1.30±0.07	7.03±0.28	-2.03±0.30	2.53±0.10 (3)	0.26±0.03	6.98±0.35	-1.51±0.19
Ronacaleret	3.35±0.04 (3)	1.53±0.26	6.61±0.21	-1.68±0.15	2.33±0.12 (4)	0.53±0.16	5.98±0.23	-1.35±0.16

2.3.3 CaSR NAMs elicit relaxation in mouse small airways

We assessed the dilator potency and efficacy of CaSR NAMs compared to salbutamol in mouse PCLS (**Figure 2.3**). Representative traces and images from airways pre-contracted with a submaximal concentration of MCh (300 nM) show that salbutamol and the CaSR NAM, NPS2143 (or Pfizer), elicit concentration-dependent (or not if images only) partial relaxation of small airways (**Figure 2.3A, B**).

In airways pre-contracted to a similar extent with 300nM MCh (**Table 2.3**), average maximal relaxation was 50±7% for salbutamol (**Figure 2.3C**). For the CaSR NAMs, Pfizer compound 1 had the highest maximal relaxation (Pfizer compound 1 70±16%; NPS2143, 32±8%; $P<0.05$). (**Figure 2.3D, E, F**). Notably, all CaSR NAMs, but not salbutamol, showed biphasic concentration-response curves (**Figure 2.3D, E, F**). Based on EC_{50}_1 values (first phase potency), CaSR NAMs were approximately 1000-fold more potent than salbutamol, but no greater efficacy than salbutamol overall (**Table 2.3**).

We then assessed the relative abilities of each bronchodilator in airways pre-contracted with 3000 nM MCh. The relaxation response to salbutamol against 3000 nM MCh was almost abolished (**Figure 2.3C**). The dilator CR curves for all NAMs were also right-shifted, with the apparent loss of the first phase of the dilator response (**Figure 2.3D, E, F**). Nevertheless, all were still able to elicit robust partial relaxation at the maximum concentration tested.

We explored this potential functional antagonism of dilator responses further, by correlating the % reduction in airway area in response to either 300 or 3000 nM MCh in individual PCLS with the matched relaxation to the highest concentration of each dilator tested (10 μM) (**Figure 2.4**). Consistent with Figure 2.3, there was a reduction in dilator responses to salbutamol or the NAMs, irrespective of the concentration of MCh used. However, extrapolation of this relationship suggested that relaxation for salbutamol and BMS would be completely abolished in maximally contracted airways, while Pfizer compound 1 and NPS2143 would retain some dilator efficacy.

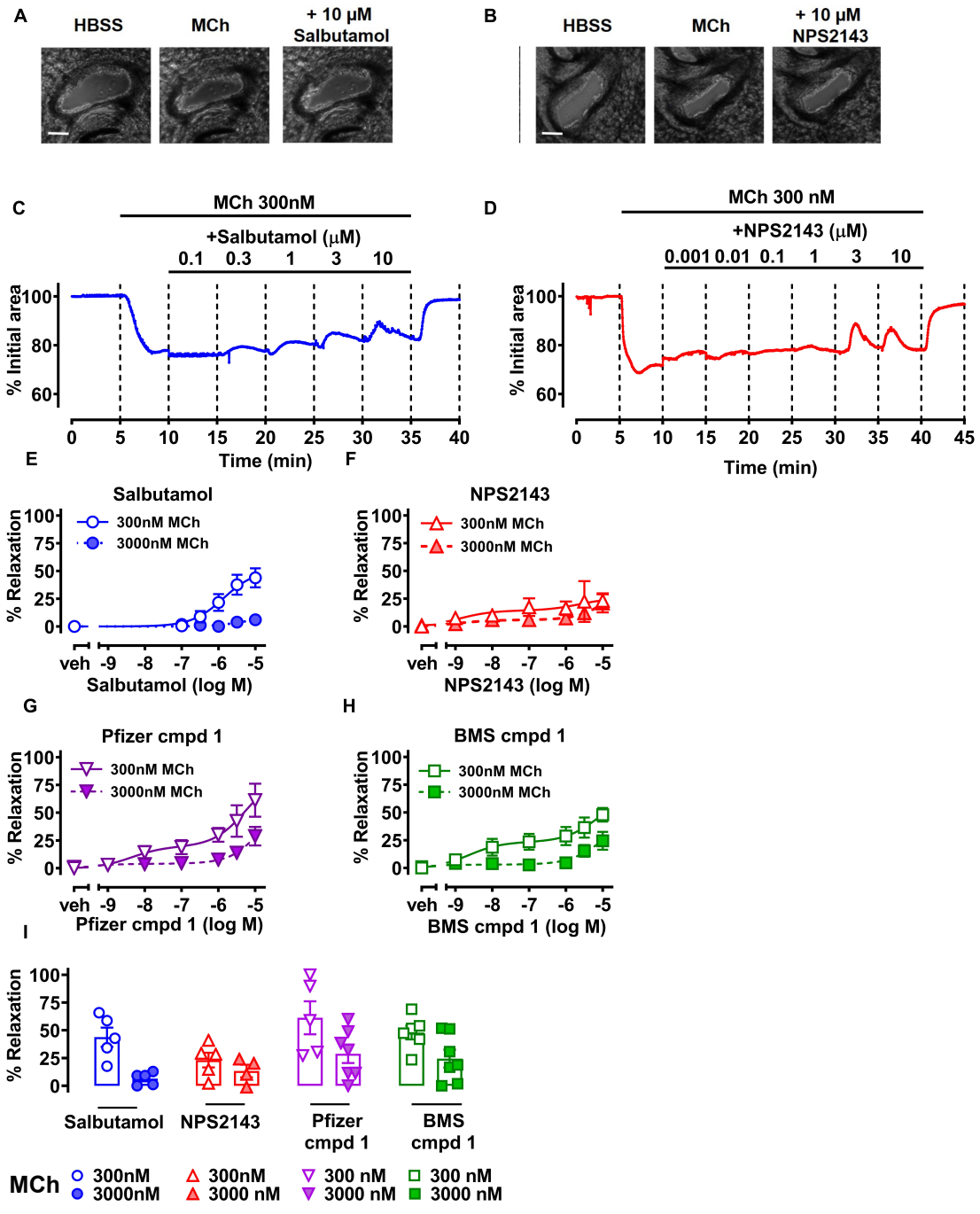

Figure 2.3. CaSR NAMs elicit concentration-dependent relaxation in mouse small airways. Airways in PCLS were pre-contracted with 300 nM or 3000 nM MCh, prior to perfusion with salbutamol, NPS2143, Pfizer compound 1 or BMS compound 1 (1 nM-10 µM). Representative images show changes in airway area during pre-contraction to 300 nM MCh and then relaxed after perfusion to 10 µM **A**) salbutamol or **B**) NPS2143. Representative traces show changes in airway area during pre-contraction to 300 nM MCh prior to cumulative perfusion of **C**) salbutamol or **D**) NPS2143. Grouped relaxation data for **E)** salbutamol, **F)** NPS2143, **G)** Pfizer compound 1 or **H)** BMS compound 1 after pre-contraction (% reduction in area) with 300 nM or 3000 nM MCh. **E-H**) Relaxation is expressed as the % relaxation of the pre-contraction to MCh, **I)** Maximum relaxation stimulated by 10 µM NAM post 300 or 3000 nM MCh-mediated contraction. All data are expressed as mean ± s.e.m, n=4-7 independent experiments. Curves through the data points are the best fit of equation 4 to the data in **C** and equation 3 to the data in D-F.

Table 2.3. Effect of pre-contraction on potency and maximum relaxation of salbutamol and CaSR NAMs. Mouse airways were pre-contracted with 300 nM or 3000 nM MCh before dilator response curves were generated. For SALBUTAMOL and CaSR NAMs, % relaxation is shown for 10 μM of each dilator post 300 nM or 3000 nM MCh. For SALB, potency (pEC_{50}) was derived from single phase curve fits using equation 1. NAM potency at the first phase (pEC_{50}_1) was derived from biphasic curve fits using equation 4. Data are mean ± s.e.m. from (n) independent experiments with NAM pEC_{50} only estimated when a plateau in the response to NAM was achieved. ****P<0.00001 compared with SALB, $^{\$}$P<0.05 compared with NPS2143, using one-way ANOVA with Tukey's multiple comparisons. ND denotes not determined due to incomplete curves.

	300 nM MCh				3000 nM MCh			
	salbutamol	NPS2143	Pfizer compound 1	BMS compound 1	salbutamol	NPS2143	Pfizer compound 1	BMS compound 1
n	5	5	5	6	5	4	7	7
pre-contraction (% initial area)	76±3	49±10	59±5	65±2	67±11	61±10	49±7	56±3
% relaxation	44±9	23±6	62±16$^{\$}$	48±6	6±3	13±6	28±8	24±8
pEC_{50}_1	5.7±0.2	8.8±0.3 ****	8.6±0.1 ****	8.7±0.2 ****	ND			
pEC_{50}_2		ND						

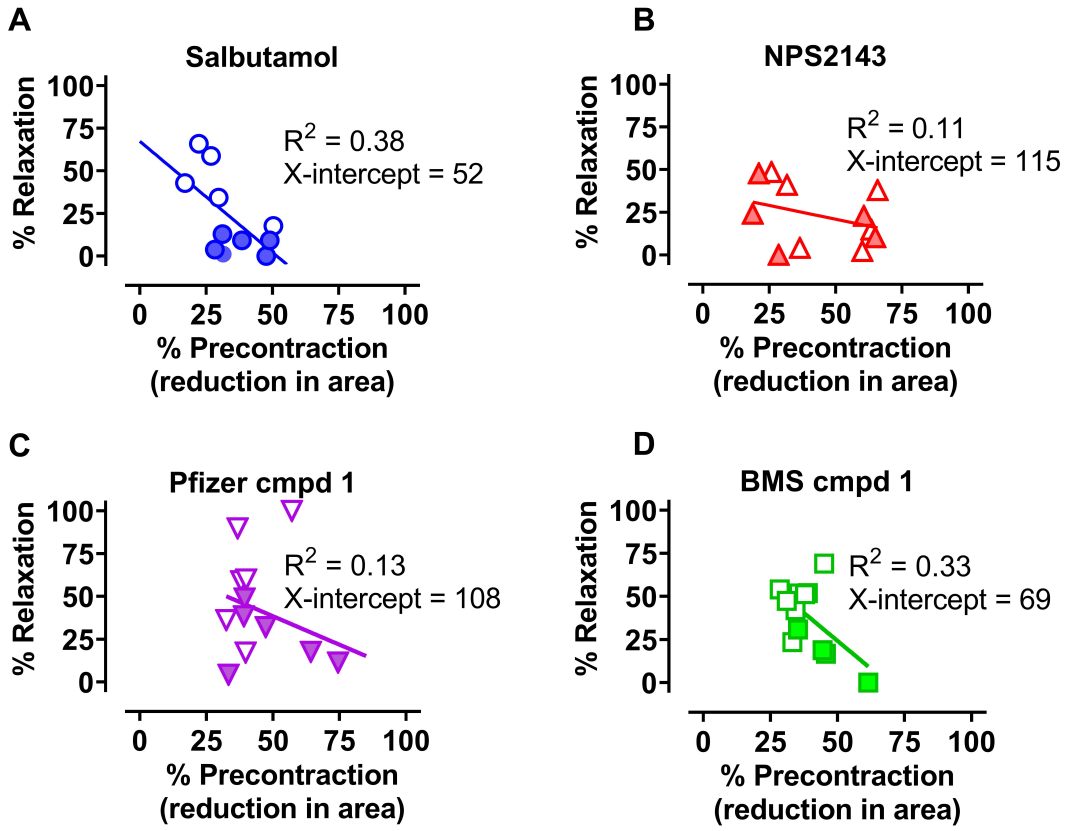

Figure 2.4. Correlation between pre-contraction to MCh and bronchodilator response to salbutamol and CaSR NAMs. Mouse small airways were pre-contracted with MCh (300 nM, open symbols or 3000 nM, closed symbols), prior to A) SALB, B) NPS2143, C) Pfizer compound 1 or D) BMS compound 1. Relaxation responses to 10 µM of each dilator were assessed. All data are expressed as mean ± s.e.m., n=10-12 independent experiments.

2.3.4 NAM-mediated airway relaxation is not due to Ca^{2+} sensitivity

Relaxation of mouse airways in PCLS to salbutamol has previously been shown to be due to inhibition of both MCh-induced Ca^{2+} oscillations and sensitivity (Donovan et al., 2014). The potential contribution of inhibition of Ca^{2+} sensitivity to NAM-mediated airway relaxation was therefore tested, using PCLS that were left untreated or treated with 20 mM caffeine and 50 µM ryanodine (**Figure 2.5A, B**). This treatment abolishes Ca^{2+} oscillations so that MCh-induced airway contraction following caffeine/ryanodine treatment is then attributed to increased Ca^{2+} sensitivity alone.

In untreated slices, dilator responses to the same NAM were reproducible (**Figure 2.5A, C, D, E,** shown as C1 and C2). A representative trace from a caffeine/ryanodine treated slice shows the transient contraction to treatment, due to release of $Ca^{2+}{}_i$ due to activation of ryanodine receptors, with the lack of subsequent contraction to 20 mM caffeine confirming store depletion (**Figure 2.5B**). Relaxation to 10 µM NPS2143 was completely abolished after caffeine/ryanodine (**Figure 2B, C**), indicating that this CaSR NAM cannot oppose contraction due to increased Ca^{2+} sensitivity. Dilator responses to BMS compound 1 and Pfizer compound 1 were variable and reduced overall post caffeine/ryanodine (**Figure 2D,E**), suggesting that these NAMS may also have limited efficacy when contraction is driven by Ca^{2+} sensitivity.

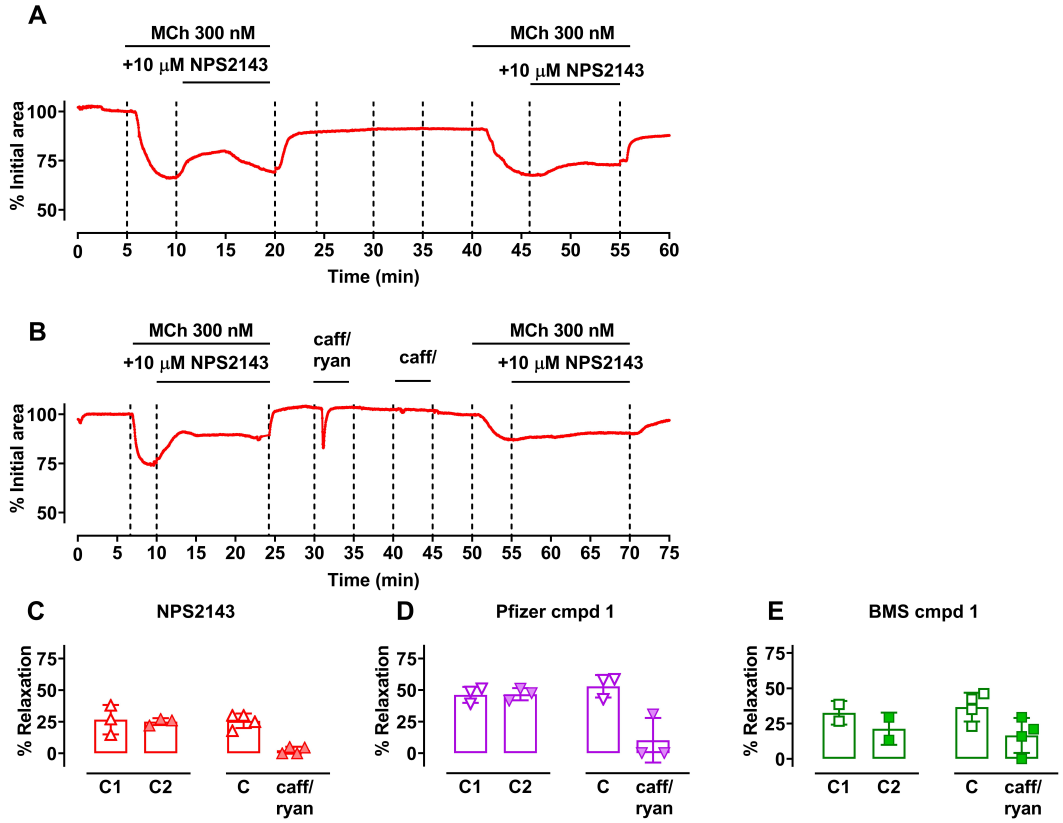

Figure 2.5. CaSR NAMs do not relax small airways following Ca^{2+}-permeabilisation. Slices were permeabilised to Ca^{2+} by simultaneous treatment with 20 mM caffeine and 50 µM ryanodine to lock ryanodine receptors open to clamp Ca^{2+}_i concentrations. Representative trace showing the response to 300 nM MCh under **A)** control and **B)** Ca^{2+} permeabilised conditions. Relaxation responses (mean ± s.e.m.) represent the % relaxation following pre-contraction mediated by MCh, averaged over the best relaxation during the perfusion with 10 µM CaSR NAMs **C)** NPS2143 **D)** Pfizer compound 1 **E)** BMS compound 1. All data are expressed as mean ± s.d., n=2-4 independent experiments. C1 and C2 refer to the two relaxation responses to CaSR NAMs on the same mouse PCLS, without caffeine/ryanodine treatment (panel A). C refers to the first relaxation to CaSR NAMs and caff/ryan refers to the relaxation to CaSR NAMs after caff/ryan treatment.

2.3.5 CaSR NAMs do not reverse MCh & spermine induced airway contraction.

As described before, the CaSR agonist spermine potentiated MCh-induced airway contraction **(Figure 2.1D**). Given the reduced efficacy of all dilators with increased MCh-induced contraction, we characterised whether CaSR NAMs could reverse the increased airway contraction induced by the combination of spermine and MCh.

Representative traces show greater reduction in airway area in response to spermine and MCh compared to MCh alone, with complete loss of dilator efficacy for Pfizer compound 1 (**Figure 2.6A, B**). Although all three CaSR NAMs caused partial relaxation of MCh-induced contraction, they were unable to reverse the increased airway contraction caused by combined spermine and MCh. In contrast, salbutamol maintained its bronchorelaxant effect irrespective of the contractile stimulus (**Figure 2.6C, D**).

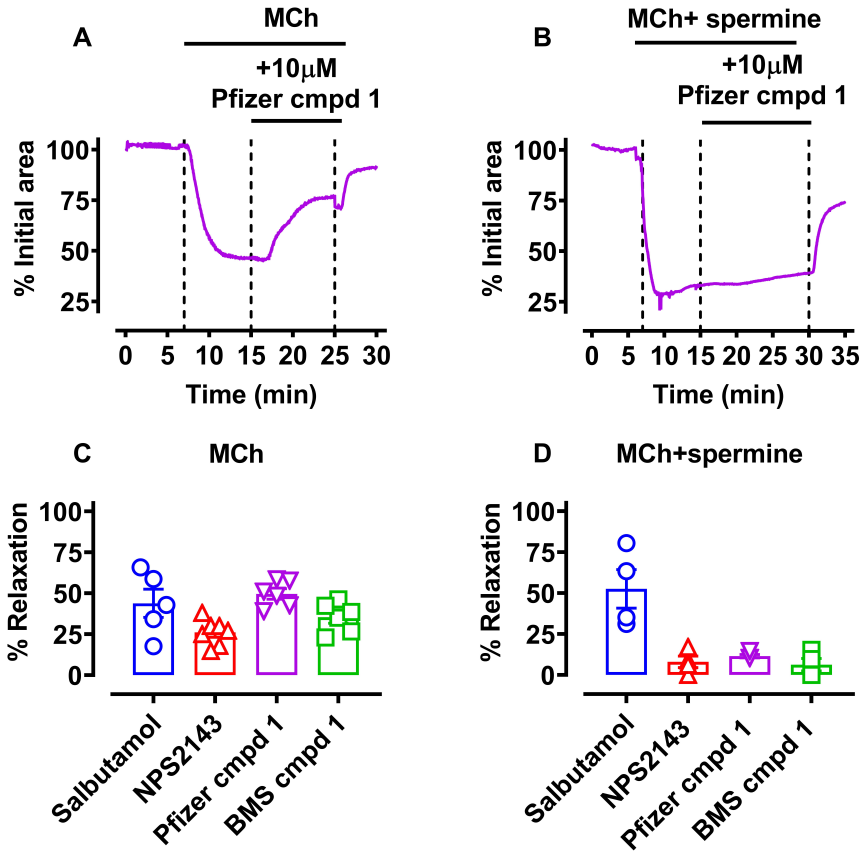

Figure 2.6. CaSR NAMs do not reverse airway contraction induced by MCh in combination with spermine. Representative trace showing contraction to 300 nM MCh in the **A)** absence or **B)** presence of 300 μM spermine added prior to addition of 10 μM Pfizer compound 1. Maximum % relaxation responses to 10 μM salbutamol or CaSR NAMs after pre-contraction to **D**) MCh or **E**) MCh and spermine (mean ± s.e.m.). All data are expressed as mean ± s.e.m, n=4-8 independent experiments

2.3.6 CaSR NAMs elicit airway relaxation in mouse small airways despite β_2-AR desensitisation.

A major limitation of current therapy with β_2-AR agonists is loss of efficacy due to receptor desensitization. To assess whether dilator responses to CaSR NAMs are affected by heterologous receptor desensitization, lung slices were incubated overnight with a high concentration of salbutamol (100 µM). β_2-AR-induced relaxation in response to 10 µM salbutamol was completely abolished, (**Figure 2.7A, B**). In contrast, NAM-mediated relaxation (NPS2143, Pfizer compound 1 and BMS compound 1) was maintained with similar potency and efficacy compared to untreated lung slices (**Figure 2.7C-E**).

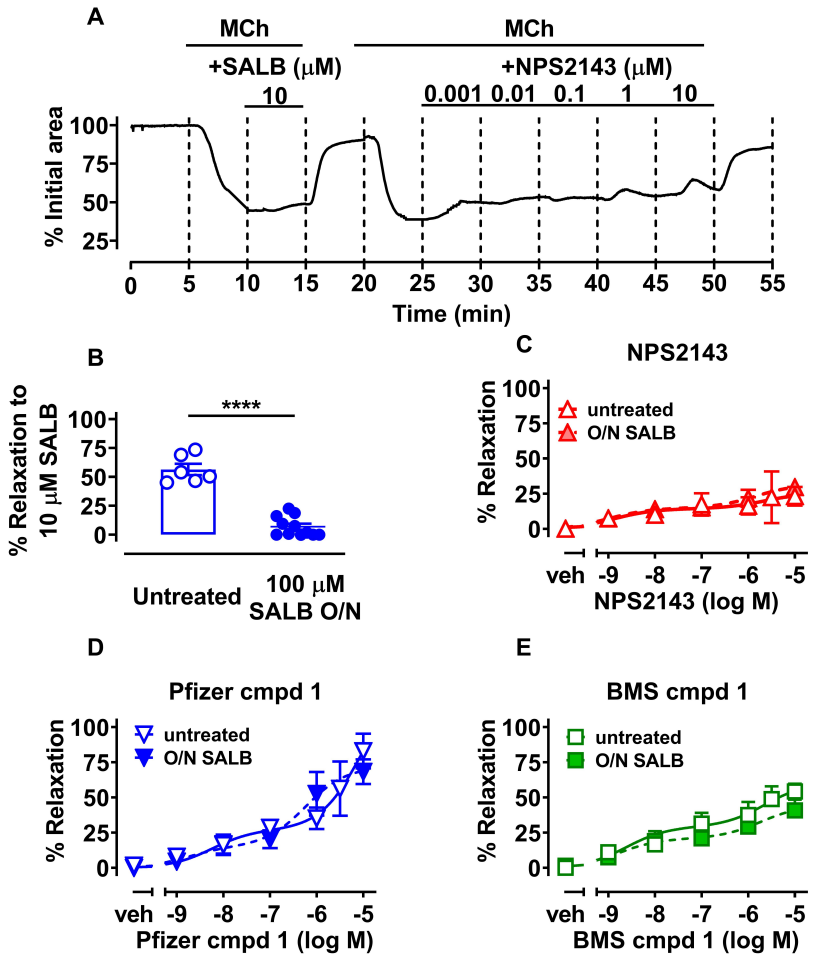

Figure 2.7. CaSR NAMs elicit concentration-dependent relaxation of mouse small airways in lung slices following β_2-AR desensitisation. Slices were incubated overnight with vehicle (0.1% distilled water) or SALBUTAMOL (100 μM). Airways were pre-contracted with 300 nM MCh prior to addition of 10 μM salbutamol (SALB) or varying concentrations of NPS2143, Pfizer compound 1 or BMS compound 1. A) Representative trace showing NPS2143 concentration-dependent responses following overnight incubation with vehicle or SALB. Grouped data for **B)** salbutamol **C)** NPS2143 **D)** Pfizer compound 1 **E)** BMS compound 1 added cumulatively. Relaxation (mean ±s.e.m.) represent the % relaxation following pre-contraction to 300 nM MCh,****P<0.0001 compared with untreated.

2.3.7 Overnight exposure to CaSR NAMs differentially prevents MCh-induced small airway contraction

Having shown that CaSR NAMs maintain efficacy under condition of β_2-AR desensitisation, we aimed to assess whether their dilator response were affected by homologous desensitisation. To address this aim, we treated PCLS overnight with increasing concentrations of NPS2143, Pfizer

compound 1or BMS Compound 1 that had been shown to relax pre-contracted airways (**Figure 2.3**).

We tested whether prolonged treatment with these NAMs affected MCh-induced contraction the next day, as a measure of maintained airway viability. Due to time constraints, dilator responses to the CaSR NAMs after overnight treatment were not assessed.

Maximum reductions in airway area to MCh in PCLS after overnight treatment with vehicle were approximately 50-60% (**Figure 2.8A, B, C**). Prior treatment with NPS2143 and Pfizer compound 1 reduced MCh-mediated contraction in a concentration-dependent manner, despite MCh contraction being assessed in the absence of CaSR NAMs. Contraction was completely abolished following 10 μM NPS2143 overnight, while 10 μM Pfizer compound 1 also significantly reduced MCh efficacy (from 59±5% reduction in airway area to 33±14%, n=8, 7). In contrast, MCh-induced airway contraction was unaltered after overnight incubation of lung slices with 1 or 10 μM BMS compound 1.

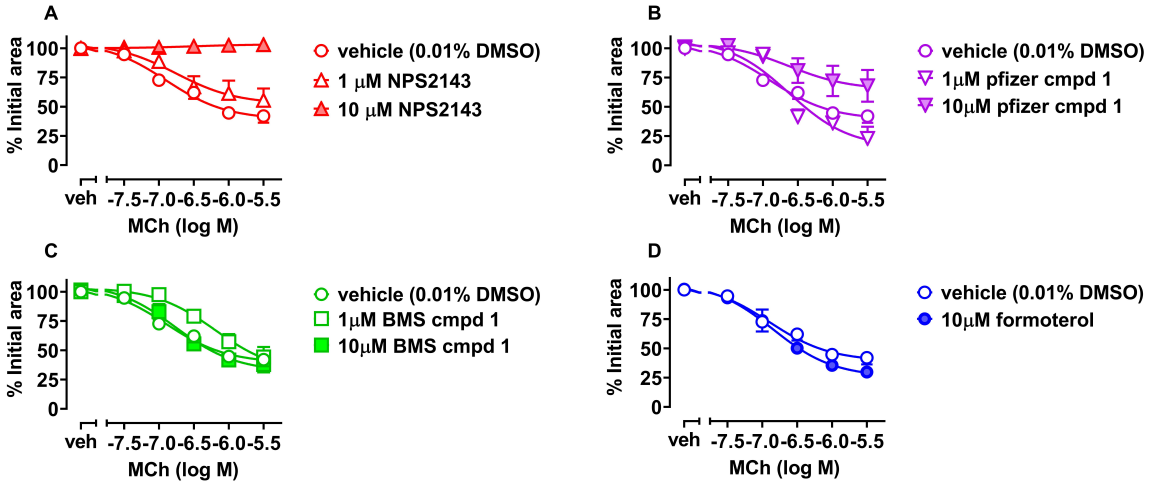

Figure 2.8. **Overnight pre-incubation with CaSR NAMs differentially prevents MCh-mediated contraction.** PCLS were pre-incubated with 0.01% DMSO (vehicle), 1 or 10 μM of **A)** NPS2143. **B)** Pfizer compound 1 or **C)** BMS compound 1. Lung slices were washed three times for 20 min with HBSS prior to perfusion with increasing concentrations of MCh. All data are expressed as mean ± s.e.m, n=4-8 independent experiments. No error bars are visible for 10 μM NPS2143 due to the error bars falling within the data point symbols

2.3.8 CaSR NAMs do not cause acute bronchoprotection of MCh-induced small airway contraction

Given the potential inhibitory effects of overnight treatment of CaSR NAMs on MCh-induced contraction (**Figure 2.8**), we then assessed whether short-term treatment with CaSR NAMs or formoterol was bronchoprotective. For these studies, a control contraction to MCh was established before PCLS were treated with 10 μM NPS2143 (or 0.1% DMSO as vehicle control) for 20 min prior to and during a single addition of spermine (300 μM) followed by MCh (300 nM). Representative traces show transient contraction to spermine in DMSO-treated PCLS, but not in the continued presence of NPS2143 (**Figure 2.9A, B**). Spermine (300 μM) caused 25±4% reduction in airway size with vehicle but only 6±4% in the presence of NPS2143 (**P<0.01, unpaired t-test; **Figure 2.9D**). In comparison, the contraction to MCh in the absence and presence of NPS2143 within the same slice remained unchanged, as showed in **Figure 2.9C**. Similarly, 20 min pre-incubation of lung slices with Pfizer compound 1 or BMS compound 1 did not reduce MCh-induced airway contraction (**Figure 2.9E**). In comparison, 20 min incubation with the LABA formoterol prevented 300 nM MCh induced airway contraction (**Figure 2.9E**).

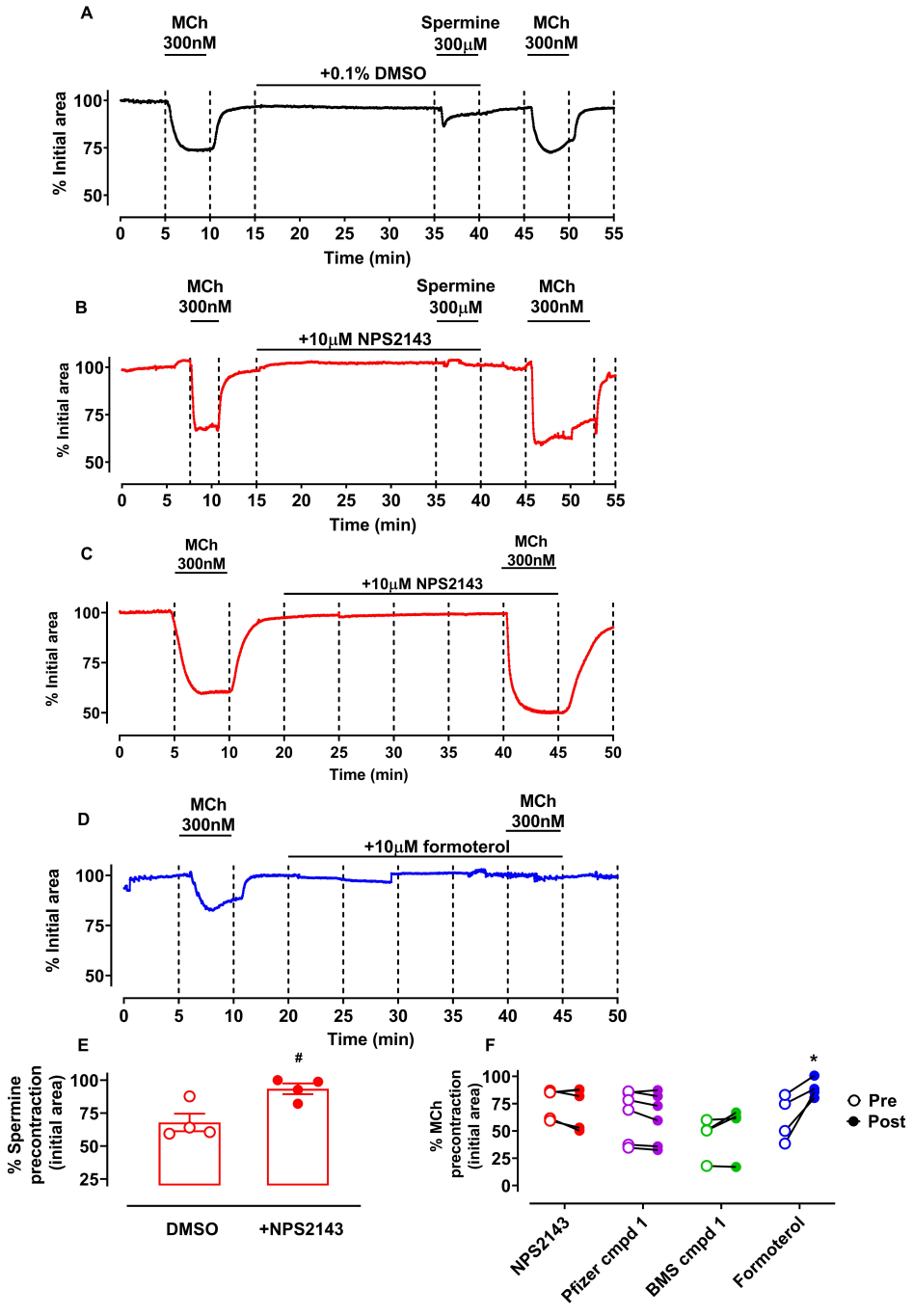

Figure 2.9. 20 min pre-incubation of lung slices with CaSR NAMs prevents contraction to spermine but not MCh. A representative trace of contraction to 300 nM MCh pre and post 20 min static incubation with **A)** 0.1% DMSO or **B)**, **C)** 10 μM NPS2143 or **D)** 10 μM formoterol followed by A), B) 300 μM spermine or C), D) 300 nM MCh. Grouped data for **E)** contraction to spermine in separate PCLS in the absence or presence of NPS2143 **F)** contraction to MCh in the matched PCLS pre and post CaSR NAMs, 0.1% DMSO, 10 μM NPS2143, Pfizer compound 1, BMS compound 1, or formoterol. Data are expressed as mean ± s.e.m (panel E), N=4-5; $^{\#}P< 0.01$, paired t-test compared with responses to spermine before NPS2143 incubation; *P<0.05, paired t-test compared with responses to MCh before formoterol incubation.

2.4 Discussion

The current study has shown that CaSR NAMs are effective bronchodilators in mouse PCLS, and when studied for their ability to reverse MCh-mediated mouse airway contraction, have higher potency and similar maximal relaxation effects compared to salbutamol. We also confirmed that the CaSR agonist, spermine, induces bronchoconstriction in mouse airways, with lower but similar efficacy to MCh. Since spermine-mediated airway contraction was transient, it was not possible to assess the effects of NAMs on spermine-mediated contraction. However, we have now demonstrated that CaSR NAMs maintain their potency and efficacy in opposing MCh-induced contraction under condition of β_2 AR desensitisation when salbutamol-mediated relaxation is abolished. Although we were unable to establish acute bronchoprotective effects, we showed that longer term treatment with selected NAMs may also prevent bronchoconstriction.

A previous study demonstrated that the amino alcohol NAM, NPS89636, stimulated a small but non-significant relaxation of small airways that had been constricted with spermine (Yarova et al., 2015). However, until now, no study had quantified the ability of CaSR NAMs to inhibit spermine-mediated CaSR activation, therefore, it was unclear whether amino alcohol NAMs were the best candidates for asthma therapeutics. We therefore assessed different NAMs in our study. Initial pharmacological characterisation was performed with a range of CaSR NAMs in FlpIn HEK293-CaSR TREx cells in Ca^{2+}_i mobilisation and IP_1 accumulation, as these two signalling pathways are important for ASM contraction (Billington & Penn, 2003). Interestingly, the potency, affinity and efficacy of spermine were higher in Ca^{2+}_i mobilisation compared to IP_1 accumulation assays. This may be because CaSR activation increases Ca^{2+}_i concentrations via IP-mediated Ca^{2+}_i release from the endoplasmic reticulum as well as via Ca^{2+}_o influx through calcium channels (Thomsen et al., 2012b), suggesting the superior ability of spermine to elevate Ca^{2+}_i is due to the contribution of Ca^{2+}_o influx through channels. Pfizer compound 1 and ATF936 had strongest cooperativity in spermine-mediated Ca^{2+}_i mobilisation and IP_1 accumulation assays, consistent with a previous study demonstrating these two NAMs showed the strongest negative cooperativity when Ca^{2+}_o was used as the agonist in Ca^{2+}_i mobilisation (Josephs et al., 2019). BMS compound 1 showed intriguing biased effects towards Ca^{2+}_i mobilisation, and was without effect in IP_1 accumulation assays. BMS compound 1 inhibited Ca^{2+}_i mobilisation presumably via inhibition of CaSR-mediated Ca^{2+}_o influx through channels. All other NAMs had inhibitory effects in both pathways.

These results are reminiscent of similar findings with CaSR PAMs, which show differential effects on $Ca^{2+}{}_i$ mobilisation versus IP_1 accumulation (Davey et al., 2012).

Having deduced that Pfizer compound 1 and BMS compound 1 had the highest and lowest affinities and cooperativities, respectively, in $Ca^{2+}{}_i$ and IP_1 assays, we chose these two NAMs to study in mouse PCLS studies, in addition to NPS2143 as a prototypical amino alcohol NAM. As we could not assess the ability of NAMs to reverse spermine-mediated airway contraction due to its transient nature, we pre-contracted airways with MCh as a gold standard bronchoconstrictor. Following airway contraction induced by a submaximal concentration of MCh, all CaSR NAMs reversed airway contraction. Intriguingly, all CaSR NAMs showed biphasic bronchorelaxation effects. Biphasic responses at the CaSR have been previously reported, where lower concentrations of $Ca^{2+}{}_o$ induced vasoconstriction but higher concentrations resulted in vasodilation in subcutaneous arteries (Li et al., 2011). Possible mechanisms of the NAM biphasic responses include NAM binding to two non-equal binding sites, or differential inhibition of two distinct spermine binding sites.

Importantly, the amino alcohol NAM, NPS2143 was the least effective NAM at reversing the effects of MCh. In contrast, Pfizer compound 1 was the most efficacious NAM at reversing MCh-mediated airway contraction, followed by BMS compound 1. The efficacy of all NAMs was reduced when airways were contracted with 3000 nM MCh, a concentration previously shown to cause maximum airway contraction in mouse PCLS. It remains to be determined whether the total biphasic response to the NAMs actually lost efficacy, or whether just the first phase was abolished, since this may provide insights into their dilator mechanisms.

Similar findings indicative of functional antagonism were observed for salbutamol, consistent with a previous study (Donovan et al., 2014). Airway relaxation was inversely correlated with MCh-induced reductions in airway area, irrespective of the concentration of MCh used. Notably, this analysis revealed that while dilator responses to both salbutamol and BMS compound 1 would be completely abolished in maximally contracted airways, both Pfizer compound 1 and NPS2143 would still elicit some bronchodilation. These findings demonstrate that different NAM chemotypes have varying capacity to act as bronchodilators, and highlight the importance of selecting the best NAM candidate for asthma.

Given these positive findings, we explored the potential mechanisms by which CaSR NAMs reversed airway contraction. We treated PCLS with caffeine and ryanodine, which abolishes the MCh-induced increase in Ca^{2+}_i-oscillations, to assess whether CaSR NAMs can elicit relaxation when contraction is due to Ca^{2+}_i-dependent mechanisms. These mechanisms are mediated by activation of RhoA/Rho kinase and/or PKC/CPI-17 pathways to decrease the activity of myosin light chain phosphatase and oppose relaxation, termed Ca^{2+}sensitivity (Bai & Sanderson, 2006; Bourke et al., 2014).

Previous studies have demonstrated that SABAs elicit relaxation via inhibition of Ca^{2+} oscillations, measured by confocal microscopy of ASM cells in PCLS, and inhibition of Ca^{2+}sensitivity in caffeine/ryanodine-treated PCLS (Delmotte & Sanderson, 2008; Donovan et al., 2014). Since CaSR NAMs lost their bronchodilator effects after caffeine and ryanodine treatment, it is possible that CaSR NAMs cannot reverse airway contraction when it is due to increases in Ca^{2+} sensitivity alone. These combined findings suggest possible complementary actions in severe asthma, whereby CaSR NAMs may be more effective in opposing functional antagonism, while SABA may be required to oppose increased Ca^{2+} sensitivity

Because spermine is elevated in asthma and potentiates MCh-induced airway contraction (Kurosawa et al., 1992; Yarova et al., 2015), we also assessed CaSR NAMs and salbutamol against MCh-induced airway contraction in the presence of spermine. In comparison to the comparable maximum bronchorelaxation effects of CaSR NAMs and salbutamol against MCh alone, CaSR NAMs lost their bronchodilator effects against airway contraction mediated by a combination of MCh and spermine, whereas salbutamol maintained its bronchodilator effects. When combine with evidence of their differential abilities to oppose contraction in caffeine/ryanodine treated PCLS, these results may reflect an increased contribution of Ca^{2+} sensitivity to contraction in response to the combination of MCh and spermine.

The lack of bronchorelaxation effects of NAM in the presence of MCh plus spermine is likely to also be because spermine and the NAMs both target the same receptor, therefore it is harder for CaSR NAMs to reverse the effects of spermine-mediated CaSR activation. The latter may be because CaSR NAMs and spermine bind to similar sites in the CaSR 7TM meaning spermine competes with the NAMs for binding thus reducing NAM activity (Josephs et al., 2019). The

development of NAMs that bind to alternative binding sites may therefore be important for future drug discovery.

β_2-AR desensitisation limits the therapeutic efficacy of salbutamol and formoterol. Therefore, we assessed the bronchodilation of CaSR NAMs following overnight salbutamol incubation, which causes β_2-AR desensitisation (Donovan et al., 2014). CaSR NAMs maintained their efficacy and potency following β_2-AR desensitisation. Further, CaSR NAMs maintained their bronchodilator effects to successive applications (shown in untreated PCLS used as controls for Ca^{2+} sensitivity studies), suggesting that CaSR NAMs may not induce acute receptor desensitisation themselves. Therefore, CaSR NAMs could serve as alternative bronchorelaxants in patients where frequent use of β_2-AR agonists such as salbutamol reduces β_2-AR agonist efficacy.

Due to time constraints, it was not possible to complete planned studies to address whether prolonged exposure to high concentrations of CaSR NAMs induces homologous desensitisation, potentially limiting their dilator efficacy in reversing MCh-induced contraction. However, our preliminary data revealed an unexpected finding, showing that PCLS treated overnight with increasing concentrations of NPS2143 and Pfizer compound 1, but not or BMS Compound 1, resulted in reduced MCh-induced contraction, despite these experiments being conducted after the PCLS were washed three times with assay buffer to remove the CaSR NAMs. NPS2143 The effects of Pfizer compound 1 and NPS2143 may be due to a NAM-mediated reduction in CaSR expression or to the ability of NPS2143 and Pfizer compound 1 to remain bound to the CaSR after PCLS were washed with assay buffer. These data suggest that the different NAMs may be mechanistically distinct in their capacity to prevent MCh-mediated bronchoconstriction. Alternatively, while BMS compound 1 may be readily washed from the lung slices following overnight treatment and washing of lung slices, NPS2143 and Pfizer compound 1 could bind pseudo-irreversibly to the CaSR, given them longer-term activity in preventing airway contraction. These possibilities remain a topic for future research, with implications for clinical translation.

Acute bronchoprotective effects are also clinically relevant given the prophylactic use of SABA for exercise-induced bronchoconstriction and the use of LABA in combination with GCS as preventer medication in asthma. However, in contrast to formoterol, 20 min pre-incubation with the CaSR NAMs did not prevent MCh-mediated airway contraction. The observation that neither Pfizer compound 1 or NPS2143 showed acute bronchoprotection but prevented airway contraction

after overnight treatment is consistent with a long-term mechanism underlying their inhibitory effects, and suggests that some CaSR NAMs could have long-term efficacy in protecting against bronchoconstriction.

It was interesting to note that the bronchodilator and bronchoprotection patterns of CaSR NAMs were not exactly as would be predicted based on their pharmacological profile in HEK293 cells in Ca^{2+}_i or IP_1 accumulation assays, despite the contributions of these pathways to airway contraction. For instance, while BMS compound 1 affinity and cooperativity in these assays were significantly lower than those of NPS2143, its dilator efficacy in mouse PCLS was not. Other potential second messengers that could be involved in NAM-mediated bronchodilation are cAMP and cGMP as both are important for inducing bronchorelaxation in response to β_2-AR agonists (Billington et al., 2013). Furthermore, receptor-mediated signalling events can be cell type-specific, therefore the effects of CaSR NAMs against spermine in recombinant FlpIn HEK293 Trex cells may not reflect pathways coupled to the interactions of CaSR NAMs with MCh-induced contraction in ASM cells. This highlights the importance of investigating CaSR NAMs in primary cell cultures, such as human primary ASM cells.

In summary, there are current limitations of β_2-AR agonists including limited efficacy and receptor desensitisation, suggesting they should not be used as a sole therapy even for mild asthma. There is still a clinical need for safe and effective bronchodilators that could provide alternate and additional benefits in asthma, and particularly in more severe asthma or following β_2-AR desensitisation (Barnes & Woolcock, 1998; Dockrell et al., 2007). In addition to our current findings, CaSR NAMs reduce airway inflammation, remodelling and hyperresponsiveness in preclinical models of chronic asthma (Lee et al., 2017; Thompson et al., 2016; Yarova et al., 2021; Yarova et al., 2015), suggesting CaSR NAMs may be beneficial in treating multiple aspects of asthma. Future studies should validate that CaSR NAMs retain bronchodilator effectiveness in preclinical models of asthma, including models that display airway inflammation, remodelling and AHR induced by asthma-relevant allergens, such as HDM.

Chapter 3

CaSR characterisation in human ASM cells

3.1 Introduction

Human airways are composed of different airway cell types, including epithelial, endothelial and ASM cells. While these airway cell types all contribute to airway structure and function, ASM cells have a critical role in regulating airway tone and contractility. Therefore, ASM itself is an important drug target in asthma and bronchodilators used clinically to treat asthma act via receptors expressed on ASM.

The molecular mechanisms underlying ASM contraction were discussed in detail in section 1.8.2.1. Briefly, G_q-coupled GPCRs are activated by contractile mediators, including ACh acting via the M_3 mAChR and spermine activating the CaSR. Receptor coupling to G_q leads to IP_3 synthesis, which induces the release of $Ca^{2+}{}_i$ from the sarcoplasmic reticulum into the cytosol, causing airway contraction via actin and myosin cross bridge formation. In contrast, airway relaxation is predominantly mediated by G_s-coupled GPCRs, which stimulate cAMP production resulting in PKA-mediated inhibition of $Ca^{2+}{}_i$ release. The β_2-AR mediates bronchodilation when activated by agonists, such as salbutamol and formoterol. However, other GPCRs also have bronchorelaxant roles in the lungs including the G_s-coupled adenosine 2B (A2B) receptor, bitter taste receptors, GABA receptors (Barnes, 2004b; Breschi et al., 2007; Brown et al., 2008; Pera & Penn, 2016).

The CaSR is expressed in both human fetal and adult ASM (Yarova et al., 2015) and is upregulated at both the gene and protein level in human asthmatics compared to healthy individuals (Yarova et al., 2015). Fetal lungs have a higher $Ca^{2+}{}_o$ concentration than adult lungs. Compared to adult ASM, CaSR expression in fetal ASM was shown to be higher and more sensitive to activation by $Ca^{2+}{}_o$ (Roesler et al., 2019). In asthma, IL-1β and other cytokines are responsible for increasing CaSR expression in ASM cells (Yarova et al., 2015). Upregulation of CaSR expression enhances its responsiveness to contractile stimuli such as spermine.

In Chapter 2, we demonstrated that CaSR NAMs have different bronchodilator efficacies in airways in mouse PCLS and distinct abilities to prevent MCh-induced airway contraction after overnight PCLS incubation. However, the underlying signalling pathways that drive NAM-mediated bronchodilation in ASM are yet to be fully characterised. It is important to identify signalling pathways contributing to (patho) physiological ASM functions for the future rational design of CaSR NAMs that inhibit these pathways.

Therefore, the aim of this study was to characterise the CaSR in human ASM cells and investigate CaSR related (patho) physiological signalling pathways in ASM cells. Previous studies have shown that activation of the CaSR in ASM cells leads to increased Ca^{2+}_i concentrations, reduced cAMP and activation of MAPK (Roesler et al., 2019; Yarova et al., 2015). In this study, we sought to detect CaSR mRNA expression in human ASM cells from healthy, mild asthmatic or severe asthmatic donors using real-time quantitative polymerase chain reaction (RT-qPCR). We also measured the Ca^{2+}_i mobilisation responses of the human ASM cells to the endogenous contractile mediators MCh, spermine and Ca^{2+}_o, because Ca^{2+}_i mobilisation is an important signalling pathway for ASM contraction.

3.2 Methods

3.2.1 Materials

The following materials were purchased: DMEM, penicillin streptomycin, TaqMan™ Fast Advanced Master Mix, Hard-Shell ® 96-well PCR plates, RNase Zap RNase Decontamination Solution, ULtraPure™ DNase/RNase-Free Distilled water, SYBR Safe DNA Gel Stain, 5x Gelpilot DNA Loading Dye, agarose, DNA ladder, TURBO DNA-free kit, iScript™ Reverse Transcription Supermix, trypsin, ethanol, TRI reagent, chloroform (Sigma Aldrich); Taqman probes (CaSR, ADORA2B and β-actin) (Thermo Fisher, Melbourne, Vic, Australia); Human ASM cells were a gift from A/Prof Brian Oliver (University of Technology Sydney). Cells were harvested from healthy donors, or donors with mild, moderate or severe asthma.

3.2.2 Harvesting human ASM cells

Human ASM cells were provided by A/Prof Brian Oliver (University of Technology Sydney), harvested from bronchial biopsies from healthy donors, or donors with mild or severe asthma, as previously described (Tan et al., 2013),

Table 3.1. Characteristics of donor subjects whose human ASM cells was used for RT-PCR or $Ca^{2+}{}_i$ mobilisation assays as shown.

Subject ID	Diagnosis	Sex	Age	RT-PCR	Ca^{2+}
2724	Healthy	M	20	✓	✓
2727	Healthy	F	27	✓	
3205	Mild asthma	M	23		✓
3226	Mild asthma	M	22		✓
3254	Mild asthma	M	21	✓	
4358	Severe asthma	M	63		✓
4270	Severe asthma	F	64	✓	
4445	Severe asthma	M	58		✓

3.2.3 Maintenance of cell lines

Human ASM cells were maintained in DMEM with 10% FBS, supplemented with 25 mM HEPES and 1% penicillin and streptomycin at 37^{o}C in a humidified atmosphere of 5% CO_2, 95% O_2. Cells were detached from tissue culture flasks using phosphate saline solution (PBS) (137 mM NaCl, 2.7 mM KCl, 4.3 mM Na_2HPO_4, 1.5 mM KH_2PO_4) supplemented with 0.67 mM ethylenediaminetetraacetic acid (EDTA) and 0.1% trypsin. Cells were centrifuged at 350 *x g* for 3 min, resuspended in media and reseeded into T75cm^2 flasks at a dilution of 1:2. Cells were passaged up to passage 10.

3.2.4 Freezing and thawing cells

Cells in T75cm^2 flasks reaching 70% confluence were harvested with 0.67 mM EDTA and 0.1% trypsin-supplemented PBS and centrifuged at 350 *x g* for 5 min. Cells were re-suspended in 1 mL freezing solutions (pre-cooled to 4°C, 90% FBS, 10% DMSO) and transferred into cyro-vials. Cryo-vials containing cells were placed in an isopropanol bath at -80°C for at least 24 hours before transfer to liquid nitrogen tanks or a vapour phase nitrogen storage system. For thawing cells, cells were bought up from storage by rapid defrosting at 37 °C and immediately transferred into a T75cm^2 flask containing pre-warmed DMEM supplemented with 10% FBS. Cells were allowed to adhere and grow prior to use in assays.

3.2.5 RNA extraction

Human ASM cells were processed and assessed for mRNA expression using established TRIzol methods, which have been described in detail previously (Zhong et al., 2004). Cells were harvested and stored at -80 ^{o}C immediately. Total RNA was extracted and purified by adding 1 mL Trizol in the fume hood according to the manufacturer's instructions. Following incubation at room temperature for 5 min, 200 µL of chloroform was added and samples were inverted vigorously for 15 secs. After incubation for 3 min at room temperature, samples were centrifuged at 12,000 *x g* for 15 min at 4 °C resulting in separation into 3 layers. The upper clear supernatant was collected carefully and mixed with 500 µL isopropanol. The samples were then incubated for 10 min at room

temperature and centrifuged again at 12, 000 *x g* for 10 min at 4 °C. The white pellet (RNA sample) was collected and washed with 200 µL 75% ethanol. Ethanol was subsequently removed after centrifuging at 7,500 *x g* for 5 min at 4 °C. RNA was dissolved in 20 µL of DNase/RNase-free water and the RNA concentration was detected using a Nanodrop Spectrophotometer at 260 nm. The purity of RNA was confirmed by a $\boldsymbol{\lambda}$ 260/280 absorbance ratio of 1.8-2.0, indicating the RNA was not contaminated by reagents used during extraction.

3.2.6 cDNA synthesis

Before cDNA synthesis, all RNA samples were run on an agarose gel (0.13%) to check the integrity and purity of the sample. RNA samples were treated with Turbo DNase and DNase Inactivation Reagents according to the manufacturer's instruction to remove genomic DNA contamination. The concentration of mRNA used to produce cDNA was equalised for all samples to minimise any errors due to differences arising from small amounts of starting mRNA. 2 µL 5x iScript RT Supermix was added to 500 ng RNA or negative control containing only iScript RT Supermix. Reverse transcription to generate cDNA was performed on an Applied Biosystems 2720 Thermal cycler (conditions outlined in **Table 3.2**), prior to. Samples being collected and stored at -20 °C.

Table 3.2. The program used for reverse transcription cycle.

1x	**25 °C for 5 min**
1x	42 °C for 30 min
2x	85 °C for 5 min
1x	4 °C until stored at -20 °C

3.2.7 RT- PCR

RT- PCR was performed using Taqman® primers (*CASR*: Hs01047795_m1; *ADORA2B*: Hs00248984_m1; β-actin: Hs01060665_g1) and Taqman master mix (ThermoFisher). A mixture of 6 ul of probe-master mix and 4 µL of cDNA was added into each well of a qPCR plate. The

plate was carefully sealed and quickly centrifuged. qPCR was performed in duplicate using a qPCR BioRad machine, using the following protocol (**Table 3.3**).

Table 3.3. The program used for RT-qPCR

1x	**50 ºC for 2 min**
2x	95 ºC for 10 min
39x	95 ºC for 15 sec 60 ºC for 1 min
	4 ℃ until sample transferred to fridge

3.2.8 $Ca^{2+}{}_i$ mobilisation assays

Human ASM cells were harvested and seeded into 96-well cleared bottom plates at a density of $1x10^4$ cells/well. Cells were allowed to grow to 70% confluency (approximately 7 days of growth). Cell media was changed every 3-4 days. Assays were performed in an isotonic buffer consisting of 150 mM NaCl, 2.6 mM KCl, 1.2 mM $CaCl_2$, 1.18 mM $MgCl_2$, 10 mM D-glucose, 25 mM HEPES, 4 mM probenecid and 0.5% w/v BSA, pH 7.4. Assay buffer was prepared as a 10x stock (without probenecid or BSA). A 1x stock (500mL) of assay buffer was prepared by adding 50 mL 10x stock, 2.5 g BSA and 5 mL of 400 mM probenecid (dissolved in 1 M NaOH) to 450 mL MQ, and pH adjusted to 7.4 with 1 M HCl or 1M NaOH. Cells were washed with 100 µL assay buffer before being loaded with 50 µL assay buffer containing 1 µM Fluo-8-AM. After one-hour incubation at 37°C in a humidified atmosphere of 5% CO_2, 95% CO_2, Fluo-8-AM containing buffer was aspirated and 90 µL assay buffer added to each well. Ligands were added using a Flexstation 1 or 3 microplate reader (Molecular Devices; Sunnyvale, California). Peak fluorescence within 120 sec was detected at 485 nm excitation and 525 nm emission using a Flexstation 1 or 3 microplate reader.

3.2.9 Data analysis

For qPCR experiments, mRNA expression was determined using RNA extracted and processed under identical conditions for each sample to avoid any procedural differences. Expression of

CASR and *ADORA2B* mRNA was calculated relative to the housekeeping gene, β-actin, and expressed, where Cq is the crossing point threshold of the sample for the amplified gene cycle number required for the fluorescent signal to exceed the background fluorescence (equation 1). Multiplication of all values by 1,000 does not change the relative expression levels and facilitates viewing of the data for poorly expressed genes.

Relative mRNA level = $2^{-Cq} * 1000$

For $Ca^{2+}{}_i$ mobilisation experiments, responses to ligands were normalised as fold over the average of the baseline readings taken prior to ligand addition. Peak fold over basal responses to ligands were retrieved for data analysis. All experiments were performed in duplicate.

3.3.Results

3.3.1. Human ASM cells did not express *CASR* or *ADORA2B*

We first investigated *CASR* and *ADORA2B* gene expression in ASM cells from healthy, mild asthma and severe asthma donors (**Table 3.1**). Untransfected FlpIn HEK293 TRex cells or FlpIn HEK293 cells stably transfected with the CaSR (HEK293-CaSR) were used as negative and positive controls, respectively. The adenosine A_2B receptor contributes to ASM relaxation, as described previously (Zhong et al., 2004), but its expression levels are lower than M_3 mAChR (Barnes, 2004b; Brown et al., 2008) so this qPCR assay was performed to validate detection of transcripts of a GPCR that is present but not expressed abundantly in human ASM cells.

As expected, abundant *CASR* mRNA expression was detected in HEK293-CaSR cells (**Figure 3.1**), demonstrating the integrity of the CaSR Taqman probes and that *CASR* mRNA was not degraded during the RNA extraction or RT-PCR experiments.

Only the #2724 cell line from a healthy donor demonstrated *CASR* mRNA expression at levels greater than those observed in untransfected HEK293 cells. Similarly, only minimal *ADORA2B* mRNA expression was detected in any of the ASM cell lines or in either the untransfected or transected HEK293 cells (**Figure 3.1**). Overall, our RT-qPCR data suggested minimal gene expression of either the *CASR* or *ADORA2B* in human ASM cells from healthy donors or donors with mild or severe asthma.

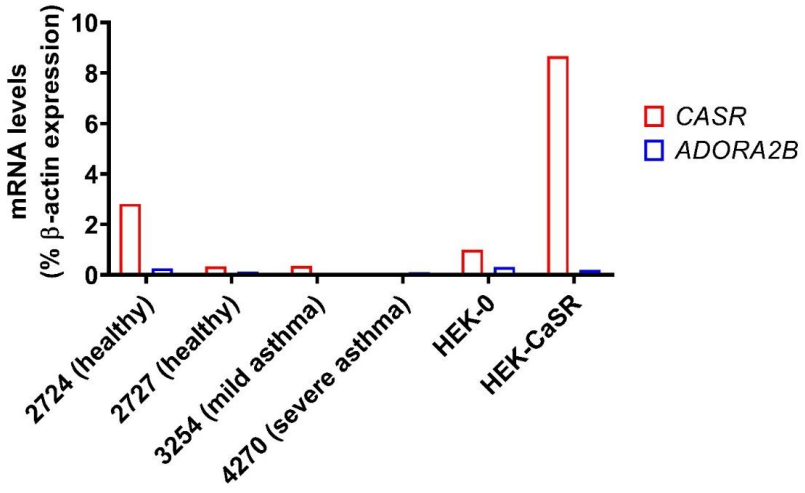

Figure 3.1. Human ASM cells demonstrate minimal *CASR* or *ADORA2B* gene expression. *CASR* and *ADORA2B* mRNA levels were normalised to β-actin in each sample using Equation 1. Data are expressed as mean from n=1.

3.3.2. Contractile stimuli induce variable Ca^{2+}_i mobilisation responses in ASM cells

We next investigated Ca^{2+}_i mobilisation in response to contractile mediators in human ASM cells, testing Ca^{2+}_o as a stimulus as well as spermine and MCh. Each mediator was tested at two different concentrations, based on their effective concentration ranges in studies performed in FlpIn HEK293-CaSR cells and mouse PCLS in Chapter 2.

The Ca^{2+}_i mobilisation responses induced by the higher concentrations of each agonist tested over 2 min are presented in **Figure 3.2** and the peak responses following drug additions at both concentrations are summarised in **Table 3.4**. The peak responses occurred ~30 sec following drug addition and responses returned to baseline within 2 min (**Figure 3.2**).

These data represent technical replicates performed in ASM from a subject without asthma (#2724) and four subjects with mild (#3205, #3226) or severe asthma (#4358, #4445). The average peak responses to ionomycin were less than 1.5- fold over basal in all samples (**Table 3.4**). However, there were considerable differences between some technical replicates, particularly in response to high Ca^{2+}_o in samples #3205 (mild asthma) and #4445 (severe asthma) (**Figure 3.2**).

To be more specific, in the healthy ASM cells (#2724), the responses to various agonists ranged from 1.1- to 1.4-fold over basal, with the highest responses seen in response to 10 mM Ca^{2+}_o (**Table 3.4**). Of note, one mild asthma ASM cell line (#3226) was more sensitive to contractile agonists compared to other cell lines, with 1.3- and 1.5-fold over basal responses to 10 µM MCh and 1 mM spermine, respectively. In terms of severe asthma ASM donors, the responses to various agonists were quite similar to the same agonist in different cell lines, with 1.1- to 1.2-fold over basal. However, one severe asthma ASM cell line (#4445) gave 1.4-fold over basal responses to 10 mM Ca^{2+}_o.

Since only a single experimental replicate was performed to measure Ca^{2+}_i mobilisation in response to MCh, spermine and Ca^{2+}_o for each ASM cell line, no further interpretation can be made on this limited data. Due to restrictions imposed by COVID-19-related lockdowns in Melbourne, there was insufficient time to continue with these studies in ASM cells during the course of this thesis, and further experiments were therefore discontinued.

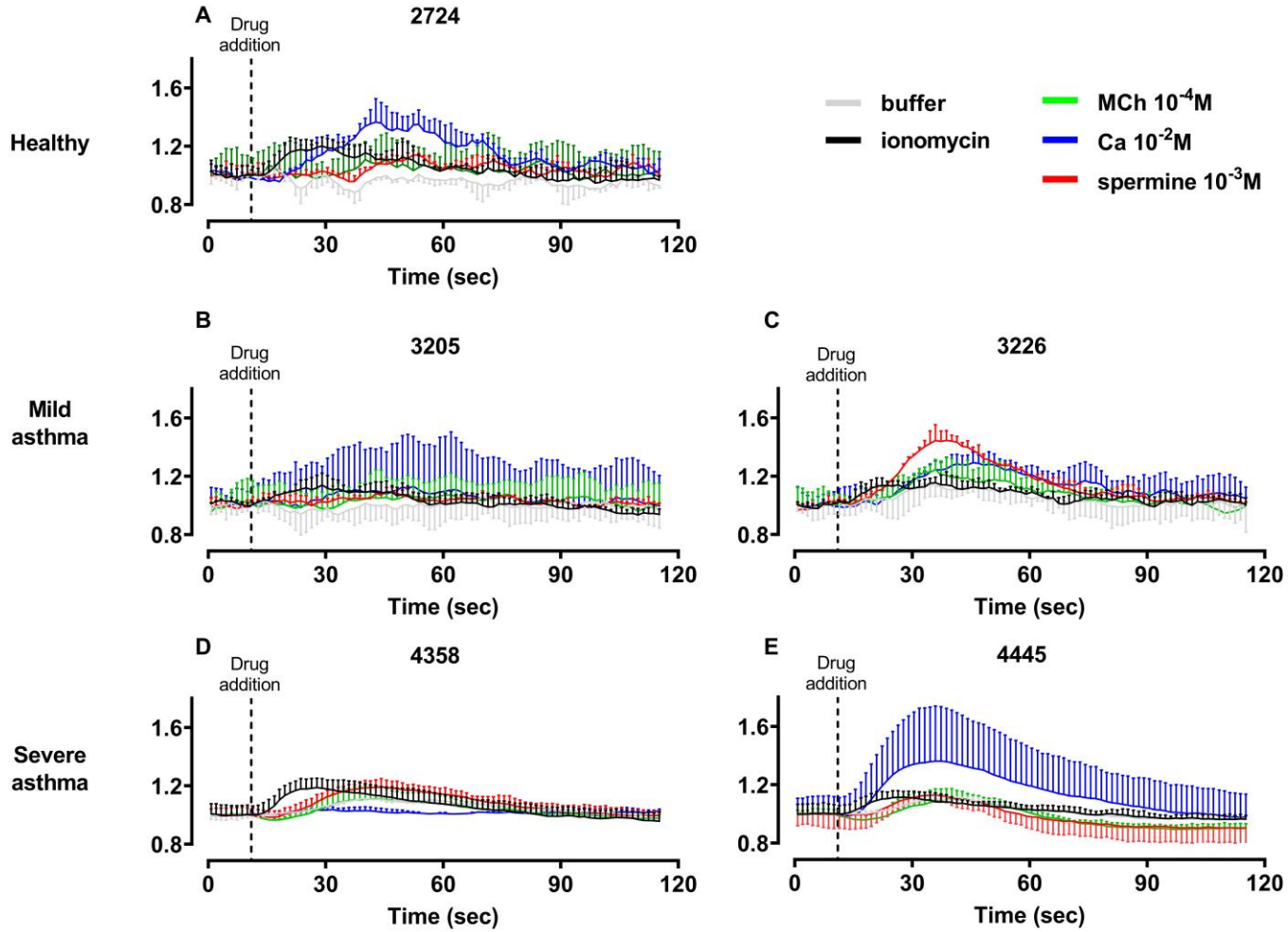

Figure 3.2. Contractile mediators stimulate $Ca^{2+}{}_i$ mobilisation in human ASM cells. The trace graphs of $Ca^{2+}{}_i$ mobilisation of **A)** healthy, **B**) & **C**) mild asthmatic, **D**) & **E**) severe human asthmatic ASM cells to various agonists. Responses after drug additions are expressed as the fold over the basal response prior to ligand addition. Data are mean± s.d. from technical duplicates.

Table 3.4. Peak Ca^{2+}_i mobilisation responses to contractile mediators in human ASM cells. Peak responses after drug addition are expressed as the fold over the basal response prior to ligand addition. Data are mean± s.d. from technical replicates.

	Cell line number	**Buffer**	**Spermine**		**MCh**		**Ca^{2+}_o**		**Ionomycin**
			10^{-4} M	10^{-3} M	10^{-5} M	10^{-4} M	10^{-3} M	10^{-2} M	10^{-6} M
Healthy	2724	1.08±0.02	1.12±0.05	1.15±0.02	1.13±0.07	1.13±0.11	1.08±0.05	1.39±0.09	1.21±0.04
Mild asthma	3205	1.07±0.07	1.08±0.01	1.10±0.02	1.09±0.03	1.10 ± 0.09	1.06±0.06	1.16±0.22	1.14±0.05
	3226	1.17±0.06	1.16±0.06	1.46±0.05	1.28±0.02	1.25±0.05	1.15±0.06	1.30±0.05	1.17±0.04
Severe asthma	4358	1.11±0.01	1.07±0.04	1.19±0.04	1.12±0.01	1.11±0.06	1.05±0.01	1.04±0.01	1.19±0.05
	4445	1.10±0.01	1.01±0.01	1.13±0.03	1.06±0.03	1.11±0.04	1.14±0.11	1.36±0.27	1.15±0.03

3.4 Discussion

The aim of the current study was to compare CaSR mRNA expression and Ca^{2+}_i mobilisation responses to ASM contractile mediators (MCh, spermine and Ca^{2+}_o) in human ASM cells from donors of varying health status; healthy, mild asthma or severe asthma. Collectively, we detected minimal CaSR and A2B receptor mRNA expression and variable Ca^{2+}_i mobilisation responses to these contractile mediators that were not related to asthma status.

We could not detect considerable *CASR* or *ADORA2B* gene expression in human ASM cells. These findings were not consistent with multiple studies that have validated *CASR* or *ADORA2B* mRNA expression in human ASM cells (Lazrak et al., 2020; Yarova et al., 2015; Zhong et al., 2004). A few possible explanations are discussed. First, *CASR* and *ADORA2B* gene expression could have been lost during passaging and maintenance of the cells in culture media. Previous studies that detected *CASR* or *ADORA2B* gene expression in human ASM cells used younger primary cells (passage number 2-4) compared to our study (passage number 7-8) (Yarova et al., 2015; Zhong et al., 2004). Second, multiple studies have evaluated poor correlations between mRNA and protein levels of GPCRs of interest (Koussounadis et al., 2015). Thirdly, different mRNA techniques could detect different levels of mRNA in the same sample (Sriram et al., 2019). Numerous techniques have been developed to measure mRNA levels of genes of interest, including TaqMan arrays and RNA sequencing (RNA-seq). However, when directly compared, these techniques detect significantly different mRNA levels of the same gene (Sriram et al., 2019) demonstrating differences in sensitivities. Therefore, we could apply more sensitive techniques to measure CaSR mRNA levels in the future.

Several *CASR* gene expression regulatory elements have been identified and could be used in the future to maintain *CASR* gene expression to detectable levels. These factors include vitamin D and IL-1β, a pro-inflammatory cytokine involved in asthma (reviewed in Hendy & Canaff, 2016; Schepelmann et al., 2016; Yarova et al., 2015). These regulatoy elements are present in *in vivo* systems but absent in the media used in this study.

Alternatively, we could also measure CaSR protein levels in addition to CaSR mRNA. Multiple studies have validated CaSR protein expression in human fetal and adult smooth muscle cells using immunofluorescence and western blot analysis of cell lysates and increased CaSR protein expression (Roesler et al., 2019; Yarova et al., 2015). Indeed, CaSR protein was detected in human ASM cells and also increased after treatment with TNF-α and IL-13 (Yarova et al., 2015).

We did detect Ca^{2+}_i mobilisation responses to the CaSR agonists Ca^{2+}_o and spermine, as well as the M3 agonist MCh, in human ASM cells. The reason for variable responses detected within some technical replicates for the same agonist tested in the same cell line is unclear. All cells were checked under a microscope after Ca^{2+}_i mobilisation assays and no abnormalities in cell phenotype, health or distribution of cell numbers in different wells were observed. All agonists stimulated responses that were approximately 1.2 to 1.5-fold above basal. Somewhat surprisingly, responses in each cell line to a single agonist were generally similar when comparing the low and high concentrations of MCh, spermine and Ca^{2+}_o, apart from two experiments (Ca^{2+}_o in a healthy cell line, spermine in a mild asthma line). Furthermore, there were no marked differences with asthma status when comparing Ca^{2+}_i mobilisation to the same agonist between different cell lines originating from healthy, mild asthma and severe asthma.

Although we did not validate M3 receptor expression, there was a detectable response to MCh in the Ca^{2+}_i mobilisation assays that was similar in healthy and asthmatic ASM. Increased M3 expression is not thought to contribute to AHR in asthma, but changes in downstream signalling have been implicated in increased contraction (Zaagsma et al., 1997). The current findings do not provide any evidence of increased Ca^{2+}_i mobilisation in response to MCh in human ASM with increased disease severity. Although a single study has reported increased Ca^{2+}_i oscillations in ASM from asthmatics (Sweeney et al., 2014), the current findings are consistent with another study which showed similar basal Ca^{2+}_i concentrations and no difference in bradykinin-stimulated increases in Ca^{2+}_i in ASM from subjects with and without asthma (Sweeney et al., 2015). The contribution of altered Ca^{2+} signalling to AHR remains an active subject of investigation.

Since only minimal *CASR* gene expression was detected in ASM cells, and protein expression was not measured, we could not define whether Ca^{2+}_i mobilisation in response to spermine were mediated via the CaSR. In the future, we could measure and compare responses to these agonists after pre-incubation with CaSR NAMs to validate CaSR-specific responses in human ASM cells. Future experiments should also involve elucidation of additional signalling pathways in human ASM, including $ERK_{1/2}$ phosphorylation, cAMP inhibition and accumulation. These pathways are potentially important in asthma pathophysiology, since cAMP has relaxant effects in ASM (Kume et al., 1994)., while phosphorylation of $ERK_{1/2}$ regulates ASM proliferation and hypertrophy (Pascual & Peters, 2005).

Overall, minimal *CASR* gene expression was detected in ASM, irrespective of asthma status, suggesting that further optimisation using more sensitive detection methods is required to explore the role of CaSR in asthma. Future experiments could also use asthma-relevant inflammatory cytokines to stimulate CaSR expression in culture. Until then, the contribution of CaSR to multiple processes contributing to altered airway structure and functions in asthma, and their potential targeting by CaSR NAMs, remains to be elucidated.

Chapter 4

Probing the binding and function of polyamines at the CaSR

4.1 Introduction

As described in chapter 1, the CaSR is a multimodal sensor that maintains diverse physiological functions. In addition to its primary physiological agonist, Ca^{2+}_o, the CaSR responds to a wide range of endogenous and exogenous ligands, including divalent and trivalent ions, L-amino acids, polyamines and pH. However, little is known about how many of the endogenous ligands of the CaSR interact with and activate the receptor; only Ca^{2+}_o and L-amino acid binding sites have been elucidated so far (Geng et al., 2016; Ling et al., 2021; Zhang et al., 2016). Major obstacles in understanding the molecular mechanisms of CaSR ligand binding and activation include a lack of high resolution full-length active-state CaSR structures, as well as difficulties in quantifying CaSR ligand binding and efficacy. The latter has hindered studies seeking to elucidate how agonist binding and efficacy are altered by amino acid substitutions, which are typically undertaken to probe the involvement of residues in receptor structure and function.

The full-length and ECD structures of the CaSR have been solved recently (Geng et al., 2016; Ling et al., 2021; Zhang et al., 2016). Similar to other class C GPCRs, the CaSR ECD is composed of two protomers, which each consist of three domains, lobe (LB) 1, LB2 and a cysteine rich domain **(**CRD; **Figure 4.1**). Activation of the CaSR stabilises large conformational changes in the CaSR ECD (Geng et al., 2016; Ling et al., 2021; Zhang et al., 2016). In the inactive state, the ECD protomers are in an "open" conformation (**Figure 4.1A**), while in the active state, both ECD protomers adopt a so-called closed conformation bound to agonist (closed-closed) (**Figure 4.1B**). The closed-closed state refers to the fact that LB1 and LB2 in both protomers are closed around a cleft, which in all other class C GPCRs is a conserved binding site for orthosteric agonists. However, in the CaSR, the cleft is an allosteric binding site for L-amino acids and other molecules (Geng et al., 2016; Zhang et al., 2016).

While structural studies indicate di- and trivalent cations bind to the CaSR VFT (Geng et al., 2016; Ling et al., 2021; Zhang et al., 2016), pharmacological studies have shown Ca^{2+}_o, Gd^{3+} and polyamines activate the CaSR in the absence of the ECD, demonstrating endogenous agonist binding sites outside the ECD (Leach et al., 2016; Ray & Northup, 2002). Similarly, a number of synthetic molecules bind in the 7TM and/or ECL domains of the CaSR (Josephs et al., 2019; Keller et al., 2018; Leach et al., 2016). The details of binding sites were discussed in Chapter 1 and are summarised in **Figure 4.1C**. In the structures of the ECD in isolation, four Ca^{2+}_o binding sites were discovered (sites 1-4; **Figure 4.1C**). Binding sites 1 and 2 were suggested to be high affinity sites because these sites were occupied by Ca^{2+}_o in the inactive

state, whereas sites 3 and 4 were only occupied in the active state (Geng et al., 2016). However, in the active-state full-length CaSR, only site 4 was occupied by Ca^{2+}_o as well as a fifth site in the ECD cleft (Ling et al., 2021). Given the differences in Ca^{2+}_o binding sites identified in different structures, it is unclear whether these sites are physiologically relevant or simply an artefact of the conditions used for structural determination. Efforts to validate these binding sites using mutagenesis relied on changes in agonist potency or E_{max} after mutation of amino acids suggested to contribute to Ca^{2+}_o binding (Geng et al., 2016; Zhang et al., 2016). However, changes in potency or E_{max} alone can reflect mutation-induced alterations in receptor expression, agonist efficacy or agonist affinity. Without delineation of these effects, none of the Ca^{2+}_o binding sites have been experimentally validated.

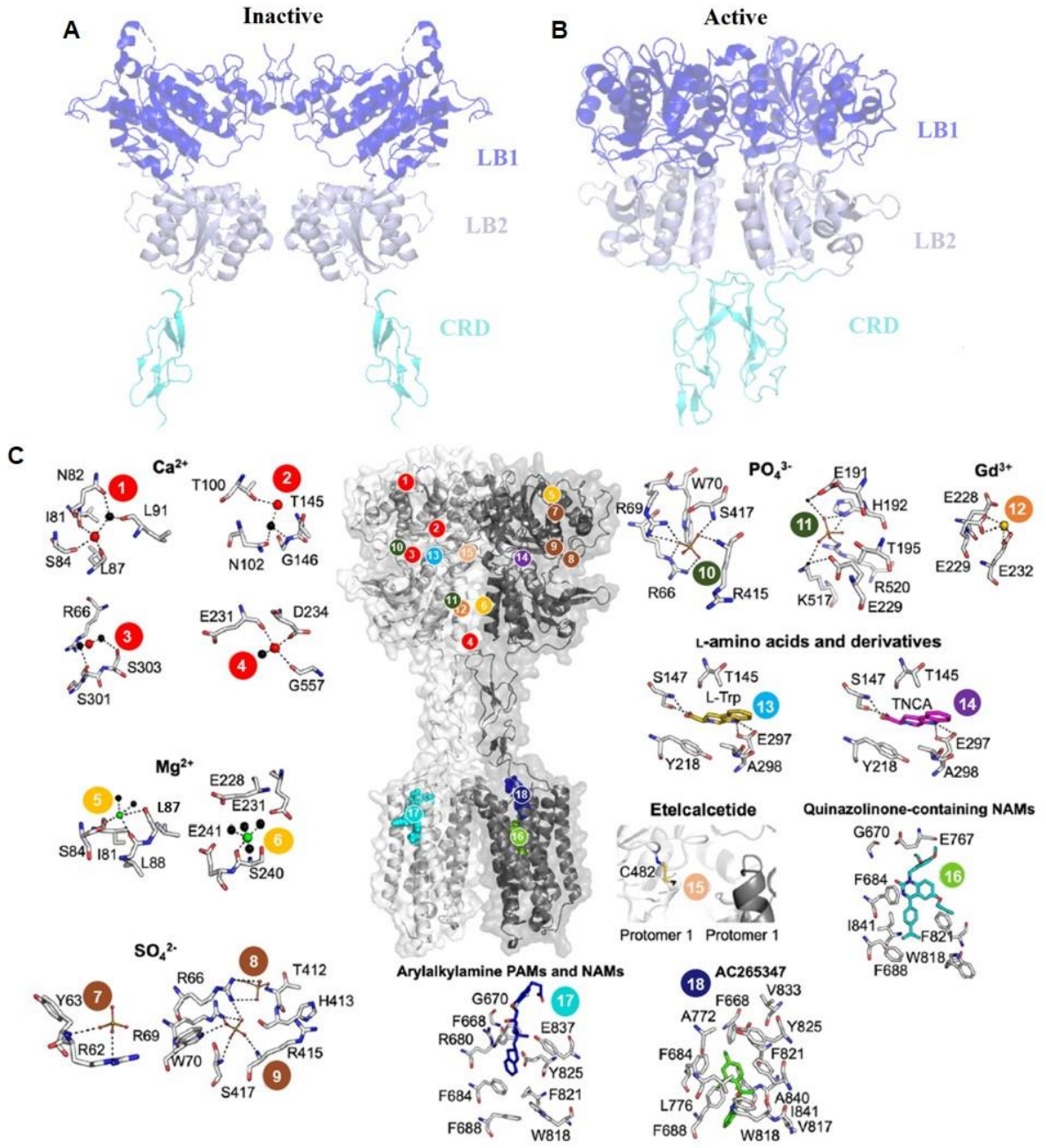

Figure 4.1. Structures of the CaSR ECD determined using x-ray crystallography. **A**) CaSR ECD inactive-state structure following ECD purification in the presence of 2 mM Ca^{2+}_o (PDB ID: 5k5t) **B**) CaSR ECD active-state structure following ECD purification in the presence of 10 mM Ca^{2+}_o and 10 mM L-Trp (PDB ID: 5k5s). Structures are shown in cartoon form (ligands not shown). The CaSR ECD is composed of two protomers that each consist of three domains: LB1 (blue), LB2 (grey) and CRD (cyan). **C**) CaSR ECD active-state structure (PDB: 5k5s) was superimposed onto a published model of the CaSR's 7TM (Josephs et al., 2019), ECLs and ICLs based on homology with the metabotropic glutamate receptor 5 crystal structure (PDB: 4OO9). Numbers correspond to ligand binding sites predicted as follows: Ca^{2+} (sites **1-4**), SO_4^{3-} (**7-9**), PO_4^{3-} (**12-13**) and L-Trp (**10**) by electron density distribution in the crystallised ECD (Geng et al., 2016); Mg^{2+} (**5-6**), Gd^{3+} (**15**) and TNCA (**11**) by electron density distribution in the crystallised VFT (Zhang et al., 2016); etelcalcetide (**14**) from mutagenesis and mass spectrometry (Alexander et al., 2015); AC265347 (**16**), quinazolinone-containing NAMs (**17**) and arylalkylamine PAMs and NAMs (**18**), from mutagenesis combined with homology modelling and computational docking (Josephs et al., 2019). Panel C is adapted from (Diao et al., 2021).

In addition to the aforementioned shortcomings in validating Ca^{2+}_o binding sites, little is known about the location of polyamine binding sites in the CaSR, or how polyamines activate the CaSR. Polyamine and CaSR expression are upregulated in asthma, and inhibition of CaSRs in the lungs attenuates airway hyperresponsiveness, airway inflammation and remodelling in murine asthma models (Kurosawa et al., 1992; Lee et al., 2017; North et al., 2013; Thompson et al., 2016; Yarova et al., 2015), suggesting blockade of CaSR activation by polyamines may be beneficial in asthma. Therefore, understanding how polyamines bind to and activate the CaSR will inform future drug discovery efforts seeking to disrupt the polyamine-CaSR interaction in asthma.

Herein, we undertook a structure-function approach combining mutagenesis, cellular assays (Ca^{2+}_i release) and analytical pharmacology (**Figure 4.2**), to probe how different CaSR residues affect the binding of, and activation by, polyamines and Ca^{2+}_o. Since there are no commercially available radioligands for the CaSR, we measured Ca^{2+}_i mobilisation in response to agonists and quantified agonist affinity and efficacy using an operational model of agonism called the cooperative agonist operational model (Gregory et al., 2020). The cooperative agonist operational model is based on the operational model of agonism postulated by Black and Leff (1983) (referred to herein as the Black and Leff operational model of agonism). The Black and Leff operational model of agonism assumes agonist-receptor interactions are governed by the law of mass action, i.e. the rate at which drug-receptor complexes form is dependent on the ligand concentration, the number of unoccupied receptors, and the association rate constant (K_{on}). If complex formation is reversible, the ligand-receptor complex dissociates into free receptor and ligand, which is dependent on the concentration of ligand-receptor complexes and the dissociation rate constant (K_{off}). The Black and Leff operational model of agonism dictates that agonist responses are governed by agonist affinity (equilibrium dissociation constant, K_A) and agonist efficacy in a given system (transducer ratio, τ; a ratio of the total receptor number and a transducer parameter that defines the avidity with which a given agonist-occupied receptor complex promotes the final observed pharmacological effect), which accounts for both the intrinsic efficacy of an agonist and tissue-specific factors that influence the sensitivity of the response, such as receptor expression (**Figure 4.2**). When receptor expression levels are high, there is an increase in the number (but not proportion) of agonist-receptor complexes that form compared to when expression levels are low. Therefore, in high expressing systems, agonist responses are enhanced, and lower agonist concentrations are required to elicit such responses, resulting in: 1) an upward shift of the maximum asymptote of the agonist

concentration-response curve until the maximum system response (E_m) is reached; and 2) a leftward shift in the agonist concentration-response curve because E_m is achieved at submaximal receptor occupancy. The latter scenario is referred to as receptor reserve. When receptor reserve is high and an agonist stimulates E_m (i.e. the agonist is a full agonist), τ can only be calculated if K_A is known. One means to calculate τ for a full agonist using the operational model of agonism is to fix K_A determined, for example, in a radioligand binding assay, thus enabling determination of the extent to which agonist potency (EC_{50}) deviates from K_A. Alternatively, receptor expression levels may be titrated down to diminish receptor reserve and convert a full agonist to a partial agonist, where EC_{50} approaches K_A and both τ and K_A can be calculated from the maximum agonist response relative to E_m and from the agonist EC_{50}. (**Figure 4.2**).

The Black and Leff operational model of agonism can be used to analyse both rectangular hyperbolic or non-hyperbolic concentration-response curves that are normally empirically characterised by Hill slopes that are equal to or different from unity, respectively. Therefore, the operational model of agonism can be used to characterise agonist actions at the CaSR, which have steep concentration-response curves. However, the Black and Leff operational model assumes that the steepness of the agonist response curve is due to post-receptor mechanisms that transduce agonist responses, and that the initial agonist binding event follows a simple one-to-one agonist-receptor binding interaction. In this instance, steep agonist concentration-response curves are described by a transducer function, nT. However, for the CaSR, steep concentration-response curves are presumed to arise from the binding of multiple agonist molecules in a positive cooperative manner. As such, our lab developed and validated a "cooperative agonist operational model" that accounts for orthosteric agonist binding to multiple sites in a cooperative manner (Gregory et al., 2020). In the cooperative agonist operational model, steep agonist concentration-response curves are described by a binding function, nB. The development and validation of this model is described in detail in Appendix 2, but the same principles can be applied to calculate agonist efficacy and affinity as are used for the Black and Leff operational model of agonism.

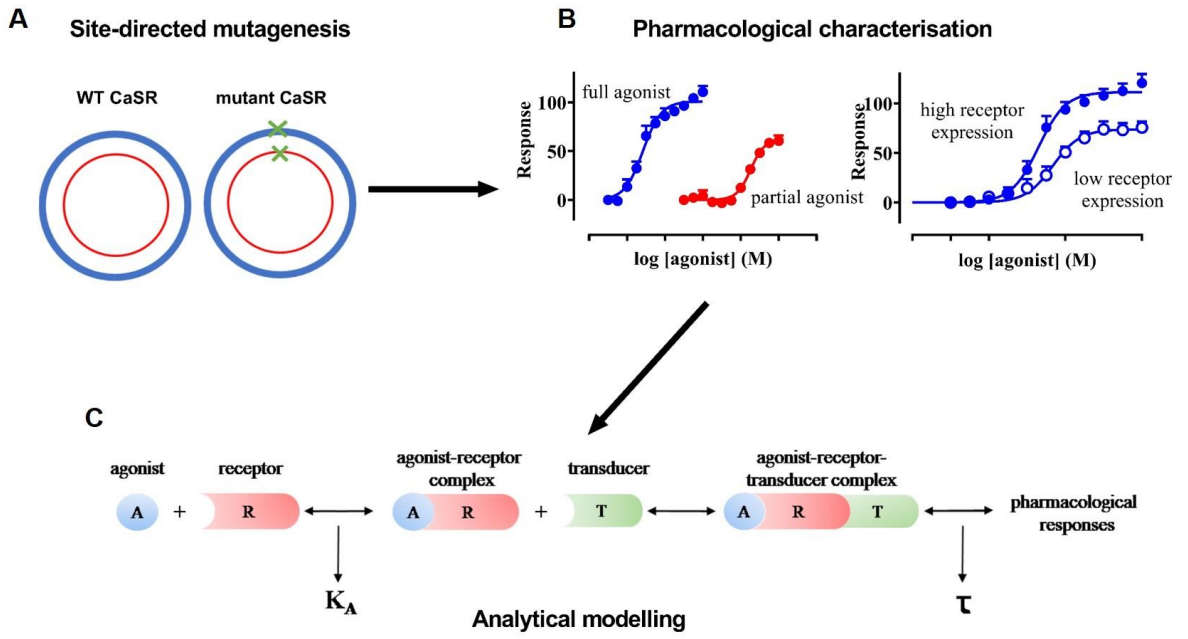

Figure 4.2. Schematic outline of the structure-function approach to quantify agonist binding and function, with a combination of **A**) site-directed mutagenesis, **B**) pharmacological assays and **C**) analytical modelling. Agonist-receptor complex is driven by K_A in the operational model of agonism and the response mediated by this complex is governed by transducer effector, **τ**, taken account into receptor expression and efficacy of agonist.

In the present study, we used FlpIn HEK293 TREx cells stably transfected with WT and mutant CaSRs to quantify the effects of single amino acid substitutions on receptor expression, and on polyamine and Ca^{2+}_o affinity and efficacy. The HEK293 TREx system is a tetracycline-inducible expression system that allowed us to titrate receptor expression levels down to calculate the affinity and efficacy of agonists that were full-agonists when receptor expression levels were maximally induced. Comparison of agonist affinity and efficacy at WT versus mutant CaSRs established residues that contribute to the binding or signalling of CaSR agonists, thus unravelling agonist binding and activation residues.

4.2 Methods

4.2.1. Reagents

The following materials were purchased: Dulbecco's Modified Eagle's medium (DMEM) and fetal bovine serum (FBS; Sigma Aldrich, St Louis, USA); hygromycin B (Roche, Mannheim, Germany); tetracycline (tet; dissolved in 100% ethanol, stored at 3mg/mL at -20°C), FlpIn HEK293 TRex Cells (Human Embryonic Kidney 293-Tet Regulated Expression), poly-D-lysine (PDL) and blasticidin HCl (Invitrogen, Carlsbad, USA); Fluo-4-AM (Molecular Probes, Eugene, USA) and Fluo-8-AM (Abcam, Cambridge, United Kingdom); ionomycin (Sigma Aldrich, St Louis, USA).

4.2.2. Molecular biology

Protocols for the generation of c-myc-tagged CaSR DNA in pcDNA^{TM}5/frt/TO and FlpIn HEK293 Trex cell lines expressing the cmyc-tagged CaSR have been described previously (Davey et al., 2012; Leach et al., 2016). C-myc-tagged CaSR or c-myc-tagged N-terminally truncated CaSR were subjected to Quikchange® II site-directed mutagenesis (Agilent Technologies) according to the manufacturer's instructions. Primers for mutagenesis are listed in **Table S1**. Briefly, 2 ng of template c-myc-tagged CaSR DNA in pcDNA^{TM}5/frt/TO was incubated with 2 µM of primer (both sense and anti-sense), Pfu Ultra II HF HS Phusion, 1 µL of Pfu reaction buffer, 0.2 µM of free nucleotides (dNTPs), 0.25 µL of DMSO in a final volume of 10 µL with MilliQ water. Solutions were heated at 60 °C for 30 sec and 68 °C for 6 min for 10 cycles, then heated at 95 °C for 30 sec (to allow primer denaturation), 55 °C for 1 min and 68 °C for 6 min for 10 cycles.

To amplify the DNA constructs, 2 µL of mutated DNA was added to 30 µL of competent bacterial cells and placed on ice for 20 min. Competent cells were then heat shocked at 42 °C for 30 sec. Cells were added to 150 µL Luria-Bertani medium (LB; 10 g peptone 140, 5 g/L yeast extract, 5g/L NaCl) and incubated at 37 °C for 30 min. Cells were then evenly spread onto LB-agar (LB with 12g/L Agar) containing carbenicillin (100 µg/mL) and incubated at 37 °C overnight. A single bacterial colony was picked and transferred to 5 mL LB containing 50 µg/mL ampicillin, incubated for overnight. The bacterial culture was harvested after 16-20 hr. DNA was extracted from the culture using the Promega Wizard Plus SV Miniprep DNA

purification System following the manufacturer's instructions. All constructs were sequenced to verify their integrity and accuracy.

4.2.3. Cell culture

4.2.3.1. Generation of stable cell lines

FlpIn HEK293 Trex cells were allowed to grow to 70% confluency in T25 cm^2 flasks in DMEM containing 5% FBS. On the day of transfection, 5 µg DNA and lipofectamine 2000 or polyethylenimine (PEI) were added to the cells using a ratio of 1:4. Twenty-four hours following transfection, cells were detached and transferred to a T75 cm^2 flask, and one day after, cell media was changed to DMEM with 5% FBS, 200 µg/ml hygromycin B and 5 µg/ml blasticidin S HCl. Selection media was changed every 2-4 days if necessary, for 3-4 weeks.

4.2.3.2.Maintenance of cells

FlpIn HEK293 Trex cells transfected with either WT or mutated CaSR were selected and maintained in DMEM, 5% FBS, 5 µg/mL blasticidin and 200 µg/mL hygromycin B at 37°C in a humidified atmosphere of 5% CO_2, 95% O_2. Cells were passaged every 3-4 days up to passage number 30. Cells were detached from tissue culture flasks using PBS supplemented with 2 mM EDTA. Cells were centrifuged at 350 x *g* for 3-10 min, re-suspended in media and reseeded into T175 cm^2 flasks at a dilution of between 1:20 and 1:2.

4.2.3.3. Freezing and thawing cells

Cells were expanded into 6x 175 cm^2 flasks and upon reaching 70% confluence were harvested with 2 mM EDTA-supplemented PBS and centrifuged at 350 x *g* for 5 min. Cells were re-suspended in 4 mL freezing solution (pre-cooled to 4°C, 50% FBS, 45% DMEM, 5% DMSO) and 400 µL aliquots were dispensed into 10x cryo-vials. Cryo-vials containing cells were placed in an isopropanol bath at -80°C for at least 24 hours before transfer to liquid nitrogen tanks or a vapour phase nitrogen storage system.

For thawing cells, cells were bought up from storage by rapid defrosting at 37°C and immediately transferred into a 75 cm^2 flask containing DMEM supplemented with 10% FBS. Cells were allowed to adhere and grow for a minimum of seven days prior to use in assays.

4.2.4. Cell seeding for Ca^{2+}_i mobilisation and flow cytometry assays

For Ca^{2+}_i mobilisation assays, prior to seeding cells, plastic plates were coated with PDL to allow for sufficient cell adherence. 96-well plates (0.92 cm^2/well) were coated with 32-50 µL 50 µg/mL PDL (stored for up to eight weeks at 4°C) for at least 15 min followed by 1x wash with 50 µL PBS. For flow cytometry assays, cells were seeded into uncoated plates. 50 µl media with or without tetracycline (10-100 ng/ml) were added to wells. Cells were harvested, centrifuged, and re-suspended in DMEM containing 5% FBS. Cells were then seeded into 96-well plates at a density of 80,000 cells/well (100 µL per well) and incubated overnight.

4.2.5. Flow cytometry for cell-surface c-myc-CaSR expression

On the day of the experiment, media was aspirated, and cells were harvested with 50 µL 2mM EDTA in PBS. Cells were transferred to a V-bottom shaped 96 well plate and centrifuged for 3 min at 350 *x g* and 4°C. EDTA/PBS was removed, and cells were re-suspended in 50 µL blocking buffer (137 mM NaCl, 2.7 mM KCl, 4.3 mM Na_2HPO_4, 1.5 mM KH_2PO_4, 10 % bovine serum albumin (BSA)) containing 1 µg/µL mouse 9E10 anti-c-myc antibody conjugated to AF647, and incubated on ice for 30 min, away from light. Following centrifugation (at 350 *x g* and 4°C) and removal of the primary antibody, cells were re-suspended in 200 µL wash buffer (137 mM NaCl, 2.7 mM KCl, 4.3 mM Na_2HPO_4, 1.5mM KH_2PO_4, 5% BSA) and centrifuged for 3 min at 350 x *g* and 4°C. Cells were then re-suspended in 200 µL wash buffer containing 1 µg/mL propidium iodide (PI). Following centrifugation and 1x wash with washing buffer, cells were transferred to filter-top tubes in a final volume of 400 µL wash buffer. Only live cells were gated and analysed and fluorescence was quantified using a BD FACS Canto II. Data was analysed using FlowJo to determine the mean AF647 fluorescence per live cell.

4.2.6. Ca^{2+}_i mobilisation assays

Assays were performed in an isotonic buffer consisting of 150 mM NaCl, 2.6 mM KCl, 0.1 mM $CaCl_2$, 1.18 mM $MgCl_2$, 10 mM D-glucose, 10 or 25 mM HEPES, 4 mM probenecid and 0.5% w/v BSA, pH 7.4. Assay buffer was prepared as a 10x stock (without probenecid or BSA). A 1x stock (500 mL) of assay buffer was prepared by adding 50 mL 10x stock, 2.5 g BSA and 5 mL of 400 mM probenecid (dissolved in 1 M NaOH) to 450 mL MQ, and pH adjusted to 7.4 with 1 M HCl or 1M NaOH. Cells were washed with 100 µL assay buffer before being loaded with 50 µL assay buffer containing 1 µM Fluo-4-AM or Fluo-8-AM. After one-hour incubation at 37°C in a humidified atmosphere of 5% CO_2, 95% CO_2, Fluo-4-AM or Fluo-8-AM containing buffer was removed and 90 µL assay buffer added into each well. Ligands were added on a Flexstation 1 or 3 microplate reader (Molecular Devices; Sunnyvale, California). Peak fluorescence within 30 sec was detected using 485 nm excitation and 525 nm emission filters. Results were normalised to the response to 1 µM ionomycin.

4.2.7. Data analysis

For Ca^{2+}_i mobilisation assays, data from individual experiments were fitted to a four-parameter Hill equation (equation 1) or to a cooperative agonist operational model of agonism (equation 2) (Gregory et al., 2020) using Graphpad Prism 8.0.2. Data are represented as mean ± s.e.m of the stated number (n) of experiments performed in duplicate.

Equation 1.

$$\text{Effect}=\text{basal}+\frac{(\text{Emax}-\text{basal})\ \text{x}\ [A]^{nH}}{A^{nH}+EC50^{\text{nH}}}$$

Where [A] is the agonist concentration, basal is the response in the absence of agonist, nH is the hill slope and EC_{50} is the concentration of agonist, A, that gives the mid-point response between basal and E_{max}, which are the lower and upper asymptotes of the response, respectively.

Equation 2.

$$\text{Effect}=\frac{Em\ \tau A^{nT}[A]^{nBnT}}{\tau A^{nT}[A]^{nBnT}+([A]^{nB}+KA^{nB})^{nT}}$$

Where [A] is agonist concentration, K_A is the agonist equilibrium dissociation constant; τ_A is the agonist efficacy; E_m is the maximal system response and was determined from the response to Gd^{3+} at the WT or headless CaSR; *nT* is the logistic transducer function linking agonist concentration to response and was fixed to 1; *nB* is the slope of agonist binding linking agonist concentration to occupancy. An F-test was performed to determine whether equation 1 or 2 was fitted best to the grouped data when nH in equation 1 or nB in Equation 2 was the same or differed between agonists at each mutant and WT CaSR. Statistical differences in pK_A and $log\tau_A$ between WT and mutant CaSR were determined via a one-way ANOVA followed by Dunnett's post-test, where significance was defined as $P<0.05$.

For FACS analysis, statistical differences between the expression levels of the WT versus mutant receptors were determined by the 95% confidence interval (CI), where only CIs excluding 100% were considered significant.

4.3 Results

4.3.1. Rationale for location of mutations

Mutations were introduced at residues predicted to contribute to: **i**) polyvalent ion binding sites in the VFT: Ca^{2+}_o (I81, S84, T100, N102, E231, D234, S303), Mg^{2+} (I81, S84, E228, E231, E241), Gd^{3+} (E228, E232), L-Trp (S170) (Geng et al., 2016; Zhang et al., 2016); and ii) 7TM and ECL small molecule allosteric binding pocket residues: F668$^{2.56}$A, F684$^{3.36}$A, F688$^{3.40}$A, E767^{ECL2}A, E837$^{7.32}$I, I841$^{7.36}$A, in an N-terminally truncated CaSR otherwise known as the headless CaSR (Leach et al., 2016) in addition to other 7TM or ECL residues such as S750^{ECL2}A, R752^{ECL2}A, Q754^{ECL2}A, E755^{ECL2}A, I760^{ECL2}A, I761^{ECL2}A, to remove potential compensatory effects of the presence of primary binding sites in the VFT (**Figure 4.1C**).

4.3.2. CaSR mutations alter cell surface expression

First, the effects of amino acid substitutions on CaSR cell surface expression were investigated. While the majority of amino acid substitutions in the VFT had no effect on surface expression (**Figure 4.3A & Table 4.1)**, five out of thirteen mutations altered receptor expression, four of which were located on the top of LB1 (I81A and S84A) or on the bottom of LB1 (T100A, N102A and S170A). In contrast, mutations in LB2 did not affect receptor expression (**Figure 4.3A & Table 4.1**). Among all VFT mutants, I81A and T100A were expressed at the lowest level at 8±1% and 10±10% of the WT CaSR, respectively. These data suggest that amino acids on the top or bottom of LB1 are critical for receptor expression.

For analysis of 7TM and ECL mutants, we used a "headless" CaSR that lacked its entire ECD. F668$^{2.56}$A and I841$^{7.36}$A mutations almost abolished headless CaSR cell surface expression (**Figure 4.3B & Table 4.2**). F688$^{3.40}$A, I760^{ECL2}A, E767^{ECL2}A and E837$^{7.32}$I mutations significantly reduced receptor expression levels, whereas the other 7TM or ECL mutants had no effect on headless CaSR expression (**Figure 4.3B & Table 4.2**). These results suggest that some amino acids in the ECL and 7TM are important for receptor expression.

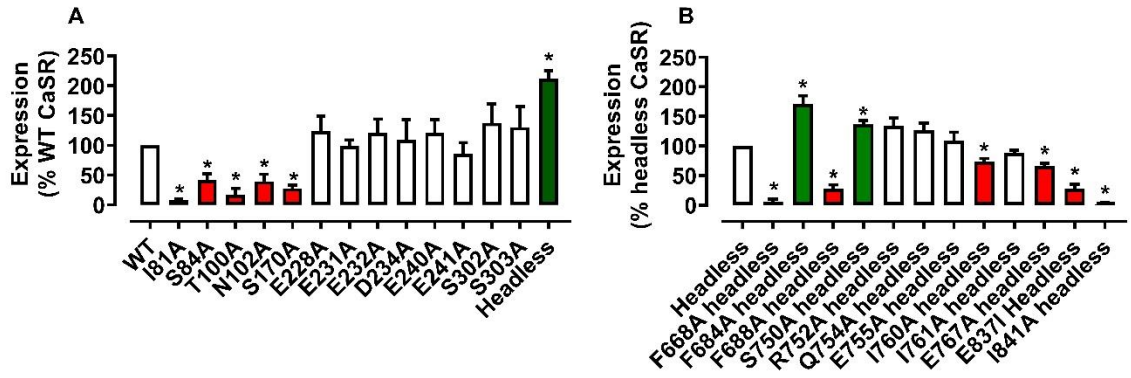

Figure 4.3. Cell surface expression of A) VFT mutants and headless CaSR compared to WT CaSR (represented as % WT CaSR); B) ECL and 7TM headless mutants compared to headless CaSR. Red or green bar = 95% CI excluding 100%, *significantly different to WT or headless CaSR, white bar = not significant. Data are mean ± s.e.m from 3-14 independent experiments.

Table 4.1. WT and VFT mutant expression levels determined in FACs experiments. Data are mean ± s.e.m from the indicated number of experiments (n). Expression levels are represented as a percentage of WT CaSR. *95% CI excluding 100% were considered significant.

Full length WT or mutant	Expression (% WT CaSR)	n	Full length mutant	Expression (% WT CaSR)	n
WT	100	21	**E231A**	99±10	3
I81A	8±1*	5	**E232A**	121±23	5
S84A	42±10*	5	**D234A**	110±24	4
T100A	10±10*	5	**S240A**	121±23	4
N102A	53±5*	5	**E241A**	86±19	6
S170A	28±6*	7	**S302A**	138±32	5
E228A	124±26	5	**S303A**	138±32	5
Headless	212±13*	11			

Table 4.2. Headless and headless mutant expression levels determined in FACs experiments. Data are mean ± s.e.m. from the indicated number of experiments. Expression levels are represented as a percentage of N-terminally truncated CaSR. *CI excluding 100% were considered significant.

Headless or headless mutant	Expression (% headless CaSR)	n	Headless mutant	Expression (% headless CaSR)	n
Headless	100	14	**E755^{ECL2}A headless**	109±14	7
F668$^{2.56}$A headless	5±5*	3	**I760^{ECL2}A headless**	74±5*	6
F684$^{3.36}$ headless	171±14*	6	**I761^{ECL2}A headless**	89±4	7
F688$^{3.40}$A headless	28±7*	7	**E767^{ECL2} headless**	66±5*	8
S750^{ECL2}A headless	137±6*	7	**E837$^{7.32}$I headless**	28±7*	5
R752^{ECL2}A headless	134±13	7	**I841$^{7.36}$A headless**	2±2*	3
Q754^{ECL2}A headless	127±11	7			

4.3.3. Polycations stimulate Ca^{2+}_i mobilisation via the CaSR

The concentration-response profiles of polycations in Ca^{2+}_i mobilisation assays were first characterised at the WT CaSR. All agonists stimulated a concentration-dependent increase in Ca^{2+}_i mobilisation in HEK293-CaSR cells, whereas none of the agonists stimulated a significant response in non-transfected HEK293 cells (**Figure 4.4A & B**). Data were analysed using Equation 1 to quantify agonist Hill slopes, potencies (pEC_{50}) and maximum responses (E_{max}). Gd^{3+} and spermine were the most potent agonists sharing similar potencies, whereas putrescine was the least potent agonist, being 40-fold less potent than Gd^{3+} or spermine (**Table 4.3**). Gd^{3+}, Ca^{2+}_o, spermidine and spermine were full agonists with maximum responses close to 100% of the ionomycin response (**Table 4.3**). Putrescine and agmatine were partial agonists, inducing 60% or 84% of the ionomycin response, respectively (**Table 4.3**). When Equation 1 was fitted to agonist-mediated stimulation of Ca^{2+}_i mobilisation, an F-test established the Hill slope was not significantly different between agonists at the WT CaSR, which was 2.3±0.1. Such steep Hill slopes suggest polyamines bind to multiple sites at the WT CaSR, similar to Ca^{2+}_o and Gd^{3+}.

We next sought to fit Equation 2 to agonist concentration-response data at the WT CaSR to derive agonist pK_A and $log\tau_A$ values. Equation 2 was fitted to putrescine and agmatine concentration-response data to quantify partial agonist affinity and efficacy, where the maximal

response to Gd^{3+} was used to define the maximum system response (E_m). Since Ca^{2+}_o, Gd^{3+}, spermidine and spermine were full agonists at the WT CaSR, thus preventing determination of pK_A, we took advantage of the tetracycline-inducible HEK293 TRex system and titrated receptor expression levels by exposing cells to different tetracycline concentrations (0-30 ng/mL) (**Figure 4.5)**. Equation 2 was subsequently fitted to agonist concentration-response data under high (100 ng/ml tetracycline) and low (0-30 ng/ml tetracycline) expression conditions to derive Ca^{2+}_o, Gd^{3+}, spermidine and spermine pK_A and $log\tau_A$ values. This analysis demonstrated that the affinity and efficacy of polycations varied widely (**Table 4.3**). The rank pK_A order was as follows (from low to high): putrescine < agmatine = spermidine < Ca^{2+}_o < spermine = Gd^{3+} and the rank order of agonist efficacies under the highest expression level induced by 100 ng/mL tetracycline was: putrescine < agmatine = spermidine < spermine = Ca^{2+}_o < Gd^{3+} (**Table 4.3**). Spermine had the highest efficacy and affinity among the polyamines, with values 3- and 20-fold higher than putrescine, respectfully (**Table 4.3**).

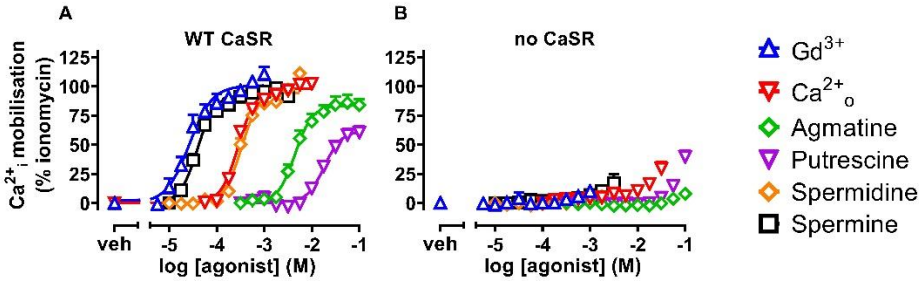

Figure 4.4. Polycations stimulate Ca^{2+}_i mobilisation in FlpIn HEK293 TREx cells stably expressing the WT CaSR, but do not stimulate responses in non-transfected FlpIn HEK293 TREx cells. A) FlpIn HEK293 TREx cells were stably transfected with WT CaSR. B) FlpIn HEK293 TRex cells were non-transfected. Data are mean ± s.e.m. from 4-6 pooled independent experiments performed in duplicate. Curves through the data points are the best fit of Equation 2 to the grouped data.

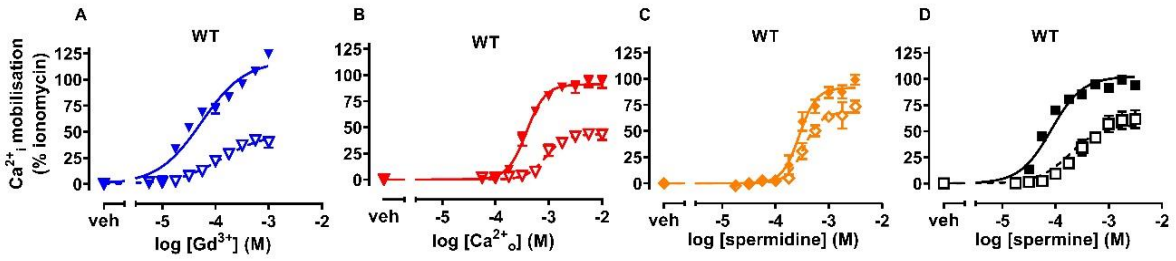

Figure 4.5. Polycation concentration-response curves at the WT CaSR upon titration of receptor expression. FlpIn HEK293 TREx cells were pre-incubated with different concentrations of tetracycline overnight and then treated with A) Gd^{3+}, B) Ca^{2+}_o, C) spermidine, or D) spermine. Closed symbol = 100 ng/mL tetracycline, open symbol=0-30 ng/mL tetracycline. Data are mean ± s.e.m. from 4 independent experiments performed in duplicate. Curves through the data points are the best fit of Equation 2 to the grouped data.

4.3.4. Polycations stimulate Ca^{2+}_i mobilisation via VFT and 7TM residues

Next, we aimed to investigate whether polycations bind to and signal through both the extracellular and 7TM domains of the CaSR. Previous studies suggest that Ca^{2+}_o, Gd^{3+} and polyamines bind to both regions (Geng et al., 2016; Leach et al., 2016; Ray & Northup, 2002). To address this, the headless CaSR was used to assess polycation responses in the absence of the CaSR ECD. When headless CaSR expression was maximally induced with 100 ng/ml tetracycline, all polycations except putrescine stimulated Ca^{2+}_i mobilisation via the headless CaSR (**Figure 4.6)**. The complete loss of response to putrescine was due to either reduced affinity or efficacy.

Next, CaSR agonist potencies, E_{max}, affinities and efficacies at the headless CaSR were quantified using Equations 1 and 2. In contrast to the WT CaSR, an F-test determined that Hill slopes were not significantly different to unity and shared among all agonists, demonstrating a significant reduction in Hill slope at the headless CaSR compared to at the WT CaSR (**Table 4.3**). Gd^{3+} stimulated responses at the headless CaSR significantly higher than responses at the full-length WT CaSR (**Table 4.3**), whereas the other agonists that were full agonists at the WT CaSR (i.e., spermidine, spermine and Ca^{2+}_o) were partial agonists compared to Gd^{3+} at the headless CaSR, stimulating only 50-70% of the ionomycin response **(Table 4.3 & Figure 4.4C)**. The response to agmatine was also reduced by 40% after removal of the N-terminus **(Table 4.3 & Figure 4.4C)**. Equation 2 was fitted to partial agonist concentration-response data to quantify agonist affinity and efficacy, where the maximal response to Gd^{3+} was used to define the maximum system response (E_m). All partial agonists except agmatine had reduced affinity at the headless CaSR (**Table 4.3**). For instance, the affinity of Ca^{2+}_o was reduced 10-fold and spermine 3-fold after the removal of the CaSR N-terminus (**Table 4.3**). Further, binding slopes (nB) were not significantly different to unity for all agonists (F-test), indicating a loss in positive cooperativity between agonist binding sites upon removal of the N-terminus. These findings suggest that CaSR agonists likely bind to both the CaSR VFT and 7TM.

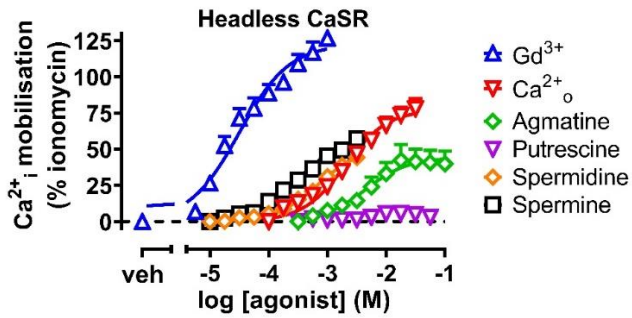

Figure 4.6. Polycations stimulate Ca^{2+}_i mobilisation at the headless CaSR. FlpIn HEK293 TREx cells were stably transfected with the headless CaSR. Data are mean ± s.e.m. from 6 independent experiments performed in duplicate. Curves through the data points are the best fit of Equation 2 to the grouped data.

Table 4.3. Hill slope (nH), potencies (pEC_{50}), maximum response (E_{max}) as a % of ionomycin, functional affinity (pK_A) and efficacy ($log\tau_A$) for polycations at WT and headless (ΔH) CaSRs determined in $Ca^{2+}{}_i$ mobilisation assays. Data are represented as mean ± s.e.m. from n=4-6 independent experiments performed in duplicate and analysed via one-way ANOVA followed by Dunnett's post-test compared with WT CaSR value, *P<0.05, **P<0.01, ***P<0.001. $^{\#}$nH is not significantly different from unity, determined by F-tests. NR denotes no response.

	Gd^{3+}		$Ca^{2+}{}_o$		Agmatine		Putrescine		Spermidine		Spermine	
	WT	ΔH	WT	ΔH	WT	ΔH	WT	ΔH	WT	ΔH	WT	ΔH
pEC_{50}	4.61±0.03	4.51±0.08	3.56±0.02	2.52±0.18	2.35±0.03	2.37±0.14	1.75±0.04	NR	3.45±0.01	3.07±0.20	4.51±0.02	3.35±0.12
nH	2.3±0.1	1.0$^{\#}$	2.30±0.12	1.0$^{\#}$	2.30±0.12	1.0$^{\#}$	2.30±0.12	NR	2.30±0.12	1.0$^{\#}$	2.30±0.12	1.0$^{\#}$
E_{max}	98±2	123±6 *	97±1	82±7	84±3	43±5****	61±3	NR	98±4	56±1 **	120±3	63±6**
pK_A	3.62±0.14	ND	3.07±0.05	1.93±0.09 **	1.93±0.04	2.07±0.01	1.59±0.03	NR	3.32±0.05	2.70±0.03 **	3.80±0.04	3.21±0.01**
$Log\tau_A$	0.94±0.10	ND	0.56±0.04	0.21±0.09 ***	0.85±0.08	-0.34±0.08**	0.12±0.03	NR	0.48±0.05	0.09±0.19**	0.66±0.05	0.11±0.15*
nB	2.4±0.1	1.0±0.1	2.4±0.1	1.0±0.1	2.4±0.1	1.0±0.1	2.4±0.1	NR	2.4±0.1	1.0±0.1	2.4±0.1	1.0±0.1

4.3.5. VFT and 7TM mutations alter polycation pEC_{50}, maximum responses and nH

Having established that spermidine, spermine and Ca^{2+}_o signal through both the CaSR ECD and ECLs/7TM domains, we sought to determine amino acid residues in these domains that contribute to polycation binding and signaling. We focused on key residues previously identified to be important for the binding or function of Ca^{2+}_o in the VFT (Geng et al., 2016; Zhang et al., 2016), as well as residues within a large cavity in the 7TM that accommodates the binding of small molecule NAMs and PAMs (Leach et al., 2016).

First, we investigated the effects of amino acid substitutions in four Ca^{2+}_o binding sites located in the CaSR VFT (Geng et al., 2016). Agonist concentration-response curves at VFT mutants, and parameter estimates from the data analyses are summarised in **Figure 4.7 & Table S4.2**. Ala substitution of E228 reduced all agonist Hill slopes from 2.3±0.1 to 1.2±0.1, suggesting the E228A mutation reduces positive cooperativity between sites (**Table S4.2**). E231A, E232A, D234A and S240A also reduced the Hill slope of Gd^{3+} responses but did not affect the Hill slope of any other agonists. The reduction in Gd^{3+} Hill slopes upon mutation of these aforementioned residues is consistent with abolishment of the direct interaction between Gd^{3+} and E232, or disruption of the Gd^{3+} binding site by virtue of E231A, E232A and S240A mutations being in close proximity to the Gd^{3+} binding site and therefore likely disrupting the integrity of the site (**Figure 4.1**). Consistent with the large (72% or greater) reduction in cell surface expression caused by I84A, T100A and S170A, these three mutations reduced the potency or E_{max} of all agonists tested. Interestingly, S84A and N102A, which also reduced CaSR surface expression, reduced putrescine, agmatine, spermidine and spermine potencies and E_{max} but did not affect Ca^{2+}_o or Gd^{3+} (**Table S4.2**). Intriguingly, agmatine's potency was increased 3-fold by E228A. For mutants on the interface between LB2 on the two protomers (referred to herein as the LB2-LB2 interface), D234A, S240A, E241A, S302A and S303A reduced agmatine's maximum response and S302A reduced putrescine's maximum response, but these mutations did not alter maximal responses to the other agonists. These results suggest that polycation potency and E_{max} are affected by some common but also different amino acids in the CaSR VFT.

We also investigated substitutions of 7TM and ECL amino acids in the headless CaSR to remove the possibility of compensatory effects of ECD binding sites (Leach et al., 2016). Concentration-response data and parameter estimates from the data analyses are summarised in **Figure 4.8 & Table S4.2**. With the exception of Gd^{3+}, agonists were partial agonists at all

headless mutants where responses were stimulated (**Figure 4.8 & Table S4.2**). Consistent with a large reduction in cell surface expression caused by F688$^{3.40}$A, E837$^{7.32}$I and I841$^{7.36}$A, the E_{max} of Gd^{3+} at F688$^{3.40}$A and E837$^{7.32}$I headless was reduced compared to headless CaSR. Further Gd^{3+} stimulated no responses at I841$^{7.36}$A headless. Similarly, no other agonist stimulated responses at these three loss-of-expression mutants (**Figure 4.8 & Table S4.2 & Table 4.2**). Gd^{3+} potency was decreased at I760^{ECL2}A, I761^{ECL2}A and E767^{ECL2} (**Table S4.3**), and Gd^{3+} potency and effifcacy were reduced at F684$^{3.36}$A headless. F684$^{3.36}$A also completely abolished the responses to $Ca^{2+}{}_o$ and polyamines despite good cell surface expression. These findings suggest that F684$^{3.36}$ is crucial for polycation function. One amino acid substitution, I760^{ECL2}A, reduced the E_{max} of all polyamines but did not affect Gd^{3+} or $Ca^{2+}{}_o$ E_{max} values (**Table 4.2 & Table S4.3**), while spermine potency was increased 6-fold at R752^{ECL2}A. Of note, putrescine could signal via two gain-of-function headless CaSR mutants, E767^{ECL2}A and R752^{ECL2}A (**Figure 4.8E & I**). These results suggest putrescine can bind to the CaSR 7TM domains, but the responses were not detectable at the headless CaSR, most likely because putrescine lost efficacy.

No other agonist potencies were affected by CaSR 7TM or ECL mutations. The Hill slopes of Gd^{3+} were increased significantly at F684$^{3.36}$A and E837$^{7.32}$I compared to at the headless CaSR whereas no other mutations affected polycation Hill slopes (**Table S4.3**). Together, these findings suggest that polycations are sensitive to mutations in both the CaSR VFT and 7TM.

4.1.1. VFT and 7TM mutations alter polycation affinity

Similar to quantification of agonist affinity at the WT and headless CaSRs, we used the cooperative agonist operational model (Equation 2) to quantify agonist affinity at full length and headless mutant CaSRs. To quantify partial agonist affinity, we defined the system maximum response (E_m) using the Gd^{3+} E_{max} if the Gd^{3+} E_{max} at the mutant was comparable to the WT or headless CaSR E_{max}. If Gd^{3+} E_{max} was significantly reduced at a mutant CaSR compared to the WT or headless CaSR, we used the Gd^{3+} E_{max} at the WT or headless CaSR to define the system E_m. To quantify full agonist affinity at mutant CaSRs, we titrated receptor expression levels by using different tetracycline concentrations (0, 30 or 100 ng/mL), and equation 2 was fitted to concentration-response data under different receptor expression levels (summarised in **Figure 4.7 & 4.8 & 4.9**). Where nB is not significantly different to unity (e.g.

at the headless CaSR and many of the mutants thereof), the cooperative agonist operational model of agonism collapses down to the Black and Leff operational model of agonism.

Surprisingly, Ca^{2+}_o affinity was not affected by any of the VFT mutations, despite many of the mutations being located at residues suggested from structural studies to contribute to Ca^{2+}_o binding (**Figure 4.10 & Table 4.4**). In contrast, VFT mutations, specifically those located at the top of LB1, altered polyamine affinity, albeit differentially (**Figure 4.10 & Table 4.6**). With the exception of S84A, mutations on the LB1 completely abolished the putrescine response, therefore we could not quantify putrescine affinity at these mutants (**Figure 4.10 & Table 4.4**). I81A reduced the affinity of all the polyamines (**Table 4.4**). To be more specific, Ala substitution of I81 (located in Ca^{2+}_o binding site 1 at the top of LB1) and N102 (located in Ca^{2+}_o binding site 2) reduced agmatine affinity by 2-fold (**Figure 4.10 & Table 4.4**). I81A, S84A, and T100A reduced spermidine affinity 3 to 9-fold (**Figure 4.10 & Table 4.4**). Furthermore, E228A located on LB2 increased putrescine and decreased spermidine affinity, respectively, by 4-fold (**Figure 4.10 & Table 4.4**). Overall, the mutations on the top and bottom of LB1 and the LB1-LB2 interface (within the same protomer) affected polyamine affinity.

As discussed earlier, Ca^{2+}_o and polyamines did not signal at several 7TM mutant headless CaSRs, including F668$^{2.56}$A headless, F688$^{3.40}$A headless, E837$^{7.32}$I headless and I841$^{7.36}$A headless mutants, which significantly reduced receptor expression (**Figure 4.3B & Table 4.2& Figure 4.8**). Also as mentioned previously, Ala substitution of F684$^{3.36}$A headless also abolished the responses to Ca^{2+}_o and polyamines, despite good cell surface expression of this mutant (**Figure 4.8**). Therefore, agonist affinities could not be quantified at these mutants. Intriguingly, two mutations in ECL2, R752^{ECL2}A headless and E767^{ECL2}A headless, significantly increased spermidine and spermine affinity by 4 to 7-fold (**Table 4.7**), but had no effect on the affinity of the other agonists. Collectively, these data suggest that mutations in the small molecule binding pocket affect spermidine and spermine affinity. Residues where mutations affect polycation affinity are highlighted in the CaSR VFT structure or 7TM homology model in **Figure 4.14A, 4.15A, 4.16A and 4.17A**.

4.1.2. VFT and 7TM mutations reduce polycation efficacy

We next quantified polycation efficacy at each full length and headless mutant CaSR. Following derivation of agonist logτA with the cooperative agonist operational model

(Equation 2), we corrected logτA at each mutant to account for mutant-induced changes in receptor expression levels where mutant expression was significantly different compared to the WT or headless CaSR (**Table 4.1 & Table 4.2**). The corrected logτA is expressed as logτC. In the CaSR VFT, some common mutations that affected polyamine affinity also had effects on efficacy, including N102A and E228A (**Table 4.6**). For example, E228A reduced agmatine but increased spermidine and spermine efficacy (**Table 4.6**). Other mutations that did not have effects on Ca^{2+}_o or polyamine affinity, such as D234A, reduced the efficacy of agmatine by ~10-fold (**Table 4.6**). Mutations E231A, S240A and E241A located on LB2 also reduced agmatine efficacy. However, these mutations had no effect on putrescine, spermidine or spermine efficacy (**Table 4.6**). Furthermore, when efficacy was corrected for differences in receptor expression levels, mutations that reduced both the receptor expression and E_{max} of polycations, including I81A and S84A, did not alter the logτC of Ca^{2+}_o or polyamines, indicating that reductions in E_{max} were due solely to the reduced cell surface receptor expression and not due to impairments in agonist efficacy (**Table 4.6**).

With regards to 7TM or ECL mutations in the headless CaSR, the logτC of Ca^{2+}_o and polyamines was differentially altered. As discussed earlier, Ca^{2+}_o and polyamines lost their responses at several headless mutants preventing quantification (**Figure 4.8** & **Table 4.5**). Further, $E755^{ECL2}A$ headless and $I760^{ECL2}A$ headless reduced spermidine and spermine efficacy by 3 to 6- fold but had no effect on Ca^{2+}_o or agmatine, whereas $Q754^{ECL2}A$ headless reduced agmatine efficacy by 6-fold but did not affect Ca^{2+}_o, spermidine or spermine (**Table 4.6**). Mutations that affect polycation efficacy are shown in the CaSR VFT structure and 7TM homology model in **Figure 4.14B, 4.15B, 4.16B and 4.17B**.

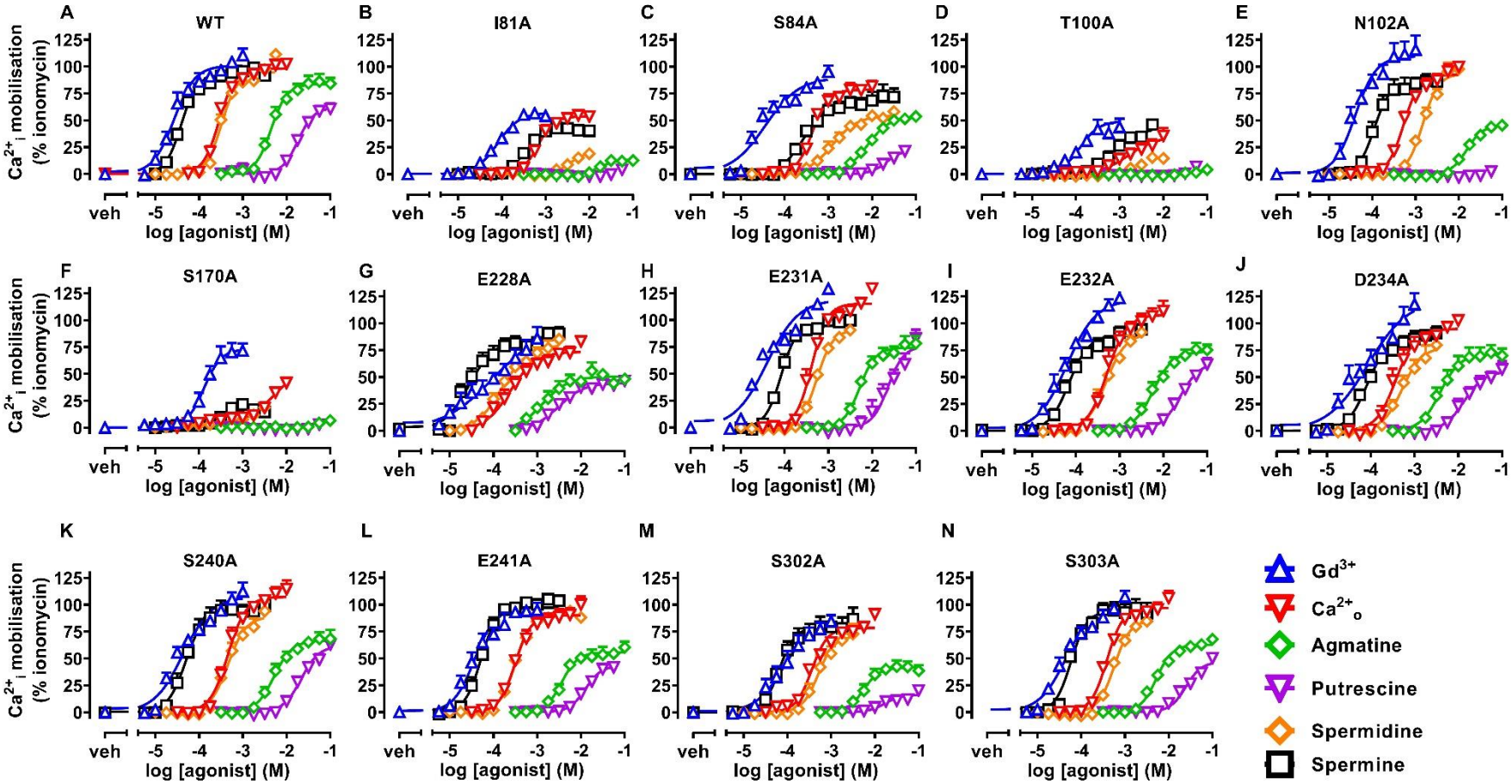

Figure 4.7. VFT mutations alter the activity of polycations at the CaSR. Concentration-response curves to polycations were determined in Ca^{2+}_i mobilisation assays to identify mutations that altered polycation activity. FlpIn HEK293 TRex cells were stably transfected with: **A**) WT, **B**) I81A, **C**) S84A, **D**) T100A, **E**) N102A, **F**) S170A, **G**) E228A, **H**) E231A, **I**) E232A, **J**) D234A, **K**) S240A, **L**) E241A, **M**) S302A, **N**) S303A CaSR. Data are mean ± s.e.m. from 4-7 pooled independent experiments performed in duplicate. Curves through the data points are the best fit of Equation 2 to the pooled data.

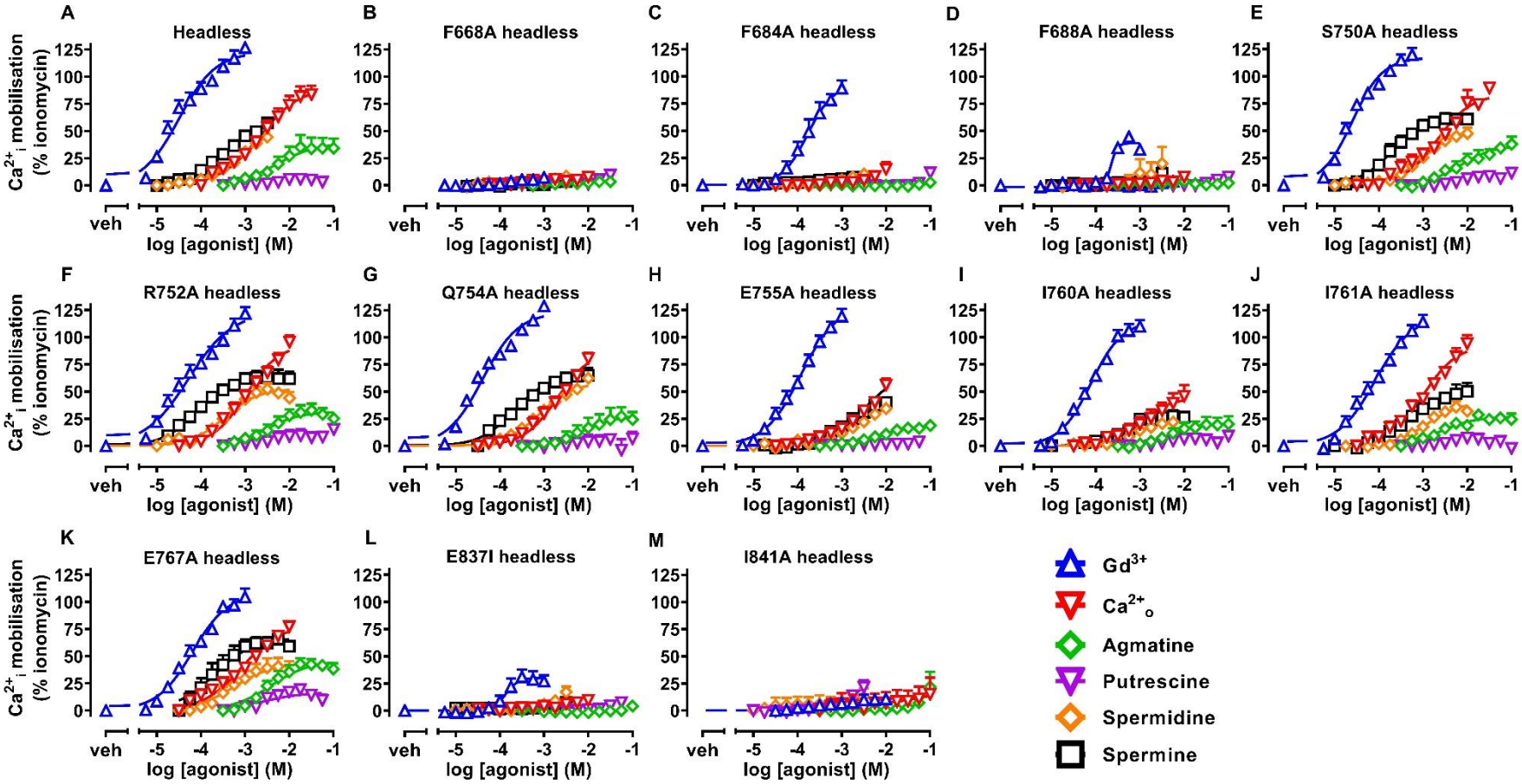

Figure 4.8. 7TM and ECL mutations alter the activity of polycations at the CaSR. Concentration-response curves to polycations were determined in Ca^{2+}_i mobilisation assays to identify mutations that altered polycation activity. FlpIn HEK293 Trex cells were stably transfected with: **A**) headless, **B**) $F668^{2.56}A$, **C**) $F684^{3.36}A$, **D**) $F688^{3.40}A$, **E**) $S750^{ECL2}A$; **F**) $R752^{ECL2}A$, **G**) $Q754^{ECL2}A$, **H**) $E755^{ECL2}A$, **I**) $I760^{ECL2}A$, **J**) $I761^{ECL2}A$, **K**) $E767^{ECL2}A$, **L**) $E837^{7.32}I$, **M**) $I841^{7.36}A$ headless CaSR. Data are represented as mean ± s.e.m. from 3-7 pooled independent experiments performed in duplicate. Curves through the data points are the best fit of Equation 2 to the pooled data.

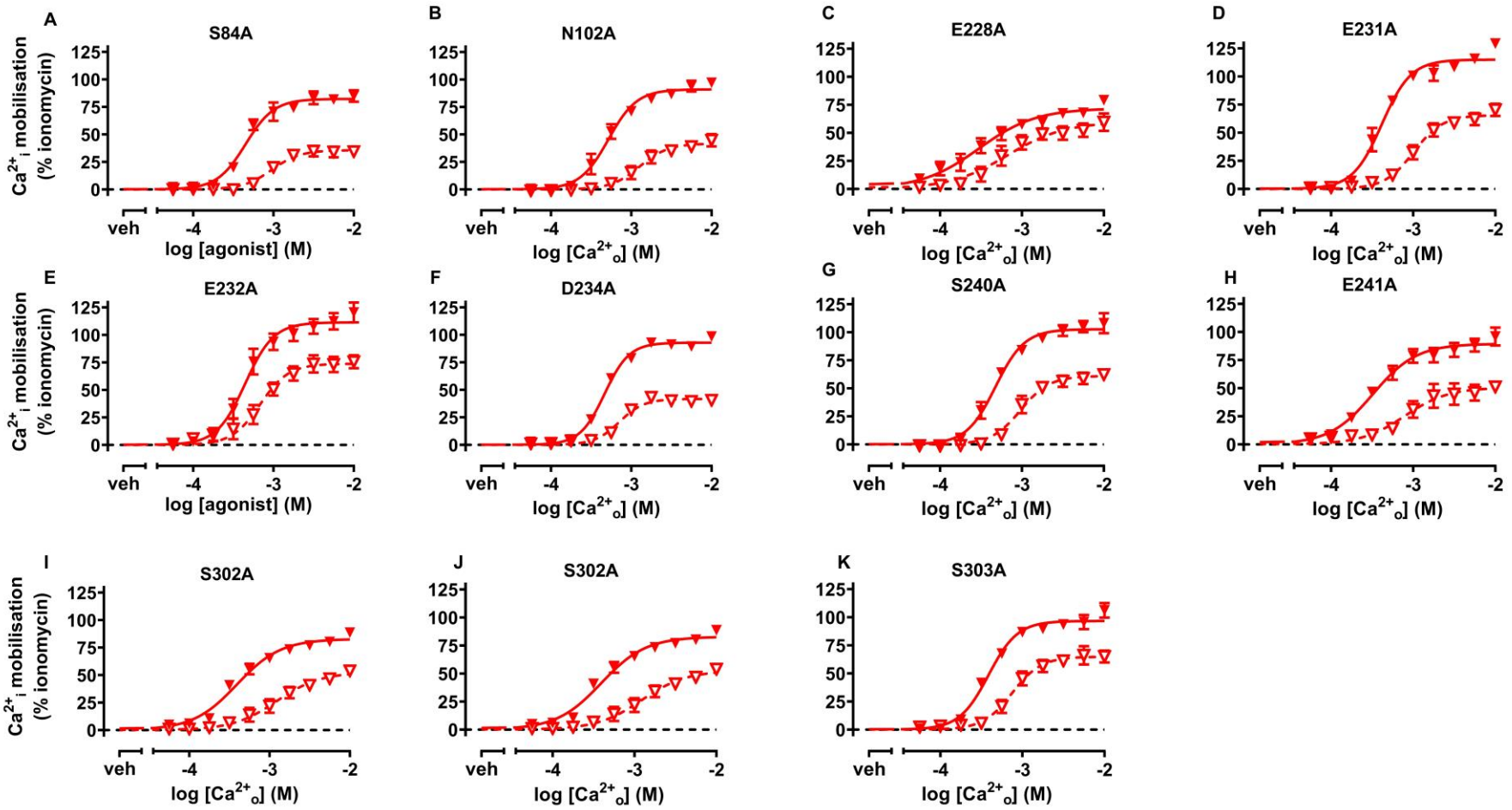

Figure 4.9. Ca^{2+}_o stimulated Ca^{2+}_i mobilisation via mutant CaSR after overnight pre-incubation with different concentrations of tetracycline. FlpIn HEK293-Trex cells were transfected with **A**) S84A, **B**) N102A, **C**) E228A, **D**) E231A, **E**) E232A, **F**) D234A, **G**) S240A, **H**) E241A, **I**) S302A, **J**) S303A CaSR, pre-incubated with different concentrations of tetracycline. Closed symbol = 100ng/mL tetracycline, open symbol=0-30 ng/mL tetracycline. Data are represented as mean ± s.e.m from 3-4 independent experiments performed in duplicate. Curves through the data points are the best fit of Equation 2 to the pooled data.

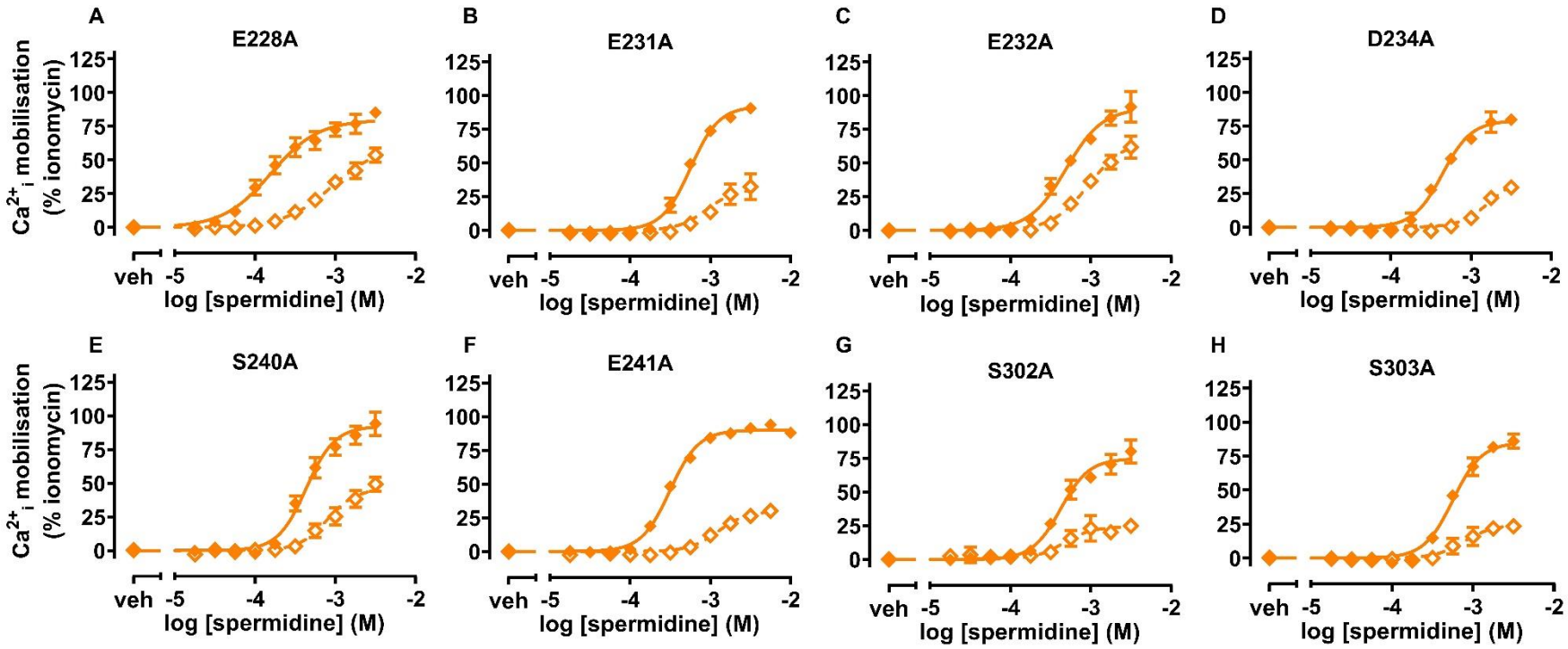

Figure 4.10. The concentration-response curve of spermidine in HEK293-Trex transfected with **A**) E228A, **B**) E231A, **C**) E232A, **D**) D234A, **E**) S240A, **F**) E241A, **G**) S302A **H**) S303A CaSR, pre-incubated with different concentrations of tetracycline overnight. Closed symbol = 100ng/mL tetracycline, open symbol=0-30 ng/mL tetracycline. Data are represented as mean ± s.e.m from 4 independent experiments performed in duplicate. Curves through the data points are the best fit of Equation 2 to the pooled data.

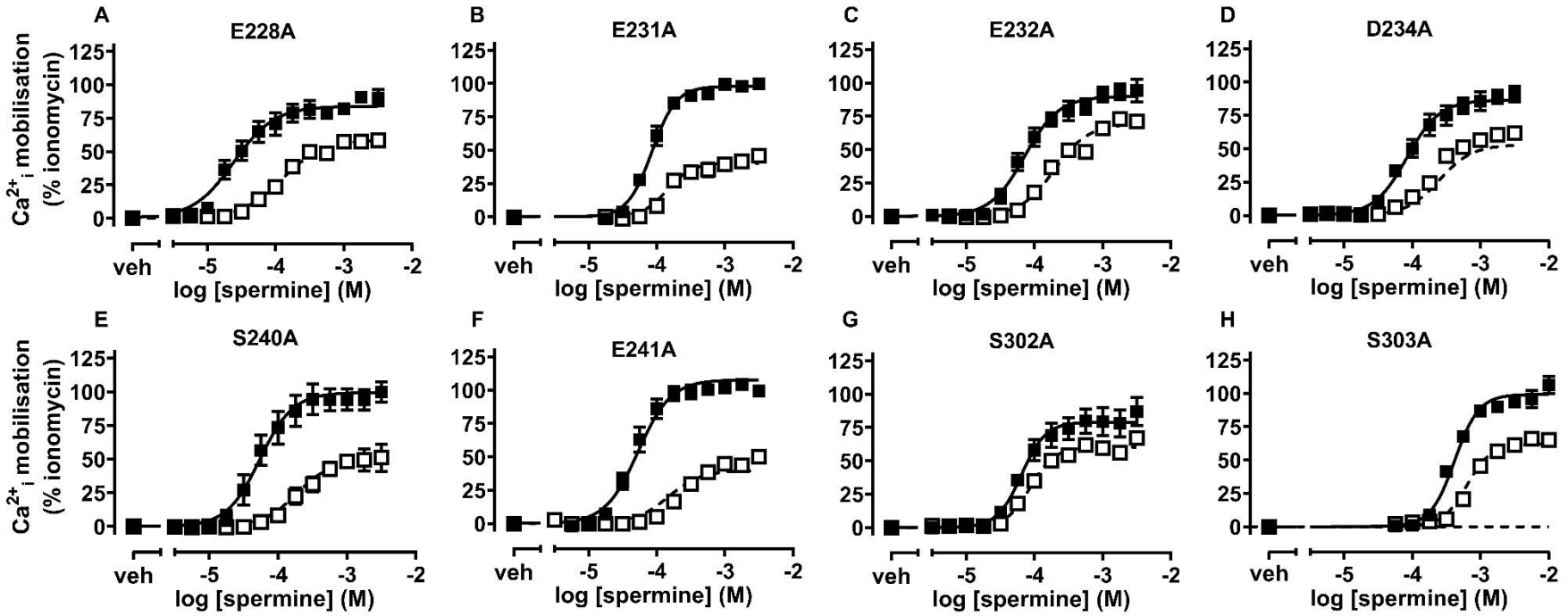

Figure 4.11. The concentration-response curve of spermine in HEK293-Trex transfected with **A**) E228A, **B**) E231A, **C**) E232A, **D**) D234A, **E**) S240A, **F**) E241A, **G**) S302A **H**) S303A CaSR, pre-incubated with different concentrations of tetracycline overnight. Closed symbol = 100ng/mL tetracycline, open symbol=0-30 ng/mL tetracycline. Data are represented as mean ±s.e.m from 4-5 independent experiments performed in duplicate. Curves through the data points are the best fit of Equation 2 to the pooled data.

Table 4.4. Functional affinity (pK_A), corrected efficacy (logτC) and binding slope (nB) parameters for polycations at WT and VFT mutants determined in Ca^{2+}_i mobilisation assays. Data are mean ± s.e.m. from 3-6 independent experiments performed in duplicate, and analysed via one-way ANOVA followed with Dunnett's post-test, *P<0.05, **P<0.01, ***P<0.001, significantly different to WT CaSR. . $^{\#}$nB at each mutant CaSR is not significantly different from nB at WT CaSR, determined by F-tests. NR denotes no responses.

	Ca^{2+}_o			Agmatine			Putrescine			Spermidine			Spermine		
	pK_A	logτC	nB	pK_A	logτC	nB	pK_A	logτC	nB	pK_A	logτC	nB	pK_A	logτC	nB
WT	2.95±0.06	1.11±0.19	2.4±0.1	1.93±0.04	0.85±0.08	2.4±0.1	1.59±0.03	0.12±0.03	2.4±0.1	3.28±0.04	0.66±0.07	2.4±0.1	3.81±0.04	0.64±0.04	2.4±0.1
I81A	2.61±0.13	1.58±0.17	2.4$^{\#}$	1.65±0.02**	0.29±0.11	2.4$^{\#}$	NR		2.4$^{\#}$	2.61±0.08*	0.80±0.09	2.4$^{\#}$	3.38±0.03***	0.95±0.03	2.4$^{\#}$
S84A	2.93±0.07	1.43±0.19	1.8±0.1	1.89±0.07	0.67±0.04	1.8±0.1	1.59±0.11	0.41±0.09	1.8±0.1	2.46±0.08*	0.57±0.06	1.8±0.1	3.30±0.06***	0.72±0.07	1.8±0.1
T100A	2.73±0.13	1.21±0.23	1.4±0.3	NR			NR			2.39±0.25*	0.72±0.37	1.4±0.3	3.15±0.06**	0.84±0.11	1.4±0.3
N102A	2.80±0.06	1.37±0.20	2.4$^{\#}$	1.64±0.06**	0.26±0.07**	2.4$^{\#}$	NR			2.73±0.11*	0.74±0.24	2.4$^{\#}$	3.66±0.05	0.94±0.10	2.4$^{\#}$
S170A	2.71±0.09	1.54±0.21	1.0±0.2*	NR			NR			3.13±0.23	0.17±0.11**	1.0±0.2	3.44±0.08	0.13±0.07**	1.0±0.2
E228A	2.68±0.24	1.01±0.32	1.6±0.1	2.23±0.06	0.38±0.03**	1.6±0.1	2.20±0.09***	0.24±0.07	1.6±0.1	2.71±0.08*	1.78±0.03**	1.6±0.1	3.74±0.09	1.52±0.23*	1.6±0.1
E231A	2.86±0.049	1.27±0.14	2.4$^{\#}$	1.95±0.04	0.35±0.08**	2.4$^{\#}$	1.61±0.06	0.24±0.11	2.4$^{\#}$	3.03±0.02	0.48±0.04	2.4$^{\#}$	3.75±0.02	0.64±0.03	2.4$^{\#}$
E232A	3.02±0.07	0.74±0.25	2.4$^{\#}$	2.09±0.02	0.25±0.08**	1.6±0.2	1.48±0.02	0.09±0.03	2.4$^{\#}$	2.91±0.05	0.55±0.07	2.4$^{\#}$	3.73±0.04	0.51±0.04	2.4$^{\#}$
D234A	3.00±0.08	0.70±0.27	2.4$^{\#}$	2.11±0.05	0.48±0.03**	2.4$^{\#}$	1.70±0.03	0.12±0.05	2.4$^{\#}$	3.18±0.04	0.15±0.05	2.4$^{\#}$	3.66±0.05	0.42±0.04	1.7±0.2
S240A	2.88±0.05	1.06±0.15	2.4$^{\#}$	2.01±0.06	0.35±0.03**	2.4$^{\#}$	1.43±0.08	0.19±0.059	2.4$^{\#}$	3.09±0.04	0.64±0.07	2.4$^{\#}$	3.76±0.06	1.07±0.12	2.4$^{\#}$

E241A	2.92±0.12	0.88±0.24	2.4[#]	2.20±0.03	0.33±0.03**	2.4[#]	1.74±0.04	-0.05±0.14	2.4[#]	2.90±0.07	0.69±0.09	2.4[#]	3.42±0.08	0.92±0.07	2.4[#]
S302A	2.67±0.10	1.15±0.19	1.6±0.2*	2.08±0.04	0.00±0.05**	2.4[#]	1.84±0.06*	-0.80±0.19**	1.0±0.4	3.05±0.08	0.62±0.14	2.4[#]	3.63±0.08	0.81±0.10	2.4[#]
S303A	2.95±0.05	1.07±0.17	2.44[#]	1.95±0.06	0.33±0.03	1.9±0.3	1.45±0.05	0.04±0.08	1.4±0.4	2.95±0.03	0.74±0.06	2.8±0.4	3.59±0.09	0.67±0.04	2.8±0.4

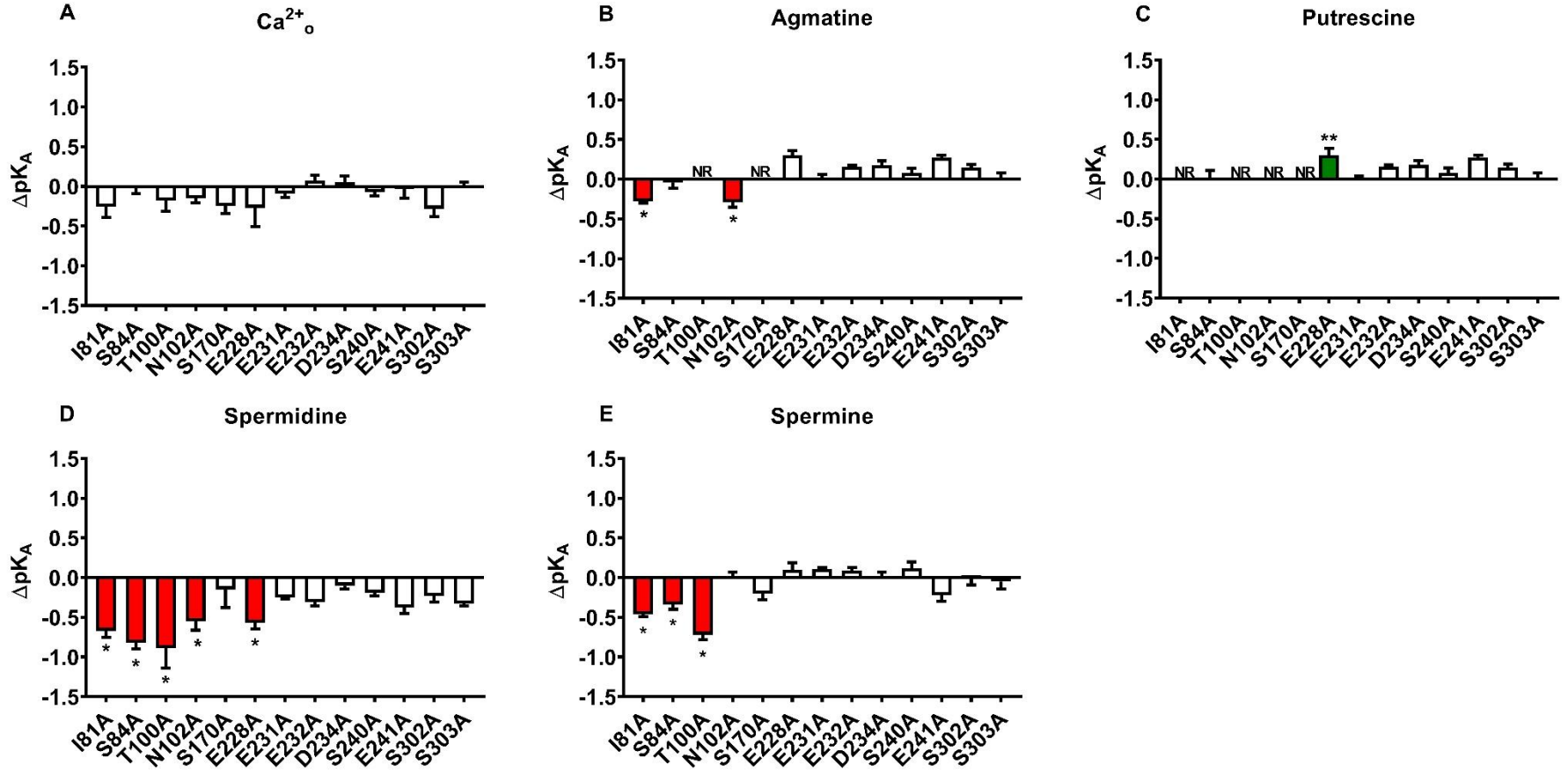

Figure 4.12. Change in pK_A of: **A**) Ca^{2+}_o, **B**) agmatine, **C**) putrescine; **D**) spermidine and **E**) spermine at VFT mutations compared to WT CaSR. Equation 2 was fitted to agonist concentration-response data determined in Ca^{2+}_i mobilisation assays and the change in agonist pK_A (ΔpK_A) at the VFT mutants compared to the WT CaSR were calculated. Bars that sit above and below zero represent an increase or decrease in pK_A, respectively. Green and red bars represent mutations that caused a significant increase or decrease in pK_A in comparison to the WT CaSR, respectively. White bars represent no significant changes in pK_A. NR denotes no agonist response. Data are mean ± s.e.m. from 3-6 independent experiments performed in duplicate, and analysed via one-way ANOVA followed with Dunnett's post-test, *P<0.05, **P<0.01.

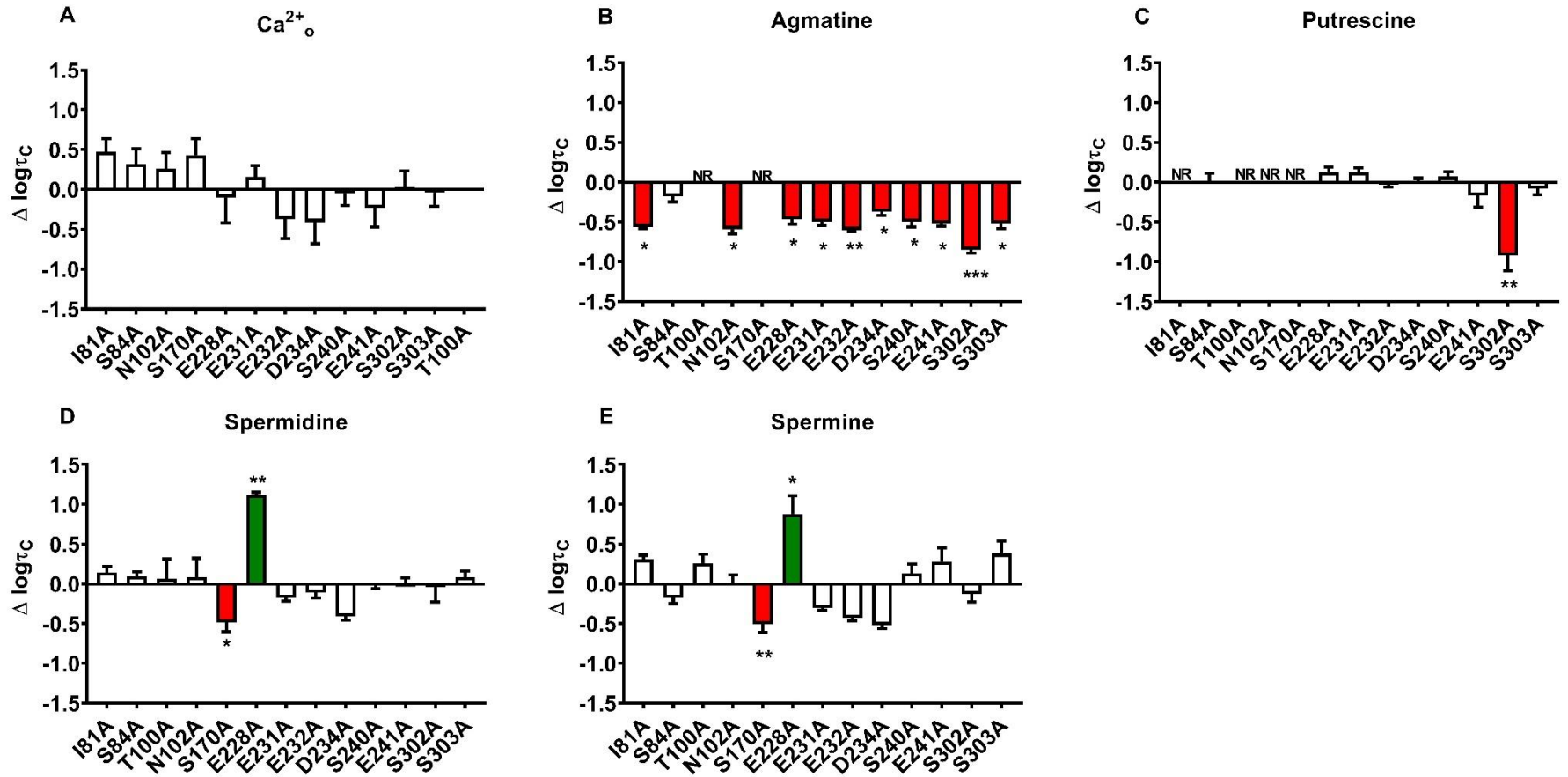

Figure 4.13. Change in $\log\tau_c$ of **A)** Ca^{2+}_o, B) agmatine, **C)** putrescine, **D)** spermidine, **E)** spermine at VFT mutations compared with WT CaSR. Equation 2 was fitted to agonist concentration-response data determined in Ca^{2+}_i mobilisation assays and the change in agonist $\log\tau_c$ ($\Delta\log\tau_c$) at the VFT mutants compared to the WT receptor CaSR were calculated. Bars that sit above and below zero represent an increase or decrease in $\log\tau_C$ in comparison to the WT receptor, respectively. Green and red bars represent mutations that caused a significant increase or decrease in $\log\tau_c$, respectively. White bars represent no significant changes in $\log\tau_C$. NR denotes for no responses. Data are mean ± s.e.m from 3-6 independent experiments performed in duplicate, and analysed via one-way ANOVA followed with Dunnett's post-test, *P<0.05, **P<0.01, ***P<0.001.

Table 4.5. Functional affinity (pK_A), corrected efficacy ($log\tau_C$) and binding slope (nB) parameters for polycation ligands at WT and headless CaSR, and 7TM and ECL mutant CaSRs determined in $Ca^{2+}{}_i$ mobilisation assays and analysed with Equation 2. Data are mean ± s.e.m. from 4-7 independent experiments performed in duplicate. Parameters for 7TM and ECL mutant CaSR were analysed via one-way ANOVA followed with Dunnett's post-test, *P<0.05, **P<0.01, ***P<0.001, ****P<0.0001, significantly different to headless CaSR. NR denotes for no responses. NP denotes for not performed.

	$Ca^{2+}{}_o$			Agmatine			Putrescine			Spermidine			Spermine		
	pK_A	$log\tau_C$	nB	pK_A	$log\tau_C$	nB	pK_A	$log\tau_C$	nB	pK_A	$log\tau_C$	nB	pK_A	$log\tau_C$	nB
ΔH	1.93±0.06	0.44±0.14	1.0±0.1	2.24±0.18	-0.27±0.07	1.0±0.1	NR		1.0±0.1	2.60±0.08$^{\$\$}$	0.01±0.12	1.0±0.1	3.03±0.09$^{\$\$}$	0.03±0.04	1.0±0.1
$F668^{2.56}A$ ΔH	NR														
$F684^{3.36}A$ ΔH	NR														
$F688^{3.40}A$ ΔH	NR														
$S750^{ECL2}A$ ΔH	2.27±0.10	0.32±0.13	1.0$^{\#}$	2.25±0.02	-0.36±0.08	1.0$^{\#}$	NR		1.0$^{\#}$	2.89±0.09	0.13±0.05	1.0$^{\#}$	3.29±0.11	0.27±0.06	1.0$^{\#}$
$R752^{ECL2}A$ ΔH	2.65±0.34	0.11±0.14	1.0$^{\#}$	2.44±0.14	0.11±0.14	1.0$^{\#}$	2.28±0.40	-0.99±0.18	1.0$^{\#}$	3.32±0.03*****	-0.17±0.03	1.0$^{\#}$	3.89±0.05*	-0.02±0.02	1.0$^{\#}$
$Q754^{ECL2}A$ ΔH	2.32±0.21	0.48±0.01	1.0$^{\#}$	2.01±0.30	0.48±0.01*	1.0$^{\#}$	NR		1.0$^{\#}$	2.83±0.05	-0.03±0.04	1.0$^{\#}$	3.34±0.06	-0.09±0.03	1.0$^{\#}$
$E755^{ECL2}A$ ΔH	2.37±0.15	0.02±0.14	0.7±	2.07±0.03	0.02±0.14		NR			2.82±0.12	-0.51±0.05*		2.79±0.09	-0.40±0.04*	

I760^{ECL2}A ΔH	2.68±0.17	0.18±0.38	1.0$^{\#}$	2.27±0.18	0.18±0.38	1.0$^{\#}$	NR		1.0$^{\#}$	2.85±0.08	-0.72±0.08**	1.0$^{\#}$	3.30±0.12	-0.51±0.05*	1.0$^{\#}$
I761^{ECL2}A ΔH	2.42±0.22	0.36±0.10	1.0$^{\#}$	2.51±0.11	-0.54±0.04	1.0$^{\#}$	NR		1.0$^{\#}$	2.75±0.10	-0.19±0.05	1.0$^{\#}$	3.04±0.08	-0.04±0.04	1.0$^{\#}$
E767^{ECL2}A ΔH	NP		1.0$^{\#}$	2.17±0.08	-0.13±0.06	2.51±0.43	-0.72±0.13	1.0$^{\#}$	3.23±0.13***	-0.30±0.05	1.0$^{\#}$	3.60±0.11*	-0.07±0.05	1.0$^{\#}$	
E837$^{7.32}$I ΔH	NR														
I841$^{7.36}$A ΔH	NR														

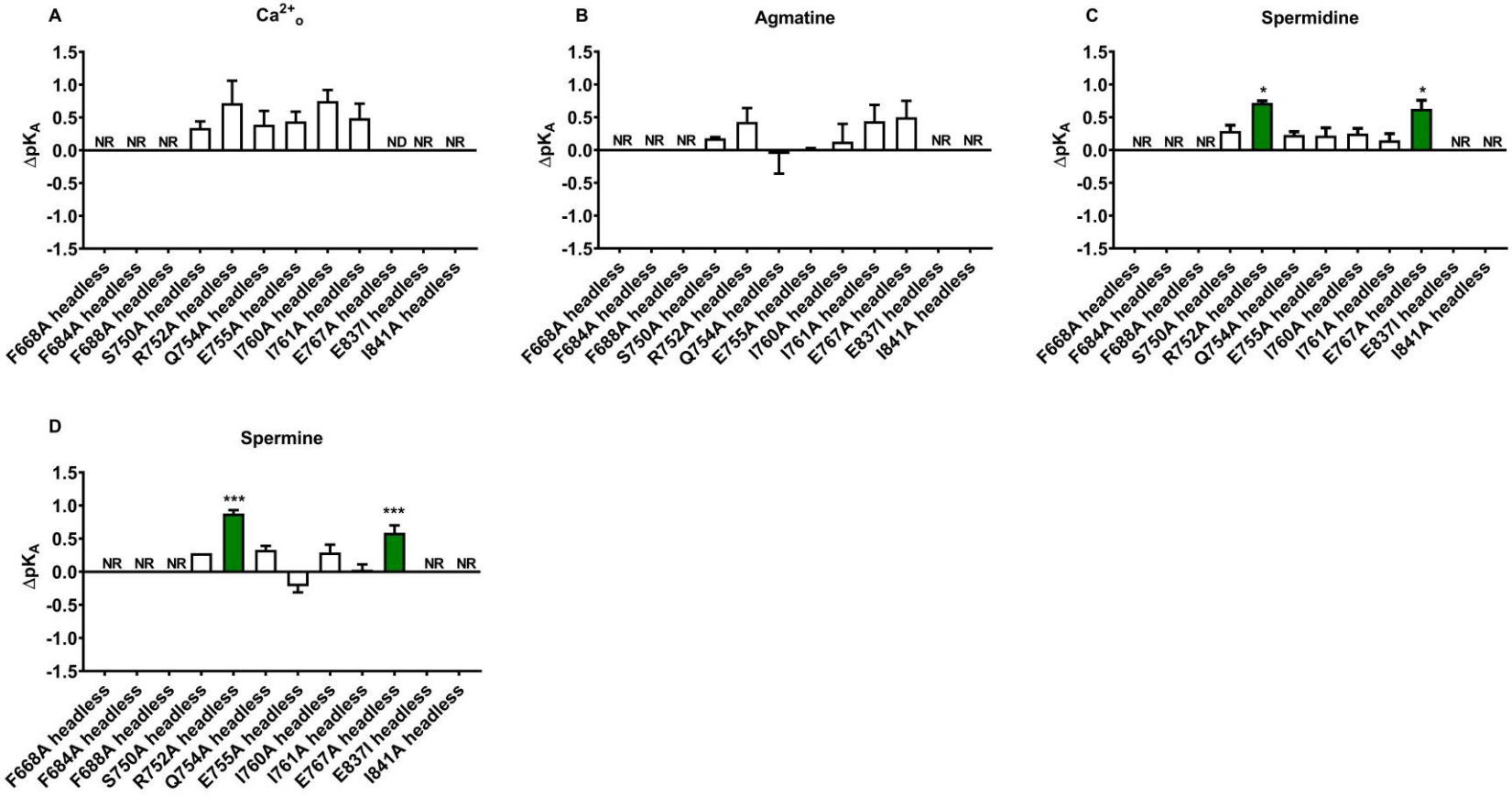

Figure 4.14. Change in pK_A of: **A**) Ca^{2+}_o, **B**) agmatine, **C**) spermidine, **D**) spermine at ECL/7TM mutations within the headless CaSR. Equation 2 was fitted to agonist concentration-response data determined in Ca^{2+}_i mobilisation assays and the change in agonist pK_A (ΔpK_A) at the ECL/7TM compared to the headless CaSR receptor were calculated. Bars that sit above and below zero represent ΔpK_A, respectively. Green and red bars represent mutations that caused a significant increase or decrease in pK_A in comparison to the WT headless receptor, respectively. White bars represent no significant changes in pK_A. Data are mean ± s.e.m from 3-6 independent experiments performed in duplicate, and analysed via ONE-WAY ANOVA followed with Dunnett's post-test, *P<0.05, **P<0.01, ***P<0.001. NR denotes for no response. Significant difference in comparison to the WT (*P < 0.05, **P<0.01, ***P<0.001, one-way ANOVA with Dunnett's multiple comparisons post-test)

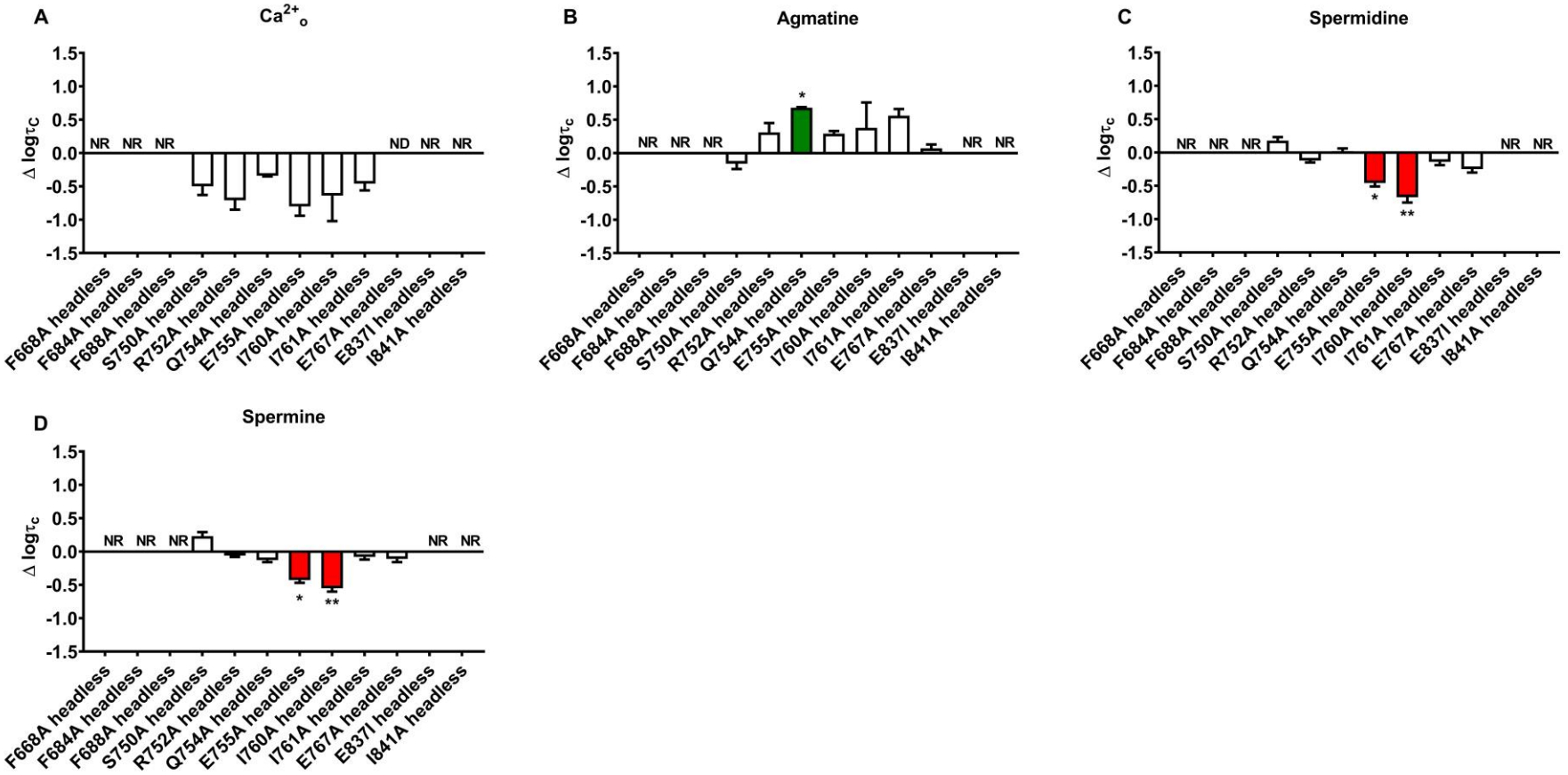

Figure 4.15. Change in $\log\tau_c$ of **A**) $Ca^{2+}{}_o$, **B**) agmatine, **C**) putrescine, **D**) spermidine, **E**) spermine at ECL/7TM mutations within the headless CaSR. Equation 2 was fitted to agonist concentration-response data determined in $Ca^{2+}{}_i$ mobilisation assays and the change in agonist $\log\tau_c$ ($\Delta\log\tau_c$) at the ECL/7TM mutants compared to the headless receptor CaSR were calculated. Bars that sit above and below zero represent an increase or decrease in $\log\tau_C$ in comparison to the WT receptor, respectively. Green and red bars represent mutations that caused a significant increase or decrease in $\log\tau_c$, respectively. White bars represent no significant changes in $\log\tau_C$. NR denotes for no responses. Data are mean ± s.e.m from 3-6 independent experiments performed in duplicate, and analysed via ONE-WAY ANOVA followed with Dunnett's post-test, *P<0.05, **P<0.01.

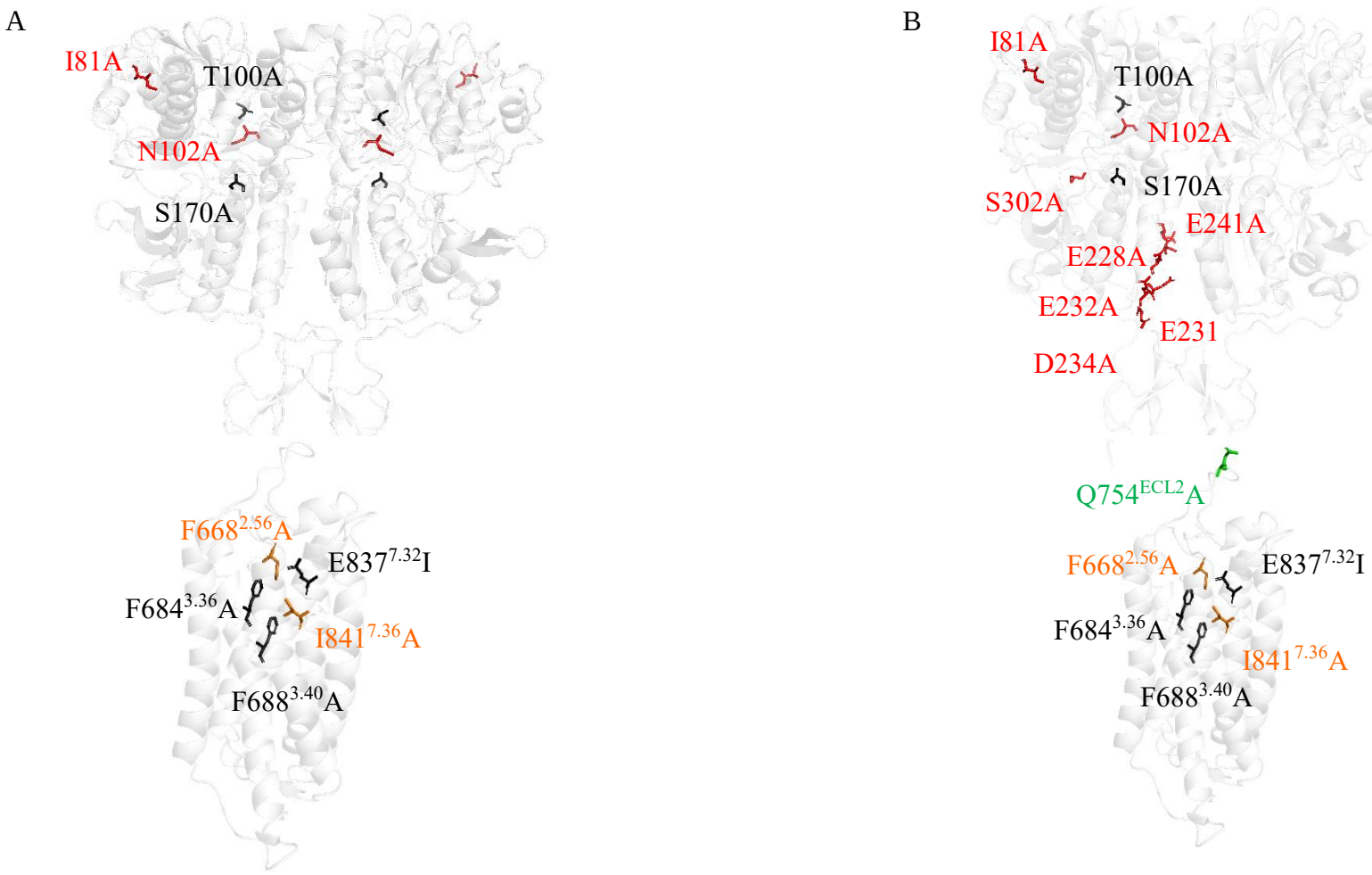

Figure 4.16. Residues that alter **A**) affinity and **B**) efficacy of agmatine, labelled in the CaSR VFT structure (PDB: 5k5s) and 7TM homology models (mGlu5; PDB: 4OO9). Residues coloured red are those where mutations reduce affinity or efficacy. Residues coloured green are those where mutations increase efficacy. Residues coloured orange are those where mutations abolish receptor expression and residues coloured black are those where mutations abolish the response to agmatine.

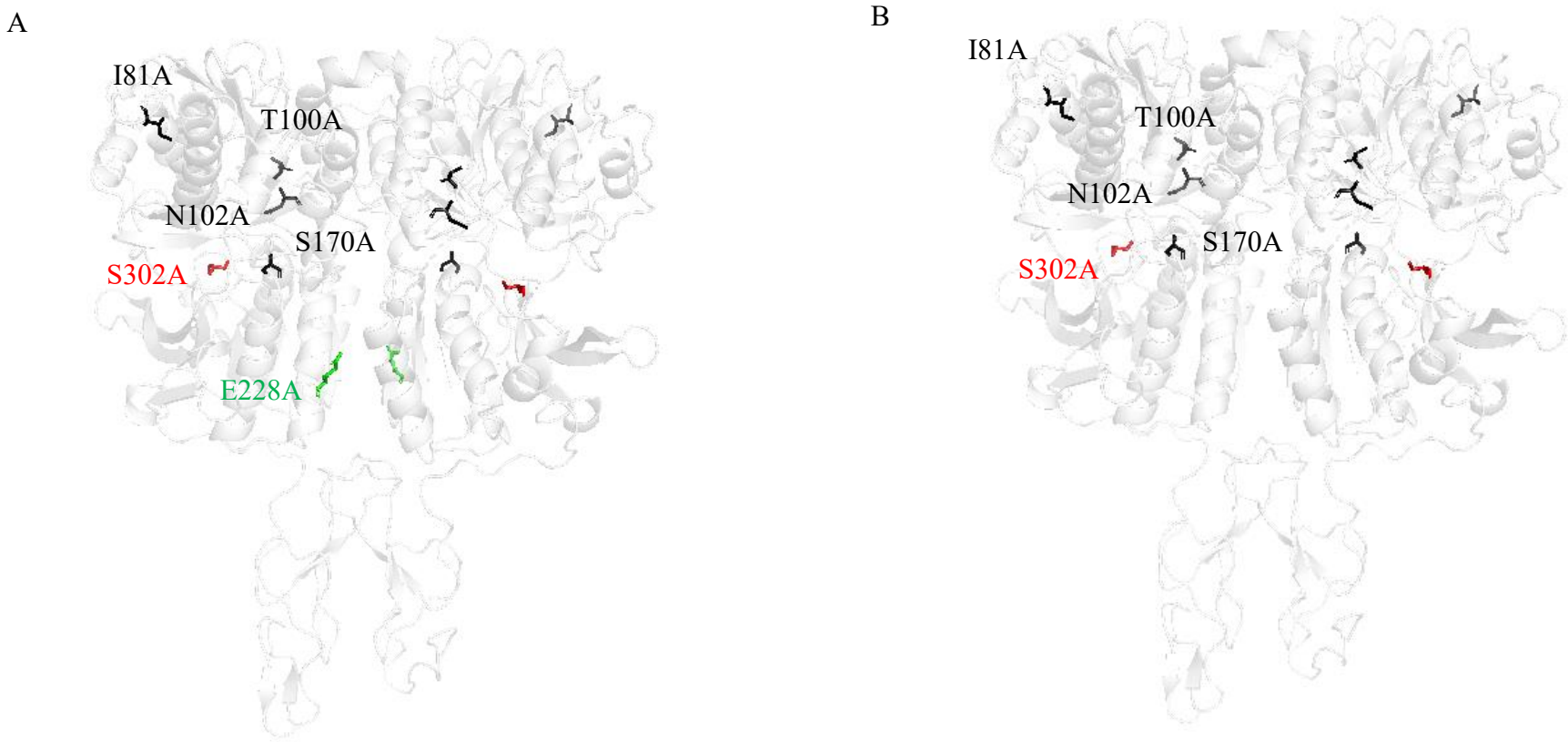

Figure 4.17. Residues that alter **A**) affinity and **B**) efficacy of putrescine, labelled in CaSR VFT crystal structures. Residues coloured red are those where mutations reduce affinity or efficacy. Residues coloured green are those where mutations increase affinity. Residues coloured black are those where mutations abolish the response to putrescine.

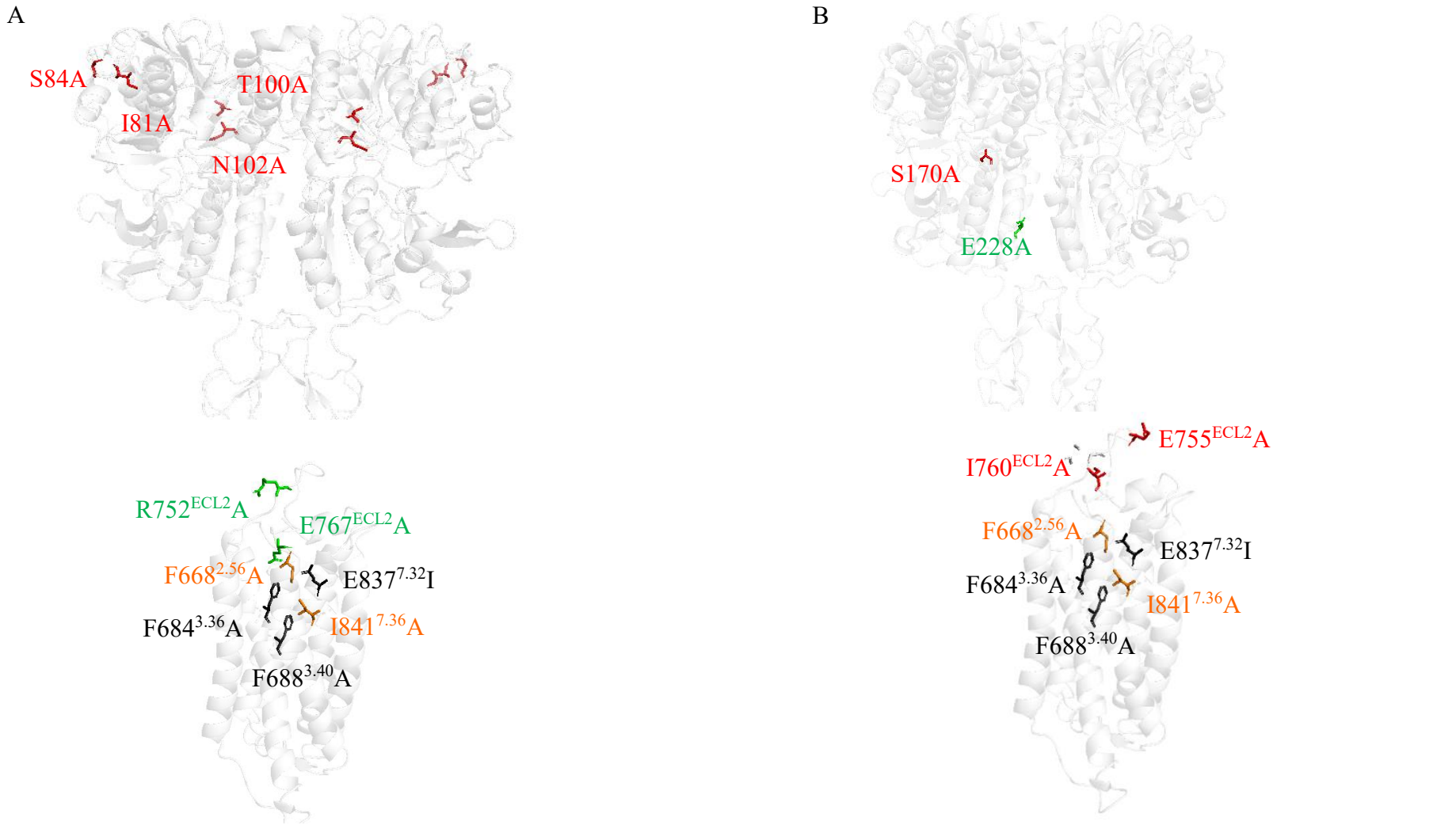

Figure 4.18. Residues that alter **A**) affinity and **B**) efficacy of spermidine, labelled in CaSR VFT crystal structures and 7TM homology models (mGlu5). Residues coloured red are those where mutations reduce affinity or efficacy. Residues coloured green are those where mutations increase affinity. Residues coloured orange are those where mutations abolish receptor expression and residues coloured black are those where mutations abolish the response to spermidine.

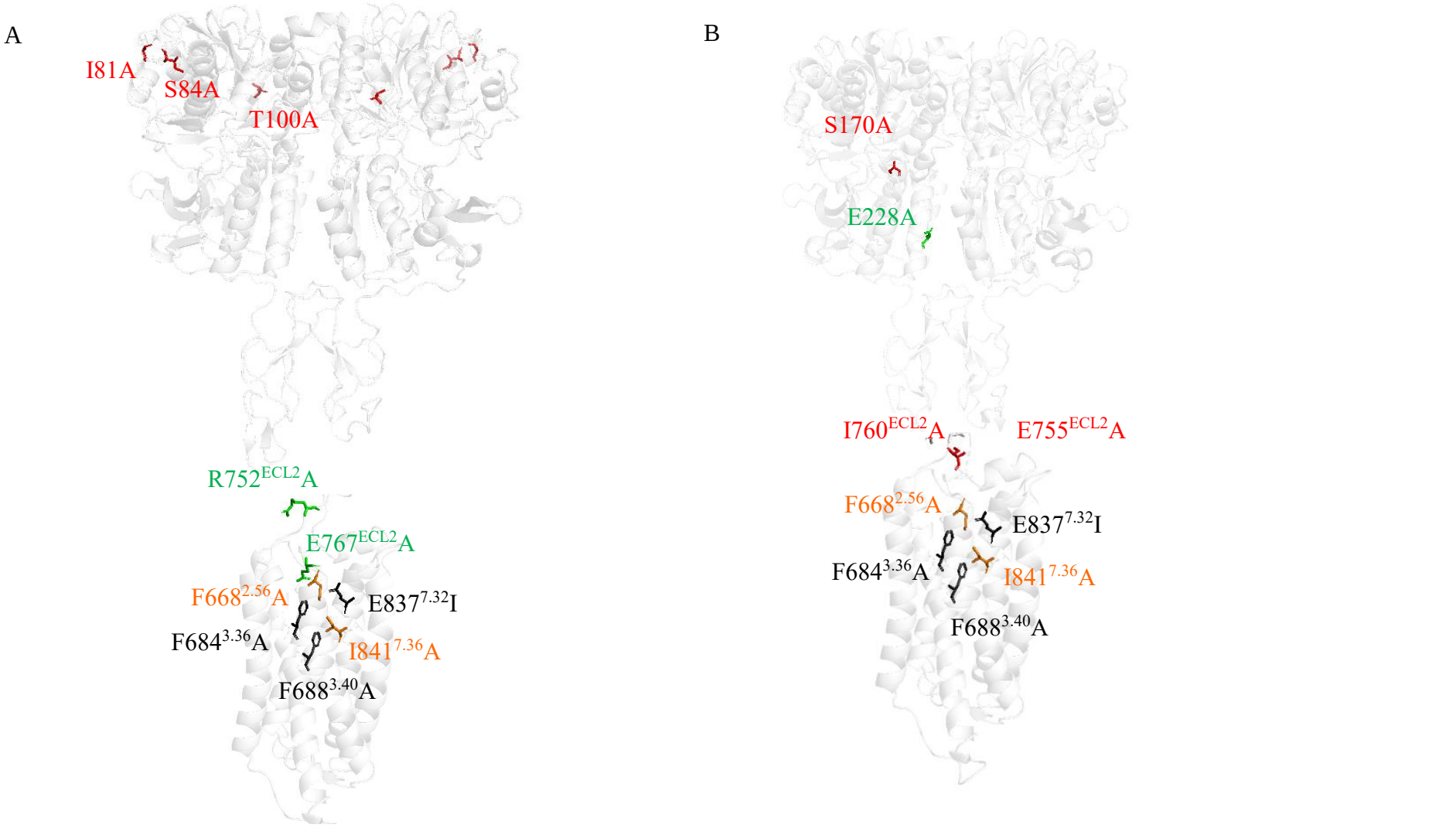

Figure 4.19. Residues that alter the **A**) affinity and **B**) efficacy of spermine at the CaSR, labelled in CaSR VFT crystal structures and 7TM homology models (mGlu5). Residues coloured red are those where mutations reduce affinity or efficacy. Residues coloured green are those where mutations increase affinity. Residues coloured orange are those where mutations abolish receptor expression and residues coloured black are those where mutations abolish the response to spermidine.

4.2 Discussion

The current study probed the location of agonist binding sites and activation residues in the CaSR VFT, 7TM and ECL domains. We applied mutagenesis and Ca^{2+}_i mobilisation assays combined with a cooperative agonist operational model of agonism to quantify the affinity and efficacy of six polycations (Gd^{3+}, Ca^{2+}_o, putrescine, agmatine, spermidine, and spermine) at the WT CaSR, headless CaSR, and mutants thereof. We provide evidence that agonists bind to multiple binding sites located both in the CaSR VFT and 7TM or ECL domains, but binding sites and activation residues likely differ between agonists.

First, we demonstrated distinct agonist affinities and efficacies at the WT CaSR. Agmatine and putrescine affinities were ~20-fold lower than spermine. Spermine had higher affinity than the orthosteric agonist, Ca^{2+}_o. The rank orders of agonist affinity and efficacy was consistent with previous findings demonstrating that the potency of polyamines depends on the number of positive charges (Quinn et al., 1997) and that trivalent cations are better than divalent cations at activating the CaSR (reviewed in Leach et al., 2020).

Next, we investigated how removal of the CaSR's N-terminus affects the pharmacological properties of different polycations. All polycations except for putrescine signalled through the headless CaSR. However, removal of the N-terminus reduced the affinity of Ca^{2+}_o, spermine and spermidine but not agmatine (Gd^{3+} affinity at the headless CaSR was not determined in the current study and putrescine affinity could not be determined due to its loss of activity). These findings suggest the N-terminus of the CaSR may contain binding sites for Ca^{2+}_o, spermine and spermidine. In support of this, removal of the N-terminus reduced spermidine and spermine affinity by 3-fold and reduced Ca^{2+}_o affinity 10-fold, consistent with the CaSR ECD containing the primary binding sites for Ca^{2+}_o and other polycations.

Also consistent with this notion, polycation Hill slopes were reduced at the headless CaSR including those for agmatine and Gd^{3+}, suggesting a loss in positive cooperativity between multiple binding sites after removal of the CaSR N-terminus. A loss in positive cooperativity upon removal of the N-terminus would be expected to result in a loss in agonist affinity because positive binding cooperativity is reciprocal. The fact that agmatine affinity and Gd^{3+} potency were not reduced at the headless CaSR suggests agmatine and Gd^{3+} bind more favourably to the 7TM in the absence of the VFT, thus counteracting the loss in positive cooperativity between the VFT and 7TM binding sites.

Next, we investigated how different amino acid substitutions affect agonist binding at the CaSR. Surprisingly, VFT mutations located at sites occupied by Ca^{2+}_o in the solved VFT and full-length structures did not affect Ca^{2+}_o affinity in our study. Of note, previous studies seeking to validate Ca^{2+}_o binding sites did not quantify effects of mutations on agonist affinity or efficacy but instead relied on mutation-induced changes in agonist potency and E_{max} with no consideration of the effect of mutations on receptor expression levels (Geng et al., 2016; Zhang et al., 2016). In the current study, reductions in Ca^{2+}_o potency were indeed observed at VFT mutants, consistent with previous studies (Geng et al., 2016; Zhang et al., 2016). However, in the presence of receptor reserve, potency is a composite value of agonist affinity and efficacy. Therefore, we delineated Ca^{2+}_o affinity at WT and VFT mutant CaSRs and found that VFT mutations do not affect Ca^{2+}_o affinity. This inconsistency could be because Ca^{2+}_o interacts with the CaSR via multiple binding sites and single amino acid substitutions do not significantly alter its binding affinity.

In comparison to Ca^{2+}_o, polyamine affinity was affected by several VFT mutations. For example, I81A and S84A located in Ca^{2+}_o binding site 1 reduced spermidine and spermine affinity, suggesting that spermidine and spermine either interact directly with the primary Ca^{2+}_o binding site or these amino acid mutations cause indirect conformational changes that reduce polyamine affinity. Of note, as mentioned before, removal of the N-terminus did not reduce agmatine affinity, but I81A and S84A mutations caused a small (~2-fold) but significant decrease in agmatine affinity. This inconsistency could be due to the fact that these mutational effects were minimal and were not reflected when removing the N-terminus, or because while agmatine binding to the 7TM may be favoured by complete N-terminal removal, the same is not true when the agmatine VFT binding site alone is removed.

Ca^{2+}_o and polyamines lost their ability to signal at five headless 7TM and ECL mutants. Among them, Ala substitution of $F668^{2.56}$, $I841^{7.36}$ or $F688^{3.40}$, and Ile substitution of $E837^{7.32}$ abolished or significantly reduced receptor expression, demonstrating the importance of these residues for correct receptor folding and expression. Intriguingly, Ca^{2+}_o and polyamines lost responses at the $F684^{3.36}$A headless mutant, despite this mutant maintaining considerable receptor expression, and Gd^{3+} retaining agonism. These results suggest Ca^{2+}_o and polyamines exhibit distinct binding or activation mechanisms compared to Gd^{3+}. While we have established that $F684^{3.36}$ is critical to Ca^{2+}_o and polyamine activity, we cannot distinguish whether this mutation caused a loss in Ca^{2+}_o and polyamine binding versus efficacy.

Spermidine and spermine affinities were increased, and putrescine signalling restored, by two ECL mutations in the headless CaSR: R752^{ECL2}A and E767^{ECL2}A, the latter of which contributes to a small molecule binding pocket (Leach et al., 2016). Of note, these two mutations did not alter Ca^{2+}_o or agmatine affinity. This is unsurprising as spermidine and spermine share similar chemical structures therefore it is likely that they interact with common amino acids or are similarly affected by mutations that stabilise conformational changes that have indirect effects on agonist affinity.

In addition to residues involved in agonist binding, we also investigated residues that contribute to agonist efficacy. The CaSR VFT undergoes large conformational rearrangements that include movement of LB1-LB2 and LB2-LB2 towards each other, resulting in a closed-closed conformation (Geng et al., 2016; Ling et al., 2021; Zhang et al., 2016) (**Figure 4.1**). Therefore, mutations at amino acids on the LB1-LB2 and LB2-LB2 likely disrupt rearrangements and stabilisation of the VFT upon agonist activation, affecting the signalling efficacy of agonists. However, interestingly, mutations at the LB2-LB2 interface only reduced agmatine efficacy and had no effects on Ca^{2+}_o or the other polyamines. Furthermore, previous structural studies demonstrated that T100A and S170A mutations (located in the LB1-LB2 interdomain cleft) reduced Ca^{2+}_o potency and maximal responses and concluded that these two residues were involved in Ca^{2+}_o binding (Geng et al., 2016; Zhang et al., 2016). However, we demonstrated that both T100A and S170A lost significant receptor expression, causing a reduction in potency and maximal agonist responses, but neither Ca^{2+}_o affinity nor efficacy was reduced after correcting for receptor expression levels. Changes in E_{max} alone are therefore a gross misinterpretation when deducing affinity or efficacy residues. In comparison, we demonstrated S170A reduced spermidine and spermine efficacy when corrected for expression levels and abolished agmatine and putrescine responses. Similarly, in the CaSR 7TM, two mutations affected spermidine and spermine affinity (E755^{ECL2}A) or efficacy (I760^{ECL2}A) but did not affect other agonists, suggesting unique binding and activation residues utilised by spermidine and spermine. However, it is difficult to draw conclusions about where polycations bind in the 7TM as most mutations abolished polycation responses thereby preventing delineation of mutation effects on agonist affinity versus efficacy.

In conclusion, this study provides structure-function evidence that CaSR agonists bind to both the CaSR's VFT and 7TM. We demonstrate polycations likely interact with residues in Ca^{2+}_o binding site 1 in the VFT as well as residues in a small molecule 7TM binding site, and polyamines utilise similar residues to transmit agonism. Further investigation including

computational docking of polyamines as well as solving an active CaSR structure in the presence of polyamines would be essential to support the mutagenesis results presented herein. Together, these results will inform future rational drug design seeking to disrupt polyamine-CaSR signalling in asthma.

4.3 Supplementary information

Table S1. Primers used to generate mutant CaSR constructs via Quikchange II site-directed mutagenesis

	Sense (5'-3')	Antisense (5'-3')
I81A	Aagggctgggctgctgtttgcctcctctatggcaaatatc	gatatttgccatagaggaggcaaacagcagcccagccctt
S84A	Gggaagaagggctggggcgctgtttatctcctct	agaggagataaacagcgccccagcccttcttccc
T100A	Ttagaaacggtgttgcaagcgtcaaatatcctgtatccc	gggatacaggatatttgacgcttgcaacaccgtttctaa
N102A	Caaggccttagaaacggtggcgcaagtgtcaaatatcctg	caggatatttgacacttgcgccaccgtttctaaggccttg
S170A	Tgaggagtctgctggcggaggcataactgac	gtcagttatgcctccgccagcagactcctca
E228A	Ccctttcctcagcttccgctcggaatttctcaatc	gattgagaaattccgagcggaagctgaggaaaggg
E231A	Ttccgagaggaagctgcggaaagggatatctgc	gcagatatccctttccgcagcttcctctcggaa
E232A	Gatgcagatatcccttgcctcagcttcctctcg	cgagaggaagctgaggcaagggatatctgcatc
D234A	Tgaagtcgatgcagatagccctttcctcagcttcc	ggaagctgaggaaagggctatctgcatcgacttca
S240A	Gtactgggagatgagttcagcgaagtcgatgcagatatcc	ggatatctgcatcgacttcgctgaactcatctcccagtac
E241A	Agtactgggagatgagtgcactgaagtcgatgcag	ctgcatcgacttcagtgcactcatctcccagtact
S302A	Cgatcagggaggcgctggcccaggc	gcctgggccagcgcctccctgatcg
S303 A	Ggcgatcagggcggagctggccc	gggccagctccgccctgatcgcc
F668$^{2.56}$A	Ccagctccctgttcgccatcggggagcccc	ggggctccccgatggcgaacagggagctgg
F684$^{3.36}$A	Gcgccagccggccgctggcatcagcttc	gaagctgatgccagcggccggctggcgc
F688$^{3.40}$A	Ggcctttggcatcagcgccgtgctctgcatctca	tgagatgcagagcacggcgctgatgccaaaggcc
S750^{ECL2}A	Ctggttgcggtaggctgaggggggcgcg	cgcgccccccctcagcctaccgcaaccag
R752^{ECL2}A	Ccagctcctggttggcgtagcttgaggggg	ccccctcaagctacgccaaccaggagctgg
Q754^{ECL2}A	Ctcatcctccagctccgcgttgcggtagcttgag	ctcaagctaccgcaacgcggagctggaggatgag
E755^{ECL2}A	Tctcatcctccagcgcctggttgcggtag	ctaccgcaaccaggcgctggaggatgaga
I760^{ECL2}A	Ggcacgtgatgaagatggcctcatcctccagctcct	aggagctggaggatgaggccatcttcatcacgtgcc
I761^{ECL2}A	Cgtggcacgtgatgaaggcgatctcatcctccagct	agctggaggatgagatcgccttcatcacgtgccacg
E767^{ECL2}A	Atcacgtgccacgcgggctccctcatg	catgagggagcccgcgtggcacgtgat
E837$^{7.32}$I	Gcaagtttgtctctgccgtaatagtgattgccatcctggcag	ctgccaggatggcaatcactattacggcagagacaaacttgc
I841$^{7.36}$A	Cgtagaggtgattgccgccctggcagccagcttt	gcatctccactaacggcgggaccgtcggtcgaaa

Table S4.2. Potency (pEC_{50}), maximal response (E_{max}) and Hill slope (nH) parameters at WT and full-length mutants determined in $Ca^{2+}{}_i$ mobilisation assays. Data are represented as mean ± SEM from 3-6 independent experiments performed in duplicate, and analysed via one-way ANOVA followed by Dunnett's post-test, *P<0.05, **P<0.01, ***P<0.001, ****P<0.0001

	Gd^{3+}			$Ca^{2+}{}_o$			Agmatine			Putrescine			Spermidine			Spermine		
	pEC_{50}	E_{max}	nH	pEC_{50}	E_{max}	nH	pEC_{50}	E_{max}	nH	pEC_{50}	E_{max}	nH	pEC_{50}	E_{max}	nH	pEC_{50}	E_{max}	nH
WT	4.61±0.03	98±2	2.3±0.1	3.56±0.02	97±1	2.3±0.1	2.35±0.03	84±3	2.3±0.1	1.75±0.04	61±3	2.3±0.1	3.45±0.01	98±4	2.3±0.1	4.51±0.02	120±3	2.3±0.1
I81A	4.10±0.04	57±2****	1.8±0.2	3.18±0.04*	53±2****	2.6±0.1	1.78±0.05****	18±2****	2.8±0.5	NR	NR	NR	2.74±0.05***	18±2****	2.5±0.3	3.46±0.02****	43±1****	2.5±0.3
S84A	4.56±0.04	83±2	1.0	3.33±0.04	82±3	2.7±0.4	2.13±0.07	54±3****	1.7±0.2	1.60±0.25	31±11**	1.9±0.7	2.93±0.06**	53±3****	1.5±0.3	3.56±0.04****	67±2****	1.7±0.3
T100A	3.92±0.08	49±4****	1.0	2.89±0.16****	34±5****	1.0	NR			NR			2.64±0.30****	13±10****	2.6±0.6	3.11±0.06****	35±3****	1.7±0.4
N102A	4.41±0.03	108±3	1.9±0.1	3.25±0.04	95±3	1.9±0.1	1.78±0.08****	47±4****	1.9±0.1	NR			2.79±0.04***	100±5	1.9±0.1	3.94±0.04*	87±3	1.9±0.1
S170A	3.83±0.06**	80±5	1.5±0.2	2.43±0.15****	50±10****	1.5±0.2	NR			NR			2.79±0.16***	33±7****	1.5±0.2	3.58±0.41****	19±6****	1.5±0.2
E228A	4.33±0.08	77±4	1.2±0.1*	3.58±0.07	76±3**	1.2±0.1*	2.86±0.09****	51±1***	1.2±0.1	2.48±0.11**	46±3	1.2±0.1*	3.76±0.06	83±4	1.2±0.1*	4.61±0.05	86±2	1.2±0.1
E231A	4.40±0.07	121±7	1.1±0.1	3.38±0.03	116±3*	2.3±0.3	2.28±0.04	75±3	2.3±0.4	1.64±0.13	98±21	1.4±0.4	3.28±0.02	89±2	2.7±0.2	4.08±0.02	97±2	2.7±0.2
E232A	4.20±0.06	123±6*	2.2±0.1	3.30±0.04	106±4	2.2±0.4	2.01±0.06	76±3	1.6±0.2	1.60±0.06	66±5	1.8±0.3	3.30±0.05	92±5	1.9±0.3	4.14±0.04	90±3	1.7±0.3
D234A	4.05±0.18	125±16*	1.0	3.44±0.05	94±4	2.0±0.4	2.42±0.06	71±3	2.0±0.6	1.87±0.06	76±4	2.1±0.6	3.30±0.06	76±6	2.0±0.5	4.07±0.04	87±3	1.7±0.2

S240A	4.39±0.05	106±4	1.3±0.2	3.34±0.03	107±3	2.3±0.3	2.28±0.04	67±3***	2.0±0.3	1.66±0.05	62±4	2.1±0.4	3.36±0.04	87±5	2.4±0.4	4.31±0.04	95±3	2.2±0.4
E241A	4.54±0.05	94±4	2.1±0.1	3.49±0.04	92±3	2.1±0.1	2.44±0.04	55±2***	2.1±0.1	1.90±0.04	43±3	2.1±0.1	3.50±0.02	90±2	2.1±0.1	4.27±0.03	102±2	2.1±0.1
S302A	4.14±0.05	79±3*	1.77±0.14	3.41±0.05	82±3	1.8±0.1	2.24±0.09	43±3***	1.8±0.1	1.68±0.30	18±6***	1.8±0.1	3.24±0.06	77±5	1.8±0.1	4.17±0.04	81±3	1.8±0.1
S303A	4.35±0.05	99±4	1.4±0.1	3.41±0.02	97±2	2.4±0.3	2.26±0.02	65±1**	1.9±0.1	1.42±0.07	61±5	1.4±0.2	3.26±0.02	83±2	2.7±0.6	4.24±0.04	93±3	2.8±0.6

Table S4.3. Potency (pEC_{50}), maximal response (E_{max}) and Hill slope (nH) parameters at headless and headless mutants determined in Ca^{2+}_i mobilisation assays. Data are represented as mean ± SEM from 4-7 independent experiments performed in duplicate, and analysed via one-way ANOVA followed by Dunnett's post-test, *P<0.05, **P<0.01, ***P<0.001, ****P<0.0001.

	Gd^{3+}			Ca^{2+}_o			Agmatine			Putrescine			Spermidine			Spermine		
	pEC_{50}	E_{max}	nH	pEC_{50}	E_{max}	nH	pEC_{50}	E_{max}	nH	pEC_{50}	E_{max}	nH	pEC_{50}	E_{max}	nH	pEC_{50}	E_{max}	nH
ΔH	4.51± 0.08	123 ±6	1.0#	2.52± 0.18	90± 8	1.0#	2.37± 0.14	43±5	1.0#	NR			3.07± 0.20	56±11	1.0#	3.35± 0.12	63±6	1.0#
F668$^{2.56}$A ΔH	NR																	
F684$^{3.36}$A ΔH	3.77± 0.09****	91± 6**	1.6 ±0.2**	NR														
F688$^{3.40}$A ΔH	3.79± 0.07	57± 5	2.3 ±0.7	NR														
S750^{ECL2}A ΔH	4.54± 0.03	125 ±3	1.2 ±0.1	2.69± 0.11	83± 7	1.2 ±0.1	2.16± 0.21	36±5	1.16 ±0.07	NR			3.00± 0.14	51±6	1.2± 0.1	3.69± 0.09	63±3	1.2 ±0.1
R752^{ECL2}A ΔH	4.34± 0.05	119 ±4	1.0#	2.85± 0.09	107 ±7	1.0#	2.47± 0.21	33±4	1.0#	2.22± 0.67	12±5	1.0#	3.42± 0.13	55±4	1.6± 0.3	4.10± 0.12****	65±3	1.0#
Q754^{ECL2}A ΔH	4.39± 0.04	123 ±4	1.0#	2.45± 0.23	112 ±23	1.0#	2.17± 0.24	27±6	1.0#	NR			3.01± 0.08	64±4	1.0#	3.64± 0.08	68±3	1.0#
E755^{ECL2}A ΔH	3.93± 0.05****	130.3±5.34	1.0#	2.47± 0.15	69± 11	1.0#	2.13± 0.30	19±4**	1.0#	NR			2.58± 0.19	42±8	1.0#	2.80± 0.16*	46±7*	1.0#
I760^{ECL2}A ΔH	4.11± 0.05**	115 ±5	1.0#	2.67± 0.33	70± 18	1.0#	2.35± 0.18	20±3**	1.0	NR			3.10± 0.15	23±3**	1.0#	3.38± 0.15	28±3****	1.0

I761^{ECL2}A ΔH	4.10±0.05***	119±4	1.0$^{\#}$	2.97±0.08	96±6	1.0	2.60±0.25	27±4	1.0$^{\#}$	NR			2.88±0.16	42±6	1.0$^{\#}$	3.28±0.11	51±4	1.0$^{\#}$
E767^{ECL2}A ΔH	4.11±0.12***	125±11	1.0	2.35±0.44	125±34	0.6±0.1	2.52±0.07	41±2	1.8±0.5	2.62±0.08	15±1	3.5±1.8	3.35±0.10	43±3	1.5±0.5	3.80±0.08	59±3	1.3±0.3
E837$^{7.32}$I ΔH	3.95±0.04****	37±2*****	3.90±0.26****	NR														
I841$^{7.36}$A ΔH	NR																	

Chapter 5
General discussion

Asthma is a heterogeneous chronic airway disease, characterised by airway inflammation and remodelling leading to airway hyperresponsiveness. Asthma affects ~340 million patients worldwide and 10% of patients have poorly controlled asthma (World Health Organization, 2017b). Of note, no current drug therapies target all the pathophysiological features of asthma. First-line drugs, including β_2-AR agonists and ICSs, only target bronchoconstriction and airway inflammation, respectively (Dockrell et al., 2007). Notably, the efficacy of β_2-AR agonists is limited in severe asthma and reduced after repeated doses due to β_2-AR desensitisation (Barnes & Woolcock, 1998; Dockrell et al., 2007). Further, ICSs are ineffective in severe asthma patients and have side effects that lead to poor compliance (Barnes, 2004a). Therefore, new therapies are needed for severe asthma, particularly those that treat all the pathological features.

The main aim of this study was to validate the CaSR as a novel therapeutic drug target for the treatment of asthma. The current study combined mutagenesis, cell biology, analytical pharmacology, and computational biology and *ex vivo* PCLS studies to progress preclinical CaSR drug discovery (**Figure 5.1**). The best-characterised role of the CaSR is to maintain whole body Ca^{2+}_o homeostasis by detecting small changes in Ca^{2+}_o, but CaSR is expressed on ASM cells and CaSR agonists (e.g. polyamines) are upregulated in asthmatic patients and in murine asthma models (Kurosawa et al., 1992; Yarova et al., 2015), suggesting additional CaSR (patho)physiological roles. Indeed, CaSR NAMs reduce airway inflammation, remodelling and bronchoconstriction in murine asthma models (Lee et al., 2017; Thompson et al., 2016; Yarova et al., 2021; Yarova et al., 2015). The current knowledge gap involves: **i**) lack of comparison of bronchodilator effects between CaSR NAMs and standard-of-care treatments, **ii**) lack of *in vitro* characterisation of different CaSR NAM classes against the most potent polyamine, spermine (i.e., biased agonism and probe dependence as demonstrated in chapter 1), and **iii**) lack of understanding how polyamines bind and activate the receptor.

We now provide further evidence that CaSR NAMs are as efficacious as the standard-of-care bronchodilator, salbutamol, as acute bronchodilators that reverse MCh-mediated bronchoconstriction in *ex vivo* mouse PCLSs. We attempted to elucidate CaSR-induced signalling pathways in healthy and asthmatic ASM cells that may contribute to NAM bronchodilator effects, but this part of the study was only partially completed due to time limitations presented by the COVID-19 pandemic, which slowed research efforts during 2020. Finally, using mutagenesis

combined with functional assays in recombinant HEK293-CaSR cells and analytical pharmacology, we identified key amino acid residues that contribute to the binding and signalling of different polyamines, providing a better understanding of polyamine-CaSR interactions at a molecular level. As a whole, this study will inform the future development of CaSR NAMs for asthma, by contributing knowledge that will facilitate how best to undertake lead identification and drug candidate selection, *in vitro* cell and preclinical mouse models of asthma in which to test CaSR NAMs.

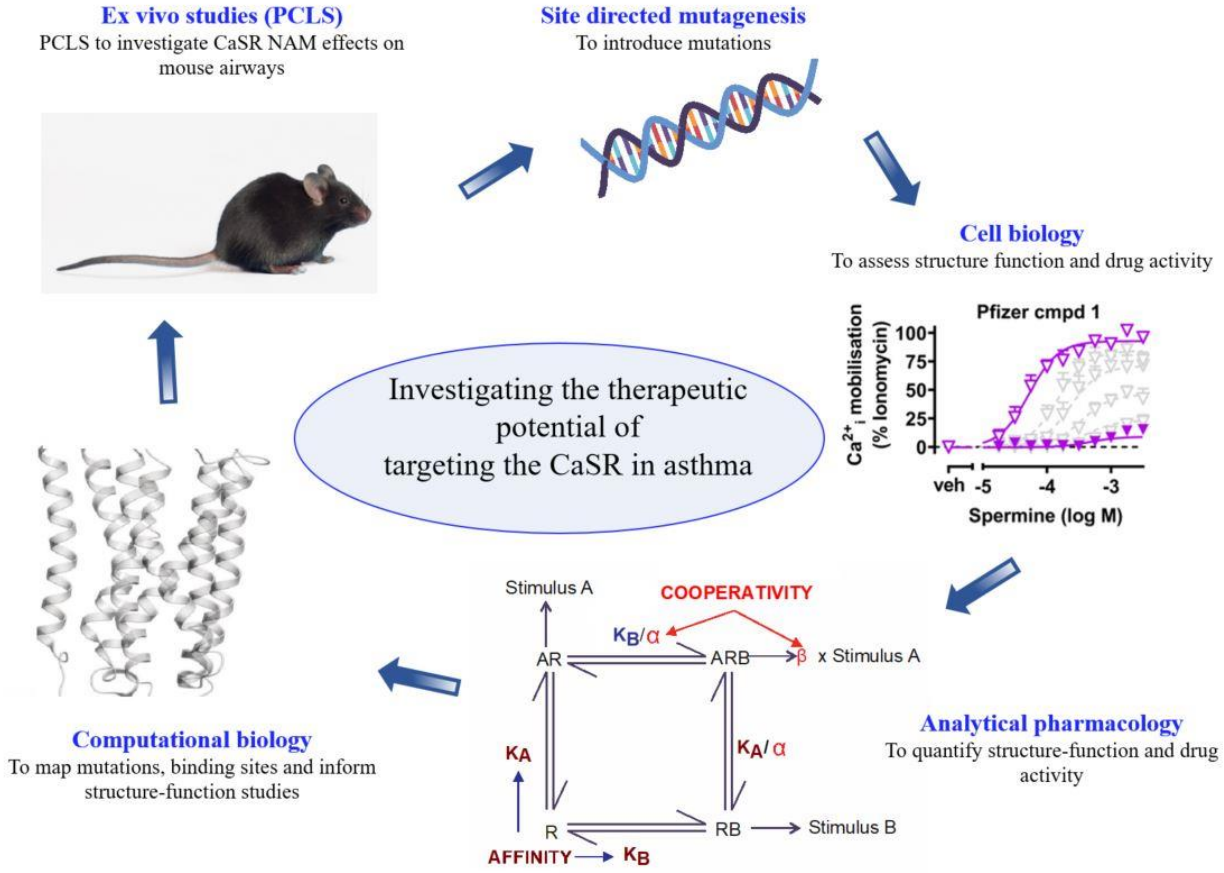

Figure 5.1. A schematic diagram of the drug discovery process undertaken in this study.

In Chapter 2, we demonstrated that spermine both induced airway contraction and enhanced MCh-mediated airway contraction in mouse airways, consistent with a previous study (Yarova et al., 2015). We applied high throughput functional assays ($Ca^{2+}{}_i$ mobilisation and IP_1 accumulation) to evaluate the cellular and molecular effects of five chemically distinct CaSR NAMs (NPS2143, Pfizer compound 1, BMS compound 1, ATF936 and ronacaleret), before applying them to mouse

PCLS to assess CaSR NAMs for their ability to reverse airway contraction. Intriguingly, we observed differences in the affinity and cooperativity of the different CaSR NAMs, and more importantly, BMS compound 1 demonstrated significant bias towards inhibition of spermine-induced Ca^{2+}_i mobilisation over IP_1 accumulation. We thereby progressed three NAMs to use to validate the CaSR as a druggable target for reversing or preventing bronchoconstriction: Pfizer compound 1 for its overall greatest negative cooperativity, BMS compound 1 for its biased modulation (inhibitory effects in Ca^{2+}_i mobilisation but no effects in IP_1 accumulation) and NPS2143, a prototypical CaSR NAM.

Interestingly, CaSR NAMs showed differential effects on MCh-induced airway contraction, with Pfizer compound 1 exhibiting greater bronchodilator efficacy than NPS2143 as well as greater efficacy and potency than salbutamol, a current standard-of-care β_2-AR agonist treatment. However, NPS2143 showed complete prevention of MCh-induced airway contraction after overnight incubation with PCLS even though slices were washed to remove NAMs prior to measuring MCh-mediated contraction. In contrast, Pfizer compound 1 showed partial prevention of MCh-induced airway contraction following overnight incubation, while BMS compound 1 was unable to prevent contraction in this experimental paradigm despite demonstrating comparable ability to Pfizer compound 1 for reversing MCh-mediated airway contraction. Importantly, all CaSR NAMs maintained their bronchodilator effects after β_2-AR desensitisation, which is important as β_2-AR desensitisation is a major clinical problem that reduces salbutamol efficacy (Billington & Penn, 2003).

Combined with previous findings by others demonstrating that CaSR NAMs have anti-inflammatory and anti-remodelling effects in murine asthma models, our findings validating CaSR NAMs are as effective as salbutamol as bronchodilators indicate that CaSR NAMs have the potential to target multiple aspects of asthma pathobiology. However, our findings that NAMs had distinct effects depending on the assay paradigm, and that Pfizer compound 1 had the highest cooperativity, correlating with its superior efficacy for reversing MCh-mediated airway contraction, demonstrate the importance of screening and filtering CaSR NAMs in *in vitro* cell models before applying them to mouse models to ensure the most efficient progression to *ex vivo* studies and beyond.

It is interesting to note that CaSR NAMs did not demonstrate acute bronchoprotection effects after 20 min incubation with PCLS, demonstrating the NAMs could reverse but not prevent MCh-induced airway contraction after only 20 min. Nonetheless, the fact that overnight incubation of PCLS with NPS2143 and Pfizer compound 1 prevented MCh-induced airway contraction suggests long-term modulatory effects of CaSR NAMs worthy of further investigation. This is important because CaSR NAMs have potential as long term bronchoprotective drugs similar to the standard-of-care treatment, formorterol, which is used for acute bronchoprotection before a potential asthma attack.

Unfortunately, CaSR NAMs lost bronchodilator effects against combined MCh and spermine induced airway contraction. This could be due to the fact that spermine and CaSR NAMs target the same receptor, therefore it is harder for the NAMs to reverse MCh-mediated airway contraction when CaSR activity is enhanced by spermine. Findings from mutagenesis studies indicated that spermine binds to the 7TM of the CaSR, similar to small molecule NAMs (Josephs et al., 2019). A better understanding of polyamine binding sites could aid the development of novel NAMs that bind to alternative sites on the CaSR.

Furthermore, CaSR NAM bronchodilator effects should be assessed in preclinical severe and exacerbated asthma models. The house dust mite (HDM)-induced asthma model is one of the potential platforms to investigate such effects, in which mice develop airway remodelling, and inflammation (mostly eosinophilic infiltration) (Woo et al., 2018). In addition to the acute effects of CaSR NAMs on established AHR in these models, we could also investigate whether chronic treatment with CaSR NAMs inhibits the development of other asthma aspects, such as airway inflammation and remodelling, cytokine secretion and collagen production. Current drug treatments do not adequately oppose these aspects in severe asthma (reviewed in Pera & Penn, 2016). These *in vivo* mouse models may reflect the potential role of CaSR NAMs in regulating *in situ* responses relevant to asthma.

In addition to using mouse models, it is also important to validate the role of the CaSR in human ASM cells, rather than recombinant FlpIn HEK293 TRex cells stably transfected with the CaSR, to support clinical translation of CaSR NAMs. Therefore, following evaluation of bronchodilator and bronchoprotective effects of CaSR NAMs in mouse airways, we aimed to elucidate the full scope of ASM (patho) physiological signalling pathways in healthy and asthmatic ASM cells. The

advantage of using healthy and asthmatic ASM cells compared to mouse PCLS experiments includes: **i**) the (patho) physiological cellular signalling pathways in ASM cells can be determined; **ii**) studies are undertaken in human cells, which is important because animal experiments often do not translate into human asthmatic conditions (Bracken, 2009). We showed that in ASM cells isolated from healthy and asthmatic human donors, only a low level of *CASR* gene expression was detected (including in cells from asthmatics with mild and severe asthma). Preliminary results indicated that $Ca^{2+}{}_i$ release was stimulated by contractile agonists (e.g., MCh, spermine and $Ca^{2+}{}_o$) in some ASM cell lines. However, responses to different stimuli were variable and so assays need further optimisation. The low level of *CASR* gene expression may indicate that primary ASM cells in culture may not be suitable to investigate CaSR-mediated signalling pathways in ASM. However, CaSR expression in these cells still needs to be determined using SDS PAGE and western blotting to establish whether the CaSR protein is present. Further progress of our studies on ASM cells was largely compromised due to the COVID-19 pandemic, which hindered additional experiments to confirm these findings and to extend analysis to additional signalling pathways.

Finally, we probed the binding and function of polyamines at the CaSR. Previous mutagenesis and structural studies have focused on investigating $Ca^{2+}{}_o$-mediated CaSR activation but polyamine binding and function at the CaSR have not been investigated in detail. It is important to probe the polyamine-mediated CaSR binding and activation network compared to $Ca^{2+}{}_o$-mediated networks due to the possibility of probe dependence. Previous mutagenesis studies suggest that polyamines bind to both the CaSR VFT and 7TM (Northup et al.), similar to $Ca^{2+}{}_o$. Therefore, we first investigated the effects of removal of the N-terminus of the CaSR. Removal of the N-terminus had less effect on polyamine binding affinity (~3-fold reduction) compared to the ~10-fold reduction in $Ca^{2+}{}_o$ affinity, suggesting that polyamine primary binding sites are most likely located in the 7TM. Furthermore, the affinity and efficacy of polyamines were similarly affected by distinct amino acid residues, suggesting similar binding or function networks for different polyamines. The affinity and efficacy of spermidine and spermine (which share the most similar chemical structure compared to other polyamines) were affected by the same amino acid substitutions, suggesting that it is likely that spermidine and spermine utilise similar residues to transmit signals. However, further investigation such as computational docking of polyamines or solving active CaSR structures bound to polyamines are important to validate these mutagenesis results. In

conclusion, this study provides mutagenesis evidence that CaSR agonists bind to both the CaSR's VFT and 7TM. We demonstrate that polycations likely interact with residues in Ca^{2+}_o binding site 1 in the VFT as well as residues in a small molecule 7TM binding site. However, further investigation including computational docking of polyamines as well as solving an active CaSR structure when bound to polyamines would be essential to support the mutagenesis results in this study.

Overall, current drug treatments for asthma, including SABAs and LABAs, have limited efficacy and receptor desensitisation therefore safe and more effective bronchodilators are required for treating asthma, particularly in more severe asthma condition or after β2-AR desensitisation. We herein demonstrate that CaSR NAMs elicite bronchodilator effects in naïve mice, suggesting their potential therapeutic effects for treating asthma.

References

Agostinelli E, Marques MPM, Calheiros R, Gil FPSC, Tempera G, Viceconte N, *et al.* (2010). Polyamines: fundamental characters in chemistry and biology. Amino Acids 38**:** 393-403.

Akinbami LJ, Moorman JE, Bailey C, Zahran HS, King M, Johnson CA, *et al.* (2012). Trends in asthma prevalence, health care use, and mortality in the United States, 2001-2010. NCHS Data Brief 94**:** 1-8.

Akizawa T, Shimazaki R, Fukagawa M, & Group ES (2018). Phase 2b study of evocalcet (KHK7580), a novel calcimimetic, in Japanese patients with secondary hyperparathyroidism undergoing hemodialysis: A randomized, double-blind, placebo-controlled, dose-finding study. PLOS One 13**:** e0204896-0204815.

Alamshah A, Spreckley E, Norton M, Kinsey-Jones JS, Amin A, Ramgulam A, *et al.* (2017). l-phenylalanine modulates gut hormone release and glucose tolerance, and suppresses food intake through the calcium-sensing receptor in rodents. International Journal of Obesity (Lond) 41**:** 1693-1701.

Alangari AA (2014). Corticosteroids in the treatment of acute asthma. Annals of Thoracic Medicine 9**:** 187-192.

Alexander ST, Hunter T, Walter S, Dong J, Maclean D, Baruch A, *et al.* (2015). Critical Cysteine Residues in Both the Calcium-Sensing Receptor and the Allosteric Activator AMG 416 Underlie the Mechanism of Action. Molecular Pharmacology 88**:** 853-865.

Alon US, & VanDeVoorde RG (2010). Beneficial effect of cinacalcet in a child with familial hypocalciuric hypercalcemia. Pediatric Nephrology 25**:** 1747-1750.

Amrani Y, & Panettieri RA (2002). Modulation of calcium homeostasis as a mechanism for altering smooth muscle responsiveness in asthma. Current Opinion in Allergy and Clinical Immunology 2**:** 39-45.

Amrani Y, & Panettieri RA (2003). Airway smooth muscle: contraction and beyond. The International Journal of Biochemistry & Cell Biology 35**:** 272-278.

Atay Z, Bereket A, Haliloglu B, Abali S, Ozdogan T, Altuncu E, *et al.* (2014). Novel homozygous inactivating mutation of the calcium-sensing receptor gene (CASR) in neonatal severe hyperparathyroidism—lack of effect of cinacalcet. Bone 64**:** 102-107.

Atchison D, K., Ortiz-Capisano MC, & Beierwaltes W, H. (2010). Acute activation of the calcium-sensing receptor inhibits plasma renin activity in vivo. The American Journal of Physiology - Regulatory, Integrative and Comparartive Physiology 299**:** 1020-1026.

Australian Bureau of Statistics (2015). National Health Survey: First Results, 2014-15: Australian Bureau Statistics.

Australian Centre for Asthma Monitoring (2007). Asthma in Australia: findings from the 2004-05 National Health Survey Cat. no. ACM.10.: Canerra: Australian Institute of Health and Welfare.

Australian Centre for Asthma Monitoring (2008). Asthma in Australia 2008 AIHW Asthma Series no.3. Cat. no. ACM 14.: Canberra: Australian Institute of Health and Welfare.

Awata H, Huang C, Handlogten ME, & Miller RT (2001). Interaction of the Calcium-sensing Receptor and Filamin, a Potential Scaffolding Protein. Journal of Biological Chemistry 276**:** 34871-34879.

Ba J, Brown D, & Friedman PA (2003). Calcium-sensing receptor regulation of PTH-inhibitable proximal tubule phosphate transport. American Journal of Physiology-Renal Physiology 285**:** F1233-F1243.

Babinsky VN, Hannan FM, Gorvin CM, Howles SA, Nesbit MA, Rust N, *et al.* (2016). Allosteric modulation of the calcium-sensing receptor rectifies signaling abnormalities associated with G-protein alpha-11 mutations causing hypercalcemic and hypocalcemic disorders. Journal of Biological Chemistry 291**:** 10876-10885.

Bai M, Trivedi S, Lane CR, Yang Y, Quinn S, & Brown EM (1998). Protein kinase C phosphorylation of threonine at position 888 in Ca^{2+o}-sensing receptor stably expressed in HEK293 cells. American Journal of Physiology-Cell Physiology 292**:** 1895-1905.

Bai Y, & Sanderson MJ (2006). Modulation of the Ca2+ sensitivity of airway smooth muscle cells in murine lung slices. The American Journal of Physiology-Lung Cellular and Molecular Physiology291**:** 208-221.

Balan G, Bauman J, Bhattacharya S, Castrodad M, Healy DR, Herr M, *et al.* (2009). The discovery of novel calcium sensing receptor negative allosteric modulators. Bioorganic & Medicinal Chemistry Letters 19**:** 3328-3332.

Bara I, Ozier A, Tunon DLJ, Marthan R, & Berger P (2010). Pathophysiology of bronchial smooth muscle remodelling in asthma. European Respiratory Journal 36**:** 1174-*1184.

Barnes PJ (2004a). Corticosteroid resistance in airway disease. Proceedings of the American Thoracic Society 1**:** 264-268.

Barnes PJ (2004b). Distribution of Receptor Targets in the Lung. Proceedings of the American Thoracic Society 1**:** 345-351.

Barnes PJ (2006a). Corticosteroid effects on cell signalling. European Respiratory Journal 27**:** 413-426.

Barnes PJ (2006b). How corticosteroids control inflammation. British Journal of Pharmacology 148**:** 245-254.

Barnes PJ, Greening AP, & Crompton GK (1995). Glucocorticoid resistance in asthma. American Journal of Respiratory and Critical Care Medicine 152**:** S125-S140.

Barnes PJ, & Woolcock AJ (1998). Difficult asthma. European Respiratory Journal 12**:** 1209-1218.

Bateman ED, Hurd SS, Barnes PJ, Bousquet J, Drazen JM, FitzGerald M, *et al.* (2008). Global strategy for asthma management and prevention: GINA executive summary. European Respiratory Journal 31**:** 143-178.

Berridge MJ (1993). Inositol triphosphate and calcium signaling. Nature 361**:** 315-325.

Bert B, Fink H, Rothe J, Walstab J, & Bönisch H (2008). Learning and memory in 5-HT1A-receptor mutant mice. Behavioural Brain Research 195**:** 78-85.

Bevilacqua M, Dominguez LJ, Righini V, Valdes V, Toscano R, Sangaletti O, *et al.* (2005). Increased Gastrin and Calcitonin Secretion after Oral Calcium or Peptones Administration in Patients with Hypercalciuria: A Clue to an Alteration in Calcium-Sensing Receptor Activity. The Journal of Clinical Endocrinology & Metabolism 90**:** 1489-1494.

Billington CK, Ojo OO, Penn RB, & Ito S (2013). cAMP regulation of airway smooth muscle function. Pulmonary Pharmacology & Therapeutics 26**:** 112-120.

Billington CK, & Penn RB (2003). Signaling and regualtion of G-protein-coupled receptors in airway smooth muscle. Respiratory Research 4**:** 2.

Black JW, & Leff P (1983). Operational Models of Pharmacological Agonism. Proceedings of the Royal Society of London Series B, Biological Sciences 220**:** 141-162.

Blanchard C, & Rothenberg ME (2009). Biology of the eosinophil. Advance in Immunology 101**:** 81-121.

Blier P, Bergeron R, & de Montigny C (1997). Selective Activation of Postsynaptic 5-HT1A Receptors Induces Rapid Antidepressant Response. Neuropsychopharmacology 16**:** 333.

Block GA, Bushinsky DA, Cheng S, Cunningham J, Dehmel B, Drueke TB, *et al.* (2017a). Effect of etelcalcetide vs cinacalcet on serum parathyroid hormone in patients receiving hemodialysis with secondary hyperparathyroidism: A randomized clinical trialetelcalcetide vs cinacalcet in hemodialysis with secondary hyperparathyroidism etelcalcetide vs cinacalcet in hemodialysis with secondary hyperparathyroidism. The Journal of the American Medical Association 317**:** 156-164.

Block GA, Bushinsky DA, Cunningham J, Drueke TB, Ketteler M, Kewalramani R, *et al.* (2017b). Effect of Etelcalcetide vs Placebo on Serum Parathyroid Hormone in Patients Receiving Hemodialysis With Secondary Hyperparathyroidism: Two Randomized Clinical Trials. JAMA 317**:** 146-155.

Block GA, Martin KJ, de Francisco ALM, Turner SA, Avram MM, Suranyi MG, *et al.* (2009). Cinacalcet for secondary hyperparathyroidism in patients receiving hemodialysis. The New England Journal of Medicine 350**:** 1516-1525.

Bochner BS, Klunk DA, Sterbinsky SA, Coffman RL, & Schleimer RP (1995). IL-13 selectively induces vascular cell adhesion molecule-1 expression in human endothelial cells Journal of Immunology 154**:** 799-803.

Boivin B, Vaniotis G, Allen BG, & Hebert TE (2008). G Protein-Coupled Receptors in and on the Cell Nucleus: A New Signaling Paradigm? Journal of Receptors and Signal Transduction 28**:** 15-28.

Bourke JE, Bai Y, Donovan C, Esposito JG, Tan X, & Sanderson MJ (2014). Novel small airway bronchodilator responses to rosiglitazone in mouse lung slices. American Journal of Respiratory Cell and Molecular Biology 50**:** 748-756.

Bouvier M, Collins S, O'Dowd BF, Campbell PT, Deblasi A, Kobilka BK, *et al.* (1989). Two distinct pathways for cAMPmediated down-regulation of the beta2-adrenergic receptor: phosphorylation of the receptor and regulation of its mRNA levels. Journal of Biological Chemistry 264**:** 16786-16792.

Bover J, Ureña P, Ruiz-García C, daSilva I, Lescano P, Del Carpio J, *et al.* (2016). Clinical and practical use of calcimimetics in dialysis patients with secondary hyperparathyroidism. Clinical Journal of the American Society of Nephrology 11**:** 161.

Bracken MB (2009). Why animal studies are often poor predictors of human reactions to exposure. Journal of the Royal Society of Medicine 102**:** 120-122.

Brennan SC, Wilkinson WJ, Tseng H-E, Finney B, Monk B, Dibble H, *et al.* (2016). The extracellular calcium-sensing receptor regulates human fetal lung development via CFTR. Scientific Reports 6**:** 21975.

Brenner BE, Clavda KK, & Camargo CA (2000). Randomized trial of inhaled flunisolide versus placebo among asthmatic patients discharged from the emergency department. Annals of Emergency Medicine 36**:** 417-426.

Breschi MC, Blandizzi C, Fogli S, Martinelli C, Adinolfi B, Calderone V, *et al.* (2007). In vivo adenosine A2B receptor desensitization in guinea-pig airway smooth muscle: Implications for asthma. European Journal of Pharmacology 575**:** 149-157.

Brixen KT, Christensen B, Ejersted C, & Langdahl BL (2004). Teriparatide (biosynthetic human parathyroid hormone 1–34): A new paradigm in the treatment of osteoporosis. Basic & Clinical Pharmacology & Toxicology 94**:** 260-270.

Broadhead GK, Mun H, Avlani VA, Jourdon O, Church WB, Christopoulos A, *et al.* (2011). Allosteric modulation of the calcium-sensing receptor by γ-glutamyl peptides. Journal of Biological Chemistry 286**:** 8786-8797.

Brown EM, Gamba G, Riccardi D, Lombardi M, Butters R, Kifor O, *et al.* (1993). Cloning and characterization of an extracellular Ca2+-sensing receptor from bovine parathyroid. Nature 366**:** 575-580.

Brown EM, Katz C, Butters R, & Kifor O (1991). Polyarginine, polylysine, and protamine mimic the effects of high extracellular calcium concentrations on dispersed bovine parathyroid cells. Journal of Bone and Mineral Research 6**:** 1217-1226.

Brown EM, & Macleod RJ (2001). Extracellular calcium sensing and extracellular calcium signaling. Physiological Reviews 81**:** 239-297.

Brown RA, Spina D, & Page CP (2008). Adenosine receptors and asthma. British Journal of Pharmacology 153 Suppl 1**:** S446-456.

Bu L, Michino M, Wolf RM, & Brooks CL (2008). Improved model building and assessment of the Calcium-sensing receptor transmembrane domain. Proteins 71**:** 215-226.

Buchan AMJ, Squires PE, Ring M, & Meloche RM (2001). Mechanism of action of the calcium-sensing receptor in human antral gastrin cells. Gastroenterology 120**:** 1128-1139.

Bush A (2019). Pathophysiological Mechanisms of Asthma. Frontiers in Pediatrics 7**:** 68.

Bushinsky DA, Chertow GM, Cheng S, Deng H, Kopyt N, Martin KJ, *et al.* (2019). One-year safety and efficacy of intravenous etelcalcetide in patients on hemodialysis with secondary hyperparathyroidism. Nephrology Dialysis Transplantation.

Busque SM, Kerstetter JE, Geibel JP, & Insogna K (2005). l-Type amino acids stimulate gastric acid secretion by activation of the calcium-sensing receptor in parietal cells. American Journal of Physiology-Gastrointestinal and Liver Physiology 289**:** G664-G669.

Calebiro D, Nikolaev VO, Persani L, & Lohse MJ (2010). Signaling by internalized G-protein-coupled receptors. Trends in Pharmacological Sciences 31**:** 221-228.

Caltabiano S, Dollery CT, Hossain M, Kurtinecz MT, Desjardins JP, Favus MJ, *et al.* (2013). Characterization of the effect of chronic administration of a calcium-sensing receptor antagonist, ronacaleret, on renal calcium excretion and serum calcium in postmenopausal women. Bone 56**:** 154-162.

Capozza M, Chinellato I, Guarnieri V, Di lorgi N, Accadia M, Traggiai C, *et al.* (2018). Case report: acute clinical presentation and neonatal management of primary hyperparathyroidism due to a novel CaSR mutation. BMC Pediatrics 18**:** 340.

Cazzola M, Page CP, Calzetta L, & Matera MG (2012). Pharmacology and therapeutics of bronchodilators. Pharmacological Reviews 64**:** 450-504.

Cha SK, Huang C, Ding Y, Qi X, Huang C, & Miller RT (2011). Calcium-sensing Receptor Decreases Cell Surface Expression of the Inwardly Rectifying K+ Channel Kir4.1. Journal of Biological Chemistry 286**:** 1828-1835.

Chakrabarty S, Radjendirane V, Appelman H, & Varani J (2003). Extracellular Calcium and Calcium Sensing Receptor Function in Human Colon Carcinomas. Promotion of E-Cadherin Expression and Suppression of β-Catenin/TCF Activation 63**:** 67-71.

Chang W, Chen T-H, Pratt S, & Shoback D (2000). Amino acids in the second and third intracellular lopps of the parathyroid Ca^{2+}-sensing receptor mediate effcient coupling to phospholipase C. Journal of Biological Chemistry 275.

Chang W, Pratt S, Chen T, Bourguignon L, & Shoback D (2001). Amino Acids in the Cytoplasmic C Terminus of the Parathyroid Ca2+-sensing Receptor Mediate Efficient Cell-surface Expression and Phospholipase C Activation. Journal of Biological Chemistry 276**:** 44129-44136.

Chang W, Tu C, Chen T-H, Bikle D, & Shoback D (2008). The extracellular calcium-sensing receptor (CaSR) is a critical modulator of skeletal development. Science Signalling 1**:** ra1-ra1.

Chang W, Tu C, Cheng Z, Rodriguez L, Chen T-H, Gassmann M, *et al.* (2007). Complex Formation with the Type B γ-Aminobutyric Acid Receptor Affects the Expression and Signal Transduction of the Extracellular Calcium-sensing Receptor: STUDIES WITH HEK-293 CELLS AND NEURONS. Journal of Biological Chemistry 282**:** 25030-25040.

Chattopadhyay N, Cheng I, Rogers K, Riccardi D, Hall A, Diaz R, *et al.* (1998). Identification and localization of extracellular Ca2+-sensing receptor in rat intestine. American Journal of Physiology-Gastrointestinal and Liver Physiology 274**:** G122-G130.

Chattopadhyay N, Jeong K-H, Yano S, Huang S, Pang J, L. , Ren X, *et al.* (2007). Calcium receptor stimulates chemotaxis and secretion of MCP-1 in GnRH neurons in vitro: potential impact on reduced GnRH neuron population in CaR-null mice. American Journal of Physiology-Endocrinology and Metabolism 292**:** 523-532.

Chattopadhyay N, Yano S, H.J. T, Rooney P, Kanuparthi D, Bandyopadhyay S, *et al.* (2004). Mitogenic Action of Calcium-Sensing Receptor on Rat Calvarial Osteoblasts. Endocrinology 145**:** 3451-3462.

Chen CJ, Barnett JV, Congo DA, & Brown EM (1989). Divalent Cations Suppress 3′,5′-Adenosine Monophosphate Accumulation by Stimulating a Pertussis Toxin-Sensitive Guanine Nucleotide-Binding Protein in Cultured Bovine Parathyroid Cells. Endocrinology 124**:** 233-239.

Cheng I, Klingensmith ME, Chattopadhyay N, Kifor O, Butters RR, Soybel DI, *et al.* (1998). Identification and localization of the extracellular calcium-sensing receptor in human breast. The Journal of Clinical Endocrinology & Metababolism 83**:** 703-707.

Chiarini A, Armato U, Liu D, & Dal Prà I (2017). Calcium-Sensing Receptor Antagonist NPS 2143 Restores Amyloid Precursor Protein Physiological Non-Amyloidogenic Processing in Aβ-Exposed Adult Human Astrocytes. Scientific Reports 7**:** 1277.

Christopoulos A, Changeux J-P, Catterall WA, Fabbro D, Burris TP, Cidlowski JA, *et al.* (2014). International Union of Basic and Clinical Pharmacology. XC. multisite pharmacology: recommendations for the nomenclature of receptor allosterism and allosteric ligands. Pharmacological Reviews 66**:** 918-947.

Clark AR, Martins JR, & Tchen CR (2008). Role of dual specficity phosphatases in biological responses to glucocortiocids. Journal of Biological Chemistry 283**:** 25765-256769.

Cohn L, Elias JA, & Chupp GL (2004). Asthma: mechanisms of disease persistence and progression. Annual Review in Immunology 22**:** 789-815.

Conigrave AD, & Hampson DR (2010). Broad-spectrum amino acid-sensing class C G-protein coupled receptors: Molecular mechanisms, physiological significance and options for drug development. Pharmacology & Therapeutics 127**:** 252-260.

Conigrave AD, Mun H, Delbridge L, Quinn SJ, Wilkinson M, & Brown EM (2004). L-Amino Acids Regulate Parathyroid Hormone Secretion. Journal of Biological Chemistry 279**:** 38151-38159.

Conigrave AD, Quinn SJ, & Brown EM (2000). L-Amino acid sensing by the extracellular Ca2+-sensing receptor. Proceedings of the National Academy of Sciences 97**:** 4814-4819.

Conigrave AD, & Ward DT (2013). Calcium-sensing receptor (CaSR): Pharmacological properties and signaling pathways. Best Practice & Research Clinical Endocrinology & Metabolism 27**:** 315-331.

Conley YP, Mukherjee A, Kammerer C, DeKosky ST, Kamboh MI, Finegold DN, *et al.* (2009). Evidence supporting a role for the calcium-sensing receptor in Alzheimer disease. American Journal of Medical Genetics Part B: Neuropsychiatric Genetics 150B**:** 703-709.

Cook AE, Mistry SN, Gregory KJ, Furness SG, Sexton PM, Scammells PJ, *et al.* (2015). Biased allosteric modulation at the CaS receptor engendered by structurally diverse calcimimetics. British Journal of Pharmacology 172**:** 185-200.

Corbetta S, Lania A, Filopanti M, Vicentini L, Ballaré E, & Spada A (2002). Mitogen-activated protein kinase cascade in human normal and tumoral parathyroid cells. Journal of Clinical Endocrinology and Metabolism 87**:** 2201-2205.

Cosman F, Gilchrist N, McClung M, Foldes J, de Villiers T, Santora A, *et al.* (2016). A phase 2 study of MK-5442, a calcium-sensing receptor antagonist, in postmenopausal women with osteoporosis after long-term use of oral bisphosphonates. Osteoporosis International 27**:** 377-386.

Dahl R, Lundback B, Malso JL, Mazza JA, Nieminen MM, Saarelainen P, *et al.* (1993). A dose-ranging study of fluticasone propionate in adult patients with moderate asthma. Chest `104**:** 1352-1358.

Davey AE, Leach K, Valant C, Conigrave AD, Sexton PM, & Christopolous A (2012). Positive and negative allosteric modulators promote biased signaling at the calcium-sensing receptor. Endocrinology 153**:** 1232-1241.

Davies SL, Gibbons CE, Vizard T, & Ward DT (2006). Ca^{2+}-sensing receptor induces Rho kinase-mediated actin stress fiber assembly and altered cell morphology, but not in response to aromatic amino acids. American Journal of Physiology-Cell Physiology 290**:** C1542-C1551.

Delmotte P, & Sanderson MJ (2008). Effects of albuterol isomers on the contraction and Ca2+ signaling of small airways in mouse lung slices. American Journal of Respiratory Cell and Molecular Biology 38**:** 524-531.

Dershem R, Gorvin CM, Metpally RPR, Krishnamurthy S, Smelser DT, Hannan FM, *et al.* (2020). Familial hypocalciuric hypercalcemia type 1 and autosomal-dominant hypocalcemia type 1: Prevalence in a large healthcare population. American Journal of Human Genetics 106**:** 734-747.

Deshpande DA, & Penn RB (2006). Targeting G protein-coupled receptor signaling in asthma. Cellular signaling 18**:** 2105-2120.

Diao J, DeBono A, Josephs TM, Bourke JE, Capuano B, Gregory KJ, *et al.* (2021). Therapeutic Opportunities of Targeting Allosteric Binding Sites on the Calcium-Sensing Receptor. ACS Pharmacology & Translational Science 4**:** 666-679.

Dobnig H, & Turner RT (1997). The effects of programmed administration of human parathyroid hormone fragment (1-34) on bone histomorphometry and serum chemistry in rats. Endocrinology 138**:** 4607-4612.

Dockrell M, Partridge MR, & Valovirta E (2007). The limitations of severe asthma: the results of a European survey. Allergy 62**:** 134-141.

Dong B, Endo I, Ohnishi Y, Kondo T, Hasegawa T, Amizuka N, *et al.* (2015). Calcilytic ameliorates abnormalities of mutant calcium-sensing receptor (CaSR) knock-in mice mimicking autosomal dominant hypocalcemia (ADH). Journal of Bone and Mineral Research 30**:** 1980-1993.

Donovan C, Simoons M, Esposito J, Cheong JN, FitzPatrick M, & Bourke JE (2014). Rosiglitazone is a superior bronchodilator compared to chloroquine and beta-adrenoceptor agonists in mouse lung slices. Respiratory Research 15**:** 29-29.

Douglas KA, Ortiz-Capisano MC, & William HB (2010). Acute activation of the calcium-sensing receptor inhibits plasma renin activity in vivo. The American Journal of Physiology - Regulatory, Integrative and Comparative Physiology. 299**:** 1020-1026.

Ducharme FM, Lasserspm TJ, & Cates CJ (2006). Long-acting beta2-agonists versus anti-leukogtrienes as add-on therapy to inhaled corticosteroids for chronic asthma. Cochrane Data Systematic Review**:** CD003137.

Dvorak-Ewell MM, Chen TH, Liang N, Garvey C, Liu B, Tu C, *et al.* (2011). Osteoblast extracellular Ca2+-sensing receptor regulates bone development, mineralization, and turnover. Journal of Bone and Mineral Research 26**:** 2935-2947.

Dvorak MM, Siddiqua A, Ward DT, Carter DH, Dallas SL, Nemeth EF, *et al.* (2004). Physiological changes in extracellular calcium concentration directly control osteoblast function in the absence of calciotropic hormones. Proceedings of the National Academy of Sciences of the United States of America 101**:** 5140-5145.

Eller-Vainicher C, Battista C, Guarnieri V, Muscarella S, Palmieri S, Salcuni AS, *et al.* (2014). Factors associated with vertebral fracture risk in patients with primary hyperparathyroidism. European Journal of Endocrinology 171**:** 399-406.

Fahy JV, Kim KW, Liu J, & Boushey HA (1995). Prominent neutrophilic inflammation in sputum from subjects with asthma exacerbation. Journal of Allergy and Clinical Immunology 95**:** 843-852.

Fan Y, Liu W, Bi R, Densmore M, J. , Sato T, Mannstadt M, *et al.* (2018). Interrelated role of Klotho and calcium-sensing receptor in parathyroid hormone synthesis and parathyroid hyperplasia. Proceedings of the National Academy of Sciences of the United States of America 115**:** E3749-E3758.

Feng J, Petersen CD, Coy DH, Jiang J-K, Thomas CJ, Pollak MR, *et al.* (2010). Calcium-sensing receptor is a physiologic multimodal chemosensor regulating gastric G-cell growth and gastrin secretion. Proceedings of the National Academy of Sciences 107**:** 17791-17796.

Fergeson JE, Patel SS, & Lockey RF (2017). Acute asthma, prognosis, and treatment. Journal of Allergy and Clinical Immunology 139**:** 438-447.

Finney BA, del Moral PM, Wilkinson WJ, Cayzac S, Cole M, Warburton D, *et al.* (2008). Regulation of mouse lung development by the extracellular calcium-sensing receptor, CaR. Journal of Physiology 586**:** 6007-6019.

Fisher MM, Cabrera SM, & Imel EA (2015). Successful treatment of neonatal severe hyperparathyroidism with cinacalcet in two patients. Endocrinology, Diabetes & Metabolism Case Reports 2015**:** 102-107.

Fitzpatrick LA, Dabrowski CE, Cicconetti G, Gordon DN, Fuerst T, Engelke K, *et al.* (2012). Ronacaleret, a calcium-sensing receptor antagonist, increases trabecular but not cortical bone in postmenopausal women. Journal of Bone and Mineral Research 27**:** 255-262.

Fitzpatrick LA, Dabrowski CE, Cicconetti G, Gordon DN, Papapoulos S, Bone HG, *et al.* (2011). The Effects of Ronacaleret, a Calcium-Sensing Receptor Antagonist, on Bone Mineral Density and Biochemical Markers of Bone Turnover in Postmenopausal Women with Low Bone Mineral Density. The Journal of Clinical Endocrinology & Metabolism 96**:** 2441-2449.

Foord SM (2002). Receptor classification: post genome. Current Opinion in Pharmacology 2**:** 561-566.

Foord SM, Bonner TI, Neubig RR, Rosser EM, Pin JP, Davenport AP, *et al.* (2005). International Union of Pharmacology. XLVI. G-protein-coupled receptor list. Pharmacological Reviews 57**:** 279-288.

Fredriksson R, Langerstorm MC, Lundin LG, & Schioth HB (2003). The G protein-coupled receptors in the human genome form five main families. Phylogenetic analysis, paralogon groups, and fingerprints. Molecular Pharmacology 63**:** 1256-1272.

Fredrujssib R, Lagerstrom MC, Lundin LG, & Schioth HB (2003). The G-protein-coupled receptors in the human genome form five main families. Phylogenetic analysis, paralogon groups, and fingerprints. Molecular Pharmacology 63**:** 1256-1272.

Freyer AM, Johnson SR, & Hall JR (2001). Effects of growth factors and extracellular matrix on survival of human airway smooth muscle cells. American Journal of Respiratory Cell and Molecular Biology 25**:** 569-576.

Fromigué O, Haÿ E, Barbara A, Petrel C, Traiffort E, Ruat M, *et al.* (2009). Calcium sensing receptor-dependent and receptor-independent activation of osteoblast replication and survival by strontium ranelate. Journal of Cellular and Molecular Medicine 13**:** 2189-2199.

Fujisawa Y, Yamaguchi R, Satake E, Ohtaka K, Nakanishi T, Ozono K, *et al.* (2013). Identification of AP2S1 mutation and effects of low calcium formula in an infant with hypercalcemia and hypercalciuria. The Journal of Clinical Endocrinology & Metabolism 98**:** E2022-E2027.

Fukagawa M, Shimazaki R, & Akizawa T (2018). Head-to-head comparison of the new calcimimetic agent evocalcet with cinacalcet in Japanese hemodialysis patients with secondary hyperparathyroidism. Kidney International 94**:** 818-825.

Fukumoto K, Noguchi T, Toriie S, Shimazu E, & Miyake S (2010). The mechanism of upper-gastrointestinal complication after taking cinacalcet hydrochloride. Nihon Toseki Igakkai Zasshi 43**:** 309-315.

Gama L, & Breitwieser GE (1998). A carboxyl-terminal domain controls the cooperativity for extracellular Ca^{2+} activation of the human calcium sensing receptor. Journal of Biological Chemistry 273**:** 29712-29718.

Gama L, Wilt SG, & Breitwieser GE (2001). Heterodimerization of Calcium Sensing Receptors with Metabotropic Glutamate Receptors in Neurons. Journal of Biological Chemistry 276**:** 39053-39059.

Ganesan S, Comstock AT, & Saijan US (2013). Barrier function of airway tract epithelium. Tissue Barriers 1**:** e24997.

Gannon AW, Monk HM, & Levine MA (2014). Cinacalcet Monotherapy in Neonatal Severe Hyperparathyroidism: A Case Study and Review. The Journal of Clinical Endocrinology & Metabolism 99**:** 7-11.

García-Faroldi G, Rodríguez CE, Urdiales JL, Pérez-Pomares JM, Dávila JC, Pejler G, *et al.* (2010). Polyamines are present in mast cell secretory granules and are important for granule homeostasis. Plos One 5**:** e15071.

García Soblechero E, Ferrer Castillo MT, Jiménez Crespo B, Domínguez Quintero ML, & González Fuentes C (2013). Neonatal Hypercalcemia due to a Homozygous Mutation in the Calcium-Sensing Receptor: Failure of Cinacalcet. Neonatology 104**:** 104-108.

Garrett JE, Capuano I, Hammerland LG, Hung BC, Brown EM, Hebert SC, *et al.* (1995). Molecular cloning and functional expression of human parathyroid calcium receptor cDNAs. Journal of Biological Chemistry 270**:** 12919-12925.

Geng Y, Mosyak L, Kurinov I, Zuo H, Sturchler E, Cheung CT, *et al.* (2016). Structural mechanism of ligand activation in human calcium-sensing receptor. eLife 5.

Geng Y, Xiong D, Mosyak L, Malito DL, Kniazeff J, Chen Y, *et al.* (2012). Structure and functional interaction of the extracellular domain of human GABAB receptor GBR2. Nature Neuroscience 15**:** 970-978.

George SR, O'Dowd BF, & Lee SP (2002). G-protein-coupled receptor oligomerization and its potential for drug discovery. Nature Reviews Drug Discovery 1**:** 808-820.

Ghanemi A (2015). Targeting G protein coupled receptor-related pathways as emerging molecular therapies. Saudi Pharmaceutical Journal 23**:** 115-129.

Gincherman Y, Moloney K, Mckee C, & Coyne DW (2010). Assessment of adherence to cinacalcet by prescription refill rates in hemodialysis patients. Hemodialysis International 14**:** 68-72.

Gleich GJ (2000). Mechanisms of eosinophil-associated inflammation. Journal of Allergy and Clinical Immunology 105**:** 651-663.

Godwin SL, & Soltoff SP (2002). Calcium-sensing receptor-mediated activation of phospholipase C-γ1 is downstream of phospholipase C-β and protein kinase C in MC_3T_3-E1 osteoblasts. Bone 30**:** 559-566.

Gong T, Lundholm C, Rejno G, Langstrom N, & Almqvist C (2014). Parental socioeconomic status, childhood asthma and medication use - a population-based study. Plos One 9**:** e106579.

Goodman OBJ, Krupnick JG, Gurevich VV, Benovic KL, & Keen JH (1997). Arrestin/clathrin interaction. Localization of the arrestin binding locus to the clathrin terminal domain. Journal of Biological Chemistry 279**:** 15017-15022.

Goolam MA, Ward JH, Avlani VA, Leach K, Christopoulos A, & Conigrave AD (2014). Roles of intraloops-2 and -3 and the proximal C-terminus in signalling pathway selection from the human calcium-sensing receptor. FEBS Letters 588**:** 3340-3346.

Gorvin CM (2019). Molecular and clinical insights from studies of calcium-sensing receptor mutations. Journal of Molecular Endocrinology 63**:** R1-R16.

Gorvin CM, Hannan FM, Cranston T, Valta H, Makitie O, Schalin-Jantti C, *et al.* (2018a). Cinacalcet rectifies hypercalcemia in a patient with Familial Hypocalciuric Hypercalcemia Type 2 (FHH2) caused by a germline loss-of-function Galpha11 mutation. Journal of Bone and Mineral Research 33**:** 32-41.

Gorvin CM, Hannan FM, Howles SA, Babinsky VN, Piret SE, Rogers A, *et al.* (2017). Gα11 mutation in mice causes hypocalcemia rectifiable by calcilytic therapy. JCI Insight 2**:** e91103.

Gorvin CM, Metpally R, Stokes VJ, Hannan FM, Krishnamurthy SB, Overton JD, *et al.* (2018b). Large-scale exome datasets reveal a new class of adaptor-related protein complex 2 sigma subunit (AP2σ) mutations, located at the interface with the AP2 alpha subunit, that impair calcium-sensing receptor signalling. Human Molecular Genetics 27**:** 901-911.

Gowen M, Stroup GB, Dodds RA, James IE, Votta BJ, Smith BR, *et al.* (2000a). Antagonizing the parathyroid calcium receptor stimulates parathyroid hormone secretion and bone formation in osteopenic rats. Journal of Clinical Investigation 105**:** 1595-1604.

Gowen M, Stroup GB, Dodds RA, James IE, Votta BJ, Smith BR, *et al.* (2000b). Antagonizing the parathyroid calcium receptor stimulates parathyroid hormone secretion and bone formation in osteopenic rats. The Journal of Clinical Investigation 105**:** 1595-1604.

Grasemann H, Shehnaz D, Enomoto M, Leadley M, Belik J, & Ratjen F (2012). L-Ornithine Derived Polyamines in Cystic Fibrosis Airways. PLoS ONE 7**:** e46618.

Gregory KJ, Giraldo J, Diao J, Christopoulos A, & Leach K (2020). Evaluation of Operational Models of Agonism and Allosterism at Receptors with Multiple Orthosteric Binding Sites. Molecular Pharmacology 97**:** 35-45.

Gregory KJ, Kufareva I, Keller AN, Khajehali E, Mun HC, Goolam MA, *et al.* (2018). Dual action calcium-sensing receptor modulator unmasks novel mode-switching mechanism. ACS Pharmacology & Translational Science 1**:** 96-109.

Grzegorzewska AE, Bednarski D, Swiderska M, Mostowska A, & Jagodzinski PP (2018). The calcium-sensing receptor gene polymorphism rs1801725 and calcium-related phenotypes in hemodialysis patients. Kidney & Blood Pressure Research 43**:** 719-734.

Guarnieri C, Georgountzos A, Caladarera I, Flamigni F, & Ligabue A (1987). Polyamines stimulate superoxide production in human neutrophils activated by N-fMet-Leu-Phe but not by phorbol myristate acetate. Biochimica et Biophysica Acta 930**:** 135-139.

Guerman M, Sean J, Simon F, Jeanette B, Hendrik L, Rosemary B, *et al.* (2007). Extracellular calcium-sensing receptor is functionally expressed in human artery. American Journal of Physiology-Renal Physiology 293**:** 946-955.

Gunganah K, Grossman A, & Druce M (2014). Recurrent pancreatitis in a patient with familial hypocalciuric hypercalcaemia treated successfully with cinacalcet. Endocrinology, Diabetes & Metabolism Case Reports 2014**:** 675-673.

Gunst SJ (2012) *Airway Smooth Muscle and Asthma*. First edition edn.

Gunst SJ, & Stropp JQ (1988). Pressure-volume and length-stress relationships in caine bronchi in vitro. Journal of Applied Physiology 64**:** 2522-2531.

Gustafsson M, Jensen J, Bertozzi SM, Currier EA, Ma JN, Burstein ES, *et al.* (2010). Discovery of a class of calcium sensing receptor positive allosteric modulators; 1-(benzothiazol-2-yl)-1-phenylethanols. Bioorganic & Medicinal Chemistry Letters 20**:** 5918-5921.

Hall IP (2000). Second messengers, ion channels and pharmacology of airway smooth muscle. European Respiratory Journal 15**:** 1120-1127.

Halse J, Greenspan S, Cosman F, Ellis G, Santora A, Leung A, *et al.* (2014a). A Phase 2, Randomized, Placebo-Controlled, Dose-Ranging Study of the Calcium-Sensing Receptor Antagonist MK-5442 in the Treatment of Postmenopausal Women With Osteoporosis. The Journal of Clinical Endocrinology & Metabolism 99**:** E2207-E2215.

Halse J, Greenspan S, Cosman F, Ellis G, Santora A, Leung A, *et al.* (2014b). A phase 2, randomized, placebo-controlled, dose-ranging study of the calcium-sensing receptor antagonist MK-5442 in the treatment of postmenopausal women with osteoporosis. The Journal of Clinical Endocrinology and Metabolism 99**:** E2207-2215.

Hammond AS, Rodriguez AL, Townsend SD, Niswender CM, Gregory KJ, Lindsley CW, *et al.* (2010). Discovery of a novel chemical class of mGlu(5) allosteric ligands with distinct modes of pharmacology. ACS Chemical Neuroscience 1**:** 702-716.

Handlogten ME, Huang C, Shiraishi N, Awata H, & Miller RT (2001). The Ca^{2+}-sensing receptor activates cytosolic phospholipase A_2 via a $G\alpha_q$-dependent ERK-independent pathway. Journal of Biological Chemistry 276**:** 13941-13948.

Hannan F, Babinsky V, & Thakker RV (2016). Disorders of the calcium-sensing receptor and partner proteins: insights into the molecular basis of calcium homeostasis. Journal of Molecular Endocrinology 57**:** R127-R142.

Hannan F, Kallay E, Chang W, Brandi M, & Thakker R (2019). The calcium-sensing receptor in physiology and in calcitropic and noncalcitropic diseases. Nature Reviews Endocrinology 15**:** 33-51.

Hannan FM, Howles SA, Rogers A, Cranston T, Gorvin CM, Babinsky VN, *et al.* (2015a). Adaptor protein-2 sigma subunit mutations causing familial hypocalciuric hypercalcaemia type 3 (FHH3) demonstrate genotype-phenotype correlations, codon bias and dominant-negative effects. Human molecular genetics 24**:** 5079.

Hannan FM, Nesbit MA, Zhang C, Cranston T, Curley AJ, Harding B, *et al.* (2012). Identification of 70 calcium-sensing receptor mutations in hyper- and hypo-calcaemic patients: evidence for

clustering of extracellular domain mutations at calcium-binding sites. Human Molecular Genetics 21**:** 2768-2778.

Hannan FM, Walls GV, Babinsky VN, Nesbit MA, Kallay E, Hough TA, *et al.* (2015b). The calcilytic agent NPS 2143 rectifies hypocalcemia in a mouse model with an activating calcium-sensing receptor (CaSR) mutation: Relevance to Autosomal Dominant Hypocalcemia Type 1 (ADH1). Endocrinology 156**:** 3114-3121.

Hart L, Lim S, Adcock I, Barnes PJ, & Chung KF (2000). Efffects of inhaled corticosteroid therapy on expression and DNA-binding activity of nuclear factor-kB in asthma. American Journal of Respiratory and Critical Care Medicine 161**:** 224-231.

Heath Hr, Odelberg S, Jackson CE, Teh BT, Hayward N, Larsson C, *et al.* (1996). Clustered inactivating mutations and benign polymorphisms of the calcium receptor gene in familial benign hypocalciuric hypercalcemia suggest receptor functional domains. The Journal of clinical endocrinology and metabolism 81**:** 1312-1317.

Heijink IH, Nawijn MC, & Hackett TL (2014). Airway epithelial barrier function regulates the pathogenesis of allergic asthma. Clinical & Experimental Allergy 44**:** 620-630.

Hendy GN, & Canaff L (2016). Calcium-Sensing Receptor Gene: Regulation of Expression. Frontiers in Physiology 7.

Hendy NG, Canaff SL, Newfield LR, Tripto-Shkolnik PL, Wong CBY, Lee CBS, *et al.* (2014). Codon Arg15 Mutations of the AP2S1 Gene: Common Occurrence in Familial Hypocalciuric Hypercalcemia Cases Negative for Calcium-Sensing Receptor (CASR) Mutations. The Journal of Clinical Endocrinology & Metabolism 99**:** E1311-E1315.

Herberger AL, & Loretz CA (2013). Vertebrate extracellular calcium-sensing receptor evolution: Selection in relation to life history and habitat. Comp Biochem Physiol Part D Genomics Proteomics 8**:** 86-94.

Hjälm G, MacLeod RJ, Kifor O, Chattopadhyay N, & Brown EM (2001). Filamin-A binds to the carboxyl-terminal tail of the calcium-sensing receptor, an interaction that participates in CaR-mediated activation of mitogen-activated protein kinase. Journal of Biological Chemistry 276**:** 34880-34887.

Hobson SA, Wright J, Lee F, McNeil SE, Bilderback T, & Rodland KD (2003). Activation of the MAP kinase cascade by exogenous calcium-sensing receptor. Molecular and Cellular Endocrinology 200**:** 189-198.

Hofer AM, & Brown EM (2003). Extracellular calcium sensing and signaling. Nature Review Molecular Cell Biologoy 4**:** 531-538.

Hoff AO, Cote GJ, Fritsche HA, Qiu H, Schultz PN, & Gagel RF (1999). Calcium-Induced Activation of a Mutant G-Protein-Coupled Receptor Causes In Vitro Transformation of NIH/3T3 Cells. Neoplasia 1**:** 485-491.

Holgate ST (2012). Innate and adaptive immune responses in asthma. Nature Medicine 18**:** 673-683.

Holgate ST, Wenzel S, Postma DS, Weiss ST, Renz H, & Sly PD (2015). Asthma. Nature Reviews Disease Primers 1**:** 15025.

Howles SA, Hannan FM, Babinsky VN, Rogers A, Gorvin CM, Rust N, *et al.* (2016). Cinacalcet for symptomatic Hypercalcemia caused by AP2S1 mutations. The New England Journal of Medicine 374**:** 1396-1398.

Howles SA, Hannan FM, Gorvin CM, Piret SE, Paudyal A, Stewart M, *et al.* (2017). Cinacalcet corrects hypercalcemia in mice with an inactivating Galpha11 mutation. JCI Insight 2.

Huang C, Hujer KM, Wu Z, & Miller RT (2004). The Ca^{2+}-sensing receptor couples to $G\alpha_{12/13}$ to activate phospholipas D in Madin-Darby canine kidney cells. American Journal of Physiology-Cell Physiology 286**:** C22-C30.

Huang Y, & Breitwieser GE (2007). Rescue of calcium-sensing receptor mutants by allosteric modulators reveals a conformational checkpoint in receptor biogenesis. Journal of Biological Chemistry 282**:** 9517-9525.

Ilmarinen P, Moilanen E, Erjefalt JS, & Kankaanranta H (2015). The polyamine spermine promotes survival and activation of human eosinophils. Journal of Allergy and Clinical Immunology 136**:** 482-484. e411.

Ilmarinen P, Moilanen E, Kinnula VL, & Kankaanranta H (2012). Nitric oxide-induced eosinophil apoptosis is dependent on mitochondrial permeability transition (mPT), JNK and oxidative stress: apoptosis is preceded but not mediated by early mPT-dependent JNK activation. Respiratory Research 13**:** 73.

Innes AL, Carrington SD, Thornton DJ, Kirkham S, Rousseau K, Dougherty RH, *et al.* (2009). Ex vivo sputum analysis reveals impairment of protease-dependent mucus degradation by plasma proteins in acute asthma. American Journal of Respiratory and Critical Care Medicine 180**:** 203-210.

Jain V (2018). Role of Polyamines in Asthma Pathophysiology. Med Sci (Basel) 6.

James AL, Pare PD, & Hogg JC (1989). The mechanics of airway narrowing in asthma. American Review of Respiratory Disease 139**:** 242-246.

Jeffery PK (2001). Remodeling in asthma and chronic obstructive lung disease. American Journal of Respiratory and Critical Care Medicine 164**:** S28-S38.

Jeong S, Kim IW, Oh KH, Han N, Joo KW, Kim HJ, *et al.* (2016). Pharmacogenetic analysis of cinacalcet response in secondary hyperparathyroidism patients. Drug Design, Development and Therapy 10**:** 2211-2225.

Jiang Y, Minet E, Zhang Z, Silver PA, & Bai M (2004). Modulation of Interprotomer Relationships Is Important for Activation of Dimeric Calcium-sensing Receptor*. Journal of Biological Chemistry 279**:** 14147-14156.

John MR, Harfst E, Loeffler J, Belleli R, Mason J, Bruin GJ, *et al.* (2014). AXT914 a novel, orally-active parathyroid hormone-releasing drug in two early studies of healthy volunteers and postmenopausal women. Bone 64**:** 204-210.

Josephs TM, Keller AN, Khajehali E, Debono A, Langmead CJ, Conigrave AD, *et al.* (2019). Negative allosteric modulators of the human calcium-sensing receptor bind to overlapping and distinct sites within the 7 transmembrane domain. British journal of pharmacology.

Josephs TM, Keller AN, Khajehali E, DeBono A, Langmead CJ, Conigrave AD, *et al.* (2020). Negative allosteric modulators of the human calcium-sensing receptor bind to overlapping and distinct sites within the 7-transmembrane domain. British journal of pharmacology 177**:** 1917-1930.

Juniper EF, Kline PA, Vanzieleghem MA, Ramsdale EH, O'Byrne PM, & Hargreave FE (1990a). Effect of long-term treatment with an inhaled corticosteroid (budesonide) on airway hyperresponsivess and clinical asthma in nonsteroid-depedent asthmatics. American Review of Respiratory Disease 142**:** 832-836.

Juniper EF, Kline PA, Vanzieleghem MA, Ramsdale EH, O'Byrne PM, & Hargreave FE (1990b). Long-term effects of budesonide on airay responsivenss and clinical asthma severity in inhaled steroid-dependent asthmatics. European Respiratory Journal 3**:** 1122-1127.

Justinich CJ, Mak N, Pacheco I, Mulder D, Wells RW, Blennerhassett MG, *et al.* (2008). The extracellular calcium-sensing receptor (CaSR) on human esophagus and evidence of expression of

the CaSR on the esophageal epithelial cell line (HET-1A). American Journal of Physiology-Gastrointestinal and Liver Physiology 294**:** G120-G129.

Kantham L, Quinn SJ, Egbuna OI, Baxi K, Butters R, Pang JL, *et al.* (2009). The calcium-sensing receptor (CaSR) defends against hypercalcemia independently of its regulation of parathyroid hormone secretion. American Journal of Physiology-Endocrinology and Metabolism 297**:** E915-E923.

Katritch V, Cherezov V, & Stevens RC (2013). Structure-function of the G-protein-coupled receptor superfamily. Annual Review in Pharmacology Toxicology 53**:** 531-556.

Katsuyuki M, Hidenobu M, & Kazuki S (2010). Theoretical calculations of the thermodynamic stability of ionic substitutions in hydroxyapatite under an aqueous solution environment. Journal of Physics: Condensed Matter 22**:** 384210.

Kawata T, Tokunaga S, Murai M, Masuda N, Haruyama W, Shoukei Y, *et al.* (2018). A novel calcimimetic agent, evocalcet (MT-4580/KHK7580), suppresses the parathyroid cell function with little effect on the gastrointestinal tract or CYP isozymes in vivo and in vitro. PLOS ONE 13**:** e0195316-0195314.

Keller AN, Kufareva I, Josephs TM, Diao J, Mai VT, Conigrave AD, *et al.* (2018). Identification of Global and Ligand-Specific Calcium Sensing Receptor Activation Mechanisms. Molecular pharmacology 93**:** 619-630.

Kelly P, Casey PJ, & Meigs TE (2007). Biologic Functions of the G12 Subfamily of Heterotrimeric G Proteins: Growth, Migration, and Metastasis. Biochemistry 46**:** 6677-6687.

Kenakin T, & Christopoulos A (2013). Signalling bias in new drug discovery: detection, quantification and therapeutic impact. Nature Reviews Drug Discovery 12**:** 205-216.

Kessler A, Faure H, Petrel C, Rognan D, Cesario M, Ruat M, *et al.* (2006). N1-Benzoyl-N2-[1-(1-naphthyl)ethyl]-trans-1,2-diaminocyclohexanes: Development of 4-chlorophenylcarboxamide (calhex 231) as a new calcium sensing receptor ligand demonstrating potent calcilytic activity. Journal of Medicinal Chemistry 49**:** 5119-5128.

Kifor O, Diaz R, Butters JRR, & Brown EM (1997). The Ca^{2+}-sensing receptor (CaR) activates phopholipases C. A_2, and D in bovine parathyroid and CaR-transfected, human embryonic kidney (HEK293) cells. Journal of Bone and Mineral Research 12**:** 715-725.

Kifor O, Macleod RJ, Diaz R, Bai M, Yamanguchi T, Yao T, *et al.* (2001). Regulation of MAP kinase by calcium-sensing receptor in bovine parathyroid and CaR-transfected HEK293 cells American Journal of Physiology-Renal Physiology 280**:** F291-F302.

Kikuchi I, Kikuchi S, Kobayashi T, & Hagiwara K (2006). Eosinophil trans-basement membrane migration induced by interleukin-8 and neutrophils American Journal of Respiratory Cell and Molecular Biology 34**:** 760-765.

Kim W, & Wysolmerski JJ (2016). Calcium-Sensing Receptor in Breast Physiology and Cancer. Frontiers in Physiology 7**:** 440-440.

Kita H (2013). Eosinophils: multifunctional and distinctive properties. International Archives of Allergy Immunology 161**:** 3-9.

Kobayashi-Torii M, Takahashi Y, Sunanaga J, Fujita M, Lee EY, Ichimaru Y, *et al.* (2011). Possible participation of extracellular calcium-sensing receptor in blood pressure regulation in rats. Brain Research 1367**:** 181-187.

Koehl A, Hu H, Feng D, Sun B, Zhang Y, Robertson MJ, *et al.* (2019). Structural insights into the activation of metabotropic glutamate receptors. Nature 566**:** 79-84.

Kos CH, Karaplis A, Peng JB, Hediger M, Goltzman D, Mohammad KS, *et al.* (2003). The calcium-sensing receptor is required for normal calcium homeostasis independent of parathyroid hormone. Journal of Clinical Investigation 111**:** 1021-1028.

Koussounadis A, Langdon SP, Um IH, Harrison DJ, & Smith VA (2015). Relationship between differentially expressed mRNA and mRNA-protein correlations in a xenograft model system. Scientific Reports 5**:** 10775.

Krupnick JG, & Benovic JL (1998). The role of receptor kinases and arrestins in G protein-coupled receptor regulation. Annual Review of Pharmacology and Toxicology 38**:** 1780-1787.

Kuehn BM (2008). Asthma linked to psychiatric disorders. Medical News and Perspectives 299**:** 158-160.

Kumar S, Matheny CJ, Hoffman SJ, Marquis RW, Schultz M, Liang X, *et al.* (2010). An orally active calcium-sensing receptor antagonist that transiently increases plasma concentrations of PTH and stimulates bone formation. Bone 46**:** 534-542.

Kume H, Hall IP, Washabau RJ, Takagi K, & Kotlikoff MI (1994). Beta-adrenergic agonists regulate KCa channels in airway smooth muscle by cAMP-dependent and -independent mechanisms. Journal of Clinical Investigation 93**:** 371-379.

Kurosawa M, Shimizu Y, Tsukagoshi H, & Ueki M (1992). Elevated levels of peripheral-blood, naturally occurring aliphatic polyamines in bronchial asthmatic patients with active symptoms. Allergy 47**:** 638-643.

Lagerström MC, & Schiöth HB (2008). Structural diversity of G protein-coupled receptors and significance for drug discovery. Nature Reviews Drug Discovery 7**:** 339.

Lago MA, Callahan JF, Bhatnagar PK, Del Mar RG, Bryan WM, & Burgess JL (2006). Calcilytic compoundsed. Inc. S.B.C.a.N.P.: USA.

Lam M, Lamanna E, & Bourke JE (2019) *Regulation of Airway Smooth Muscle Contraction in Health and Disease*. vol. 1124.

Lambert RK, Codd SL, Alley MR, & Pack PJ (1994). Physical determinants of bronchial mucosal folding. Journal of Applied Physiology 64**:** 1206-1216.

Langmead CJ, & Christopoulos A (2006). Allosteric agonists of 7TM receptors: expanding the pharmacological toolbox. Trends in Pharmacological Sciences 27**:** 475-481.

Lazaar AL, & Panettieri RA (2001). Airway smooth muscle as an immunomodulatory cells: a new taret for pharmacotherapy. Current Opinion in Pharmacology 1**:** 259-264.

Lazrak A, Yu Z, Doran S, Jian MY, Creighton J, Laube M, *et al.* (2020). Upregulation of airway smooth muscle calcium-sensing receptor by low-molecular-weight hyaluronan. Am J Physiol Lung Cell Mol Physiol 318**:** L459-l471.

Leach K, Gregory KJ, Kufareva I, Khajehali E, Cook AE, Abagyan R, *et al.* (2016). Towards a structural understanding of allosteric drugs at the human calcium-sensing receptor. Cell Research 26**:** 574-592.

Leach K, Hannan FM, Josephs TM, Keller AN, Møller TC, Ward DT, *et al.* (2020). International Union of Basic and Clinical Pharmacology. CVIII. Calcium-Sensing Receptor Nomenclature, Pharmacology, and Function. Pharmacological Reviews 72**:** 558-604.

Leach K, Sexton PM, & Christopoulos A (2007). Allosteric GPCR modulators: taking advantage of permissive receptor pharmacology. Trends in Pharmacological Sciences 28**:** 382-389.

Leach K, Wen A, Cook AE, Sexton PM, Conigrave AD, & Christopoulos A (2013). Impact of clinically relevant mutations on the pharmacoregulation and signaling bias of the calcium-sensing receptor by positive and negative allosteric modulators. Endocrinology 154**:** 1105-1116.

Leach K, Wen A, Davey AE, Sexton PM, & Conigrave AD (2012). Identification of molecular phenotypes and biased signaling induced by naturally occurring mutations of the human calcium-sensing receptor. Endocrinology 153**:** 4304-4316.

LeBoff MS, Shoback D, Brown EM, Thatcher J, Leombruno R, Beaudoin D, *et al.* (1985). Regulation of parathyroid hormone release and cytosolic calcium by extracellular calcium in dispersed and cultured bovine and pathological human parathyroid cells. Journal of Clinical Investigation 75**:** 49-57.

LeDoux JE (2000). Emotion Circuits in the Brain. Annual Review of Neuroscience 23**:** 155-184.

Lee HJ, Mun HC, Lewis NC, Crouch MF, Culverston EL, Mason RS, *et al.* (2007). Allosteric activation of the extracellular Ca^{2+}-sensing receptor by L-amino acids enhances ERK1/2 phosphorylation. Biochemical Journal 404**:** 141-149.

Lee J-W, Park HA, Kwon O-K, Park J-W, Lee G, Lee HJ, *et al.* (2017). NPS 2143, a selective calcium-sensing receptor antagonist inhibits lipopolysaccharide-induced pulmonary inflammation. Molecular Immunology 90**:** 150-157.

Letz S, Haag C, Schulze E, Frank-Raue K, Raue F, Hofner B, *et al.* (2014). Amino alcohol-(NPS-2143) and quinazolinone-derived calcilytics (ATF936 and AXT914) differentially mitigate excessive signalling of calcium-sensing receptor mutants causing Bartter syndrome Type 5 and autosomal dominant hypocalcemia. PLoS One 9**:** e115178.

Letz S, Rus R, Haag C, Dorr HG, Schnabel D, Mohlig M, *et al.* (2010). Novel activating mutations of the calcium-sensing receptor: the calcilytic NPS-2143 mitigates excessive signal transduction of mutant receptors. The Journal of Clinical Endocrinology and Metabolism 95**:** E229-233.

Li B, Samp L, Sagal J, Hayward CM, Yang C, & Zhang Z (2013). Synthesis of Quinazolin-4(3H)-ones via Amidine N-Arylation. The Journal of Organic Chemistry 78**:** 1273-1277.

Li D, Opas EE, Tuluc F, Metzger DL, Hou C, Hakonarson H, *et al.* (2014). Autosomal Dominant Hypoparathyroidism Caused by Germline Mutation in GNA11: Phenotypic and Molecular Characterization. The Journal of Clinical Endocrinology & Metabolism 99**:** E1774-E1783.

Li X, & Wilson JW (1997). Increased vascularity of the bronchial mucosa in mild asthma. American Journal of Respiratory and Critical Care Medicine 156**:** 229-233.

Lindberg JS, Moe SM, Goodman WG, Coburn JW, Sprague SM, Liu W, *et al.* (2003). The calcimimetic AMG 073 reduces parathyroid hormone and calcium x phosphorus in secondary hyperparathyroidism. Kidney International 63**:** 248-254.

Ling S, Shi P, Liu S, Meng X, Zhou Y, Sun W, *et al.* (2021). Structural mechanism of cooperative activation of the human calcium-sensing receptor by Ca2+ ions and L-tryptophan. Cell Research.

Loupy A, Ramakrishnan SK, Wootla B, Chambrey R, de la Faille R, Bourgeois S, *et al.* (2012). PTH-independent regulation of blood calcium concentration by the calcium-sensing receptor. Journal of Clinical Investigation 122**:** 3355-3367.

Ma J-N, Owens M, Gustafsson M, Jensen J, Tabatabaei A, Schmelzer K, *et al.* (2011). Characterization of highly efficacious allosteric agonists of the human calcium-sensing receptor. Journal of Pharmacology and Experimental Therapeutics 337**:** 275-284.

MacLeod RJPD (2013). CaSR function in the intestine: Hormone secretion, electrolyte absorption and secretion, paracrine non-canonical Wnt signaling and colonic crypt cell proliferation. Best Practice & Research Clinical Endocrinology & Metabolism 27**:** 385-402.

Mamillapalli R, VanHouten J, Zawalich W, & Wysolmerski J (2008). Switching of G-protein Usage by the Calcium-sensing Receptor Reverses Its Effect on Parathyroid Hormone-related Protein Secretion in Normal Versus Malignant Breast Cells. Journal of Biological Chemistry 283**:** 24435-24447.

Mamillapalli R, & Wysolmerski J (2010). The calcium-sensign receptor couples to Gαs and regulates PTHrP and ACTH secretion in pituitary cells. Journal of Endocrinology 204**:** 287-297.

Mannstadt M, Harris M, Bravenboer B, Chitturi S, Dreijerink KMA, Lambright DG, *et al.* (2013). Germline Mutations Affecting Gα 11 in Hypoparathyroidism. The New England Journal of Medicine 368**:** 2532-2534.

Marinissen MJ, & Gutkind JS (2001). G-protein-coupled receptors and signaling networks: emerging paradigms. Trends in Pharmacological Sciences 22**:** 368-376.

Marquis RW, Casillas LN, Ramanjulu JM, & Callahan JF (2010). Calcilytic compoundsed. GlaxoSmithKline: USA.

Marquis RW, Lago AM, Callahan JF, Rahman A, Dong X, Stroup GB, *et al.* (2009). Antagonists of the calcium receptor. 2. amino alcohol-based parathyroid hormone secretagogues. Journal of Medicinal Chemistry 52**:** 6599-6605.

Martin JG, & Verma N (2012). Mechanisms of airway remodeling in asthma. Drug Discover Today: Disease Mechanisms 9**:** e95-e102.

Martinez FD, & Verceli D (2013). Asthma. Lancet 382**:** 1360-1372.

Marz W, Seelhorst U, Wellnitz B, Tiran B, Obermayer-Pietsch B, Renner W, *et al.* (2007). Alanine to serine polymorphism at position 986 of the calcium-sensing receptor associated with coronary heart disease, myocardial infarction, all-cause, and cardiovascular mortality. The Journal of Clinical Endocrinology and Metabolism 92**:** 2363-2369.

Masoli M, Fabian D, Holt S, & Beasley R (2004). The global burden of asthma: executive summary of the GINA Dissemination Committee report. Allergy 59**:** 469-478.

Mastromatteo E, Lamacchia O, Campo MR, Conserva A, Baorda F, Cinque L, *et al.* (2014). A novel mutation in calcium-sensing receptor gene associated to hypercalcemia and hypercalciuria. BMC Endocrine Disorders 14**:** 239-236.

May LT, Leach K, Sexton PM, & Christopoulos A (2007). Allosteric modulation of G protein-coupled receptors. Annual Reviews of Pharmacology and Toxicology 47**:** 1-51.

McGehee DS, Aldersberg M, Liu K, Hsuing S, Heath MJS, & Tamir H (1997). Mechanism of extracellular Ca2+ receptor-stimulated hormone release from sheep thyroid parafollicular cells. Journal of Physiology 502**:** 31-44.

McMurtry CT, Schranck FW, Walkenhorst DA, Murphy WA, Kocher DB, Teitelbaum SL, *et al.* (1992). Significant developmental elevation in serum parathyroid hormone levels in a large kindred with familial benign (hypocalciuric) hypercalcemia. The American Journal of Medicine 93**:** 247-258.

McNeil SE, Hobson SA, Nipper V, & Rodland KD (1998). Functional Calcium-sensing Receptors in Rat Fibroblasts Are Required for Activation of SRC Kinase and Mitogen-activated Protein Kinase in Response to Extracellular Calcium. Journal of Biological Chemistry 273**:** 1114-1120.

Mentaverri R, Yano S, Chattopadhyay N, Petit L, Kifor O, Kamel S, *et al.* (2006). The calcium sensing receptor is directly involved in both osteoclast differentiation and apoptosis. The FASEB Journal 20**:** 2562-2564.

Miedlich SU, Gama L, Seuwen K, Wolf RM, & Breitwieser GE (2004). Homology modeling of the transmembrane domain of the human calcium sensing receptor expressing taste cells. Plos One 7**:** e34489.

Mine Y, & Zhang H (2015). Calcium-Sensing Receptor (CaSR)-Mediated Anti-inflammatory Effects of l-Amino Acids in Intestinal Epithelial Cells. Journal of Agricultural and Food Chemistry 63**:** 9987-9995.

Morgan SJ, Deshpande DA, Tiegs BC, Misior AM, Yan H, Hershfeld AV, *et al.* (2014). β-Agonist-mediated relaxation of airway smooth muscle is protein kinase A-dependent. Journal of Biological Chemistry 289**:** 23065-23074.

Mukherjee S, Trice J, Shinde P, Willis RE, Pressley TA, & Perez-Zoghbi JF (2013). Ca2+ oscillations, Ca2+ sensitization, and contraction activated by protein kinase C in small airway smooth muscle. The Journal of General Physiology 141**:** 165-178.

Mun H, Culverston EL, Franks AH, Collyer CA, Clifton-Bligh RJ, & Conigrave AD (2005). A double mutation in the extracellular Ca^{2+}-sensing receptor's venus flytrap domain that selectively disables L-amino acid sensing Journal of Biological Chemistry 280**:** 29067-29072.

Mun H, Franks AH, Culverston EL, Krapcho K, Nemeth EF, & Conigrave AD (2004). The venus flytrap domain of the extracellular Ca^{2+}-sensing receptor is required for L-amino acid sensing. Journal of Biological Chemistry 279**:** 51739-51744.

Murphy H, Patrick J, Báez-Irizarry E, Lacassie Y, Gómez R, Vargas A, *et al.* (2016). Neonatal severe hyperparathyroidism caused by homozygous mutation in CASR: A rare cause of life-threatening hypercalcemia. European Journal of Medical Genetics**:** 1-5.

Nadif R, Zerimech F, Bouzigon E, & Matran R (2013). The role of eosinophils and basophils in allergic diseases considering genetic findings Current Opinion in Allergy and Clinical Immunology 13**:** 507-513.

Nagata M, Sedgwick J, Kita H, & Busse WW (1998). Granulocyte macrophage colony-stimulating factor augments ICAM-1 and VCAM-1 activation of eosinophil function American Journal of Respiratory Cell and Molecular Biology 19**:** 158-166.

Nagata M, Sedgwick JB, Bates ME, Kita H, & Busse WW (1995). Eosinophil adhesion to vascular cell adhesion molecule-1 activates superoxide anion generation. Journal of Immunology 155**:** 2194-2202.

Nagata M, Sedgwick JB, Vrtis R, & Busse WW (1999). Endothelial cells upregulate eosinophil superoxide generation via VCAM-1 expression. Clinical & Experimental Allergy 29**:** 550-561.

Nagata M, Yamamoto H, Tabe K, & Sakamoto Y (2001). Eosinophil transmigration across VCAM-1-expressing endothelial cells is upregulated by antigen-stimulated mononuclear cells. International Archives of Allergy Immunology 125**:** 7-11.

Nakagome K, Matsushita S, & Nagata M (2012). Neutrophilic inflammation in severe asthma. International Archives of Allergy Immunology 158**:** 96-102.

Nelson HS, Busse WW, Kerwin E, Church N, Emmett A, Richard K, *et al.* (2000). Fluticasone propionate/salmeterol combination provides more effective asthma control than low-dose inhaled corticosteroid plus montelukast. Journal of Allergy and Clinical Immunology 106**:** 1088-1095.

Nemeth EF (2002). The search for calcium receptor antagonists (calcilytics). Journal of Molecular Endocrinology 29**:** 15-21.

Nemeth EF, Heaton WH, Miller M, Fox J, Balandrin MF, Van Wagenen BC, *et al.* (2004). Pharmacodynamics of the type II calcimimetic compound cinacalcet HCl. The Journal of pharmacology and experimental therapeutics 308**:** 627.

Nemeth EF, & Scarpa A (1986). Cytosolic Ca2+ and the regulation of secretion in parathyroid cells. FEBS Letters 203**:** 15-19.

Nemeth EF, & Scarpa A (1987). Rapid mobilization of cellular Ca2+ in bovine parathyroid cells evoked by extracellular divalent cations. Evidence for a cell surface calcium receptor. Journal of Biological Chemistry 262**:** 5188-5196.

Nemeth EF, Van Wagenen BC, & Balandrin MF (2018). Discovery and development of calcimimetic and calcilytic compounds. Progress in Medicinal Chemistry 57**:** 1-86.

Nesbit MA, Hannan FM, Howles SA, Babinsky VN, Head RA, Cranston T, *et al.* (2013). Mutations affecting G-Protein Subunit α 11 in hypercalcemia and hypocalcemia. The New England Journal of Medicine 368**:** 2476-2486.

Noetzel MJ, Gregory KJ, Vinson PN, Manka JT, Stauffer SR, Lindsley CW, *et al.* (2013). A novel metabotropic glutamate receptor 5 positive allosteric modulator acts at a unique site and confers stimulus bias to mGlu5 signaling. Molecular Pharmacology 83**:** 835-847.

North ML, Grasemann H, Khanna N, Inman MD, Gauvreau GM, & Scott JA (2013). Increased ornithine-derived polyamines cause airway hyperresponsiveness in a mouse model of asthma. American Journal of Respiratory Cell and Molecular Biology 48**:** 694-702.

Ogata S, Kubota Y, Satoh S, Ito S, Takeuchi H, Ashizuka M, *et al.* (2006). Ca2+ stimulates COX-2 expression through calcium-sensing receptor in fibroblasts. Biochemical and Biophysical Research Communications 351**:** 808-814.

Oti AB (1983). A perspective of respiratory mechanics. Journal of Applied Physiology 54**:** 1183-1187.

Ouedraogo N, & Roux E (2014). Physiology of airway smooth muscle contraction: an overview. Pulmonary & Respiratory Medicine 4**:** 10002221.

Palmer SC, Mavridis D, Johnson DW, Tonelli M, Ruospo M, & Strippoli GFM (2020). Comparative effectiveness of calcimimetic agents for Secondary Hyperparathyroidism in adults: a systematic review and network meta-analysis. American Journal of Kidney Diseases 76**:** 321-330.

Pascual RM, & Peters SP (2005). Airway remodeling contributes to the progressive loss of lung function in asthma: an overview. Journal of Allergy and Clinical Immunology 116**:** 477-486.

Pegg AE (2016). Functions of Polyamines in Mammals. Journal of Biological Chemistry 291**:** 14904-14912.

Pera T, & Penn RB (2016). Bronchoprotection and bronchorelaxation in asthma: New targets, and new ways to target the old ones. Pharmacology & Therapeutics 164**:** 82-96.

Petrel C, Kessler A, Dauban P, Dodd RH, Rognan D, & Ruat M (2004). Positive and negative allosteric modulators of the Ca2+-sensing receptor interact within overlapping but not identical binding sites in the transmembrane domain. Journal of Biological Chemistry 279**:** 18990-18997.

Petrel C, Kessler A, Maslah F, Dauban P, Dodd RH, Rognan D, *et al.* (2003). Modeling and mutagenesis of the binding site of Calhex 231, a novel negative allosteric modulator of the extracellular Ca(2+)-sensing receptor. Journal of Biological Chemistry 278**:** 49487-49494.

Pi M, Spurney RF, Tu Q, Hinson T, & Quarles LD (2002). Calcium-sensing recpetor activation of Rho involves filamin and Rho-guanine nucleotide exchange factor. Endocrinology 143**:** 3830-3838.

Pin JP, Galvez T, & Prézeau L (2003). Evolution, structure, and activation mechanism of family 3/C G-protein-coupled receptors. Pharmacology & Therapeutics 98**:** 325-354.

Piret SE, Gorvin CM, Pagnamenta AT, Howles SA, Cranston T, Rust N, *et al.* (2016). Identification of a G-Protein subunit-α11 gain-of-function mutation, Val340Met, in a Family With Autosomal Dominant Hypocalcemia Type 2 (ADH2). Journal of Bone and Mineral Research 31**:** 1207-1214.

Qu Y, Hui J, Wang L, Tang N, Zhong H, Liu Y, *et al.* (2016). Reduced Expression of the Extracellular Calcium-Sensing Receptor (CaSR) Is Associated with Activation of the Renin-Angiotensin System (RAS) to Promote Vascular Remodeling in the Pathogenesis of Essential Hypertension. PLoS ONE 11**:** e0157456.

Quarles LD, Sherrard DJ, Adler S, Rosansky SJ, McCary LC, Liu W, *et al.* (2003). The calcimimetic AMG 073 as a potential treatment for secondary hyperparathyroidism of end-stage renal disease. Journal of the American Society of Nephrology : JASN 14**:** 575.

Quinn SJ, Ye CP, Diaz R, Kifor O, Bai M, Vassilev P, *et al.* (1997). The Ca2+-sensing receptor: a target for polyamines. American Journal of Physiology-Cell Physiology 273**:** C1315-C1323.

Ray K, Clapp P, Goldsmith PK, & Spiegel AM (1998). Identification of the sites of N-linked glycosylation on the human calcium receptor and assessment of their role in cell surface expression and signal transduction. Journal of Biological Chemistry 273**:** 34558-34567.

Ray K, Fan GF, Goldsmith PK, & Spiegel AM (1997). The carboxyl terminus of the human calcium receptor. Requirements for cell-surface expression and signal transduction. Journal of Biological Chemistry 272.

Ray K, Ghosh SP, & Northup JK (2004). The Role of Cysteines and Charged Amino Acids in Extracellular Loops of the Human Ca2+ Receptor in Cell Surface Expression and Receptor Activation Processes. Endocrinology 145**:** 3892-3903.

Ray K, & Northup J (2002). Evidence for distinct cation and calcimimetic compound (NPS568) recognition domains in the transmembrane regions of the human Ca^{2+} receptor Journal of Biological Chemistry 277**:** 18908-18913.

Re M, Pampillo M, Savard M, Dubuc C, McArdle CA, Millar RP, *et al.* (2010). The Human Gonadotropin Releasing Hormone Type I Receptor Is a Functional Intracellular GPCR Expressed on the Nuclear Membrane. PLOS ONE 5**:** e11489.

Renkema KY, Velic A, Dijkman HBPM, Verkaart SAJ, Kemp JWCMvd, Nowik M, *et al.* (2009). The calcium-sensing receptor promotes urinary acidification to prevent nephrolithiasis. Journal of the American Society of Nephrology 20**:** 1705-1713.

Rey O, Chang W, Bikle D, Rozengurt N, Young SH, & Rozengurt E (2012). Negative Cross-talk between Calcium-sensing Receptor and β-Catenin Signaling Systems in Colonic Epithelium. Journal of Biological Chemistry 287**:** 1158-1167.

Riccardi D, Hall AE, Chattopadhyay N, Xu JZ, Brown E, & Hebert SC (1998). Localization of the extracellular Ca2+/polyvalent cation-sensing protein in rat kidney. American Journal of Physiology-Renal Physiology 274**:** F611-F622.

Riccardi D, Park J, Lee WS, Gamba G, Brown EM, & Hebert SC (1995). Cloning and functional expression of a rat kidney extracellular calcium/polyvalent cation-sensing receptor. Proceedings of the National Academy of Sciences 92**:** 131-135.

Riccardi D PJ, Lee W, Gamba G, Brown EM, Hebert SC (1995). Cloning and Functional Expression of a Rat Kidney Extracellular Calcium/ Polyvalent Cation-Sensing Receptor. Proceedings of the National Academy of Sciences of the United States of America 92**:** 131-135.

Riccardi D, & Valenti G (2016). Localization and function of the renal calcium-sensing receptor. Nature Reviews Nephrology 12**:** 414-425.

Roberts MS, Gafni RI, Brillante B, Guthrie LC, Streit J, Gash D, *et al.* (2019). Treatment of Autosomal Dominant Hypocalcemia Type 1 with the calcilytic NPSP795 (SHP635). Journal of Bone and Mineral Research 34**:** 1609-1618.

Roesler AM, Wicher SA, Ravix J, Britt Jr. RD, Manlove L, Teske JJ, *et al.* (2019). Calcium sensing receptor in developing human airway smooth muscle. Journal of Cellular Physiology 234**:** 14187-14197.

Roszko KL, Bi R, Gorvin CM, Brauner-Osborne H, Xiong XF, Inoue A, *et al.* (2017). Knockin mouse with mutant Galpha11 mimics human inherited hypocalcemia and is rescued by pharmacologic inhibitors. JCI Insight 2**:** e91079.

Rothe H, Shapiro W, Sun WY, & Matalon A (2008). CaSR polymorphism Arg990Gly and response to calcimimetic agents in end-stage kidney disease patients with secondary hyperparathyroidism and in cell culture. Personalized Medicine 5**:** 109-116.

Rothe HM, Shapiro WB, Sun WY, & Chou SY (2005). Calcium-sensing receptor gene polymorphism Arg990Gly and its possible effect on response to cinacalcet HCl. Pharmacogenetics and Genomics 15**:** 29-34.

Rottembourg J, Urena-Torres P, Toledano D, Gueutin V, Hamani A, Coldefy O, *et al.* (2019). Factors associated with parathyroid hormone control in haemodialysis patients with secondary

hyperparathyroidism treated with cinacalcet in real-world clinical practice: Mimosa study. Clinical Kidney Journal 12**:** 871-879.

Rowe BH, Bota GW, Fabris L, Therrien SA, Milner RA, & Jacono J (1999). Inhaled budesonide in addition to oral corticosteroids to prevent asthma replapse following discharge from the emergency department: A randomized controlled trial. The Journal of the American Medical Association 281**:** 2119-2126.

Ruat M, Moliver ME, Snowman A, M., & Snyder S, H. (1995). Calcium Sensing Receptor: Molecular Cloning in Rat and Localization to Nerve Terminals. Proceedings of the National Academy of Sciences of the United States of America 92**:** 3161-3165.

Ruat M, Snowman AM, Hester LD, & Snyder SH (1996). Cloned and Expressed Rat Ca-sensing Receptor: DIFFERENTIAL COOPERATIVE RESPONSES TO CALCIUM AND MAGNESIUM. Journal of Biological Chemistry 271**:** 5972-5975.

Sands JM, Naruse M, Baum M, Jo I, Hebert SC, Brown EM, *et al.* (1997). Apical extracellular calcium/polyvalent cation-sensing receptor regulates vasopressin-elicited water permeability in rat kidney inner medullary collecting duct The Journal of Clincial Investigation 99**:** 1399-1405.

Savas-Erdeve S, Sagsak E, Keskin M, Magdelaine C, Lienhardt-Roussie A, Kurnaz E, *et al.* (2016). Treatment experience and long-term follow-up data in two severe neonatal hyperparathyroidism cases. Journal of Pediatric Endocrinology and Metabolism 29**:** 129-129.

Savitz J, Lucki I, & Drevets WC (2009). 5-HT1A receptor function in major depressive disorder. Progress in Neurobiology 88**:** 17-31.

Schepelmann M, Yarova PL, Lopez-Fernandez I, Davies TS, Brennan SC, Edwards PJ, *et al.* (2016). The vascular Ca2+-sensing receptor regulates blood vessel tone and blood pressure. American Journal of Physiology-Cell Physiology 310**:** C193-C204.

Schleimer RP, Sterbinsky SA, Kaiser J, Bickel CA, Klunk DA, Tomioka K, *et al.* (1992). IL-4 induces adherence of human eosinophils and basophils but not neutrophils to endothelium. Association with expression of VCAM-1**.** Journal of Immunology 148**:** 1086-1092.

Schreckenberg R, & Schlüter K-D (2018). Calcium sensing receptor expression and signalling in cardiovascular physiology and disease. Vascular Pharmacology 107**:** 35-42.

Schwartz C, & Voehringer D (2011). Basophils: important emerging players in allergic and anti-parasite responses. Bioessays 33**:** 423-426.

Schwartz TW, Frimurer TM, Holst B, Rosenkilde MM, & Elling CE (2006). Molecular mechanism of 7TM receptor activation--a global toggle switch model. Annual Review of Pharmacology and Toxicology 46**:** 481-519.

Shannon J, Ernst P, Yamauchi Y, Olivenstein R, Lemiere C, Foley S, *et al.* (2007). Differences in airway cytokine profile in severe asthma compared to moderate asthma. Chest 133**:** 420-426.

Shigematsu T, Shimazaki R, Fukagawa M, & Akizawa T (2018). Pharmacokinetics of evocalcet in secondary hyperparathyroidism patients receiving hemodialysis: first-in-patient clinical trial in Japan. Clinical Pharmacology: Advances and Applications Volume 10**:** 101-111.

Shinagawa Y, Inoue T, Katsushima T, Kiguchi T, Ikenogami T, Ogawa N, *et al.* (2011). Discovery of a potent and short-acting oral calcilytic with a pulsatile secretion of parathyroid hormone. ACS Medicinal Chemistry Letters 2**:** 238-242.

Shore SA, & Moore PE (2003). Regulation of beta-adrenergic responses in airway smooth muscle. Respiratory Physiology & Neurobiology 137**:** 179-195.

Siehler S (2009). Regulation of RhoGEF proteins by G12/13-coupled receptors. British Journal of Pharmacological Society 158**:** 41-49.

Siracusa MC, Wojno ED, & Artis D (2012). Functional heterogeneity in the basophil cell lineage. Advance in Immunology 115**:** 141-159.

Smajilovic S, Yano S, Jabbari R, & Tfelt-Hansen J (2011). The calcium-sensing receptor and calcimimetics in blood pressure modulation. British Journal of Pharmacology 164**:** 884-893.

Soda K (2010). Polyamine intake, dietary pattern, and cardiovascular disease. Medical Hypotheses 75**:** 299-301.

SözenT, Özışık L, & BaşaranNÇ (2017). An overview and management of osteoporosis. European Journal of Rheumatology 4**:** 46-56.

Sriram K, Wiley SZ, Moyung K, Gorr MW, Salmerón C, Marucut J, *et al.* (2019). Detection and Quantification of GPCR mRNA: An Assessment and Implications of Data from High-Content Methods. ACS Omega 4**:** 17048-17059.

Subbarao P, Mandhane PJ, & Sears MR (2009). Asthma: epidemiology, etiology and risk factors. Canadian Medical Association Journal 181**:** E181-E190.

Sweeney D, Hollins F, Gomez E, Mistry R, Saunders R, Challiss RA, *et al.* (2015). No evidence for altered intracellular calcium-handling in airway smooth muscle cells from human subjects with asthma. BMC Pulmonary Medicine 15**:** 12.

Tadatoshi S, Marie C, Noriko I, Yi F, Jun-ichi H, Jovana K, *et al.* (2017). Parathyroid hormone controls paracellular Ca2+ transport in the thick ascending limb by regulating the tight-junction protein Claudin14. Proceedings of the National Academy of Sciences - PNAS 114**:** E3344-E3353.

Tan X, Alrashdan YA, Alkhouri H, Oliver BG, Armour CL, & Hughes JM (2013). Airway smooth muscle CXCR3 ligand production: regulation by JAK-STAT1 and intracellular Ca^{2+}. American Journal of Physiology- Lung Cellular and Molecular Physiology 304**:** L790-802.

Tang L, Cheng CY, Sun X, Pedicone AJ, Mohamadzadeh M, & Cheng SX (2016). The Extracellular Calcium-Sensing Receptor in the Intestine: Evidence for Regulation of Colonic Absorption, Secretion, Motility, and Immunity. Frontiers in Physiology 7**:** 245-245.

Tang MLK, Wilson JW, Stewart AG, & Royce SG (2006). Airway remodelling in asthma: current understanding and implications for future therapies. Pharmacology & Therapeutics 112**:** 474-488.

Tang X, Wang Y, Li D, Luo J, & Liu M (2012). Orphan G protein-coupled receptors (GPCRs): biological functions and potential drug targets. Acta Pharmacologica Sinica 33**:** 363-371.

Tashjian AHJ, & Goltzman D (2008). On the Interpretation of Rat Carcinogenicity Studies for Human PTH(1-34) and Human PTH(1-84). Journal of Bone and Mineral Research 23**:** 803-811.

Tattersfield AE (1997). Limitations of current treatment. The Lancet 350**:** S24-S27.

Tfelt-Hansen J, & Brown EM (2005). THE CALCIUM-SENSING RECEPTOR IN NORMAL PHYSIOLOGY AND PATHOPHYSIOLOGY: A Review. Critical Reviews in Clinical Laboratory Sciences 42**:** 35-70.

Tfelt-Hansen J, MacLeod RJ, Chattopadhyay N, Yano S, Quinn S, Ren X, *et al.* (2003). Calcium-sensing receptor stimulates PTHrP release by pathways dependent on PKC, p38 MAPK, JNK, and ERK1/2 in H-500 cells. American Journal of Physiology-Endocrinology and Metabolism 285**:** E329-E337.

Thakker RV (2004). Diseases associated with the extracellular calcium-sensing receptor. Cell Calcium 35**:** 275-282.

Tharmalingam S, Wu C, & Hampson DR (2016). The calcium-sensing receptor and integrins modulate cerebellar granule cell precursor differentiation and migration. Developmental Neurobiology 76**:** 375-389.

Thompson M, Freeman MR, Manlove LJ, Fang YH, Britt R, Kuipers I, *et al.* (2016). A29 INFLAMMATION AND MECHANISMS OF AIRWAY SMOOTH MUSCLE CONTRACTION: Calcium Sensing Receptor And Airway Reactivity In Mixed Allergen Treated Mouse Model Of Asthma. American Journal of Respiratory and Critical Care Medicine 193**:** 1.

Thomsen ARB, Hvidtfeldt M, & Bräuner-Osborne H (2012a). Biased agonism of the calcium-sensing receptor. Cell Calcium 51**:** 107-116.

Thomsen ARB, Worm J, Jacobsen SE, Stahlhut M, Latta M, & Bräuner-Osborne H (2012b). Strontium Is a Biased Agonist of the Calcium-Sensing Receptor in Rat Medullary Thyroid Carcinoma 6-23 Cells. Journal of Pharmacology and Experimental Therapeutics 343**:** 638-649.

Timmers HJLM, Karperien M, Hamdy NAT, De boer H, & Hermus ARMM (2006). Normalization of serum calcium by cinacalcet in a patient with hypercalcaemia due to a de novo inactivating mutation of the calcium-sensing receptor. Journal of Internal Medicine 260**:** 177-182.

Toka HR (2014). New functional aspects of the extracellular calcium-sensing receptor. Current Opinion in Nephrology and Hypertension 23**:** 352-360.

Toka HR, Al-Romaih K, Koshy JM, Dibartolo S, Kos CH, Quinn SJ, *et al.* (2012). Deficiency of the Calcium-Sensing Receptor in the Kidney Causes Parathyroid Hormone—Independent Hypocalciuria. Journal of American Society of Nephrology 23**:** 1879-1890.

Topala CN, Schoeber JPH, Searchfield LE, Riccardi D, Hoenderop JGJ, & Bindels RJM (2008). Activation of the Ca2+ -sensing receptor stimulates the activity of the epithelial Ca2+ channel TRPV5. Cell Calcium 45**:** 331-339.

Topala CN, Schoeber JPH, Searchfield LE, Riccardi D, Hoenderop JGJ, & Bindels RJM (2009). Activation of the Ca.sup.2+-sensing receptor stimulates the activity of the epithelial Ca.sup.2+ channel TRPV5. Cell calcium (Edinburgh) 45**:** 331.

Van den Bossche J, Lamers WH, Koehler ES, Geuns JM, Alhonen L, Uimari A, *et al.* (2012). Pivotal Advance: Arginase-1-independent polyamine production stimulates the expression of IL-4-induced alternatively activated macrophage markers while inhibiting LPS-induced expression of inflammatory genes. Journal of Leukocyte Biology 91**:** 684-699.

VanHouten J, Dann P, McGeoch G, Brown EM, Krapcho K, Neville M, *et al.* (2004). The calcium-sensing receptor regulates mammary gland parathyroid hormone-related protein production and calcium transport. Journal of Clinical Investigation 113**:** 598-608.

Vargas-Poussou RR, Mansour-Hendili RL, Baron RS, Bertocchio RJ-P, Travers RC, Simian RC, *et al.* (2016). Familial Hypocalciuric Hypercalcemia Types 1 and 3 and Primary Hyperparathyroidism: Similarities and Differences. The Journal of Clinical Endocrinology & Metabolism 101**:** 2185-2195.

Vassilev PM, Ho-Pao CL, Kanazirska MP, Hong YK, Seidman CE, Seidman JG, *et al.* (1997). Ca_o-sensing receptor (CaR)-mediated activation of K^+ channels is blunted in CaR gene-deficient mouse neurons. Neuroreport 8**:** 1411-1415.

Vezzoli G, Scillitani A, Corbetta S, Terranegra A, Dogliotti E, Guarnieri V, *et al.* (2011). Polymorphisms at the regulatory regions of the CASR gene influence stone risk in primary hyperparathyroidism. European Journal of Endocrinology 164**:** 421-427.

Vezzoli G, Terranegra A, Aloia A, Arcidiacono T, Milanesi L, Mosca E, *et al.* (2013). Decreased transcriptional activity of calcium-sensing receptor gene promoter 1 is associated with calcium nephrolithiasis. The Journal of Clinical Endocrinology and Metabolism 98**:** 3839-3847.

Vizard TN, O'Keeffe GW, Gutierrez H, Kos CH, Riccardi D, & Davies AM (2008). Regulation of axonal and dendritic growth by the extracellular calcium-sensing receptor. Nature Neuroscience 11**:** 285-291.

Wadhwa R, Dua K, Adcock IM, Horvat JC, Kim RY, & Hansbro PM (2019). Cellular mechanisms underlying steroid-resistant asthma. European Respiratory Review 28**:** 190096.

Walter S, Baruch A, Dong J, Tomlinson JE, Alexander ST, Janes J, *et al.* (2013). Pharmacology of AMG 416 (Velcalcetide), a novel peptide agonist of the calcium-sensing receptor, for the treatment of Secondary Hyperparathyroidism in hemodialysis patients. Journal of Pharmacology and Experimental Therapeutics 346**:** 229.

Wang R, Xu C, Zhao W, Zhang J, Cao K, Yang B, *et al.* (2003). Calcium and polyamine regulated calcium-sensing receptors in cardiac tissues. European Journal of Biochemistry 270**:** 2680-2688.

Wang XM, Wu YW, Li ZJ, Zhao XH, Lv SM, & Wang XH (2016). Polymorphisms of CASR gene increase the risk of primary hyperparathyroidism. Journal of Endocrinological Investigation 39**:** 617-625.

Watanabe Sumiyo SF, Chang Hangil, Takeuchi Yasuhiro, Hasegawa Yukihiro, Okazaki Ryo, Chikatsu Noriko, Fujita Toshiro (2002). Association between activating mutations of calcium-sensing receptor and Bartter's syndrome. Lancet 360**:** 692.

Weller PF (2000). Human eosinophils. Journal of Allergy and Clinical Immunology 100**:** 283-287.

Wess J, Han S, Kim S, Jacobson KA, & Li JH (2008). Conformational changes involved in G-protein-coupled-receptor activation. Trends in Pharmacological Sciences 29**:** 616-625.

Wettschureck N, E. L, Libutti SK, Offermanns S, Robey PG, & Spiegel AM (2007). Parathyroid-specific double knockout of Gq and G11 alpha-subunits leads to a phenotype resembling germline knockout of the extracellular Ca2+ -sensing receptor. Molecular Endocrinology 21**:** 274-280.

White E, McKenna J, Cavanaugh A, & Breitwieser GE (2009). Pharmacochaperone-Mediated Rescue of Calcium-Sensing Receptor Loss-of-Function Mutants. Molecular Endocrinology 23**:** 1115-1123.

Widler L (2011). Calcilytics: antagonists of the calcium-sensing receptor for the treatment of osteoporosis. Future Medicinal Chemistry 3**:** 535-547.

Widler L, Altmann E, Beerli R, Breitenstein W, Bouhelal R, Buhl T, *et al.* (2010). 1-alkyl-4-phenyl-6-alkoxy-1H-quinazolin-2-ones: a novel series of potent calcium-sensing receptor antagonists. Journal of Medicinal Chemistry 53**:** 2250-2263.

Wilhelm-Bals A, Parvex P, Magdelaine C, & Girardin E (2012). Successful use of bisphosphonate and calcimimetic in neonatal severe Primary Hyperparathyroidism. Pediatrics 129**:** e812-e816.

Woo LN, Guo WY, Wang X, Young A, Salehi S, Hin A, *et al.* (2018). A 4-Week Model of House Dust Mite (HDM) Induced Allergic Airways Inflammation with Airway Remodeling. Scientific Reports 8**:** 6925.

Wootten D, Christopoulos A, & Sexton PM (2013). Emerging paradigms in GPCR allostery: implications for drug discovery. Nature Reviews Drug Discovery 12**:** 630-644.

World Health Organization (2017a). 10 facts on asthma. Fact Sheet.

World Health Organization (2017b). Medical Centre: Asthma. Fact Sheet.

Wu H, Wang C, Gregory KJ, Han GW, Cho HP, Xia Y, *et al.* (2014). Structure of a class C GPCR metabotropic glutamate receptor 1 bound to an allosteric modulator. Science 344**:** 58-64.

Yamaguchi T, Chattopadhyay N, Kifor O, Butters RR, Sugimoto T, & Brown EM (1998). Mouse Osteoblastic Cell Line (MC3T3-E1) Expresses Extracellular Calcium (Ca2+o)–Sensing Receptor and Its Agonists Stimulate Chemotaxis and Proliferation of MC3T3-E1 Cells. Journal of Bone and Mineral Research 13**:** 1530-1538.

Yamamura A, Guo Q, Yamamura H, Zimnicka AM, Pohl NM, Smith KA, *et al.* (2012). Enhanced Ca(2+)-sensing receptor function in idiopathic pulmonary arterial hypertension. Circulation Research 111**:** 469-481.

Yang W, Ruan Z, Wang Y, Van KK, Ma Z, Arey BJ, *et al.* (2009). Discovery and Structure−Activity Relationships of Trisubstituted Pyrimidines/Pyridines as Novel Calcium-Sensing Receptor Antagonists. Journal of Medicinal Chemistry 52**:** 1204-1208.

Yano S BE, Chattopadhyay N (2004). Calcium-sensing receptor in the brain. Cell Calcium 35**:** 257-264.

Yano S, Macleod RJ, Chattopadyay N, Tfelt-Hansen J, Kifor O, Butters RR, *et al.* (2004). Calcium-sensing receptor activation stimulates parathyroid hormone-related protein secretion in prostate cancer cells: role of epidermal growth factor receptor transactivation. Bone 35**:** 664-672.

Yarova PL, Huang P, Schepelmann MW, Bruce R, Ecker R, Nica R, *et al.* (2021). Characterization of Negative Allosteric Modulators of the Calcium-Sensing Receptor for Repurposing as a Treatment of Asthma. Journal of Pharmacology and Experimental Therapeutics 376**:** 51-63.

Yarova PL, Stewart AL, Sathish V, Britt RD, Thompson MAPL, Alexander P, *et al.* (2015). Calcium-sensing receptor antagonists abrogate airway hyperresponsiveness and inflammation in allergic asthma. Science Translational Medicine 7**:** 284ra260-284ra260.

Ye C, Ho-Pao CL, Kanazirska M, Quinn S, Seidman CE, Seidman JG, *et al.* (1997). Deficient Cation Channel Regulation in Neurons From Mice With Targeted Disruption of the Extracellular Ca2+-Sensing Receptor Gene. Brain Research Bulletin 44**:** 75-84.

Zaagsma J, Roffel AF, & Meurs H (1997). Muscarinic control of airway function. Life Sciences 60**:** 1061-1068.

Zhang C, Zhang T, Zou J, Miller CL, Gorkhali R, Yang J, *et al.* (2016). Structural basis for regulation of human calcium-sensing receptor by magnesium ions and an unexpected tryptophan derivative co-agonist. Science Advances 2**:** e1600241.

Zhang Z, Qiu W, Quinn S, Conigrave AD, Brown EM, & Bai M (2002). Three ajacent serines in the extracellular domains of the CaR are required for L-amino acid-mediated potentiation of receptor function. Journal of Biological Chemistry 277**:** 33727-33735.

Zhao X, Hauache O, Goldsmith PK, Collins R, & Spiegel AM (1999). A missense mutation in the seventh transmembrane domain constitutively activates the human Ca2+ receptor. FEBS Letters 448**:** 180-184.

Zhong H, Belardinelli L, Maa T, Feoktistov I, Biaggioni I, & Zeng D (2004). A(2B) adenosine receptors increase cytokine release by bronchial smooth muscle cells. American Journal of Respiratory Cell and Molecular Biology 30**:** 118-125.

Appendix

ACS Pharmacology & Translational Science

pubs.acs.org/ptsci

Review

Therapeutic Opportunities of Targeting Allosteric Binding Sites on the Calcium-Sensing Receptor

Jiayin Diao, Aaron DeBono, Tracy M. Josephs, Jane E. Bourke, Ben Capuano, Karen J. Gregory, and Katie Leach*

Cite This: *ACS Pharmacol. Transl. Sci.* 2021, 4, 666–679

Read Online

ACCESS | Metrics & More | Article Recommendations

ABSTRACT: The CaSR is a class C G protein-coupled receptor (GPCR) that acts as a multimodal chemosensor to maintain diverse homeostatic functions. The CaSR is a clinical therapeutic target in hyperparathyroidism and has emerged as a putative target in several other diseases. These include hyper- and hypocalcaemia caused either by mutations in the *CASR* gene or in genes that regulate CaSR signaling and expression, and more recently in asthma. The development of CaSR-targeting drugs is complicated by the fact that the CaSR possesses many different binding sites for endogenous and exogenous agonists and allosteric modulators. Binding sites for endogenous and exogenous ligands are located throughout the large CaSR protein and are interconnected in ways that we do not yet fully understand. This review summarizes our current understanding of CaSR physiology, signaling, and structure and how the many different binding sites of the CaSR may be targeted to treat disease.

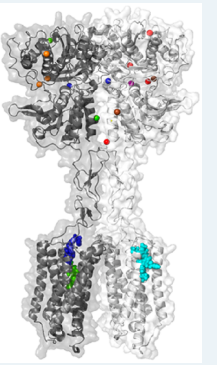

KEYWORDS: *CaSR, hyperparathyroidism, asthma, CASR gene, FHH, ADH, osteoporosis, allosteric modulator*

The CaSR is ubiquitously expressed in the human body but is found abundantly in the parathyroid glands and kidney. In these organs, the CaSR is responsible for exquisite control of extracellular Ca^{2+} (Ca^{2+}_o) to maintain systemic ionized Ca^{2+}_o concentrations within 1.2−1.4 mM (reviewed in ref 1). The CaSR negatively regulates parathyroid hormone (PTH) secretion in response to elevated Ca^{2+}_o. When Ca^{2+}_o concentrations rise, CaSR-mediated suppression of PTH synthesis and secretion decreases Ca^{2+} resorption from bone and Ca^{2+} reabsorption in the renal thick ascending limb of the loop of Henle. Within the kidneys, the CaSR responds to elevated Ca^{2+}_o independently of PTH to further decrease Ca^{2+} reabsorption.[2] Elevated Ca^{2+}_o concentrations are thus reduced. The CaSR is expressed in additional tissues involved in Ca^{2+}_o homeostasis. In the thyroid, elevated Ca^{2+}_o stimulates calcitonin release via the CaSR,[2] leading to Ca^{2+} uptake into bone. The CaSR also promotes differentiation and proliferation of bone-forming osteoblasts,[3] inhibits osteoclast-mediated bone resorption,[4] and facilitates chondrocyte-mediated skeletal growth and development.[5] In mammary epithelial cells, the CaSR mediates Ca^{2+} transport into milk[6] and suppresses mammary gland release of parathyroid hormone-related protein to reduce osteoclast-mediated release of Ca^{2+} from bone.[7]

The pivotal role of the CaSR in Ca^{2+}_o homeostasis is well-established; however, the CaSR also responds to additional stimuli to mediate a number of noncalciotropic functions. In taste buds, the CaSR responds to food-derived γ-glutamyl peptides to enhance certain tastes.[8] The CaSR is expressed along the entire gastrointestinal (GI) tract, where it senses amino acids to regulate inflammatory responses[9] as well as nutrient intake and digestion via the release of satiety and pancreatic hormones.[10,11] CaSRs in the pancreas also contribute to glucose-mediated insulin secretion, thus helping to maintain blood glucose levels.[12] In the vasculature, CaSR activation on vascular smooth muscle leads to vasodilatation, thus contributing to blood pressure control.[13] In the skin, the CaSR promotes keratinocyte differentiation, barrier function, and wound healing.[14] CaSRs located in the lungs detect fluctuations in local polyamines to mediate airway defense mechanisms such as airway contraction and inflammation.[15] In addition to responding to different stimuli in a tissue specific manner, CaSR expression in both calciotropic and non-calciotropic tissues is controlled in a tissue- and environment-specific manner. *CASR* gene promoters contain response elements for 1,25-dihydroxyvitamin D, pro-inflammatory cytokines, and the parathyroid cell-specific transcription factor, glial cells missing-2. Consequently, CaSR expression may be

Received: February 4, 2021
Published: March 8, 2021

https://dx.doi.org/10.1021/acsptsci.1c00046
ACS Pharmacol. Transl. Sci. 2021, 4, 666–679

increased in inflammation and decreased in states of vitamin D deficiency.[16,17] The many diverse CaSR functions and changes in CaSR expression during pathophysiological situations highlight that the CaSR is a multifunctional chemosensor in human (patho)physiology. This review will focus on how its many allosteric ligands bind to the CaSR and how allosteric binding sites have been targeted to manipulate CaSR activity in disease.

CASR SIGNALING

The CaSR couples primarily to $G_{i/o}$ and $G_{q/11}$ G proteins to reduce cyclic adenosine monophosphate (cAMP) levels[18] and trigger the release of intracellular Ca^{2+} (Ca^{2+}_i) from stores, respectively (Figure 1). The CaSR also increases Ca^{2+}_i via

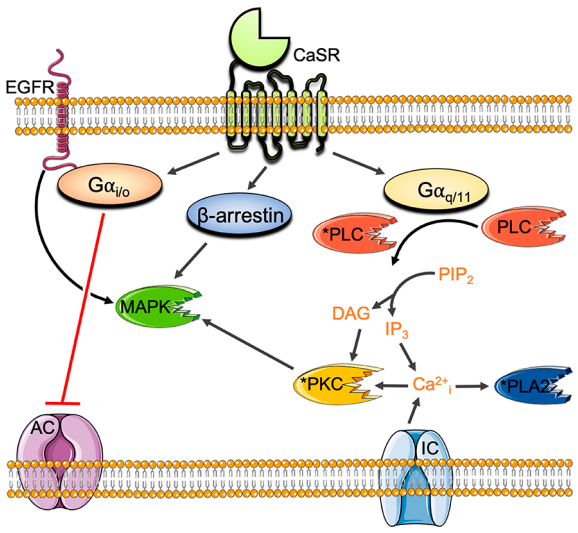

Figure 1. Principal CaSR signaling pathways. CaSR activation of $G_{i/o}$ inhibits adenylyl cyclase (AC) to reduce cAMP levels. CaSR coupling to $G_{q/11}$ activates phosphatidylinositol-specific phospholipase C (PI–PLC) to increase inositol triphosphate (IP_3) and diacyl glycerol (DAG) and trigger the release of Ca^{2+}_i from stores. Ca^{2+}_i activates phospholipase A_2 (PLA_2) and PKC. The CaSR also increases Ca^{2+}_i via influx through L-type voltage-gated and transient receptor potential ion channels (IC), in part via PKC. The CaSR activates MAPK signaling cascades via $G_{q/11}$-mediated PKC, $G_{i/o}$-mediated activation of epidermal growth factor receptor (EGFR), and β arrestin.

influx through L-type voltage-gated and transient receptor potential ion channels on the plasma membrane,[19−21] in part via a PKC-dependent mechanism.[20]

In addition to canonical G protein coupling, the CaSR stimulates mitogen activated protein kinases (MAPK) downstream from $G_{q/11}$, $G_{i/o}$, and β arrestin.[22−25] In some cell types, the CaSR couples to $G_{12/13}$,[26] although the (patho)-physiological relevance is unknown. The CaSR also activates G_s proteins in immortalized or malignant breast cells[27] and in murine pituitary corticotroph-derived AtT-20 cells,[28] resulting in increased cAMP production in these cell types. Thus, the CaSR is promiscuously coupled to several different G protein families, adding even greater pharmacological complexity.

Due to its promiscuous G protein coupling preferences, the CaSR is subject to biased agonism whereby distinct ligands activate or inhibit a subset of possible signaling pathways linked to the CaSR to the relative exclusion of others.[25,29,30] While the physiological relevance of biased CaSR agonism is not known, it likely plays an important role in regulating CaSR activation by its many varied endogenous ligands. Small molecule allosteric ligands also engender biased modulation at the CaSR (discussed in more detail below), demonstrating that CaSR function may be fine-tuned with allosteric drugs.

STRUCTURE

The CaSR protein is encoded by 7 exons and is expressed as a 1078 amino acid polypeptide. Exons 2−6 encode the large extracellular domain (ECD), while exon 7 encodes the 7 transmembrane (7TM)-spanning region and C-terminal tail. The CaSR forms a homodimer mediated by covalent and noncovalent interactions.[31,32] The ECD contains a bilobed "venus flytrap" (VFT) domain, so-called because the two lobes (named LB1 and LB2) open and close around a ligand-binding cleft[31,33] much like the VFT plant closes around its prey (Figure 2).

The VFT is linked via a cysteine-rich domain (CRD) to the 7TM and its connecting intracellular and extracellular loops (ICL and ECL, respectively). The structural integrity of the 7TM is in part maintained by a disulfide bond between C677 in ECL1 and C765 in ECL2.[34] The 7TM is proceeded by a large C-terminal tail that contributes to cell surface expression, signaling, and binding to accessory proteins.[35−37] Further, C-terminal tail residues (S875 and T888) are predicted to be key protein kinase C (PKC) phosphorylation sites, which serve to negatively regulate CaSR activity.[38,39]

ENDOGENOUS CASR LIGANDS AND THEIR BINDING SITES

The primary physiological ligand of the CaSR is Ca^{2+}. X-ray crystallography combined with anomalous scattering analysis suggest Ca^{2+} binds to four sites within the VFT domain (Figure 2)[31] in a cooperative manner, such that binding to one site positively modulates Ca^{2+} binding to the other sites.[40] A loss in Ca^{2+}_o agonism was observed upon mutation of residues located in the four Ca^{2+} sites, although the effects of mutations on receptor expression, Ca^{2+}_o affinity, and Ca^{2+}_o efficacy were not delineated. Consequently, it is unclear to what extent these mutations alter Ca^{2+}_o binding to the CaSR and therefore whether these sites are physiologically relevant or simply an artifact of the crystallization conditions. Ca^{2+} also binds to at least one site in the 7TM or ECLs, evidenced by the fact that Ca^{2+}_o retains agonist activity at a CaSR lacking its entire ECD.[41] Thus, while Ca^{2+}_o is considered the orthosteric agonist, strictly speaking Ca^{2+}_o is an allosteric modulator of itself. In addition to Ca^{2+}_o, the CaSR responds to additional divalent cations, including Mg^{2+}, as well as trivalent cations such as Gd^{3+}.[42,43] Structural studies suggest a Mg^{2+} binding site that overlaps with a Ca^{2+} binding site in the VFT, as well as other distinct binding sites for Mg^{2+} and Gd^{3+}[33] (Figure 2). However, anomalous scattering analysis was not used to assign Mg^{2+} or Gd^{3+} in the CaSR VFT crystal structure and can therefore be made with less confidence. Importantly, all six cation binding sites are topographically distinct from the VFT cleft between LB1 and LB2, which is the orthosteric agonist binding site in all other class C GPCRs.

The CaSR VFT cleft is the binding site for endogenous positive allosteric modulators (PAMs), which include aromatic L-amino acids[44] and γ-glutamyl peptides.[45] Larger aliphatic and aromatic L-amino acids, in particular L-Phe and L-Trp, are the most potent PAMs at the CaSR.[44] CaSR VFT domain structures solved by X-ray crystallography suggest the fully

https://dx.doi.org/10.1021/acsptsci.1c00046
ACS Pharmacol. Transl. Sci. 2021, 4, 666−679

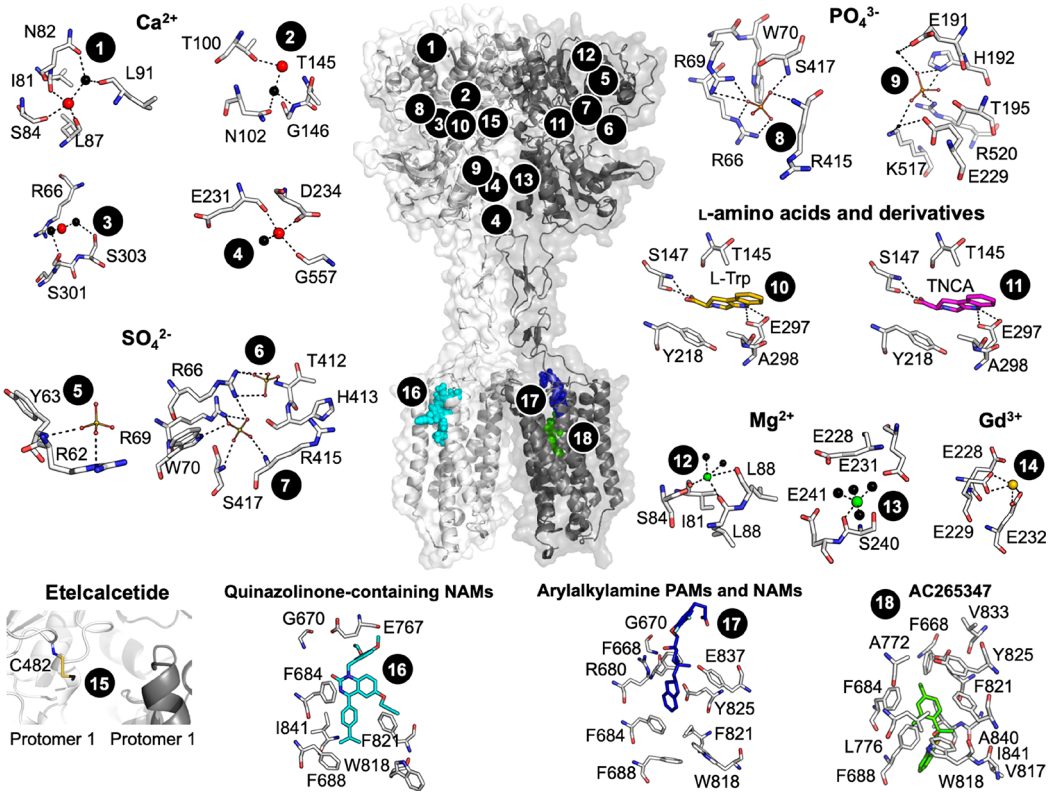

Figure 2. CaSR model and predicted ligand binding sites. The published crystal structure of the CaSR ECD (PDB 5K5S) was superimposed onto a published model of the CaSR 7TM, ECLs, and ICLs[71] based on homology with the $mGlu_5$ crystal structure (PDB 6N51). Numbers correspond to ligand binding sites predicted as follows: Ca^{2+} (sites 1−4) by anomalous scattering analysis and SO_4^{2-} (5−7), PO_4^{3-} (8−9), and L-Trp (10) by electron density distribution analysis of the crystallized ECD (PDBs 5K5S and 5K5T);[31] TNCA (11), Mg^{2+} (12−13), and Gd^{3+} (13) by electron density distribution analysis of the crystallized VFT (PDBs 5FBK and 5FBH);[33] etelcalcetide (15) from mutagenesis and mass spectrometry, where the yellow stick represents a putative disulfide bond as a rough depiction of where etelcalcetide is predicted to bind;[66] quinazolinone-containing NAMs (16), arylalkylamine PAMs and NAMs (17), and AC265347 (18) from mutagenesis combined with homology modeling and computational docking.[41,71]

active (closed) VFT conformation only exists when the cleft is occupied by an L-amino acid or similar entity.[31,33] The CaSR also responds to other positively charged endogenous ligands that interact with allosteric sites. These include polyamines such as spermine, spermidine, and putrescine.[46] Polyamines activate the CaSR in the absence of Ca^{2+}_o and are therefore agonists, but they may also act as PAMs.[46] The binding site for polyamines has not been elucidated, but it is located somewhere in the 7TM, ECLs, or ICLs.[47]

In addition to numerous endogenous activators, anions such as phosphate and sulfate, protons, or elevated osmolarity all serve to inhibit CaSR activity.[31,48−50] While anions bind in the CaSR VFT,[31] the site of action of protons is unknown.[49] These findings suggest potential clinical implications for changes in the CaSR's environment, which may occur in pathophysiological states such as alkalosis, elevated serum phosphate observed in chronic kidney disease, or increased osmolarity as occurs during dehydration. Altered levels of endogenous CaSR activators or inhibitors in different physiological or disease states may also impact discovery and validation of CaSR small molecule allosteric ligands.

EXOGENOUS ALLOSTERIC LIGANDS AND THEIR BINDING SITES

Small Molecule PAMs. Given that the endogenous ligands of the CaSR bind to a number of distinct sites in a cooperative manner, it is unsurprising that the CaSR possesses several distinct allosteric sites for exogenous molecules. The first CaSR-targeting small molecules discovered were the calcium channel blockers fendiline and prenylamine (Figure 3), which gave rise to the arylalkylamine CaSR PAMs, NPS R-467, NPS R-568, and cinacalcet (Figure 3, reviewed in ref 51). Several structurally related CaSR PAMs have since been identified, including evocalcet, calindol, and variants thereof (Figure 3). Arylalkylamine PAMs potentiate CaSR-mediated Ca^{2+}_i mobilization in recombinant cells or suppress PTH secretion from parathyroid cells in culture in the presence of physiological Ca^{2+}_o concentrations with reduced potency or affinity in the absence of Ca^{2+}_o.[52−54] However, high arylalkylamine concentrations (>1 μM) activate the CaSR in the absence of cations,[51] indicating arylalkylamines are most accurately referred to as PAM agonists. The fact that the CaSR functions in the absence of Ca^{2+}_o raises the question of whether endogenous agonists can activate the CaSR by binding to the small molecule allosteric binding site.

In the absence of a CaSR structure with a bound allosteric modulator, mutagenesis studies combined with computational docking have predicted the binding site of arylalkylamine PAMs.[41,53,55−58] Due to a lack of radiolabeled ligands, early drug discovery campaigns did not determine the affinity of CaSR PAMs; therefore, initial binding site predictions were based on the effect of mutations on PAM potency for potentiation of a single Ca^{2+}_o concentration.[55−58] However, potency changes do not discern individual effects of mutations

https://dx.doi.org/10.1021/acsptsci.1c00046
ACS Pharmacol. Transl. Sci. 2021, 4, 666−679

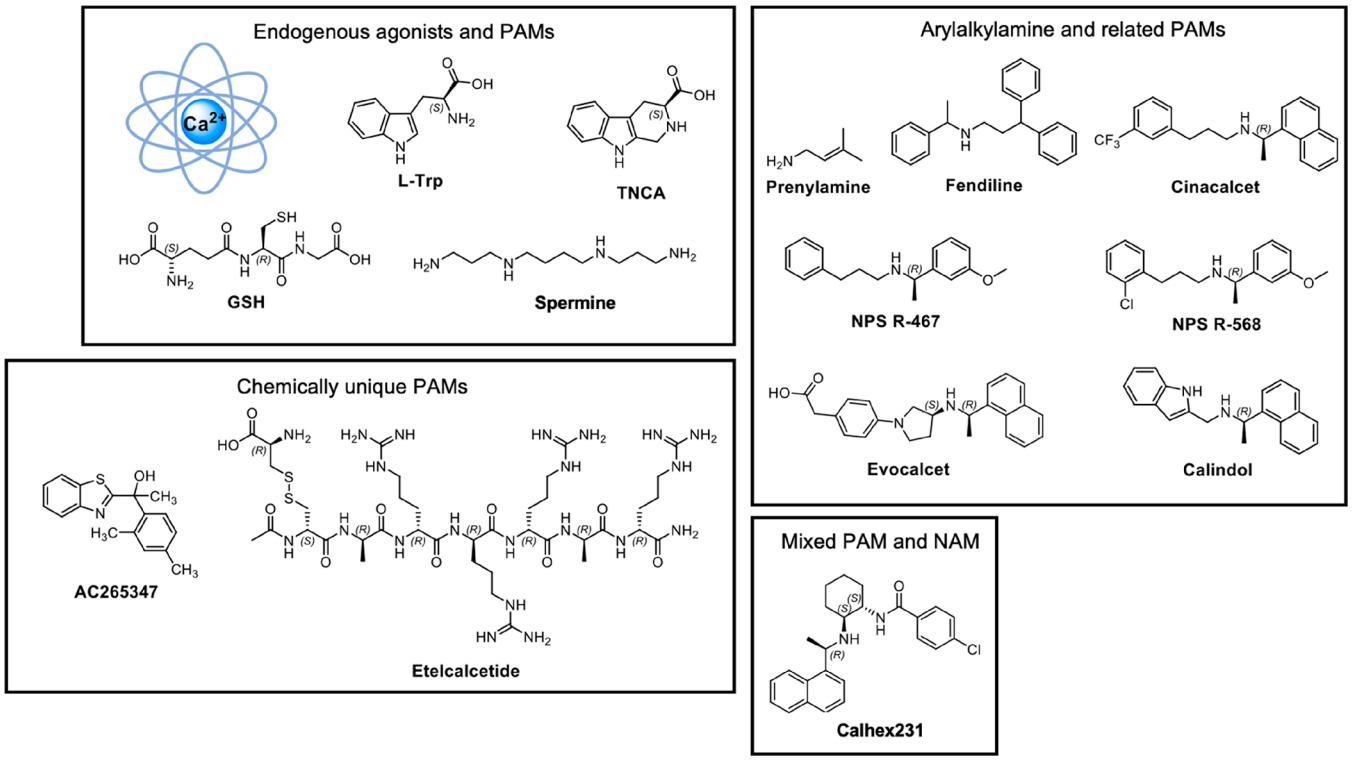

Figure 3. CaSR agonists and PAMs and their structures.

on affinity, cooperativity or efficacy. More recent studies have quantified the effect of amino acid substitutions using an operational model of allosterism[59,60] (Figure 4). Key amino

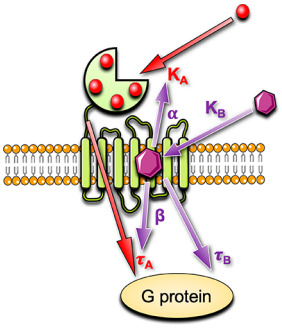

Figure 4. An operational model of allosterism to quantify CaSR agonist, PAM, and NAM actions. Endogenous CaSR agonists such as Ca^{2+}_o bind with a mean equilibrium dissociation constant, K_A, to multiple sites. When the receptor is occupied by an agonist, the agonist stimulates a response, depicted by an operational measure of efficacy, τ_A. Allosteric modulators may alter the equilibrium dissociation constant of the agonist via a cooperativity factor, α, or alter the efficacy of the orthosteric agonist via a scaling factor, β. Allosteric modulators may also have their own efficacy, τ_B.

acid residues that contribute to the affinity of arylalkylamine PAMs are located in TMs 2, 3, 5, 6, and 7 as well as ECLs 2 and 3, where numbering in superscript throughout this manuscript denotes residue positions relative to the most highly conserved residue in each TM domain across the class C GPCRs;[61] $F668^{2.56}$, $F684^{3.36}$, $F688^{3.40}$, $A772^{5.39}$, $W818^{6.50}$, $F821^{6.53}$, $Y825^{6.57}$, $E837^{7.32}$, $A840^{7.35}$, $I841^{7.36}$, $E767^{ECL2}$, and $V833^{ECL3}$.[41,53] Mapping these residues onto a homology model of the CaSR based on the metabotropic glutamate receptor subtypes 1 and 5 ($mGlu_1$ and $mGlu_5$) crystal structures revealed a large cavity that spans from the top to the middle of the 7TMs (Figure 2).[41] The arylalkylamine PAM secondary amine is protonated at physiological pH to form an ammonium salt that facilitates PAM binding by hydrogen bonding with $E837^{7.32}$ in addition to forming a strong electrostatic interaction.[41,53,55−58] The predicted 7TM binding pocket of CaSR arylalkylamine PAMs is commensurate with that observed for the binding site of a NAM cocrystallized with $mGlu_1$[62] and common across the class C GPCR family.

In 2010, Acadia Pharmaceuticals discovered benzothiazole-containing CaSR PAMs that were structurally and chemically distinct from the arylalkylamine PAMs, leading to the identification of AC265347 (Figure 3).[63,64] Like the arylalkylamines, AC265347 demonstrates agonist activity in the absence of cations, but it is a more potent agonist when compared to arylalkylamine PAMs.[54] AC265347 is also a biased CaSR allosteric modulator that preferentially enhances CaSR-mediated phosphorylation of ERK1/2 (pERK1/2) versus Ca^{2+}_i mobilization.[54] In contrast, phenylalkylamine PAMs show the reverse biased modulatory profile.[54] While AC265347 is predicted to bind within the 7TM cavity, it is unaffected by many of the mutations that reduce arylalkylamine affinity.[41,53] Importantly, AC265347 lacks an ionizable nitrogen and is therefore not predicted to form an ionic interaction with $E837^{7.32}$. Computational docking studies supported by mutagenesis suggest that AC265347 sits deeper in the 7TM bundle in comparison to the arylalkylamine PAMs[41] (Figure 2). By binding deeper within the 7TM bundle, AC265347 may stabilize distinct receptor states relative to arylalkylamine PAMs, engendering biased CaSR signaling.

The Peptide PAM, Etelcalcetide. In addition to small molecule PAMs, etelcalcetide was identified as a unique CaSR PAM, being an octapeptide comprising a linear chain of seven

https://dx.doi.org/10.1021/acsptsci.1c00046
ACS Pharmacol. Transl. Sci. 2021, 4, 666−679

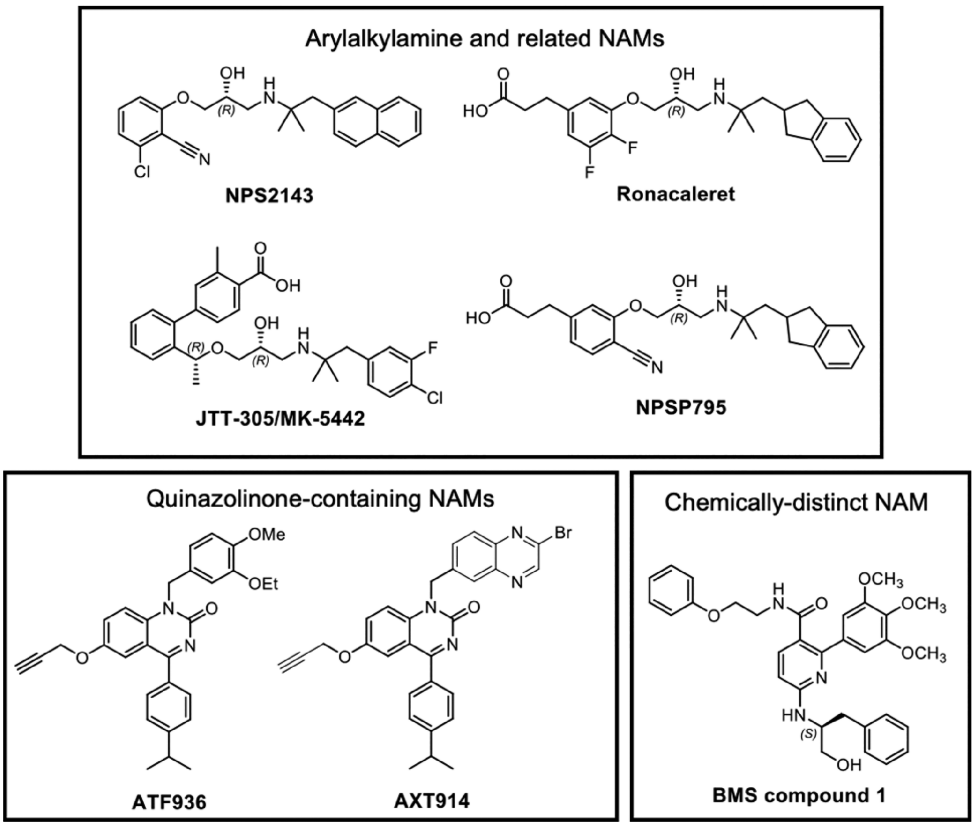

Figure 5. CaSR NAMs and their structures.

D-amino acids linked to a L-cysteine via a disulfide bond.[65] Both the C- and N-terminus are capped and the D-amino acid backbone is attached to four D-Arg residues. Etelcalcetide is predicted to bind to the CaSR VFT by forming a disulfide bond with C482 located near a "hinge" region in VFT LB1 that mediates VFT closure.[66] In the absence of Ca^{2+}_o, etelcalcetide activity in HEK293 cells is significantly decreased.[65] Nonetheless, etelcalcetide retains agonist activity in the absence of Ca^{2+}_o; therefore, it is a PAM agonist.[65] Given that etelcalcetide interacts with a unique site relative to the small molecule PAMs, etelcalcetide is likely to stabilize a distinct receptor conformation and therefore has the potential to engender biased CaSR agonism or modulation, although this remains to be determined.

CaSR NAMs. A high throughput screen and subsequent medicinal chemistry effort at NPS Pharmaceuticals and SmithKline Beecham led to the discovery of the first CaSR NAM, NPS2143 (Figure 5), which has an arylalkylamine scaffold.[67] Subsequent efforts to progress arylalkylamine NAMs clinically led to the development of several NAMs with structural and chemical similarity to NPS2143, including ronacaleret,[67,68] JTT305 (otherwise known as MK3552),[69] and NPSP795[70] (Figure 5). Arylalkylamine NAMs are predicted to bind within the same 7TM cavity as arylalkylamine PAMs, with the NAM secondary amine predicted to interact with $E837^{7.32}$ in a manner akin to the arylalkylamine PAMs.[41,71] In fact, the predicted binding pose for the arylalkylamine NAMs is very similar to the predicted pose for arylalkylamine PAMs, making it difficult to discern from computational modeling how these structurally similar PAMs and NAMs could have opposing effects on CaSR signaling. Future structural elucidation of the CaSR 7TM bound to PAMs and NAMs is needed to fully appreciate how these small molecules differentially alter CaSR structure and function.

In addition to the arylalkylamine NAMs, a screening program at Novartis identified quinazolinone-containing compounds as CaSR NAMs, which were advanced to yield ATF936 and AXT914 (Figure 5).[72,73] ATF936 has greater negative cooperativity in comparison to NPS2143, meaning that it is better at blocking CaSR activity.[71] Mutagenesis and docking studies predict the quinazolinone-containing NAMs bind in the 7TM allosteric cavity but in a distinct manner to the arylalkylamine PAMs and NAMs.[71] For instance, some mutations that reduce NPS2143 affinity have no effect on the affinity of ATF936 affinity.[71] A more detailed structural understanding of the binding of quinazolinone-containing NAMs may afford the opportunity to design NAMs with even greater affinity or cooperativity.

Intriguingly, a structurally and chemically distinct CaSR NAM, known as BMS compound 1, is predicted to bind to a second as yet unidentified allosteric site in the 7TM, ECLs, or ICLs of the CaSR.[71] Multiple allosteric binding sites within the 7TM of class C GPCRs is not unprecedented. For $mGlu_5$, several PAM chemotypes are thought to bind outside the common allosteric pocket.[74,75] Structural resolution of the BMS compound 1 binding site could provide opportunities to identify novel allosteric modulators that target this site and that may possess biased modulatory properties.

Calhex231: A Mode-Switching Allosteric Modulator. Calhex231 is structurally and chemically related to cinacalcet and the other arylalkylamine PAMs, and indeed it was discovered from an SAR study based on the PAM calindol.[76] Surprisingly, calhex231 was reported to be a NAM because it inhibited a maximally effective concentration of Ca^{2+}_o in an IP

https://dx.doi.org/10.1021/acsptsci.1c00046
ACS Pharmacol. Transl. Sci. 2021, 4, 666−679

accumulation assay.[76] Recent work, however, has revealed that calhex231 is both a PAM and a NAM depending on whether it occupies a single protomer in the CaSR dimer or both protomers.[77] The binding of calhex231 to one protomer inhibits the binding of calhex231 to the second protomer. Using an allosteric quaternary complex model, it was shown that calhex231 switches to a NAM because its negative cooperativity with itself is greater in the presence of an agonist.[77] The calhex231 binding site overlaps with the binding site for cinacalcet, NPS2143 and other arylalkylamine PAMs and NAMs.[77] The ability of calhex231, but not other PAMs and NAMs, to mode-switch is predicted to be due to a disubstituted cyclohexane ring in calhex231, which may offer more flexibility when bound to the CaSR and thus allow calhex231 to adopt at least two distinct binding poses.[77]

CLINICAL UTILITY OF CASR ALLOSTERIC MODULATORS

CaSR PAMs for Hyperparathyroidism. Given the pivotal role of the CaSR in negatively regulating PTH secretion, three CaSR PAMs are currently on the market to treat hyperparathyroidism. Hyperparathyroidism is typically caused by parathyroid adenoma or carcinoma, resulting in primary hyperparathyroidism (PHPT). Alternatively, it is secondary to chronic kidney disease, where impaired phosphate excretion and renal 1,25-dihydroxyvitamin D3 synthesis leads to decreased Ca^{2+}_o and a consequent increase in PTH synthesis and secretion as well as parathyroid hyperplasia. Cinacalcet (Sensipar) was the first CaSR-targeting drug to gain FDA approval in 2004 for hemodialysis patients with secondary hyperparathyroidism (SHPT) caused by chronic kidney disease. Cinacalcet was also the first FDA-approved GPCR allosteric modulator to reach the market. Cinacalcet has since been approved to treat hypercalcemia in adults with parathyroid carcinoma or who cannot undergo parathyroidectomy.

Cinacalcet is generally safe and well tolerated, although GI adverse events including nausea, vomiting, or loss of appetite occur in approximately 30% of patients.[78] Cinacalcet can also cause transient episodes of hypocalcaemia in some patients. Further, there is some variability in the degree to which patients respond to cinacalcet.[79] While cinacalcet responsiveness can depend on the severity of SHPT, CaSR single nucleotide polymorphisms (SNP) may influence cinacalcet efficacy. For instance, SHPT patients with an R990G SNP demonstrate higher sensitivity to cinacalcet, with a larger proportion of G990 carriers experiencing a cinacalcet-mediated suppression in PTH compared to patients with the predominant R990 allele.[80] These findings suggest that a personalized medicines approach may need to be considered when treating patients with CaSR-targeting therapies.

In 2017, etelcalcetide (Parsabiv) was approved by the FDA as an intravenous CaSR PAM for the treatment of SHPT in adults. The intravenous administration of etelcalcetide is advantageous because it can be delivered at the end of a hemodialysis session, thus ensuring patient compliance. While intravenous etelcalcetide was expected to induce fewer GI adverse events compared to oral cinacalcet, self-reported symptoms of nausea and vomiting were not significantly different between SHPT patients given etelcalcetide or cinacalcet.[81] Nonetheless, a one-year safety and efficacy trial of intravenous etelcalcetide administration revealed no major safety concerns,[82] although, like cinacalcet, etelcalcetide can cause hypocalcaemia.[83]

Recently, evocalcet (alternative names MT-4580 and KHK7580) was approved for the management of SHPT in Japanese patients that remain refractory to cinacalcet treatment because adverse GI events prevent cinacalcet dose escalation. Evocalcet has higher bioavailability in comparison to cinacalcet, and lower doses are therefore required to suppress serum PTH levels.[84] In rats, evocalcet suppresses PTH secretion while having no significant effect on gastric emptying, which is delayed in cinacalcet-treated rats and patients.[84] Evocalcet also had a reduced incidence of vomiting in marmosets.[84,85] In humans, evocalcet offers good short-term tolerability in terms of upper GI symptoms while still providing therapeutic efficacy similarly to cinacalcet.[86] However, while the severity of GI side effects is reduced compared to cinacalcet,[83] approximately 19% of evocalcet-treated patients still experience nausea and vomiting compared to 33% of patients treated with cinacalcet.[78] Evocalcet also causes hypocalcaemia in some patients.[83] Thus, while all three clinically approved CaSR PAMs are effective at reducing PTH levels in hyperparathyroidism, the risk of hypocalcaemia and incidence of GI side effects limits their use in the clinic.[83] There is still therefore a need for novel PAMs with reduced adverse effects.

PAMs for Hypercalcaemia. The importance of the CaSR in Ca^{2+}_o homeostasis is highlighted by the many naturally occurring mutations in the *CASR* gene or in genes encoding $G\alpha_{11}$ (*GNA11*), which mediates CaSR signal transduction, or adapter protein 2 sigma subunit 1 (*AP2S1*), which regulates CaSR cell surface expression. Inactivating mutations in these proteins cause familial hypocalciuric hypercalcaemia types 1 to 3 (FHH1−3) or neonatal severe primary hyperparathyroidism (NSHPT).

FHH1 (the most common form of FHH at 1 per 1350 people[87]) and NSHPT are caused by inactivating *CASR* mutations. These mutations reduce CaSR sensitivity to Ca^{2+}_o or impair the biosynthesis and post-translational processing of the CaSR within the endoplasmic reticulum or Golgi apparatus, leading to CaSR misfolding and impaired cell surface expression.[88,89] Furthermore, some mutations alter CaSR coupling to signaling pathways to the relative exclusion of others.[90] FHH1 is characterized by mild or moderate elevations of serum calcium and magnesium with mildly elevated or normal PTH levels. While FHH1 patients are often asymptomatic, up to 30% of patients experience symptomatic hypercalcaemia, whereas others develop chondrocalcinosis, acute pancreatitis, and gallstones.[91] Importantly, FHH1-causing mutations increase the risk of numerous diseases, most notably cardiovascular, neurodegenerative, and psychiatric diseases.[87] These findings suggest that it may be appropriate to treat FHH1 even in asymptomatic patients. Further, the much rarer but more severe disorder, NSHPT, is characterized by life-threatening hypercalcaemia, skeletal under-mineralization and deformities, and death if left untreated.[91] It is therefore essential that infants diagnosed with NSHPT are treated. Increasingly, cinacalcet has shown some success in treating NHSPT in addition to complications related to FHH1 in patients harboring loss-of-function or loss-of-expression CaSR mutations.[92−98] There are, however, increasing reports of NSHPT patients who do not respond adequately to cinacalcet, in some cases due to homozygous mutations that result in truncation of the CaSR before the 7TM cinacalcet binding site.[99,100] Cinacalcet-unresponsive patients may also harbor missense mutations or in-frame

https://dx.doi.org/10.1021/acsptsci.1c00046
ACS Pharmacol. Transl. Sci. 2021, 4, 666−679

deletions that result in expression of a full-length CaSR with single amino acid mutations or a shortened CaSR in which exon 5, encoding amino acids 476−536 in the ECD, is deleted.[101−103] In these instances, cinacalcet may be ineffective because the mutation may reduce cinacalcet affinity or its ability to potentiate Ca^{2+}_o by decreasing allosteric cooperativity. In cases of severe mutation-induced receptor impairment, the mutation may render cinacalcet unable to sufficiently restore receptor function even if affinity or cooperativity are unaffected.[104] Interestingly, compared to cinacalcet, AC265347 was more effective at potentiating Ca^{2+}_o-mediated signaling responses at some FHH1/NSHPT-causing CaSR mutants, suggesting that alternative PAMs may be better than cinacalcet at rescuing inactivating CaSR mutants.[64] However, as AC265347 is not approved clinically, total parathyroidectomy is currently required to normalize serum PTH levels in patients who do not respond to current pharmacological interventions.

Four *GNA11* mutations have been identified in FHH2-affected individuals (FHH2 is the least common form of FHH), which are predicted to impair guanine nucleotide binding or disrupt G protein activation of intracellular signaling proteins such as PLC.[91,105] FHH2 patients typically have mild hypercalcaemia and normal serum concentrations of PTH.[105] In recombinant cells expressing FHH2-causing *GNA11* mutations, cinacalcet restored impaired CaSR signaling.[106] Similarly, in mice with a germline loss-of-function *GNA11* mutation, cinacalcet corrected hypercalcaemia and reduced elevated serum PTH concentrations.[107] Cinacalcet also normalized serum calcium concentrations in a FHH2 patient with hypercalcaemia.[108] These studies suggest that cinacalcet stabilizes a CaSR conformation that couples more favorably to G_{11}, thus overcoming mutations that impair G_{11} function. However, given the typically asymptomatic nature of FHH2, there is no clear benefit in treating most FHH2 patients with pharmacological interventions.

Four missense *AP2S1* mutations that cause FHH3 have been identified.[109−111] FHH3-causing mutations disrupt AP2σ-mediated CaSR endocytosis and consequently impair CaSR signaling from endosomes.[105,112] FHH3 is the most severe form of FHH and is more commonly characterized by symptomatic hypercalcaemia.[109,113] FHH3 may also be associated with recurrent pancreatitis and cognitive dysfunction.[114] Cinacalcet corrected impaired CaSR signaling resulting from FHH3-causing *AP2S1* mutations and rectified symptomatic hypercalcaemia in three FHH3 patients.[115] The molecular mechanisms by which cinacalcet corrects mutation-induced impairments in AP2σ-mediated CaSR internalization are not known, but there are several possibilities. Cinacalcet may simply stabilize a CaSR conformation that interacts more favorably with AP2σ, thus restoring CaSR internalization and trafficking to endosomes. Alternatively, by crossing the cell membrane, cinacalcet may potentiate the activity of CaSRs already localized to endosomes. Regardless, these findings demonstrate that CaSR PAMs such as cinacalcet may be useful in the management of FHH3.

NAMs for Osteoporosis. The first manifestation of osteoporosis is typically a fracture.[116] Therefore, treatments are aimed at preventing further bone loss, such as with the use of bisphosphonates (e.g., alendronate), or restoring bone mass and density with recombinant human PTH(1−34) (rhPTH(1−34) or rhPTH(1−84)), which have anabolic actions by increasing the number of bone-forming osteoblasts.[117] However, rhPTH(1−34) has received a black box warning label in the United States because high doses induced osteosarcoma in long-term carcinogenicity studies in rats.[118] Further, rhPTH requires daily subcutaneous administration, and an orally active anabolic compound therefore continues to be of interest. Small molecule CaSR NAMs were consequently developed as potential orally available therapeutics for osteoporosis because they stimulate the release of endogenous PTH by mimicking a drop in Ca^{2+}_o levels.

NPS2143 was the first CaSR NAM to be evaluated in an ovariectomized rat model of postmenopausal osteoporosis. However, following 5 weeks of daily NPS2143 administration, no net increase in bone mass and density was observed.[67,119,120] The high volume of NPS2143 distribution resulted in prolonged NPS2143 exposure and sustained elevations in PTH levels, in contrast to plasma levels of rhPTH(1−34), which reached a comparable maximum concentration but returned to baseline much more rapidly. It was soon realized that CaSR NAMs would best exert an anabolic effect if they had a short half-life to ensure transient stimulation of PTH release that promptly returned to basal levels. This is because prolonged exposure to PTH mimics hyperparathyroidism, thus stimulating bone resorption at the expense of bone formation.[121]

Ronacaleret was the second CaSR NAM to be evaluated in osteoporosis. While ronacaleret is structurally similar to NPS2143, it is more metabolically labile.[122,123] However, a clinical trial in postmenopausal women given ronacaleret for 12 months demonstrated only a modest increase in bone mass and density of the lumbar spine compared to large increases seen in patients receiving rhPTH(1−34) or alendronate, while hip, femoral neck, and trochanter bone mass and density was decreased in the ronacaleret-treated group.[124] Similarly, in a phase 2 clinical trial in postmenopausal women treated with JTT305 for 6 months, no significant increase in bone mass and density was observed over placebo, despite evidence of an increase in markers of bone formation.[125] A clinical trial of AXT914 was also terminated early due to a lack of effect of AXT914 on bone formation markers and a dose-limiting increase in serum calcium after four weeks of treatment.[126]

The reasons why CaSR NAMs do not stimulate bone formation are not fully understood but may be linked to on-target CaSR effects in cells and tissues outside the parathyroid gland. For instance, CaSR NAMs may inhibit the important function of the CaSR in bone-forming osteoblasts, thus counteracting the effects of transient PTH release. Further, while the pharmacokinetic profiles of ronacaleret, JTT305, and AXT914 were more favorable than NPS2143, NAM-mediated elevations in serum PTH concentrations remained above baseline in humans for more than 3.5 h,[124−126] whereas levels of rhPTH return to baseline rapidly following rhPTH injection.[127] Prolonged PTH release was more apparent at higher NAM doses that were cleared less rapidly. The design of NAMs that can be administered at lower doses, such as those with greater affinity or cooperativity, could help to overcome this issue. Regardless of the reasons for CaSR NAM failures in the clinic, the development of NAMs for osteoporosis has been discontinued, and efforts have instead focused on repurposing CaSR NAMs for alternative disorders.

NAMs for ADH and Bartter Syndrome V. Recent interest has been garnered in repurposing CaSR NAMs for heterozygous activating mutations in the *CASR* or *GNA11* genes, which cause autosomal dominant hypocalcaemia type 1 (ADH1; caused by *CASR* mutations), Bartter syndrome V

https://dx.doi.org/10.1021/acsptsci.1c00046
ACS Pharmacol. Transl. Sci. 2021, 4, 666−679

(*CASR* mutations), or ADH2 (*GNA11* mutations). ADH is characterized by a mild or moderate decrease in serum calcium and PTH concentrations.[91] Many ADH sufferers experience symptomatic hypocalcaemia, which may include tingling and painful muscular spasms in the hands and feet as well as seizures. Some ADH1 patients also suffer from calcifications in the kidneys and basal ganglia or elevated bone mineral density.[91] In more severe cases, gain-of-function *CASR* mutations promote renal loss of sodium, potassium, magnesium, and chloride ions and consequent hypokalaemic alkalosis and hyperreninaemic hyperaldosteronism, a condition called Bartter syndrome V.[91] The prevalence of ADH1 is approximately 1 per 25 000.[87] Currently, over 90 different CaSR mutations have been linked to ADH1. Among them, over 95% are missense mutations, with the remaining 5% represented by frameshift or in-frame insertion and deletion mutations.[128] ADH2 is rarer and has been associated with six different activating missense *GNA11* mutations. ADH2-causing mutations are located at the interface between the helical and GTPase domains of the $G\alpha_{11}$ protein and involved in GDP-GTP exchange or located at the $G\alpha_{11}$ carboxyl terminal, which is involved in receptor coupling.[129,130] CaSR NAMs are a viable therapeutic strategy for reducing hyper-function caused by gain-of-function mutations in both the CaSR and $G\alpha_{11}$.

Promisingly, NPS2143 can normalize signaling responses associated with ADH-causing *CASR* and *GNA11* mutations *in vitro*[104,106,131,132] as well as increase $Ca^{2+}{}_o$ and PTH concentrations in ADH1 and ADH2 mouse models[131,133,134] and prevent nephrocalcinosis in an ADH1 mouse model.[135] However, NPS2143 is less effective, at least *in vitro*, at rectifying gain-of-function *CASR* mutations that cause Bartter syndrome V.[104,132] In contrast, quinazolinone-derived NAMs (e.g., AXT914 and ATF936) can better rectify Bartter syndrome V mutations *in vitro*[136] and may represent a class of NAMs with lower propensity to be affected by pharmacogenetic effects compared to arylalkylamine-derived NAMs like NPS2143.

Although originally developed for osteoporosis, the arylalkylamine-derived NAM, NPSP795, entered phase II clinical trials for the treatment of ADH1. NPSP795 robustly increased PTH in 3 out of 5 ADH1 trial patients and caused a small reduction in renal Ca^{2+} excretion. However, NPSP795 had no significant effect on serum $Ca^{2+}{}_o$ levels and had variable effects on PTH.[137] The high variability in NPSP795 efficacy may in part be attributable to the underlying disease-causing mutations. Some ADH1 mutations are in close proximity to the common 7TM allosteric binding site, or NPSP795 may not have sufficient affinity or cooperativity to overcome some mutation-induced enhancement in CaSR signaling.[41,104] However, pharmacogenetic effects do not completely explain interpatient variation in the efficacy of NPSP795. For instance, two patients in the study carried the same mutation (A840 V). A840 V faces into the 7TM binding cavity and contributes to the binding of the arylalkylamine NAM, NPS2143.[41] However, while serum PTH levels were robustly increased in one A840 V-harboring patient, NPSP795 had only a modest effect on PTH levels in the other, despite similar NPSP795 concentrations being reached in both patients. It therefore remains to be determined why some ADH1 patients may respond to CaSR NAMs, while others do not.

NAMs for Asthma. Asthma affects ∼340 million people worldwide, posing significant health risks particularly to approximately 10% of asthmatics whose asthma is poorly controlled with current drugs. The efficacy of asthma medications, which include β_2 adrenergic receptor agonists and corticosteroids, is further limited by acute exacerbations typically caused by respiratory virus infections or environmental pollutants.[138] Identifying novel treatments for poorly controlled asthma is therefore a key health priority.

Recently, the CaSR was identified as a putative therapeutic target in asthma. The CaSR is expressed in bronchial smooth muscle and the epithelium.[15] CaSR expression is upregulated in human bronchial biopsies from asthmatics, in murine asthma models, and in human airway smooth muscle cells exposed to asthma-associated cytokines,[15] presumably via STAT and κB response elements in the *CASR* gene promoters. Further, CaSR agonists such as polyamines are established mediators of airway inflammation, remodelling, and constriction;[139−146] polyamine concentrations are elevated in the sputum or blood of human asthmatics and in murine models of allergic airways disease.[141,143,147] While spermine potentiated airway smooth muscle contraction induced by acetylcholine, this effect was diminished in mice with selective CaSR ablation in airway smooth muscle cells.[15] These findings were consistent with observations that the CaSR NAM, NPS2143, attenuated $Ca^{2+}{}_i$ release in human airway smooth muscle cells in response to acetylcholine or histamine,[15] suggesting potential benefit in opposing CaSR signaling in asthma.

In murine models of allergic airways disease, chronic treatment with CaSR NAMs attenuated airway inflammation, fibrosis, and airway hyper-responsiveness (AHR) to the muscarinic acetylcholine receptor agonist, methacholine.[15,148,149] The CaSR NAM, NPS2143, also decreased immune cell counts in mouse bronchoalveolar lavage fluid (BALF) following allergen challenge[15] or lipopolysaccharide (LPS)-induced lung injury,[148] and suppressed serum and BALF cytokine levels.[148] The latter effects of *in vivo* treatment with NPS2143 are consistent with the established role of the CaSR in promoting pro-inflammatory cytokine release from T cells,[150] macrophages,[151,152] and airway epithelial cells *in vitro*.[148] More recent findings demonstrated that the NAMs ronacaleret, JTT-305, NPSP795, and AXT914 all reduced airway inflammation and prevented goblet cell hyperplasia in a chronic airway inflammation model.[153] Taken together, the potential benefits of CaSR NAMs in directly reducing aberrant airway smooth muscle $Ca^{2+}{}_i$ signaling and contraction as well as attenuating airway inflammation, remodelling, and inhibiting AHR in chronic disease models suggest the CaSR may be a novel therapeutic target in asthma.

CONCLUSIONS

The CaSR is a multimodal chemosensor that responds to diverse exogenous and endogenous stimuli via multiple allosteric binding sites. While great efforts have been made to therapeutically target the CaSR, to date, only CaSR PAMs have reached the clinic. Despite CaSR NAMs demonstrating promise as treatments for ADH, the reasons for the potential interpatient variability in responsiveness to NAMs need to be established to progress development of such compounds. Thus, much can still be learned about how CaSR NAMs bind to the receptor and how naturally occurring mutations alter the binding and function of the NAMs. A better identification of the CaSR's many allosteric binding sites may enable drug discovery efforts that target novel CaSR binding sites with potential to identify distinct chemotypes of allosteric modulators with unique pharmacological properties.

https://dx.doi.org/10.1021/acsptsci.1c00046
ACS Pharmacol. Transl. Sci. 2021, 4, 666−679

AUTHOR INFORMATION

Corresponding Author

Katie Leach − *Drug Discovery Biology, Monash Institute of Pharmaceutical Sciences, Monash University, Parkville, Victoria 3052, Australia; Department of Pharmacology, Biomedicine Discovery Institute, Monash University, Clayton, Victoria 3800, Australia;* orcid.org/0000-0002-9280-1803; Email: katie.leach@monash.edu

Authors

Jiayin Diao − *Drug Discovery Biology, Monash Institute of Pharmaceutical Sciences, Monash University, Parkville, Victoria 3052, Australia*

Aaron DeBono − *Drug Discovery Biology and Medicinal Chemistry, Monash Institute of Pharmaceutical Sciences, Monash University, Parkville, Victoria 3052, Australia*

Tracy M. Josephs − *Drug Discovery Biology, Monash Institute of Pharmaceutical Sciences, Monash University, Parkville, Victoria 3052, Australia;* orcid.org/0000-0002-7799-3683

Jane E. Bourke − *Department of Pharmacology, Biomedicine Discovery Institute, Monash University, Clayton, Victoria 3800, Australia*

Ben Capuano − *Medicinal Chemistry, Monash Institute of Pharmaceutical Sciences, Monash University, Parkville, Victoria 3052, Australia;* orcid.org/0000-0001-5434-0180

Karen J. Gregory − *Drug Discovery Biology, Monash Institute of Pharmaceutical Sciences, Monash University, Parkville, Victoria 3052, Australia; Department of Pharmacology, Biomedicine Discovery Institute, Monash University, Clayton, Victoria 3800, Australia;* orcid.org/0000-0002-3833-2137

Complete contact information is available at: https://pubs.acs.org/10.1021/acsptsci.1c00046

Notes

The authors declare no competing financial interest.

REFERENCES

(1) Leach, K., Hannan, F. M., Josephs, T. M., Keller, A. N., Møller, T. C., Ward, D. T., Kallay, E., Mason, R. S., Thakker, R. V., Riccardi, D., Conigrave, A. D., and Bräuner-Osborne, H. (2020) International Union of Basic and Clinical Pharmacology. CVIII. Calcium-sensing receptor nomenclature, pharmacology, and function. *Pharmacol. Rev. 72*, 558−604.

(2) Kantham, L., Quinn, S. J., Egbuna, O. I., Baxi, K., Butters, R., Pang, J. L., Pollak, M. R., Goltzman, D., and Brown, E. M. (2009) The calcium-sensing receptor (CaSR) defends against hypercalcemia independently of its regulation of parathyroid hormone secretion. *Am. J. Physiol. 297*, E915−923.

(3) Dvorak, M. M., Siddiqua, A., Ward, D. T., Carter, D. H., Dallas, S. L., Nemeth, E. F., and Riccardi, D. (2004) Physiological changes in extracellular calcium concentration directly control osteoblast function in the absence of calciotropic hormones. *Proc. Natl. Acad. Sci. U. S. A. 101*, 5140−5145.

(4) Diepenhorst, N. A., Leach, K., Keller, A. N., Rueda, P., Cook, A. E., Pierce, T. L., Nowell, C., Pastoureau, P., Sabatini, M., Summers, R. J., Charman, W. N., Sexton, P. M., Christopoulos, A., and Langmead, C. J. (2018) Divergent effects of strontium and calcium-sensing receptor positive allosteric modulators (calcimimetics) on human osteoclast activity. *Br. J. Pharmacol. 175*, 4095−4108.

(5) Chang, W., Tu, C., Chen, T. H., Bikle, D., and Shoback, D. (2008) The extracellular calcium-sensing receptor (CaSR) is a critical modulator of skeletal development. *Sci. Signal 1*, ra1.

(6) VanHouten, J., Dann, P., McGeoch, G., Brown, E. M., Krapcho, K., Neville, M., and Wysolmerski, J. J. (2004) The calcium-sensing receptor regulates mammary gland parathyroid hormone-related protein production and calcium transport. *J. Clin. Invest. 113*, 598−608.

(7) Ardeshirpour, L., Dann, P., Pollak, M., Wysolmerski, J., and VanHouten, J. (2006) The calcium-sensing receptor regulates PTHrP production and calcium transport in the lactating mammary gland. *Bone 38*, 787−793.

(8) Ohsu, T., Amino, Y., Nagasaki, H., Yamanaka, T., Takeshita, S., Hatanaka, T., Maruyama, Y., Miyamura, N., and Eto, Y. (2010) Involvement of the calcium-sensing receptor in human taste perception. *J. Biol. Chem. 285*, 1016−1022.

(9) Cheng, S. X., Lightfoot, Y. L., Yang, T., Zadeh, M., Tang, L., Sahay, B., Wang, G. P., Owen, J. L., and Mohamadzadeh, M. (2014) Epithelial CaSR deficiency alters intestinal integrity and promotes proinflammatory immune responses. *FEBS Lett. 588*, 4158−4166.

(10) Alamshah, A., Spreckley, E., Norton, M., Kinsey-Jones, J. S., Amin, A., Ramgulam, A., Cao, Y., Johnson, R., Saleh, K., Akalestou, E., Malik, Z., Gonzalez-Abuin, N., Jomard, A., Amarsi, R., Moolla, A., Sargent, P. R., Gray, G. W., Bloom, S. R., and Murphy, K. G. (2017) l-phenylalanine modulates gut hormone release and glucose tolerance, and suppresses food intake through the calcium-sensing receptor in rodents. *Int. J. Obes. 41*, 1693−1701.

(11) Engelstoft, M. S., Park, W. M., Sakata, I., Kristensen, L. V., Husted, A. S., Osborne-Lawrence, S., Piper, P. K., Walker, A. K., Pedersen, M. H., Nohr, M. K., Pan, J., Sinz, C. J., Carrington, P. E., Akiyama, T. E., Jones, R. M., Tang, C., Ahmed, K., Offermanns, S., Egerod, K. L., Zigman, J. M., and Schwartz, T. W. (2013) Seven transmembrane G protein-coupled receptor repertoire of gastric ghrelin cells. *Mol. Metab. 2*, 376−392.

(12) Babinsky, V. N., Hannan, F. M., Ramracheya, R. D., Zhang, Q., Nesbit, M. A., Hugill, A., Bentley, L., Hough, T. A., Joynson, E., Stewart, M., Aggarwal, A., Prinz-Wohlgenannt, M., Gorvin, C. M., Kallay, E., Wells, S., Cox, R. D., Richards, D., Rorsman, P., and Thakker, R. V. (2017) Mutant mice with calcium-sensing receptor activation have hyperglycemia that is rectified by calcilytic therapy. *Endocrinology 158*, 2486−2502.

(13) Schepelmann, M., Yarova, P. L., Lopez-Fernandez, I., Davies, T. S., Brennan, S. C., Edwards, P. J., Aggarwal, A., Graca, J., Rietdorf, K., Matchkov, V., Fenton, R. A., Chang, W., Krssak, M., Stewart, A., Broadley, K. J., Ward, D. T., Price, S. A., Edwards, D. H., Kemp, P. J., and Riccardi, D. (2016) The vascular Ca2+-sensing receptor regulates blood vessel tone and blood pressure. *Am. J. Physiol. 310*, C193−204.

(14) Tu, C. L., Crumrine, D. A., Man, M. Q., Chang, W., Elalieh, H., You, M., Elias, P. M., and Bikle, D. D. (2012) Ablation of the calcium-sensing receptor in keratinocytes impairs epidermal differentiation and barrier function. *J. Invest. Dermatol. 132*, 2350−2359.

(15) Yarova, P. L., Stewart, A. L., Sathish, V., Britt, R. D. J., Thompson, M. A. P., Lowe, A., Freeman, M., Aravamudan, B., Kita, H., Brennan, S. C., Schepelmann, M., Davies, T., Yung, S., Cholisoh, Z., Kidd, E. J., Ford, W. R., Broadley, K. J., Rietdorf, K., Chang, W., Bin Khayat, M. E., Ward, D. T., Corrigan, C. J. T., Ward, J., Kemp, P. J., Pabelick, C. M., Prakash, Y. S., and Riccardi, D. (2015) Calcium-sensing receptor antagonists abrogate airway hyperresponsiveness and inflammation in allergic asthma. *Sci. Transl Med. 7*, 284ra260.

(16) Hendy, G. N., and Canaff, L. (2016) Calcium-sensing receptor, proinflammatory cytokines and calcium homeostasis. *Semin. Cell Dev. Biol. 49*, 37−43.

(17) Hendy, G. N., and Canaff, L. (2016) Calcium-sensing receptor gene: regulation of expression. *Front Physiol 7*, 394.

(18) Chang, W., Pratt, S., Chen, T. H., Nemeth, E., Huang, Z., and Shoback, D. (1998) Coupling of calcium receptors to inositol phosphate and cyclic AMP generation in mammalian cells and Xenopus laevis oocytes and immunodetection of receptor protein by region-specific antipeptide antisera. *J. Bone Miner. Res. 13*, 570−580.

(19) Fajtova, V. T., Quinn, S. J., and Brown, E. M. (1991) Cytosolic calcium responses of single rMTC 44-2 cells to stimulation with external calcium and potassium. *Am. J. Physiol. 261*, E151−158.

(20) McGehee, D. S., Aldersberg, M., Liu, K., Hsuing, S., Heath, M. J. S., and Tamir, H. (1997) Mechanism of extracellular Ca2+ receptor-stimulated hormone release from sheep thyroid parafollicular cells. *J. Physiol. 502*, 31−44.
(21) Muff, R., Nemeth, E. F., Haller-Brem, S., and Fischer, J. A. (1988) Regulation of hormone secretion and cytosolic Ca2+ by extracellular Ca2+ in parathyroid cells and C-cells: role of voltage-sensitive Ca2+ channels. *Arch. Biochem. Biophys. 265*, 128−135.
(22) Ogata, S., Kubota, Y., Satoh, S., Ito, S., Takeuchi, H., Ashizuka, M., and Shirasuna, K. (2006) Ca2+ stimulates COX-2 expression through calcium-sensing receptor in fibroblasts. *Biochem. Biophys. Res. Commun. 351*, 808−814.
(23) Kifor, O., Macleod, R. J., Diaz, R., Bai, M., Yamanguchi, T., Yao, T., Kifor, I., and Brown, E. M. (2001) Regulation of MAP kinase by calcium-sensing receptor in bovine parathyroid and CaR-transfected HEK293 cells. *Am. J. Physiol. 280*, F291−F302.
(24) MacLeod, R. J., Yano, S., Chattopadhyay, N., and Brown, E. M. (2004) Extracellular calcium-sensing receptor transactivates the epidermal growth factor receptor by a triple-membrane-spanning signaling mechanism. *Biochem. Biophys. Res. Commun. 320*, 455−460.
(25) Thomsen, A. R., Hvidtfeldt, M., and Brauner-Osborne, H. (2012) Biased agonism of the calcium-sensing receptor. *Cell Calcium 51*, 107−116.
(26) Huang, C., Hujer, K. M., Wu, Z., and Miller, R. T. (2004) The Ca^{2+}-sensing receptor couples to $G\alpha_{12/13}$ to activate phospholipas D in Madin-Darby canine kidney cells. *Am. J. Physiol. 286*, C22−C30.
(27) Mamillapalli, R., VanHouten, J., Zawalich, W., and Wysolmerski, J. (2008) Switching of G-protein Usage by the Calcium-sensing Receptor Reverses Its Effect on Parathyroid Hormone-related Protein Secretion in Normal Versus Malignant Breast Cells. *J. Biol. Chem. 283*, 24435−24447.
(28) Mamillapalli, R., and Wysolmerski, J. (2010) The calcium-sensing receptor couples to Galpha(s) and regulates PTHrP and ACTH secretion in pituitary cells. *J. Endocrinol. 204*, 287−297.
(29) Kienitz, M. C., Niemeyer, A., Konig, G. M., Kostenis, E., Pott, L., and Rinne, A. (2019) Biased signaling of Ca(2+)-sensing receptors in cardiac myocytes regulates GIRK channel activity. *J. Mol. Cell. Cardiol. 130*, 107−121.
(30) Thomsen, A. R., Worm, J., Jacobsen, S. E., Stahlhut, M., Latta, M., and Brauner-Osborne, H. (2012) Strontium is a biased agonist of the calcium-sensing receptor in rat medullary thyroid carcinoma 6−23 cells. *J. Pharmacol. Exp. Ther. 343*, 638−649.
(31) Geng, Y., Mosyak, L., Kurinov, I., Zuo, H., Sturchler, E., Cheung, C. T., Subramanyam, P., Brown, A. P., Brennan, S. C., Mun, H. C., Bush, M., Chen, Y., Nguyen, T. X., Cao, B., Chang, D. D., Quick, M., Conigrave, A. D., Colecraft, H. M., McDonald, P., and Fan, Q. R. (2016) Structural mechanism of ligand activation in human calcium-sensing receptor. *eLife*, 5 DOI: 10.7554/eLife.13662.
(32) Jiang, Y., Minet, E., Zhang, Z., Silver, P. A., and Bai, M. (2004) Modulation of interprotomer relationships is important for activation of dimeric calcium-sensing receptor. *J. Biol. Chem. 279*, 14147−14156.
(33) Zhang, C., Zhang, T., Zou, J., Miller, C. L., Gorkhali, R., Yang, J., Schilmiller, A., Wang, S., Huang, K., Brown, E. M., Moremen, K. W., Hu, J., and Yang, J. J. (2016) Structural basis for regulation of human calcium-sensing receptor by magnesium ions and an unexpected tryptophan derivative co-agonist. *Sci. Adv. 2*, e1600241.
(34) Ray, K., Ghosh, S. P., and Northup, J. K. (2004) The Role of Cysteines and Charged Amino Acids in Extracellular Loops of the Human Ca2+ Receptor in Cell Surface Expression and Receptor Activation Processes. *Endocrinology 145*, 3892−3903.
(35) Ray, K., Fan, G., Goldsmith, P. K., and Spiegel, A. M. (1997) The carboxyl terminus of the human calcium receptor. Requirements for cell-surface expression and signal transduction. *J. Biol. Chem. 272*, 31355−31361.
(36) Chang, W., Pratt, S., Chen, T., Bourguignon, L., and Shoback, D. (2001) Amino acids in the cytoplasmic C terminus of the parathyroid Ca2+-sensing receptor mediate efficient cell-surface expression and phospholipase c activation. *J. Biol. Chem. 276*, 44129−44136.
(37) Hjälm, G., MacLeod, R. J., Kifor, O., Chattopadhyay, N., and Brown, E. M. (2001) Filamin-A binds to the carboxyl-terminal tail of the calcium-sensing receptor, an interaction that participates in CaR-mediated activation of mitogen-activated protein kinase. *J. Biol. Chem. 276*, 34880−34887.
(38) Bai, M., Trivedi, S., Lane, C. R., Yang, Y., Quinn, S., and Brown, E. M. (1998) Protein kinase C phosphorylation of threonine at position 888 in Ca^{2+o}-sensing receptor stably expressed in HEK293 cells. *Am. J. Physiol. 292*, 1895−1905.
(39) Binmahfouz, L. S., Centeno, P. P., Conigrave, A. D., and Ward, D. T. (2019) Identification of serine-875 as an inhibitory phosphorylation site in the calcium-sensing receptor. *Mol. Pharmacol. 96*, 204−211.
(40) Huang, Y., Zhou, Y., Castiblanco, A., Yang, W., Brown, E. M., and Yang, J. J. (2009) Multiple Ca(2+)-binding sites in the extracellular domain of the Ca(2+)-sensing receptor corresponding to cooperative Ca(2+) response. *Biochemistry 48*, 388−398.
(41) Leach, K., Gregory, K. J., Kufareva, I., Khajehali, E., Cook, A. E., Abagyan, R., Conigrave, A. D., Sexton, P. M., and Christopoulos, A. (2016) Towards a structural understanding of allosteric drugs at the human calcium-sensing receptor. *Cell Res. 26*, 574−592.
(42) Handlogten, M. E., Shiraishi, N., Awata, H., Huang, C., and Miller, R. T. (2000) Extracellular Ca(2+)-sensing receptor is a promiscuous divalent cation sensor that responds to lead. *Am. J. Physiol. 279*, F1083−1091.
(43) Brown, E. M., Fuleihan, G. e.-H., Chen, C. J., and Kifor, O. (1990) A comparison of the effects of divalent and trivalent cations on parathyroid hormone release, 3′,5′-cyclic-adenosine monophosphate accumulation, and the levels of inositol phosphates in bovine parathyroid cells. *Endocrinology 127*, 1064−1071.
(44) Conigrave, A. D., Quinn, S. J., and Brown, E. M. (2000) L-Amino acid sensing by the extracellular Ca2+-sensing receptor. *Proc. Natl. Acad. Sci. U. S. A. 97*, 4814−4819.
(45) Broadhead, G. K., Mun, H. C., Avlani, V. A., Jourdon, O., Church, W. B., Christopoulos, A., Delbridge, L., and Conigrave, A. D. (2011) Allosteric modulation of the calcium-sensing receptor by gamma-glutamyl peptides: inhibition of PTH secretion, suppression of intracellular cAMP levels, and a common mechanism of action with L-amino acids. *J. Biol. Chem. 286*, 8786−8797.
(46) Quinn, S. J., Ye, C. P., Diaz, R., Kifor, O., Bai, M., Vassilev, P., and Brown, E. (1997) The Ca2+-sensing receptor: a target for polyamines. *Am. J. Physiol. 273*, C1315−1323.
(47) Ray, K., and Northup, J. (2002) Evidence for distinct cation and calcimimetic compound (NPS 568) recognition domains in the transmembrane regions of the human Ca2+ receptor. *J. Biol. Chem. 277*, 18908−18913.
(48) Quinn, S. J., Bai, M., and Brown, E. M. (2004) pH Sensing by the calcium-sensing receptor. *J. Biol. Chem. 279*, 37241−37249.
(49) Campion, K. L., McCormick, W. D., Warwicker, J., Khayat, M. E., Atkinson-Dell, R., Steward, M. C., Delbridge, L. W., Mun, H. C., Conigrave, A. D., and Ward, D. T. (2015) Pathophysiologic changes in extracellular pH modulate parathyroid calcium-sensing receptor activity and secretion via a histidine-independent mechanism. *J. Am. Soc. Nephrol. 26*, 2163−2171.
(50) Centeno, P. P., Herberger, A., Mun, H. C., Tu, C., Nemeth, E. F., Chang, W., Conigrave, A. D., and Ward, D. T. (2019) Phosphate acts directly on the calcium-sensing receptor to stimulate parathyroid hormone secretion. *Nat. Commun. 10*, 4693.
(51) Nemeth, E. F., Van Wagenen, B. C., and Balandrin, M. F. (2018) Discovery and development of calcimimetic and calcilytic compounds. *Prog. Med. Chem. 57*, 1−86.
(52) Nemeth, E. F., Heaton, W. H., Miller, M., Fox, J., Balandrin, M. F., Van Wagenen, B. C., Colloton, M., Karbon, W., Scherrer, J., Shatzen, E., Rishton, G., Scully, S., Qi, M., Harris, R., Lacey, D., and Martin, D. (2004) Pharmacodynamics of the type II calcimimetic compound cinacalcet HCl. *J. Pharmacol. Exp. Ther. 308*, 627.
(53) Keller, A. N., Kufareva, I., Josephs, T. M., Diao, J., Mai, V. T., Conigrave, A. D., Christopoulos, A., Gregory, K. J., and Leach, K.

(2018) Identification of global and ligand-specific calcium sensing receptor activation mechanisms. *Mol. Pharmacol. 93*, 619−630.
(54) Cook, A. E., Mistry, S. N., Gregory, K. J., Furness, S. G., Sexton, P. M., Scammells, P. J., Conigrave, A. D., Christopoulos, A., and Leach, K. (2015) Biased allosteric modulation at the CaS receptor engendered by structurally diverse calcimimetics. *Br. J. Pharmacol. 172*, 185−200.
(55) Miedlich, S. U., Gama, L., Seuwen, K., Wolf, R. M., and Breitwieser, G. E. (2004) Homology modeling of the transmembrane domain of the human calcium sensing receptor and localization of an allosteric binding site. *J. Biol. Chem. 279*, 7254−7263.
(56) Bu, L., Michino, M., Wolf, R. M., and Brooks, C. L. (2008) Improved model building and assessment of the Calcium-sensing receptor transmembrane domain. *Proteins: Struct., Funct., Genet. 71*, 215−226.
(57) Petrel, C., Kessler, A., Maslah, F., Dauban, P., Dodd, R. H., Rognan, D., and Ruat, M. (2003) Modeling and mutagenesis of the binding site of Calhex 231, a novel negative allosteric modulator of the extracellular Ca(2+)-sensing receptor. *J. Biol. Chem. 278*, 49487−49494.
(58) Petrel, C., Kessler, A., Dauban, P., Dodd, R. H., Rognan, D., and Ruat, M. (2004) Positive and negative allosteric modulators of the Ca2+-sensing receptor interact within overlapping but not identical binding sites in the transmembrane domain. *J. Biol. Chem. 279*, 18990−18997.
(59) Gregory, K. J., Giraldo, J., Diao, J., Christopoulos, A., and Leach, K. (2020) Evaluation of operational models of agonism and allosterism at receptors with multiple orthosteric binding sites. *Mol. Pharmacol. 97*, 35−45.
(60) Leach, K., Sexton, P. M., and Christopoulos, A. (2007) Allosteric GPCR modulators: taking advantage of permissive receptor pharmacology. *Trends Pharmacol. Sci. 28*, 382−389.
(61) Pin, J. P., Galvez, T., and Prézeau, L. (2003) Evolution, structure, and activation mechanism of family 3/C G-protein-coupled receptors. *Pharmacol. Ther. 98*, 325−354.
(62) Wu, H., Wang, C., Gregory, K. J., Han, G. W., Cho, H. P., Xia, Y., Niswender, C. M., Katritch, V., Meiler, J., Cherezov, V., Conn, P. J., and Stevens, R. C. (2014) Structure of a class C GPCR metabotropic glutamate receptor 1 bound to an allosteric modulator. *Science 344*, 58−64.
(63) Gustafsson, M., Jensen, J., Bertozzi, S. M., Currier, E. A., Ma, J. N., Burstein, E. S., and Olsson, R. (2010) Discovery of a class of calcium sensing receptor positive allosteric modulators; 1-(benzothiazol-2-yl)-1-phenylethanols. *Bioorg. Med. Chem. Lett. 20*, 5918−5921.
(64) Ma, J.-N., Owens, M., Gustafsson, M., Jensen, J., Tabatabaei, A., Schmelzer, K., Olsson, R., and Burstein, E. S. (2011) Characterization of highly efficacious allosteric agonists of the human calcium-sensing receptor. *J. Pharmacol. Exp. Ther. 337*, 275−284.
(65) Walter, S., Baruch, A., Dong, J., Tomlinson, J. E., Alexander, S. T., Janes, J., Hunter, T., Yin, Q., Maclean, D., Bell, G., Mendel, D. B., Johnson, R. M., and Karim, F. (2013) Pharmacology of AMG 416 (Velcalcetide), a novel peptide agonist of the calcium-sensing receptor, for the treatment of Secondary Hyperparathyroidism in hemodialysis patients. *J. Pharmacol. Exp. Ther. 346*, 229.
(66) Alexander, S. T., Hunter, T., Walter, S., Dong, J., Maclean, D., Baruch, A., Subramanian, R., and Tomlinson, J. E. (2015) Critical cysteine residues in both the calcium-sensing receptor and the allosteric activator AMG 416 underlie the mechanism of action. *Mol. Pharmacol. 88*, 853−865.
(67) Marquis, R. W., Lago, A. M., Callahan, J. F., Rahman, A., Dong, X., Stroup, G. B., Hoffman, S., Gowen, M., DelMar, E. G., Van Wagenen, B. C., Logan, S., Shimizu, S., Fox, J., Nemeth, E. F., Roethke, T., Smith, B. R., Ward, K. W., and Bhatnagar, P. (2009) Antagonists of the calcium receptor. 2. amino alcohol-based parathyroid hormone secretagogues. *J. Med. Chem. 52*, 6599−6605.
(68) Marquis, R. W., Casillas, L. N., Ramanjulu, J. M., and Callahan, J. F. (2010) Calcilytic compounds. US Patent US7829594B2.
(69) Shinagawa, Y., Inoue, T., Katsushima, T., Kiguchi, T., Ikenogami, T., Ogawa, N., Fukuda, K., Hirata, K., Harada, K., Takagi, M., Nakagawa, T., Kimura, S., Matsuo, Y., Maekawa, M., Hayashi, M., Soejima, Y., Takahashi, M., Shindo, M., and Hashimoto, H. (2011) Discovery of a potent and short-acting oral calcilytic with a pulsatile secretion of parathyroid hormone. *ACS Med. Chem. Lett. 2*, 238−242.
(70) Lago, M. A., Callahan, J. F., Bhatnagar, P. K., Del Mar, R. G., Bryan, W. M., and Burgess, J. L. (2006) Calcilytic compounds. US Patent US7109238B2.
(71) Josephs, T. M., Keller, A. N., Khajehali, E., DeBono, A., Langmead, C. J., Conigrave, A. D., Capuano, B., Kufareva, I., Gregory, K. J., and Leach, K. (2020) Negative allosteric modulators of the human calcium-sensing receptor bind to overlapping and distinct sites within the 7-transmembrane domain. *Br. J. Pharmacol. 177*, 1917−1930.
(72) Widler, L., Altmann, E., Beerli, R., Breitenstein, W., Bouhelal, R., Buhl, T., Gamse, R., Gerspacher, M., Halleux, C., John, M. R., Lehmann, H., Kalb, O., Kneissel, M., Missbach, M., Müller, I. R., Reidemeister, S., Renaud, J., Taillardat, A., Tommasi, R., Weiler, S., Wolf, R. M., and Seuwen, K. (2010) 1-Alkyl-4-phenyl-6-alkoxy-1 H-quinazolin-2-ones: a novel series of potent calcium-sensing receptor antagonists. *J. Med. Chem. 53*, 2250−2263.
(73) Widler, L. (2011) Calcilytics: antagonists of the calcium-sensing receptor for the treatment of osteoporosis. *Future Med. Chem. 3*, 535−547.
(74) Noetzel, M. J., Gregory, K. J., Vinson, P. N., Manka, J. T., Stauffer, S. R., Lindsley, C. W., Niswender, C. M., Xiang, Z., and Conn, P. J. (2013) A novel metabotropic glutamate receptor 5 positive allosteric modulator acts at a unique site and confers stimulus bias to mGlu5 signaling. *Mol. Pharmacol. 83*, 835−847.
(75) Hammond, A. S., Rodriguez, A. L., Townsend, S. D., Niswender, C. M., Gregory, K. J., Lindsley, C. W., and Conn, P. J. (2010) Discovery of a novel chemical class of mGlu(5) allosteric ligands with distinct modes of pharmacology. *ACS Chem. Neurosci. 1*, 702−716.
(76) Kessler, A., Faure, H., Petrel, C., Rognan, D., Cesario, M., Ruat, M., Dauban, P., and Dodd, R. H. (2006) N1-Benzoyl-N2-[1-(1-naphthyl)ethyl]-trans-1,2-diaminocyclohexanes: Development of 4-chlorophenylcarboxamide (calhex 231) as a new calcium sensing receptor ligand demonstrating potent calcilytic activity. *J. Med. Chem. 49*, 5119−5128.
(77) Gregory, K. J., Kufareva, I., Keller, A. N., Khajehali, E., Mun, H. C., Goolam, M. A., Mason, R. S., Capuano, B., Conigrave, A. D., Christopoulos, A., and Leach, K. (2018) Dual action calcium-sensing receptor modulator unmasks novel mode-switching mechanism. *ACS Pharmacol Transl Sci. 1*, 96−109.
(78) Fukagawa, M., Shimazaki, R., and Akizawa, T. (2018) Head-to-head comparison of the new calcimimetic agent evocalcet with cinacalcet in Japanese hemodialysis patients with secondary hyperparathyroidism. *Kidney Int. 94*, 818−825.
(79) Rottembourg, J., Urena-Torres, P., Toledano, D., Gueutin, V., Hamani, A., Coldefy, O., Hebibi, H., Guincestre, T., and Emery, C. (2019) Factors associated with parathyroid hormone control in haemodialysis patients with secondary hyperparathyroidism treated with cinacalcet in real-world clinical practice: Mimosa study. *Clin. Kidney J. 12*, 871−879.
(80) Rothe, H., Shapiro, W., Sun, W. Y., and Matalon, A. (2008) CaSR polymorphism Arg990Gly and response to calcimimetic agents in end-stage kidney disease patients with secondary hyperparathyroidism and in cell culture. *Pers. Med. 5*, 109−116.
(81) Block, G. A., Bushinsky, D. A., Cheng, S., Cunningham, J., Dehmel, B., Drueke, T. B., Ketteler, M., Kewalramani, R., Martin, K. J., Moe, S. M., Patel, U. D., Silver, J., Sun, Y., Wang, H., and Chertow, G. M. (2017) Effect of etelcalcetide vs cinacalcet on serum parathyroid hormone in patients receiving hemodialysis with secondary hyperparathyroidism: A randomized clinical trialetelcalcetide vs cinacalcet in hemodialysis with secondary hyperparathyroidism

https://dx.doi.org/10.1021/acsptsci.1c00046
ACS Pharmacol. Transl. Sci. 2021, 4, 666−679

etelcalcetide vs cinacalcet in hemodialysis with secondary hyperparathyroidism. *JAMA 317*, 156−164.
(82) Bushinsky, D. A., Chertow, G. M., Cheng, S., Deng, H., Kopyt, N., Martin, K. J., Rastogi, A., Urena-Torres, P., Vervloet, M., and Block, G. A. (2020) One-year safety and efficacy of intravenous etelcalcetide in patients on hemodialysis with secondary hyperparathyroidism. *Nephrol., Dial., Transplant. 35*, 1769−1778.
(83) Palmer, S. C., Mavridis, D., Johnson, D. W., Tonelli, M., Ruospo, M., and Strippoli, G. F. M. (2020) Comparative effectiveness of calcimimetic agents for Secondary Hyperparathyroidism in adults: a systematic review and network meta-analysis. *Am. J. Kidney Dis. 76*, 321−330.
(84) Kawata, T., Tokunaga, S., Murai, M., Masuda, N., Haruyama, W., Shoukei, Y., Hisada, Y., Yanagida, T., Miyazaki, H., Wada, M., Akizawa, T., and Fukagawa, M. (2018) A novel calcimimetic agent, evocalcet (MT-4580/KHK7580), suppresses the parathyroid cell function with little effect on the gastrointestinal tract or CYP isozymes in vivo and in vitro. *PLoS One 13*, e0195316−0195314.
(85) Fukumoto, K., Noguchi, T., Toriie, S., Shimazu, E., and Miyake, S. (2010) The mechanism of upper-gastrointestinal complication after taking cinacalcet hydrochloride. *Nihon Toseki Igakkai Zasshi 43*, 309−315.
(86) Shigematsu, T., Shimazaki, R., Fukagawa, M., and Akizawa, T. (2018) Pharmacokinetics of evocalcet in secondary hyperparathyroidism patients receiving hemodialysis: first-in-patient clinical trial in Japan. *Clin Pharmacol 10*, 101−111.
(87) Dershem, R., Gorvin, C. M., Metpally, R. P.R., Krishnamurthy, S., Smelser, D. T., Hannan, F. M., Carey, D. J., Thakker, R. V., and Breitwieser, G. E. (2020) Familial hypocalciuric hypercalcemia type 1 and autosomal-dominant hypocalcemia type 1: Prevalence in a large healthcare population. *Am. J. Hum. Genet. 106*, 734−747.
(88) White, E., McKenna, J., Cavanaugh, A., and Breitwieser, G. E. (2009) Pharmacochaperone-mediated rescue of calcium-sensing receptor loss-of-function mutants. *Mol. Endocrinol. 23*, 1115−1123.
(89) Huang, Y., and Breitwieser, G. E. (2007) Rescue of calcium-sensing receptor mutants by allosteric modulators reveals a conformational checkpoint in receptor biogenesis. *J. Biol. Chem. 282*, 9517−9525.
(90) Leach, K., Wen, A., Davey, A. E., Sexton, P. M., Conigrave, A. D., and Christopoulos, A. (2012) Identification of molecular phenotypes and biased signaling induced by naturally occurring mutations of the human calcium-sensing receptor. *Endocrinology 153*, 4304−4316.
(91) Hannan, F., Babinsky, V., and Thakker, R. V. (2016) Disorders of the calcium-sensing receptor and partner proteins: insights into the molecular basis of calcium homeostasis. *J. Mol. Endocrinol. 57*, R127−R142.
(92) Timmers, H. J. L. M., Karperien, M., Hamdy, N. A. T., De boer, H., and Hermus, A. R. M. M. (2006) Normalization of serum calcium by cinacalcet in a patient with hypercalcaemia due to a de novo inactivating mutation of the calcium-sensing receptor. *J. Intern. Med. 260*, 177−182.
(93) Gannon, A. W., Monk, H. M., and Levine, M. A. (2014) Cinacalcet Monotherapy in Neonatal Severe Hyperparathyroidism: A Case Study and Review. *J. Clin. Endocrinol. Metab. 99*, 7−11.
(94) Wilhelm-Bals, A., Parvex, P., Magdelaine, C., and Girardin, E. (2012) Successful use of bisphosphonate and calcimimetic in neonatal severe Primary Hyperparathyroidism. *Pediatrics 129*, e812−e816.
(95) Fisher, M. M., Cabrera, S. M., and Imel, E. A. (2015) Successful treatment of neonatal severe hyperparathyroidism with cinacalcet in two patients. *Endocrinol Diabetes Metab Case Rep 2015*, 102−107.
(96) Alon, U. S., and VanDeVoorde, R. G. (2010) Beneficial effect of cinacalcet in a child with familial hypocalciuric hypercalcemia. *Pediatr. Nephrol. 25*, 1747−1750.
(97) Gunganah, K., Grossman, A., and Druce, M. (2014) Recurrent pancreatitis in a patient with familial hypocalciuric hypercalcaemia treated successfully with cinacalcet. *Endocrinol Diabetes Metab Case Rep 2014*, 675−673.
(98) Mastromatteo, E., Lamacchia, O., Campo, M. R., Conserva, A., Baorda, F., Cinque, L., Guarnieri, V., Scillitani, A., and Cignarelli, M. (2014) A novel mutation in calcium-sensing receptor gene associated to hypercalcemia and hypercalciuria. *BMC Endocr Disord 14*, 239−236.
(99) Atay, Z., Bereket, A., Haliloglu, B., Abali, S., Ozdogan, T., Altuncu, E., Canaff, L., Vilaça, T., Wong, B. Y. L., Cole, D. E. C., Hendy, G. N., and Turan, S. (2014) Novel homozygous inactivating mutation of the calcium-sensing receptor gene (CASR) in neonatal severe hyperparathyroidism—lack of effect of cinacalcet. *Bone 64*, 102−107.
(100) Savas-Erdeve, S., Sagsak, E., Keskin, M., Magdelaine, C., Lienhardt-Roussie, A., Kurnaz, E., Cetinkaya, S., and Aycan, Z. (2016) Treatment experience and long-term follow-up data in two severe neonatal hyperparathyroidism cases. *J. Pediatr Endocrinol Metab 29*, 129−129.
(101) Capozza, M., Chinellato, I., Guarnieri, V., Di lorgi, N., Accadia, M., Traggiai, C., Mattioli, G., Di Mauro, A., and Laforgia, N. (2018) Case report: acute clinical presentation and neonatal management of primary hyperparathyroidism due to a novel CaSR mutation. *BMC Pediatr. 18*, 340.
(102) García Soblechero, E., Ferrer Castillo, M. T., Jiménez Crespo, B., Domínguez Quintero, M. L., and González Fuentes, C. (2013) Neonatal Hypercalcemia due to a Homozygous Mutation in the Calcium-Sensing Receptor: Failure of Cinacalcet. *Neonatology 104*, 104−108.
(103) Murphy, H., Patrick, J., Báez-Irizarry, E., Lacassie, Y., Gómez, R., Vargas, A., Barkemeyer, B., Kanotra, S., and Zambrano, R. M. (2016) Neonatal severe hyperparathyroidism caused by homozygous mutation in CASR: A rare cause of life-threatening hypercalcemia. *Eur. J. Med. Genet*, 1−5.
(104) Leach, K., Wen, A., Cook, A. E., Sexton, P. M., Conigrave, A. D., and Christopoulos, A. (2013) Impact of clinically relevant mutations on the pharmacoregulation and signaling bias of the calcium-sensing receptor by positive and negative allosteric modulators. *Endocrinology 154*, 1105−1116.
(105) Nesbit, M. A., Hannan, F. M., Howles, S. A., Babinsky, V. N., Head, R. A., Cranston, T., Rust, N., Hobbs, M. R., Heath, H., and Thakker, R. V. (2013) Mutations affecting G-Protein Subunit α 11 in hypercalcemia and hypocalcemia. *N. Engl. J. Med. 368*, 2476−2486.
(106) Babinsky, V. N., Hannan, F. M., Gorvin, C. M., Howles, S. A., Nesbit, M. A., Rust, N., Hanyaloglu, A. C., Hu, J., Spiegel, A. M., and Thakker, R. V. (2016) Allosteric modulation of the calcium-sensing receptor rectifies signaling abnormalities associated with G-protein alpha-11 mutations causing hypercalcemic and hypocalcemic disorders. *J. Biol. Chem. 291*, 10876−10885.
(107) Howles, S. A., Hannan, F. M., Gorvin, C. M., Piret, S. E., Paudyal, A., Stewart, M., Hough, T. A., Nesbit, M. A., Wells, S., Brown, S. D., Cox, R. D., and Thakker, R. V. (2017) Cinacalcet corrects hypercalcemia in mice with an inactivating Galpha11 mutation. *JCI Insight*, 2 DOI: 10.1172/jci.insight.96540.
(108) Gorvin, C. M., Hannan, F. M., Cranston, T., Valta, H., Makitie, O., Schalin-Jantti, C., and Thakker, R. V. (2018) Cinacalcet rectifies hypercalcemia in a patient with Familial Hypocalciuric Hypercalcemia Type 2 (FHH2) caused by a germline loss-of-function Galpha11 mutation. *J. Bone Miner. Res. 33*, 32−41.
(109) Vargas-Poussou, R. R., Mansour-Hendili, R. L., Baron, R. S., Bertocchio, R. J.-P., Travers, R. C., Simian, R. C., Treard, R. C., Baudouin, R. V., Beltran, R. S., Broux, R. F., Camard, R. O., Cloarec, R. S., Cormier, R. C., Debussche, R. X., Dubosclard, R. E., Eid, R. C., Haymann, R. J.-P., Kiando, R. S., Kuhn, R. J.-M., Lefort, R. G., Linglart, R. A., Lucas-Pouliquen, R. B., Macher, R. M.-A., Maruani, R. G., Ouzounian, R. S., Polak, R. M., Requeda, R. E., Robier, R. D., Silve, R. C., Souberbielle, R. J.-C., Tack, R. I., Vezzosi, R. D., Jeunemaitre, R. X., and Houillier, R. P. (2016) Familial Hypocalciuric Hypercalcemia Types 1 and 3 and Primary Hyperparathyroidism: Similarities and Differences. *J. Clin. Endocrinol. Metab. 101*, 2185−2195.

(110) Fujisawa, Y., Yamaguchi, R., Satake, E., Ohtaka, K., Nakanishi, T., Ozono, K., and Ogata, T. (2013) Identification of AP2S1 mutation and effects of low calcium formula in an infant with hypercalcemia and hypercalciuria. *J. Clin. Endocrinol. Metab. 98*, E2022−E2027.
(111) Hendy, N. G., Canaff, S. L., Newfield, L. R., Tripto-Shkolnik, P. L., Wong, C. B. Y., Lee, C. B. S., and Cole, C. D. E. (2014) Codon Arg15 mutations of the AP2S1 gene: common occurrence in Familial Hypocalciuric Hypercalcemia cases negative for calcium-sensing receptor (CASR) mutations. *J. Clin. Endocrinol. Metab. 99*, E1311−E1315.
(112) Gorvin, C. M., Metpally, R., Stokes, V. J., Hannan, F. M., Krishnamurthy, S. B., Overton, J. D., Reid, J. G., Breitwieser, G. E., and Thakker, R. V. (2018) Large-scale exome datasets reveal a new class of adaptor-related protein complex 2 sigma subunit (AP2σ) mutations, located at the interface with the AP2 alpha subunit, that impair calcium-sensing receptor signalling. *Hum. Mol. Genet. 27*, 901−911.
(113) Hannan, F. M., Howles, S. A., Rogers, A., Cranston, T., Gorvin, C. M., Babinsky, V. N., Reed, A. A., Thakker, C. E., Bockenhauer, D., Brown, R. S., Connell, J. M., Cook, J., Darzy, K., Ehtisham, S., Graham, U., Hulse, T., Hunter, S. J., Izatt, L., Kumar, D., McKenna, M. J., McKnight, J. A., Morrison, P. J., Mughal, M. Z., O'Halloran, D., Pearce, S. H., Porteous, M. E., Rahman, M., Richardson, T., Robinson, R., Scheers, I., Siddique, H., Van'T Hoff, W. G., Wang, T., Whyte, M. P., Nesbit, M. A., and Thakker, R. V. (2015) Adaptor protein-2 sigma subunit mutations causing familial hypocalciuric hypercalcaemia type 3 (FHH3) demonstrate genotype-phenotype correlations, codon bias and dominant-negative effects. *Hum. Mol. Genet. 24*, 5079.
(114) McMurtry, C. T., Schranck, F. W., Walkenhorst, D. A., Murphy, W. A., Kocher, D. B., Teitelbaum, S. L., Rupich, R. C., and Whyte, M. P. (1992) Significant developmental elevation in serum parathyroid hormone levels in a large kindred with familial benign (hypocalciuric) hypercalcemia. *Am. J. Med. 93*, 247−258.
(115) Howles, S. A., Hannan, F. M., Babinsky, V. N., Rogers, A., Gorvin, C. M., Rust, N., Richardson, T., McKenna, M. J., Nesbit, M. A., and Thakker, R. V. (2016) Cinacalcet for symptomatic Hypercalcemia caused by AP2S1 mutations. *N. Engl. J. Med. 374*, 1396−1398.
(116) Sozen, T., Ozisik, L., and Calik Basaran, N. (2017) An overview and management of osteoporosis. *Eur. J. Rheumatol 4*, 46−56.
(117) Brixen, K. T., Christensen, B., Ejersted, C., and Langdahl, B. L. (2004) Teriparatide (biosynthetic human parathyroid hormone 1−34): A new paradigm in the treatment of osteoporosis. *Pharmacol. Toxicol. 94*, 260−270.
(118) Tashjian, A. H. J., and Goltzman, D. (2008) On the Interpretation of Rat Carcinogenicity Studies for Human PTH(1−34) and Human PTH(1−84). *J. Bone Miner. Res. 23*, 803−811.
(119) Gowen, M., Stroup, G. B., Dodds, R. A., James, I. E., Votta, B. J., Smith, B. R., Bhatnagar, P. K., Lago, A. M., Callahan, J. F., DelMar, E. G., Miller, M. A., Nemeth, E. F., and Fox, J. (2000) Antagonizing the parathyroid calcium receptor stimulates parathyroid hormone secretion and bone formation in osteopenic rats. *J. Clin. Invest. 105*, 1595−1604.
(120) Nemeth, E. F. (2002) The search for calcium receptor antagonists (calcilytics). *J. Mol. Endocrinol. 29*, 15−21.
(121) Dobnig, H., and Turner, R. T. (1997) The effects of programmed administration of human parathyroid hormone fragment (1−34) on bone histomorphometry and serum chemistry in rats. *Endocrinology 138*, 4607−4612.
(122) Balan, G., Bauman, J., Bhattacharya, S., Castrodad, M., Healy, D. R., Herr, M., Humphries, P., Jennings, S., Kalgutkar, A. S., Kapinos, B., Khot, V., Lazarra, K., Li, M., Li, Y., Neagu, C., Oliver, R., Piotrowski, D. W., Price, D., Qi, H., Simmons, H. A., Southers, J., Wei, L., Zhang, Y., and Paralkar, V. M. (2009) The discovery of novel calcium sensing receptor negative allosteric modulators. *Bioorg. Med. Chem. Lett. 19*, 3328−3332.
(123) Kumar, S., Matheny, C. J., Hoffman, S. J., Marquis, R. W., Schultz, M., Liang, X., Vasko, J. A., Stroup, G. B., Vaden, V. R., Haley, H., Fox, J., DelMar, E. G., Nemeth, E. F., Lago, A. M., Callahan, J. F., Bhatnagar, P., Huffman, W. F., Gowen, M., Yi, B., Danoff, T. M., and Fitzpatrick, L. A. (2010) An orally active calcium-sensing receptor antagonist that transiently increases plasma concentrations of PTH and stimulates bone formation. *Bone 46*, 534−542.
(124) Fitzpatrick, L. A., Dabrowski, C. E., Cicconetti, G., Gordon, D. N., Fuerst, T., Engelke, K., and Genant, H. K. (2012) Ronacaleret, a calcium-sensing receptor antagonist, increases trabecular but not cortical bone in postmenopausal women. *J. Bone Miner. Res. 27*, 255−262.
(125) Halse, J., Greenspan, S., Cosman, F., Ellis, G., Santora, A., Leung, A., Heyden, N., Samanta, S., Doleckyj, S., Rosenberg, E., and Denker, A. E. (2014) A phase 2, randomized, placebo-controlled, dose-ranging study of the calcium-sensing receptor antagonist MK-5442 in the treatment of postmenopausal women with osteoporosis. *J. Clin. Endocrinol. Metab. 99*, E2207−2215.
(126) John, M. R., Harfst, E., Loeffler, J., Belleli, R., Mason, J., Bruin, G. J., Seuwen, K., Klickstein, L. B., Mindeholm, L., Widler, L., and Kneissel, M. (2014) AXT914 a novel, orally-active parathyroid hormone-releasing drug in two early studies of healthy volunteers and postmenopausal women. *Bone 64*, 204−210.
(127) Caltabiano, S., Dollery, C. T., Hossain, M., Kurtinecz, M. T., Desjardins, J. P., Favus, M. J., Kumar, R., and Fitzpatrick, L. A. (2013) Characterization of the effect of chronic administration of a calcium-sensing receptor antagonist, ronacaleret, on renal calcium excretion and serum calcium in postmenopausal women. *Bone 56*, 154−162.
(128) Li, D., Opas, E. E., Tuluc, F., Metzger, D. L., Hou, C., Hakonarson, H., and Levine, M. A. (2014) Autosomal Dominant Hypoparathyroidism caused by germline mutation in GNA11: phenotypic and molecular characterization. *J. Clin. Endocrinol. Metab. 99*, E1774−E1783.
(129) Mannstadt, M., Harris, M., Bravenboer, B., Chitturi, S., Dreijerink, K. M. A., Lambright, D. G., Lim, E. T., Daly, M. J., Gabriel, S., and Jüppner, H. (2013) Germline Mutations Affecting Gα 11 in Hypoparathyroidism. *N. Engl. J. Med. 368*, 2532−2534.
(130) Piret, S. E., Gorvin, C. M., Pagnamenta, A. T., Howles, S. A., Cranston, T., Rust, N., Nesbit, M. A., Glaser, B., Taylor, J. C., Buchs, A. E., Hannan, F. M., and Thakker, R. V. (2016) Identification of a G-Protein subunit-α11 gain-of-function mutation, Val340Met, in a Family With Autosomal Dominant Hypocalcemia Type 2 (ADH2). *J. Bone Miner. Res. 31*, 1207−1214.
(131) Hannan, F. M., Walls, G. V., Babinsky, V. N., Nesbit, M. A., Kallay, E., Hough, T. A., Fraser, W. D., Cox, R. D., Hu, J., Spiegel, A. M., and Thakker, R. V. (2015) The calcilytic agent NPS 2143 rectifies hypocalcemia in a mouse model with an activating calcium-sensing receptor (CaSR) mutation: Relevance to Autosomal Dominant Hypocalcemia Type 1 (ADH1). *Endocrinology 156*, 3114−3121.
(132) Letz, S., Rus, R., Haag, C., Dorr, H. G., Schnabel, D., Mohlig, M., Schulze, E., Frank-Raue, K., Raue, F., Mayr, B., and Schofl, C. (2010) Novel activating mutations of the calcium-sensing receptor: the calcilytic NPS-2143 mitigates excessive signal transduction of mutant receptors. *J. Clin. Endocrinol. Metab. 95*, E229−233.
(133) Gorvin, C. M., Hannan, F. M., Howles, S. A., Babinsky, V. N., Piret, S. E., Rogers, A., Freidin, A. J., Stewart, M., Paudyal, A., Hough, T. A., Nesbit, M. A., Wells, S., Vincent, T. L., Brown, S. D., Cox, R. D., and Thakker, R. V. (2017) Gα11 mutation in mice causes hypocalcemia rectifiable by calcilytic therapy. *JCI Insight 2*, e91103.
(134) Roszko, K. L., Bi, R., Gorvin, C. M., Brauner-Osborne, H., Xiong, X. F., Inoue, A., Thakker, R. V., Stromgaard, K., Gardella, T., and Mannstadt, M. (2017) Knockin mouse with mutant Galpha11 mimics human inherited hypocalcemia and is rescued by pharmacologic inhibitors. *JCI Insight 2*, e91079.
(135) Dong, B., Endo, I., Ohnishi, Y., Kondo, T., Hasegawa, T., Amizuka, N., Kiyonari, H., Shioi, G., Abe, M., Fukumoto, S., and Matsumoto, T. (2015) Calcilytic ameliorates abnormalities of mutant calcium-sensing receptor (CaSR) knock-in mice mimicking autosomal dominant hypocalcemia (ADH). *J. Bone Miner. Res. 30*, 1980−1993.

https://dx.doi.org/10.1021/acsptsci.1c00046
ACS Pharmacol. Transl. Sci. 2021, 4, 666−679

(136) Letz, S., Haag, C., Schulze, E., Frank-Raue, K., Raue, F., Hofner, B., Mayr, B., and Schofl, C. (2014) Amino alcohol- (NPS-2143) and quinazolinone-derived calcilytics (ATF936 and AXT914) differentially mitigate excessive signalling of calcium-sensing receptor mutants causing Bartter syndrome Type 5 and autosomal dominant hypocalcemia. *PLoS One 9*, e115178.
(137) Roberts, M. S., Gafni, R. I., Brillante, B., Guthrie, L. C., Streit, J., Gash, D., Gelb, J., Krusinska, E., Brennan, S. C., Schepelmann, M., Riccardi, D., Bin Khayat, M. E., Ward, D. T., Nemeth, E. F., Rosskamp, R., and Collins, M. T. (2019) Treatment of Autosomal Dominant Hypocalcemia Type 1 with the calcilytic NPSP795 (SHP635). *J. Bone Miner. Res. 34*, 1609−1618.
(138) Borchers Arriagada, N., Horsley, J. A., Palmer, A. J., Morgan, G. G., Tham, R., and Johnston, F. H. (2019) Association between fire smoke fine particulate matter and asthma-related outcomes: Systematic review and meta-analysis. *Environ. Res. 179*, 108777.
(139) Koller, D. Y., Halmerbauer, G., Frischer, T., and Roithner, B. (1999) Assessment of eosinophil granule proteins in various body fluids: is there a relation to clinical variables in childhood asthma? *Clin. Exp. Allergy 29*, 786−793.
(140) Lonnkvist, K., Hellman, C., Lundahl, J., Hallden, G., and Hedlin, G. (2001) Eosinophil markers in blood, serum, and urine for monitoring the clinical course in childhood asthma: impact of budesonide treatment and withdrawal. *J. Allergy Clin. Immunol. 107*, 812−817.
(141) Kurosawa, M., Shimizu, Y., Tsukagoshi, H., and Ueki, M. (1992) Elevated levels of peripheral-blood, naturally occurring aliphatic polyamines in bronchial asthmatic patients with active symptoms. *Allergy 47*, 638−643.
(142) North, M. L., Grasemann, H., Khanna, N., Inman, M. D., Gauvreau, G. M., and Scott, J. A. (2013) Increased ornithine-derived polyamines cause airway hyperresponsiveness in a mouse model of asthma. *Am. J. Respir. Cell Mol. Biol. 48*, 694−702.
(143) Bartoli, M. L., Bacci, E., Carnevali, S., Cianchetti, S., Dente, F. L., Di Franco, A., Giannini, D., Taccola, M., Vagaggini, B., and Paggiaro, P. L. (2004) Clinical assessment of asthma severity partially corresponds to sputum eosinophilic airway inflammation. *Respir Med. 98*, 184−193.
(144) Gibson, P. G., Woolley, K. L., Carty, K., Murree-Allen, K., and Saltos, N. (1998) Induced sputum eosinophil cationic protein (ECP) measurement in asthma and chronic obstructive airway disease (COAD). *Clin. Exp. Allergy 28*, 1081−1088.
(145) Coyle, A. J., Ackerman, S. J., and Irvin, C. G. (1993) Cationic proteins induce airway hyperresponsiveness dependent on charge interactions. *Am. Rev. Respir. Dis. 147*, 896−900.
(146) Homma, T., Bates, J. H., and Irvin, C. G. (2005) Airway hyperresponsiveness induced by cationic proteins in vivo: site of action. *Am. J. Physiol. 289*, L413−418.
(147) Frigas, E., Loegering, D. A., Solley, G. O., Farrow, G. M., and Gleich, G. J. (1981) Elevated levels of the eosinophil granule major basic protein in the sputum of patients with bronchial asthma. *Mayo Clinic Proceedings 56*, 345−353.
(148) Lee, J. W., Park, H. A., Kwon, O. K., Park, J. W., Lee, G., Lee, H. J., Lee, S. J., Oh, S. R., and Ahn, K. S. (2017) NPS 2143, a selective calcium-sensing receptor antagonist inhibits lipopolysaccharide-induced pulmonary inflammation. *Mol. Immunol. 90*, 150−157.
(149) Thompson, M., Freeman, M. R., Manlove, L. J., Fang, Y. H., Britt, R., Kuipers, I., Riccardi, D., Pabelick, C., and Prakash, Y. S. (2016) Calcium sensing receptor and airway reactivity in mixed allergen treated mouse model of asthma. *Am. J. Respir Crit Care Med. 193*, A1266.
(150) Li, T., Sun, M., Yin, X., Wu, C., Wu, Q., Feng, S., Li, H., Luan, Y., Wen, J., Yan, L., Zhao, B., Xu, C., and Sun, Y. (2013) Expression of the calcium sensing receptor in human peripheral blood T lymphocyte and its contribution to cytokine secretion through MAPKs or NF-kappaB pathways. *Mol. Immunol. 53*, 414−420.
(151) Lee, G. S., Subramanian, N., Kim, A. I., Aksentijevich, I., Goldbach-Mansky, R., Sacks, D. B., Germain, R. N., Kastner, D. L., and Chae, J. J. (2012) The calcium-sensing receptor regulates the NLRP3 inflammasome through Ca2+ and cAMP. *Nature 492*, 123−127.
(152) Rossol, M., Pierer, M., Raulien, N., Quandt, D., Meusch, U., Rothe, K., Schubert, K., Schoneberg, T., Schaefer, M., Krugel, U., Smajilovic, S., Brauner-Osborne, H., Baerwald, C., and Wagner, U. (2012) Extracellular Ca2+ is a danger signal activating the NLRP3 inflammasome through G protein-coupled calcium sensing receptors. *Nat. Commun. 3*, 1329.
(153) Yarova, P. L., Huang, P., Schepelmann, M. W., Bruce, R., Ecker, R., Nica, R., Telezhkin, V., Traini, D., Gomes dos Reis, L., Kidd, E. J., Ford, W. R., Broadley, K. J., Kariuki, B. M., Corrigan, C. J., Ward, J. P. T., Kemp, P. J., and Riccardi, D. (2021) Characterisation of negative allosteric modulators of the calcium-sensing receptor, CaSR, for repurposing as a treatment for asthma. *J. Pharmacol Exp Ther 376* (1), 51−63.

https://dx.doi.org/10.1021/acsptsci.1c00046
ACS Pharmacol. Transl. Sci. 2021, 4, 666−679

1521-0111/97/1/35–47$35.00
MOLECULAR PHARMACOLOGY

https://doi.org/10.1124/mol.119.118091
Mol Pharmacol 97:35–47, January 2020

Evaluation of Operational Models of Agonism and Allosterism at Receptors with Multiple Orthosteric Binding Sites[S]

Karen J. Gregory, Jesús Giraldo, Jiayin Diao, Arthur Christopoulos, and Katie Leach

Drug Discovery Biology and Department of Pharmacology, Monash Institute of Pharmaceutical Sciences, Monash University, Parkville, Melbourne, Australia (K.J.G., J.D., A.C., K.L.); Laboratory of Molecular Neuropharmacology and Bioinformatics, Institut de Neurociències and Unitat de Bioestadística, Facultat de Medicina, Universitat Autònoma de Barcelona, Barcelona, Spain (J.G.); Instituto de Salud Carlos III, Centro de Investigación Biomédica en Red de Salud Mental, Bellaterra, Spain (J.G.); and Unitat de Neurociència Traslacional, Parc Taulí Hospital Universitari, Institut d'Investigació i Innovació Parc Taulí and Institut de Neurociències, Universitat Autònoma de Barcelona, Bellaterra, Spain (J.G.)

Received August 12, 2019; accepted November 4, 2019

ABSTRACT

Current operational models of agonism and allosterism quantify ligand actions at receptors where agonist concentration-response relationships are nonhyperbolic by introduction of a transducer slope that relates receptor occupancy to response. However, for some receptors nonhyperbolic concentration-response relationships arise from multiple endogenous agonist molecules binding to a receptor in a cooperative manner. Thus, we developed operational models of agonism in systems with cooperative agonist binding and evaluated the models by simulating data describing agonist effects. The models were validated by analyzing experimental data demonstrating the effects of agonists and allosteric modulators at receptors where agonist binding follows hyperbolic (M_4 muscarinic acetylcholine receptors) or nonhyperbolic relationships (metabotropic glutamate receptor 5 and calcium-sensing receptor). For hyperbolic agonist concentration-response relationships, no differences in estimates of ligand affinity, efficacy, or cooperativity were observed when the slope was assigned to either a transducer slope or agonist binding slope. In contrast, for receptors with nonhyperbolic agonist concentration-response relationships, estimates of ligand affinity, efficacy, or cooperativity varied depending on the assignment of the slope. The extent of this variation depended on the magnitude of the slope value and agonist efficacy, and for allosteric modulators on the magnitude of cooperativity. The modified operational models described herein are well suited to analyzing agonist and modulator interactions at receptors that bind multiple orthosteric agonists in a cooperative manner. Accounting for cooperative agonist binding is essential to accurately quantify agonist and drug actions.

SIGNIFICANCE STATEMENT

Some orthosteric agonists bind to multiple sites on a receptor, but current analytical methods to characterize such interactions are limited. Herein, we develop and validate operational models of agonism and allosterism for receptors with multiple orthosteric binding sites, and demonstrate that such models are essential to accurately quantify agonist and drug actions. These findings have important implications for the discovery and development of drugs targeting receptors such as the calcium-sensing receptor, which binds at least five calcium ions.

Introduction

The past 30 years have seen major advances in quantifying the relationship between receptor occupancy and response, with the operational model of agonism (Black and Leff, 1983) representing one of the most common analytical approaches. The operational model of agonism describes agonist effects based on agonist affinity [equilibrium dissociation constant of the orthosteric agonist (K_A)] and observed efficacy in a given test system. The latter is defined by a transducer ratio (τ),

This work was supported by the National Health and Medical Research Council of Australia [Project Grants APP1085143 (to K.L.), APP1138891 (to K.L. and K.J.G.), APP1084775 (to K.J.G.), and APP1127322 (to K.J.G.); Program Grant APP1055134 (to A.C.); and Senior Principal Research Fellowship APP1102950 (to A.C.)]; the Australian Research Council [Discovery Grant DP170104228 (to K.L. and K.J.G.), and Future Fellowships FT160100075 (to K.L.) and FT170100392 (to K.J.G.)]; and the Ministerio de Ciencia, Innovación y Universidades of Spain [Project Grant SAF2017-87199-R (to J.G.)].
https://doi.org/10.1124/mol.119.118091.
[S] This article has supplemental material available at molpharm.aspetjournals.org.

ABBREVIATIONS: AC265347, 1-(1,3-benzothiazol-2-yl)-1-(2,4-dimethylphenyl)ethanol; ACh, acetylcholine; Ca_i^{2+}, intracellular calcium; Ca_o^{2+}, extracellular calcium; calcimimetic B, R-1-(6-methoxy-4′-(trifluoromethyl)-3-biphenylyl)-N-(R)- 1-phenylethyl)ethanamine; CaSR, calcium-sensing receptor; DMEM, Dulbecco's modified Eagle's medium; DPFE, 1-(4-(2,4-difluorophenyl)piperazin-1-yl)-2-((4-fluorobenzyl)oxy)ethanone; E_m, maximal system response; E_{max}, maximum effect; GPCR, G protein–coupled receptor; HEK, human embryonic kidney; K_A, equilibrium dissociation constant of the orthosteric agonist; K_B, equilibrium dissociation constant of the allosteric ligand; LY2033298, 3-amino-5-chloro-6-methoxy-4-methyl-thieno[2,3-b]pyridine-2-carboxylic acid cyclopropylamide; M-5MPEP, 2-[2-(3-methoxyphenyl)ethynyl]-5-methylpyridine; mAChR, muscarinic acetylcholine receptor; mGlu, metabotropic glutamate receptor; MPEP, 2-methyl-6-(2-phenylethynyl)pyridine; NAM, negative allosteric modulator; n_B, binding slope linking agonist concentration to receptor occupancy; n_H, Hill slope; n_T, transducer slope linking agonist concentration to response; NPS2143, 2-chloro-6-[(2R)-2-hydroxy-3-[(2-methyl-1-naphthalen-2-ylpropan-2-yl)amino]propoxy]benzonitrile; PAM, positive allosteric modulator; WT, wild type; VE-29, 2-chloro-6-[(2R)-2-hydroxy-3-[(2-methyl-1-naphthalen-2-ylpropan-2-yl)amino]propoxy]benzonitrile.

which is a function of both tissue- and agonist-specific components; it is the ratio of the total receptor number and a transducer parameter that defines the avidity with which a given agonist-occupied receptor complex promotes the final observed pharmacological effect. As such, the operational model of agonism is a useful tool for quantifying agonism in a comparable manner across different test systems (Black and Leff, 1983), and has subsequently been extended or modified to also quantify effects of allosteric modulators and biased agonists (Leach et al., 2007, 2010; Kenakin, 2012).

The operational model of agonism has been most commonly applied to characterize the activity of agonists that display both rectangular hyperbolic or nonhyperbolic concentration-response curves, i.e., normally empirically characterized by Hill slopes that are equal to or different from unity, respectively. The key underlying assumption in the majority of instances to date where an agonist concentration-response curve displays a Hill slope significantly different from 1has been ascribed in the most common form of the operational model to differences in the postreceptor machinery that transduces occupancy to response, i.e., through introduction of a so-called transducer slope (n) (Black et al., 1985). For instance, steep or shallow Hill slopes could arise due to changes in the sensitivity of one or more steps in a receptor's signal transduction mechanism, while the initial agonist-receptor binding event is assumed to be characterized by a simple hyperbolic one-to-one relationship. However, for ion channels and a number of G protein–coupled receptors (GPCRs), particularly the class C GPCR subfamily, nonhyperbolic concentration-response relationships can also arise from cooperative binding of multiple equivalents of the same endogenous agonist molecule prior to any subsequent processing of the stimulus by the cellular transduction machinery. For example, while a number of small molecule calcium-sensing receptor (CaSR) agonists produce responses characterized by Hill slopes close to unity (Cook et al., 2015; Keller et al., 2018), indicating a transducer slope equal to unity, it is also well established that CaSR responses to its endogenous activator, extracellular calcium (Ca_o^{2+}), and other divalent cations are characterized by extremely high Hill slopes, ranging from 2 to 4 (Brown, 1983; Davey et al., 2012; Leach et al., 2015). The most parsimonious explanation to account for these disparate observations is that the operational transducer slope linking CaSR agonist occupancy to response can adequately be described by a transducer slope equal to unity, which suggests that the cooperativity observed in response to activators such as Ca_o^{2+} ions arises at the level of binding, not function. This is also in accord with known pharmacological and structural studies of the CaSR that have identified multiple binding sites for Ca_o^{2+} ions (Geng et al., 2016). As a consequence, the classic operational model of agonism as applied to concentration-response curves of nonunit Hill slopes is suboptimal for such situations.

Herein, we sought to develop and evaluate an operational model of agonism that describes orthosteric agonist binding to multiple sites in a cooperative manner, referred to as the cooperative agonist operational model. The cooperative agonist operational model was superior to the original Black-Leff operational model of agonism in fitting Ca_o^{2+}-CaSR concentration-response data. We also extended this cooperative agonist operational model to incorporate allosteric modulation of the affinity and efficacy of an agonist that binds cooperatively to multiple sites. This operational model of allosterism with cooperative agonist binding was fitted to data describing the actions of CaSR positive allosteric modulators (PAMs) and negative allosteric modulators (NAMs), and revealed that if cooperative agonist binding is not taken into consideration, under- or overestimates of PAM and NAM affinity and cooperativity can occur.

Materials and Methods

Materials. Dulbecco's modified Eagle's medium (DMEM), Flp-In human embryonic kidney (HEK) T-REx cells, blasticidin S HCl, and FBS were obtained from Invitrogen (Carlsbad, CA), while hygromycin B was obtained from Roche (Mannheim, Germany). Fluo-8 AM was obtained from Abcam (Cambridge, MA).

CaSR-Expressing HEK293 Cell Lines. The generation of DNA and Flp-In HEK T-REx cells stably expressing c-myc-tagged wild-type (WT) CaSR in pcDNA5/frt/TO have been described previously (Davey et al., 2012; Leach et al., 2016). Flp-In HEK T-REx CaSR cells were maintained in DMEM containing 5% FBS, 200 μg/ml hygromycin B, and 5 μg/ml blasticidin S HCl. To generate a tetracycline-inducible Flp-In HEK cell line stably expressing an N-terminally truncated CaSR, N-terminally truncated CaSR corresponding to amino acids 600–903 with an N-terminal influenza hemagglutinin signal peptide followed by a c-myc epitope and rhodopsin signal peptide in pcDNA3.1+ (Leach et al., 2016) was transferred to pcDNA5/frt/TO using BamHI and NotI restriction sites. Flp-In HEK T-REx cells were seeded into 25 cm^2 flasks in DMEM containing 5% FBS and allowed to reach 80% confluency. Cells were transfected with 0.5 μg pcDNA5/frt/TO containing the N-terminally truncated CaSR plus 5 μg POG44 with lipofectamine 2000 (1:4 DNA:lipofectamine 2000) according to the manufacturer's instructions. The following day, cells were transferred to a T75 cm^2 flask, and 24 hours later DMEM was replaced with DMEM containing 5% FBS, 200 μg/ml hygromycin, and 5 μg/ml blasticidin S HCl. The selection DMEM was replaced every 3 days until untransfected cells had died (~10 days), and antibiotic-resistant cells were expanded and maintained in DMEM containing 5% FBS, 200 μg/ml hygromycin, and 5 μg/ml blasticidin S HCl. All cell lines were routinely tested for mycoplasma contamination using the Lonza MycoAlert mycoplasma detection kit.

Determination of WT and N-Terminally Truncated CaSR Cell Surface Expression Using Fluorescence-Activated Cytometry. Flp-In HEK T-REx WT and N-terminally truncated CaSR-expressing cells were seeded at 80,000 cells per well into a 96-well plate and expression was induced with 100 ng/ml tetracycline overnight at 37°C. The following day, cells were harvested and washed in 1X PBS with 0.1% bovine serum albumin and 2 mM EDTA (wash buffer) by centrifugation (350g, 4°C for 3 minutes) before resuspension and 30-minute incubation in 100 μl blocking buffer (1X PBS, 5% bovine serum albumin, and 2 mM EDTA) containing 1 μg/ml AF647-conjugated 9E10 made in-house as previously described (Cook et al., 2015). Cells were washed as previously described and resuspended in wash buffer containing propidium iodide. Live cell fluorescence was measured using a BD FACS Canto analyzer (Becton Dickinson).

Calcium Mobilization Assays. Cells were seeded in clear 96-well plates coated with poly-D-lysine (50 $\mu g/ml^{-1}$) at 80,000 cells per well and incubated overnight in the presence of 0 or 100 ng/ml^{-1} tetracycline. The following day, cells were washed with assay buffer (150 mM NaCl, 2.6 mM KCl, 1.18 mM $MgCl_2$, 10 mM D-Glucose, 10 mM HEPES, 0.1 mM $CaCl_2$, 0.5% bovine serum albumin, and 4 mM probenecid at pH 7.4) and loaded with Fluo-8 AM (1 μM in assay buffer) for 1 hour at 37°C. Cells were washed with assay buffer prior to the addition of fresh assay buffer.

For all studies, each well was treated with a single agonist concentration. The release of intracellular calcium (Ca_i^{2+}) was measured at 37°C using FlexStation 1 or 3 (Molecular Devices, Sunnyvale, CA). Fluorescence was detected for 60 seconds at 490 nm excitation and 520 nm emission and the peak Ca_i^{2+} mobilization response (approximately 12 seconds after agonist addition) was used for the subsequent determination of the agonist response. Relative peak

fluorescence units were normalized to the fluorescence stimulated by 1 μM ionomycin to account for differences in cell number and loading efficiency.

Model Derivation and Data Analysis. The derivation of operational models describing the effect of an agonist in the absence or presence of an allosteric modulator at a receptor with multiple agonist binding sites is presented in the Supplemental Appendix. The script input to use the two equations in the GraphPad Prism program is also presented in the Supplemental Appendix.

Data simulations were performed using the original Black-Leff operational model of agonism, referred to hereinafter as the Black-Leff model (eq. 1), or a modified cooperative agonist operational model (eq. 2), where an additional slope [i.e., the binding slope linking agonist concentration to receptor occupancy (n_B)] was incorporated to take into account multiple agonist binding sites, and thus the steepness of the slope describing the agonist concentration-occupancy relationship:

$$\text{Effect} = \frac{E_m \tau_A^{n_T}[A]^{n_T}}{\tau_A^{n_T}[A]^{n_T} + ([A] + K_A)^{n_T}} \quad (1)$$

$$\text{Effect} = \frac{E_m \tau_A^{n_T}[A]^{n_B n_T}}{\tau_A^{n_T}[A]^{n_B n_T} + \left([A]^{n_B} + K_A^{n_B}\right)^{n_T}} \quad (2)$$

where [A] is the agonist concentration, K_A is the agonist equilibrium dissociation constant; τ_A is an operational measure of agonist efficacy; E_m is the maximal system response; and n_T is the transducer slope linking agonist concentration to response.

For simplicity, the modified cooperative operational model of agonism (eq. 2) makes the following assumptions:

1. The receptor is either empty or fully occupied, and only the fully occupied receptor exerts an effect. The lack of partially occupied receptor molecules could arise if multiple agonist molecules bind simultaneously to the receptor, or if agonist molecules bind sequentially with high positive cooperativity. Thus, once one binding site is occupied, positive cooperativity drives occupancy of all other sites. The latter scenario is most likely; hence, this is why we have called this model the cooperative agonist operational model.
2. The model cannot discern cooperativity between the multiple binding sites, thus n_B may not be the true number of binding sites; therefore, n_B is a binding slope coefficient.
3. The K_A value is a geometric mean of the microscopic dissociation constants for each binding site.

The Eqs. 1 or 2 were fitted to agonist concentration response data in order to quantify agonist affinity and efficacy. When fitting eq. 2 to experimental data, the transducer slope was constrained to unity (see *Results* for validation of this assumption).

Data describing the interaction between glutamate and PAMs and NAMs at metabotropic glutamate receptor (mGlu) subtype 5, or between acetylcholine (ACh) and 3-amino-5-chloro-6-methoxy-4-methyl-thieno[2,3-b]pyridine-2-carboxylic acid cyclopropylamide (LY2033298) at the M_4 muscarinic acetylcholine receptor (mAChR), were fitted to our original operational model of allosterism (eq. 3) or to the new operational model of allosterism with cooperative agonist binding (eq. 4). For simplicity and for the purpose of fitting experimental data, eqs. 3–8 assume a single allosteric modulator binding site; therefore, they do not take into account modulator cooperative binding:

$$\text{Effect} = \frac{E_m\{\tau_A[A](K_B + \alpha\beta[B]) + \tau_B[B][K_A]\}^{n_T}}{([A]K_B + K_A K_B + K_A[B] + \alpha[A][B])^{n_T} + \{\tau_A[A](K_B + \alpha\beta[B]) + \tau_B[B]K_A\}^{n_T}} \quad (3)$$

$$\text{Effect} = \frac{E_m\{\tau_A[A]^{n_B}(K_B + \alpha\beta[B]) + \tau_B[B][K_A]^{n_B}\}^{n_T}}{\left([A]^{n_B}K_B + K_A^{n_B}K_B + K_A^{n_B}[B] + \alpha[A]^{n_B}[B]\right)^{n_T} + \left\{\tau_A[A]^{n_B}(K_B + \alpha\beta[B]) + \tau_B[B]K_A^{n_B}\right\}^{n_T}} \quad (4)$$

where K_A is the equilibrium dissociation constant of the orthosteric agonist, which was fixed in some instances to the affinity determined in radioligand binding assays (Mutel et al., 2000; Leach et al., 2010); K_B is the equilibrium dissociation constant of the allosteric ligand; τ_A and τ_B are the operational efficacies of the orthosteric agonist and allosteric ligand, respectively; α and β are the allosteric effects on orthosteric agonist affinity and efficacy, respectively (it should be noted that β is not a reciprocal efficacy cooperativity factor) (Leach et al., 2007; Giraldo, 2015); and [A] and [B] are the orthosteric agonist and allosteric ligand concentrations, respectively.

To fit the operational model of allosterism to data describing the interaction between Ca_o^{2+} and cinacalcet at the CaSR, the original operational model of allosterism shown by eq. 3 was simplified, because for a full agonist like Ca_o^{2+} (i.e., one that generates the maximal system response at submaximal receptor occupancies) $K_A >> [A]$. Furthermore, because the CaSR's orthosteric agonist, Ca_o^{2+}, was present in the assay buffer, the contaminating agonist was included in the equations used to analyze CaSR PAM (cinacalcet) and NAM (2-chloro-6-[(2*R*)-2-hydroxy-3-[(2-methyl-1-naphthalen-2-ylpropan-2-yl)amino]propoxy]benzonitrile [NPS2143]) data (Keller et al., 2018). Therefore, data describing the interaction between Ca_o^{2+} and cinacalcet or NPS2143 at the CaSR were fitted to the original operational model of allosterism with the contaminating agonist (eqs. 5 and 6, respectively) or to an operational model of allosterism with cooperative agonist binding and contaminating agonist (eqs. 7 and 8, respectively):

$$\text{Effect} = \frac{E_m\{[A + C](K_B + \alpha\beta[B]) + \tau_B[B][EC_{50}]\}^{n_T}}{[EC_{50}]^{n_T}(K_B + [B])^{n_T} + \{[A + C](K_B + \alpha\beta[B]) + \tau_B[B][EC_{50}]\}^{n_T}} \quad (5)$$

where EC_{50} is the agonist concentration that elicits a half-maximal response, in which it should be noted that inclusion of $[EC_{50}]$ involves some simplifying assumptions that facilitate data fitting (Aurelio et al., 2009; Giraldo, 2015); [C] is the contaminating agonist concentration; and all other parameters are as described for eq. 3:

$$\text{Effect} = \frac{E_m\{\tau_A[A + C](K_B + \alpha\beta[B]) + \tau_B(B)[K_A]\}^{n_T}}{([A]K_B + K_A K_B + K_A[B] + \alpha[A + C][B])^{n_T} + \{\tau_A[A + C](K_B + \alpha\beta[B]) + \tau_B[B]K_A\}^{n_T}} \quad (6)$$

$$\text{Effect} = \frac{E_m\{[A + C]^{n_B}(K_B + \alpha\beta[B]) + \tau_B[B][EC_{50}]^{n_B}\}^{n_T}}{[EC_{50}]^{n_B n_T}(K_B + [B])^{n_T} + \{[A + C]^{n_B}(K_B + \alpha\beta[B]) + \tau_B[B][EC_{50}]^{n_B}\}^{n_T}} \quad (7)$$

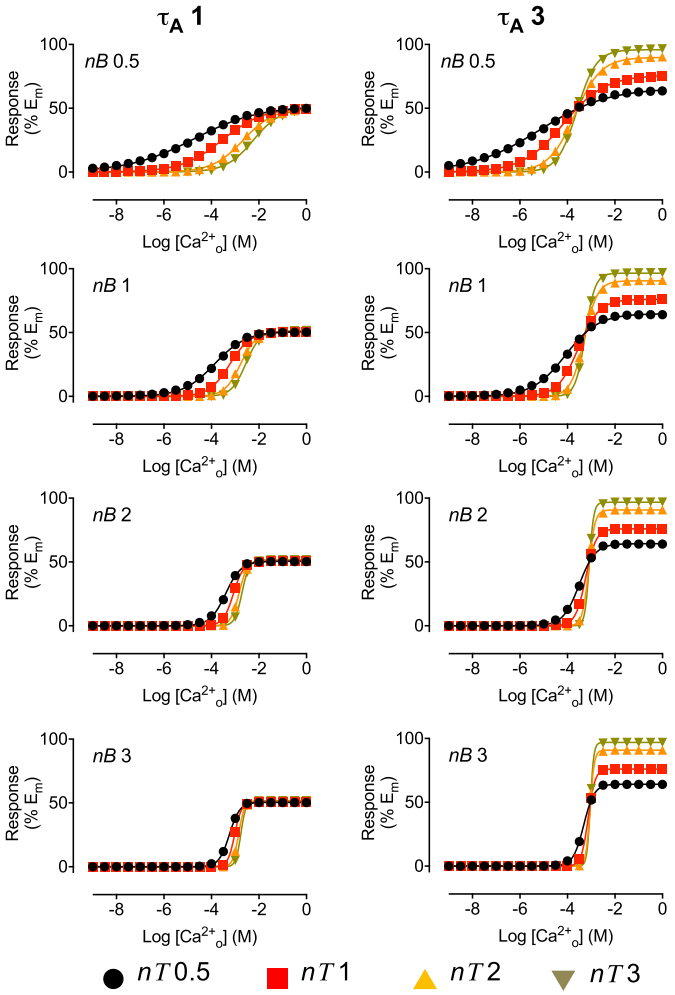

Fig. 1. The n_T and n_B values differentially contribute to agonist concentration-response relationships. Simulations demonstrating the influence of n_T or n_B on concentration-response relationships for agonists with different efficacies (τ_A). Data were simulated using the cooperative agonist operational model (eq. 2), where the affinity of the agonist (K_A) is 1.2 mM and n_T and n_B are between 1 and 3. Curves through the data are the fits to a four-parameter Hill equation (eq. 9), where the parameters describing the fits are given in Table 1.

where EC_{50}, K_B, τ_B, α, β, [A], [B], [C], and E_m are as described for eq. 5:

$$\text{Effect} = \frac{E_m\{\tau_A[A+C]^{n_B}(K_B+\alpha\beta[B])+\tau_B[B][K_A]^{n_B}\}^{n_T}}{\left([A+C]^{n_B}K_B+K_A^{n_B}K_B+K_A^{n_B}[B]+\alpha[A+C]^{n_B}[B]\right)^{n_T}+\{\tau_A[A]^{n_B}(K_B+\alpha\beta[B])+\tau_B[B]K_A^{n_B}\}^{n_T}} \quad (8)$$

where all other parameters are as described for eq. 4.

The Hill equation (Eq 9) was fitted to simulated data:

$$\text{Effect} = \frac{[A]^{n_H}E_{max}}{[A]^{n_H}+EC_{50}^{n_H}} \quad (9)$$

where [A] is the agonist concentration; E_{max} is the maximum agonist effect; and n_H is the Hill slope.

Nonlinear regression analysis was performed in GraphPad Prism 7 or 8. Potency, affinity, cooperativity, and efficacy parameters were estimated as logarithms (Christopoulos, 1998). An extra sum of squares F test was used to determine whether data were fitted best when the Hill slope, binding slope, or transducer slope (n_H, n_B, or n_T, respectively) were significantly different from unity, where $P < 0.05$ was considered significant.

Results

The Contribution of Slope Factors to Agonist Concentration-Response Relationships. We first evaluated the contribution of the agonist binding slope (n_B) or transducer slope (n_T) to the concentration-response curve of two agonists with different efficacies by simulating variations in n_B or n_T using the cooperative agonist operational model (eq. 2). We specifically wanted to evaluate a system with cooperative agonist binding; therefore, we based our simulations on Ca_o^{2+} activation of the CaSR. The Ca_o^{2+} concentration-response relationship for the CaSR's best characterized physiologic role, inhibition of parathyroid hormone secretion, occurs over a Ca_o^{2+} concentration range of 0.8–1.5 mM with an EC_{50} value of ~1.2 mM (Brown, 1983). Thus, for these simulations, the affinity of the agonist (K_A) was assumed to be 1.2 mM and n_B or n_T were assumed to be between 1 and 3. Simulated data were subsequently fitted to a Hill equation (eq. 9). Unsurprisingly, increasing n_B or n_T increases the Hill slope of the agonist concentration-response curve (Fig. 1; Table 1). Furthermore, increasing n_T decreases agonist potency. Interestingly, the effect of n_B on agonist potency depends on the magnitude of n_T and τ_A. For instance, increasing n_B decreases agonist potency for higher efficacy agonists (τ_A 3). However, for lower efficacy agonists (τ_A 1), increasing n_B decreases agonist potency when $n_T \leq 1$, but increases agonist potency when $n_T \geq 2$.

We next sought to directly compare the influence of the binding or transducer slope by simulating concentration-response curves for agonists with varying efficacies using the Black-Leff operational model (eq. 1, which contains a transducer slope, n_T) and the cooperative agonist operational model (eq. 2, which contains transducer and binding slopes, n_T and n_B, respectively). As can be seen in Fig. 2 and Table 2, when n_T or n_B are equal to 1, variations in τ_A have an identical effect on empirical agonist concentration-response parameters (potency, Hill slope, or E_{max}) regardless of the model. In contrast, when n_T or n_B are greater than 1, variations in τ_A result in major differences in the agonist concentration-response profile predicted with the two different operational models of agonism. Specifically, the Black-Leff model predicts that high-efficacy agonists have greater potency relative to affinity (due to amplification of the steps between agonist binding and response), while for low-efficacy agonists, the EC_{50} value may be less than the K_A value for curves that possess nonunity Hill slopes. The latter was previously noted by Black et al. (1985). Furthermore, the Hill slope decreases alongside decreases in τ_A. In comparison, the

TABLE 1

Simulation of agonist concentration-response relationships upon changes in binding or transducer slopes and τ_A

Data were simulated using the cooperative agonist operational model (eq. 2) and a Hill equation (eq. 9) was fitted to simulated data to determine agonist potency, maximum effect, and Hill slope.

Parameter	eq. 2											
	n_B 0.5			n_B 1			n_B 2			n_B 3		
	pEC_{50}	E_{max}	n_H	pEC_{50}	E_{max}	n_H	pEC_{50}	E_{max}	n_H	pEC_{50}	E_{max}	n_H
τ_A 1												
n_T 0.5	4.8	51	0.3	3.9	50	0.7	3.4	50	1.3	3.3	50	2.0
n_T 1	3.5	51	0.5	3.2	51	1.0	3.1	51	2.0	3.0	51	3.0
n_T 2	2.6	51	0.6	2.8	51	1.3	2.8	51	2.4	2.9	51	3.5
n_T 3	2.2	52	0.7	2.6	52	1.4	2.7	52	2.9	2.8	52	4.1
τ_A 3												
n_T 0.5	5.2	66	0.3	4.1	65	0.6	3.5	64	1.3	3.3	64	1.9
n_T 1	4.2	76	0.5	3.5	76	1.0	3.2	76	2.0	3.1	76	3.0
n_T 2	3.7	90	0.8	3.3	90	1.5	3.1	91	3.3	3.1	91	4.9
n_T 3	3.6	96	1.1	3.3	97	2.1	3.1	97	4.7	3.0	97	6.0

pEC_{50}, agonist potency.

cooperative agonist operational model predicts that when $n_T = 1$, agonist EC_{50} may approach but not be less than its K_A value, regardless of whether $n_B > 1$, and there is no effect of τ_A on the Hill slope of the agonist concentration-response curve (Fig. 2; Table 2).

Quantification of Experimentally Derived Agonist Concentration-Response Data. We next tested whether our simulations were recapitulated in a functional assay that measures CaSR activation. To do so, we measured Ca_o^{2+}-mediated Ca_i^{2+} mobilization following titration of CaSR expression using a tetracycline inducible system. In the absence of tetracycline, the maximal response to Ca_o^{2+} is approximately 50% of the maximal response obtained under full induction of receptor expression (100 ng/ml tetracycline). In this system, fitting a Hill equation (eq. 9) to both data sets indicated that the data were fitted best when the Hill slope was unchanged with different receptor expression levels, i.e., different magnitudes of τ_A ($P < 0.05$, extra sum-of-squares F test; data not shown). For the CaSR, the small molecule allosteric agonists 1-(1,3-benzothiazol-2-yl)-1-(2,4-dimethylphenyl)ethanol (AC265347) and R-1-(6-methoxy-4′-(trifluoromethyl)-3-biphenylyl)-N-(R)- 1-phenylethyl)ethanamine (calcimimetic B) activate the CaSR with a Hill slope of 1

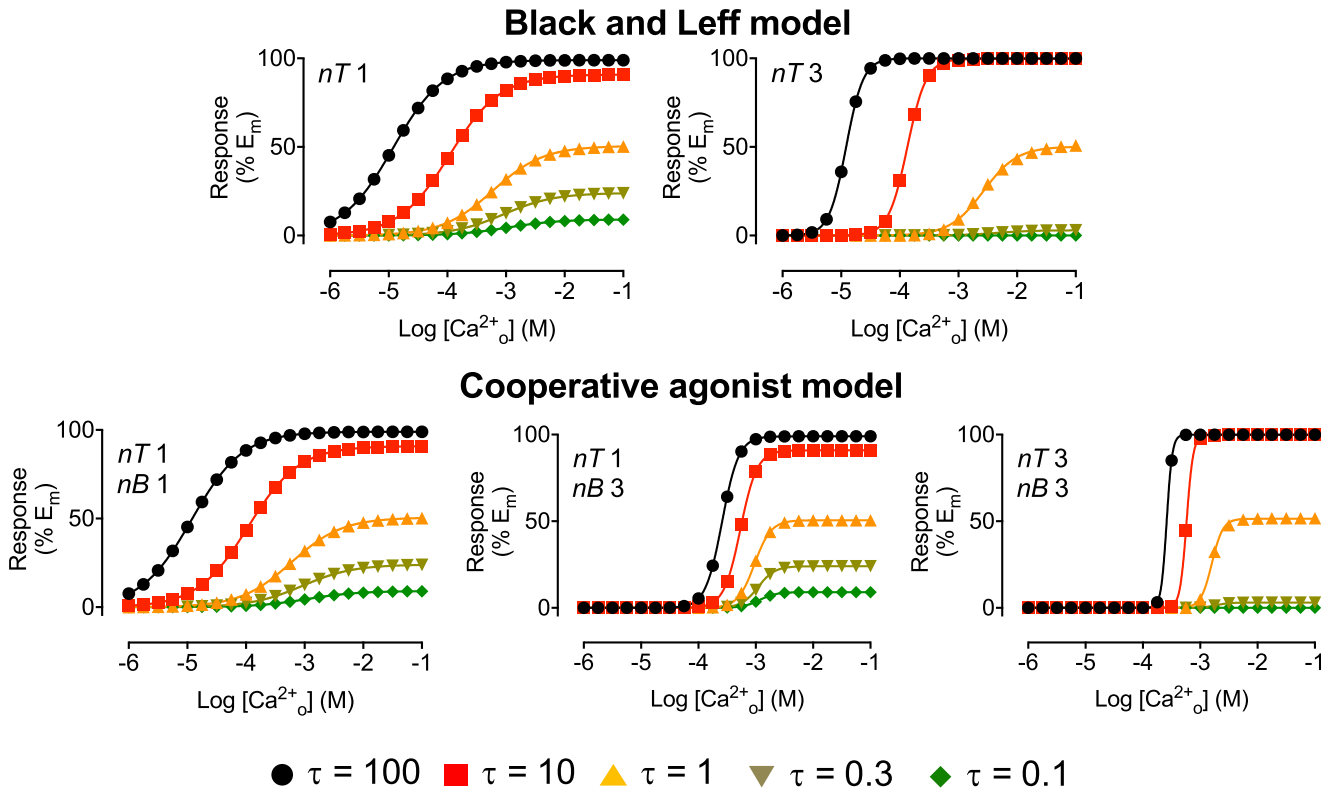

Fig. 2. Cooperative agonist binding influences agonist concentration-response relationships. Simulations demonstrating the influence of agonist efficacy (τ_A) on agonist concentration-response relationships when the slope is governed by the transducer slope (n_T, Black-Leff operational model of agonism) or the agonist binding slope (n_B, cooperative agonist operational model). Data were simulated using the Black-Leff model (eq. 1) or the cooperative agonist operational model (eq. 2), where the affinity of the agonist (K_A) is 1.2 mM and n_T and n_B are between 1 and 3. Curves through the data are the fits to a Hill equation (eq. 9), where the parameters describing the fits are given in Table 2.

TABLE 2

Simulation of agonist concentration-response relationships upon changes in binding or transducer slopes and τ_A

Data were simulated using the Black-Leff model (eq. 1) or the cooperative agonist operational model (eq. 2) and a Hill equation (eq. 9) was fitted to simulated data to determine agonist potency, maximum effect, and Hill slope.

τ_A	eq. 1; n_T 1			eq. 1; n_T 3			eq. 2; n_T 1, n_B 1			eq. 2; n_T 1, n_B 3			eq. 2; n_T 3, n_B 3		
	pEC_{50}	E_{max}	n_H	pEC_{50}	E_{max}	n_H	pEC_{50}	E_{max}	n_H	pEC_{50}	E_{max}	n_H	pEC_{50}	E_{max}	n_H
100	4.9	99	1.0	4.9	100	3.0	4.9	99	1.0	3.6	99	3.0	3.6	100	8.9
10	4.0	91	1.0	3.9	100	2.7	4.0	91	1.0	3.3	91	3.0	3.2	100	7.6
1	3.2	51	1.0	2.6	50	1.5	3.2	51	1.0	3.0	51	3.0	2.8	51	4.5
0.3	3.0	24	1.0	2.4	3.0	1.4	3.0	24	1.0	3.0	24	3.0	2.7	3.0	3.9
0.1	3.0	9.0	1.0	2.3	0.1	1.4	3.0	9.0	1.0	3.0	9.0	3.0	2.7	0.1	3.8

pEC_{50}, agonist potency.

(Cook et al., 2015; Keller et al., 2018). Similarly, when cooperative agonist binding is prevented by removal of the CaSR's N-terminal domain, and consequently the primary Ca_o^{2+} binding sites, the Hill slope for Ca_o^{2+} is not significantly different from unity (as shown subsequently). This provides experimental evidence that the CaSR's transducer slope is equal to unity, and that the steep Hill slopes observed for Ca_o^{2+} at the full-length CaSR thus likely arise from a binding slope greater than 1. Thus, when fitting CaSR experimental data to the cooperative agonist operational model, n_T was constrained to unity.

When the data were fitted to the classic Black-Leff model, the estimated K_A value was 0.2 mM (Fig. 3A; Table 3). In comparison, the cooperative agonist operational model yielded a K_A estimate of 1.1 mM, which is in close agreement with the EC_{50} value (1.2 mM) of Ca_o^{2+} for suppressing parathyroid hormone release (Brown, 1983) and Ca_o^{2+} affinity estimates for the CaSR extracellular domain determined using spectroscopic approaches (Huang et al., 2009; Zhang et al., 2014). For both analyses, data were fitted best when the binding slope (cooperative agonist operational model) or transducer slope (Black-Leff model) were different from unity ($P < 0.05$, extra sum of squares F test).

To further validate our simulations in a functional assay, we next sought to quantify the affinity and efficacy of a CaSR partial agonist. To do so, we took advantage of observations that in comparison with at the WT CaSR (Fig. 3B), Ca_o^{2+} acting via the 7 transmembrane domain is a partial agonist at an N-terminally truncated CaSR (depicted in Fig. 3C) relative to the extracellular trivalent gadolinium cation (Fig. 3D). The fluorescence-activated cytometry analysis confirmed cell surface expression of the WT and N-terminally truncated CaSR (Supplemental Fig. 1). We quantified Ca_o^{2+} affinity and efficacy at the N-terminally truncated CaSR using the original Black-Leff model or the cooperative agonist operational model (Table 3). In both instances, data were best fitted when the binding slope (the cooperative agonist operational model) or transducer slope (the Black-Leff model) were not different from unity ($P < 0.05$, extra sum of squares F test), which is consistent with a reduction in positively cooperative Ca_o^{2+} binding, as would be expected upon removal of the four primary Ca_o^{2+} binding sites located in the N-terminal domain (Geng et al., 2016). Thus, the parameters determined at the N-terminally truncated receptor were identical regardless of the equation used to analyze the data. The Ca_o^{2+} affinity and cooperativity estimates at the N-terminally truncated receptor were compared with those determined at the full-length WT CaSR, indicating a reduction in Ca_o^{2+} affinity at the N-terminally truncated receptor in comparison with WT (Table 3), again consistent with removal of the primary

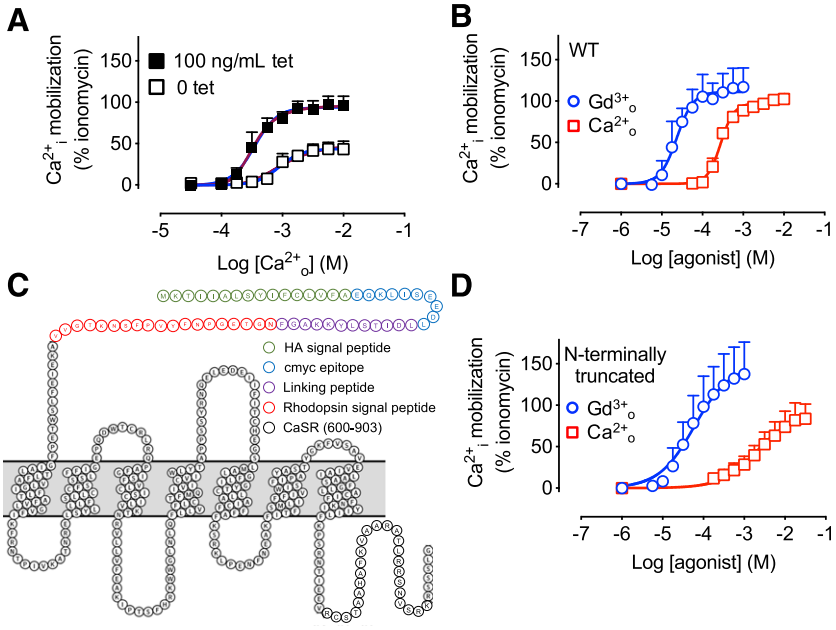

Fig. 3. Ca_o^{2+}-CaSR concentration-response relationships fit well to the cooperative agonist operational model. (A) Ca_o^{2+}-mediated Ca_i^{2+} mobilization at the WT CaSR following overnight receptor induction with 100 ng/ml tetracycline (tet) or in the absence of tetracycline. Data are mean + S.D. from four independent experiments performed in duplicate. Curves through the data are the fits to the Black-Leff model (blue line) or the cooperative agonist operational model (red line), where the parameters describing the fits are given in Table 3. Although both models fit the data, the cooperative agonist operational model more accurately predicts the expected affinity of Ca_o^{2+} at the CaSR (Table 3). (B) Extracellular trivalent gadolinium (Gd_o^{3+}) and Ca_o^{2+} concentration-response curves at the WT CaSR following overnight receptor induction with 100 ng/ml tetracycline. Data are mean + S.D. from four independent experiments performed in duplicate. Curves through the data are the fits to a four-parameter Hill equation. (C) N-terminally truncated CaSR snake diagram. (D) Gd_o^{3+} and Ca_o^{2+} concentration-response curves at an N-terminally truncated CaSR following overnight receptor induction with 100 ng/ml tetracycline. Data are mean + S.D. from five independent experiments performed in duplicate. Curves through the data are the fits to the cooperative agonist operational model, where the parameters describing the fits are given in Table 3.

TABLE 3

Quantification of Ca_o^{2+} affinity and efficacy for CaSR-Ca_i^{2+} mobilization using the operational model of agonism

Ca_o^{2+} concentration-response curves were generated at the WT receptor following overnight incubation of cells with or without 100 ng/ml tetracycline to induce receptor expression. For N-terminally truncated CaSRs, Ca_o^{2+} and Gd_o^{3+} concentration-response curves were generated upon induction of expression with 100 ng/ml tetracycline, where Ca_o^{2+} is a partial agonist and Gd_o^{3+} is a full agonist. The Black-Leff model (eq. 1) or the cooperative agonist operational model (eq. 2) was fitted to data to determine agonist affinity, efficacy, and transducer or binding slope.

Parameter	WT		N-terminally truncated CaSR	
	eq. 1	eq. 2	eq. 1	eq. 2
pK_A [K_A (mM)]	3.7 ± 0.3 (0.2)	3.0 ± 0.1 (1.0)	2.3 ± 0.2 (5.0)	2.3 ± 0.2 (5.0)
Log τ_A (τ_A)	100 ng/ml tet: 0.2 ± 0.1 (1.6) 0 tet: −0.01 ± 0.01 (1.0)	100 ng/ml tet: 1.2 ± 0.2 (16) 0 tet: −0.1 ± 0.1 (0.8)	0.2 ± 0.1 (1.6)	0.2 ± 0.1 (1.6)
n	6.0 ± 3.0[a]	2.0 ± 0.3[a]	1.0[b]	1.0[b]

Dfd, degrees of freedom denominator; Dfn, degrees of freedom numerator; Log τ_A (τ_A), efficacy; n, transducer or binding slope; pK_A (K_A), agonist affinity; tet, tetracycline.
[a]An F test determined that data were fitted best when the binding or transducer slopes were different from unity. The F data used to test the hypothesis that n differed from 1 were the following: eq. 1 $P < 0.0001$, F [(Dfn, Dfd) 48.57 (1, 74)]; and eq. 2 $P < 0.0001$, F [(Dfn, Dfd) 45.78 (1, 74)].
[b]An F test determined that data were fitted best when the binding or transducer slopes were not different from unity. The F data used to test the hypothesis that n differed from 1 were the following: eq. 1 $P < 0.2282$, F [(Dfn, Dfd) 1.470 (1, 101)]; and eq. 2 $P < 0.5332$, F [(Dfn, Dfd) 0.3910 (1, 101)].

Ca_o^{2+} binding sites. However, due to a lower estimate of Ca_o^{2+} efficacy at the WT receptor when WT data were analyzed using the Black-Leff model, only the cooperative agonist operational model accurately quantified a reduction in Ca_o^{2+} efficacy at the N-terminally truncated receptor in comparison with at the WT receptor. This is consistent with a lower Ca_o^{2+} E_{max} value at the N-terminally truncated receptor (~60% of the maximum response stimulated by extracellular trivalent gadolinium) in comparison with WT (~100% extracellular trivalent gadolinium E_{max}) (Table 3). Thus, only the cooperative agonist operational model accurately estimated Ca_o^{2+} partial agonism at the N-terminally truncated receptor.

Quantifying Allosteric Interactions in Systems with Different Degrees of Cooperative Agonist Binding. Having established that the cooperative agonist operational model best fitted our Ca_o^{2+}-WT CaSR concentration-response curves with Hill slopes greater than 1, we next extended this model to allow for quantification of allosteric modulation of an agonist response. The operational model of agonism and allosterism (Leach et al., 2007, 2010) (referred to herein as the original operational model of agonism and allosterism), which takes into account the allosteric effects on agonist affinity and efficacy, combines the allosteric ternary complex models developed by Stockton et al. (1983) and Ehlert (1988) and the Black-Leff operational model of agonism. In our original model (Leach et al., 2007), the allosteric modulator can also possess intrinsic efficacy. Introduction of a slope in that model once again assumed that the slope linked occupancy to response, not to the original binding events, which were assumed to be described as simple one-to-one hyperbolic functions. Therefore, we adapted this operational model of allosterism to account for cooperative agonist binding, referred to hereinafter as the operational model of allosterism with cooperative agonist binding. To validate this operational model of allosterism with cooperative agonist binding, we reanalyzed existing data demonstrating positive and negative allosteric modulation at three model GPCRs with different agonist Hill slopes: CaSR (a class C GPCR where the primary endogenous agonist, Ca_o^{2+}, has a Hill slope of 2–4), $mGlu_5$ (a class C GPCR where the primary endogenous agonist, L-glutamate, has a Hill slope of ~1.8) (Sengmany and Gregory, 2016), and M_4 mAChR (a class A GPCR where the endogenous agonist, acetylcholine, has a Hill slope of 1) (Leach et al., 2010, 2011) (Supplemental Fig. 2). In all instances, n_T was assumed to be unity and all allosteric modulators were assumed to bind to a single site (i.e., the modulator binding slope is unity).

For the CaSR, we analyzed allosteric modulation of Ca_o^{2+} by cinacalcet (PAM) or NPS2143 (NAM) (Leach et al., 2016) with the original operational model of agonism and allosterism with contaminating (i.e., ambient buffer) agonist (eqs. 5 or 6, respectively) and the newly derived operational model of allosterism with cooperative agonist binding and contaminating agonist (eqs. 7 or 8, respectively) (Fig. 4). Similar to our analysis of agonist concentration-response curves, data were fitted best when the binding slope (operational model of allosterism with cooperative agonist binding) or transducer slope (original operational model of agonism and allosterism) was different from unity ($P < 0.05$, extra sum of squares F test). Compared with the original operational model of agonism and allosterism, the estimated affinity for Ca_o^{2+} determined using the operational model of allosterism with cooperative agonist binding (1.4 mM) (Table 4) was once again closer to the assumed Ca_o^{2+} affinity based on its EC_{50} value for suppression of parathyroid hormone release (1.2 mM) and quantification of the Ca_o^{2+} K_A at the extracellular domain using spectroscopic approaches (3–5 mM) (Huang et al., 2009; Zhang et al., 2014). Furthermore, the estimated affinity and negative cooperativity of NPS2143 were greater (5.5- and 35-fold, respectively) when cooperative agonist binding was factored into the analysis (Table 4). For the PAM, cinacalcet,

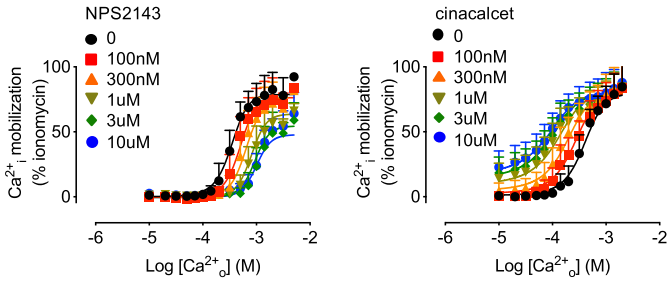

Fig. 4. Allosteric modulation at the CaSR is fitted well by an operational model of allosterism with cooperative agonist binding. Allosteric modulation of Ca_o^{2+}-mediated Ca_i^{2+} mobilization at the CaSR by NPS2143 (NAM) or cinacalcet (PAM). Data were previously published (Leach et al., 2016) and are mean + S.D. from at least 11 independent experiments performed in duplicate. Curves through the data are the fits to the operational model of allosterism with cooperative agonist binding and contaminating agonist (eq. 7 for cinacalcet and eq. 8 for NPS2143), where the parameters describing the fits are given in Table 4.

TABLE 4

Comparison of parameters describing CaSR allosteric interactions analyzed with different allosteric models

CaSR allosteric interactions with Ca_o^{2+} in Ca_i^{2+} mobilization assays were analyzed with the original operational model of agonism and allosterism (eqs. 5 or 6) vs. the operational model of allosterism with cooperative agonist binding (eqs. 7 or 8) to determine Ca_o^{2+} potency, efficacy, and affinity; modulator affinity, cooperativity, and transducer or binding slope; and maximum system response.

Parameter	Ca_o^{2+} vs. Cinacalcet		Ca_o^{2+} vs. NPS2143	
	eq. 5	eq. 7	eq. 6	eq. 8
pEC_{50}	3.3 ± 0.01	3.3 ± 0.01	n.d.	n.d.
pK_A [K_A (mM)]	n.d.	n.d.	3.6 ± 0.2 (0.3)	2.9 ± 0.1 (1.3)
pK_B [K_B (μM)]	6.3 ± 0.04 (0.5)	5.8 ± 0.1 (1.6)	6.6 ± 0.04 (0.3)	7.3 ± 0.1 (0.05)
Log τ_A (τ_A)	n.d.	n.d.	0.2 ± 0.1 (1.6)	1.8 ± 0.1 (63)
Log τ_B (τ_B)	n.a. (0)	n.a. (0)	n.a. (0)	n.a. (0)
Log $\alpha\beta$ ($\alpha\beta$)	0.5 ± 0.01 (3.2)	1.4 ± 0.1 (25)	−0.2 ± 0.1 (0.6)	−1.7 ± 0.1 (0.02)
n	2.8 ± 0.1[a]	2.8 ± 0.1[a]	12 ± 4.0[a]	3.5 ± 0.2[a]
E_m (% ionomycin)	79 ± 1.0	80 ± 1.0	78 ± 1.0	80 ± 2

Dfd, degrees of freedom denominator; Dfn, degrees of freedom numerator; E_m, maximum system response; Log $\alpha\beta$ ($\alpha\beta$), modulator cooperativity; Log τ_A (τ_A), Ca_o^{2+} efficacy; Log τ_B (τ_B), modulator efficacy; Ca_o^{2+} efficacy; n, transducer or binding slope; n.a., no agonist activity [log τ_B fixed to −100 (τ_B 0)]; n.d., not determined; pEC_{50}, Ca_o^{2+} potency; pK_A (K_A), Ca_o^{2+} affinity; pK_B (K_B), modulator affinity .

[a]An F test determined that data were fitted best when the transducer or binding slopes were different from unity. The F data used to test the hypothesis that n differed from 1 were the following: eq. 5 cinacalcet $P < 0.0001$, F [(Dfn, Dfd) 1249 (1, 2429)]; eq. 5 NPS2143 $P < 0.0001$, F [(Dfn, Dfd) 1022 (1, 908]; eq. 7 cinacalcet $P < 0.0001$, F [(Dfn, Dfd) 1241 (1, 2429)]; and eq. 7 NPS2143 $P < 0.0001$, F [(Dfn, Dfd) 504.5 (1, 907)].

the operational model of allosterism with cooperative agonist binding yielded a 3-fold lower affinity estimate but an 8-fold greater magnitude of positive cooperativity.

We next analyzed allosteric modulation of glutamate at $mGlu_5$ (eqs. 3 or 4) by a representative full NAM (2-methyl-6-(2-phenylethynyl)pyridine [MPEP]) that completely inhibits glutamate-mediated activation of Ca_i^{2+} mobilization, a partial NAM (2-[2-(3-methoxyphenyl)ethynyl]-5-methylpyridine [M-5MPEP]) that only partially inhibits glutamate-mediated activation of Ca_i^{2+} mobilization (Sengmany et al., 2019), a pure PAM (*N*-(1,3-Diphenyl-1H-pyrazolo-5-yl)-4-nitrobenzamide [VU-29]), and a mixed PAM-agonist (1-(4-(2,4-difluorophenyl)piperazin-1-yl)-2-((4-fluorobenzyl)oxy)ethanone [DPFE]) (Sengmany et al., 2017). Similar to analyses at the CaSR, all data were fitted best when the binding slope (operational model of allosterism with cooperative agonist binding) or transducer slope (original operational model of agonism and allosterism) was different from unity ($P < 0.05$, extra sum of squares F test). However, for each modulator, the affinity and cooperativity estimates were similar (within 3-fold) irrespective of the analytical model applied (Fig. 5; Table 5). Therefore, although the glutamate-$mGlu_5$ concentration-response relationship has a Hill slope greater than unity, quantification of allosteric interactions at $mGlu_5$ is largely unaffected by whether the empirical slope is assumed to be determined by the transducer slope or the agonist binding slope.

For the M_4 mAChR, we analyzed previously published positive allosteric modulation of ACh by the PAM agonist LY2033298 in guanosine 5′-*O*-(3-[^{35}S]thio)triphosphate binding assays (Leach et al., 2010) (eqs. 3 or 4). As expected, in the absence of cooperative ACh binding at the M_4 mAChR, data for the interaction between ACh and LY2033298 were fitted best by both operational models of agonism and allosterism when the slope was not different from unity ($P < 0.05$, extra sum of squares F test); therefore, both equations yielded identical estimates of affinity and cooperativity (Fig. 6; Table 6).

We next sought to establish why quantification of PAM and NAM affinity and cooperativity were not greatly affected by the assignment of the slope at $mGlu_5$, where the glutamate Hill slope is greater than unity. To do so, we simulated the interaction between an orthosteric agonist and a NAM or PAM with the operational model of allosterism with cooperative agonist binding and analyzed the simulated data with the original operational model of agonism and allosterism. For these simulations, orthosteric agonist affinity (1 μM), τ_A (10), and modulator affinity (10 nM) were held constant, and different magnitudes of positive or negative cooperativity were examined alongside changes in the magnitude of cooperative agonist binding. Consistent with our analysis of $mGlu_5$ allosteric interaction data, when the agonist binding

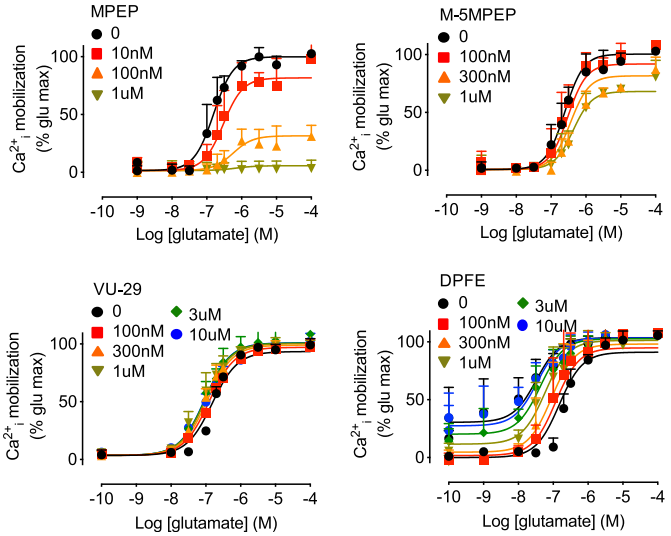

Fig. 5. Allosteric modulation at $mGlu_5$ is fitted well by an operational model of allosterism with cooperative agonist binding. Allosteric modulation of glutamate-mediated Ca_i^{2+} mobilization at $mGlu_5$ by MPEP (full NAM), M-5MPEP (partial NAM), VU-29 (PAM), and DPFE (ago-PAM). Data were previously published (Sengmany et al., 2017, 2019) and are mean + S.D. from at least three independent experiments performed in duplicate previously published. Curves through the data are the fits to the operational model of allosterism with cooperative agonist binding (eq. 4), where the parameters describing the fits are given in Table 5.

TABLE 5
Comparison of parameters describing $mGlu_5$ allosteric interactions analyzed with different allosteric models
$mGlu_5$ allosteric interactions with glutamate in Ca_i^{2+} mobilization assays were analyzed with the original operational model of agonism and allosterism (eq. 3) or the operational model of allosterism with cooperative agonist binding (eq. 4) to determine modulator affinity, glutamate or modulator efficacy, respectively), cooperativity, transducer or binding slopes, and maximum system response.

Parameter	Glutamate vs. MPEP[a]		Glutamate vs. M-5MPEP[a]		Glutamate vs. VU-29[b]		Glutamate vs. DPFE[b]	
	eq. 3	eq. 4	eq. 3	eq. 4	eq. 3	eq. 4	eq. 3	eq. 4
pK_A [K_A (μM)]	6.2 (0.6)[c]	6.2 (0.6)[c]	6.2 (0.6)[c]	6.2 (0.6)[c]	6.2 (0.6)[c]	6.2 (0.6)[c]	6.2 (0.6)[c]	6.2 (0.6)[c]
pK_B [K_B (μM)]	7.9 ± 0.1 (0.01)	8.4 ± 0.1 (0.004)	6.8 ± 0.2 (0.2)	6.8 ± 0.2 (0.2)	6.7 ± 0.2 (0.2)	6.7 ± 0.2 (0.2)	6.0 ± 0.3 (1.0)	5.6 ± 0.1 (2.5)
Log τ_A (τ_A)	0.7 ± 0.1 (5.0)	1.0 ± 0.2 (10)	0.6 ± 0.1 (3.9)	0.6 ± 0.2 (4.0)	0.7 ± 0.03 (5.0)	0.7 ± 0.1 (5.0)	0.6 ± 0.1 (4.0)	0.8 ± 0.1 (6.3)
Log τ_B (τ_B)	n.a. (0)	n.a. (0)	n.a. (0)	n.a. (0)	n.a. (0)	n.a. (0)	−0.2 ± 0.1 (0.6)	−0.4 ± 0.1 (0.4)
Log $\alpha\beta$ ($\alpha\beta$)	−100 (~0)[d]	−100 (~0)[d]	−0.5 ± 0.1 (0.3)	−0.8 ± 0.2 (0.2)	0.3 ± 0.03 (2.0)	0.3 ± 0.04 (0.2)	0.6 ± 0.1 (4.0)	1.1 ± 0.1 (13)
n	1.7 ± 0.2[e]	1.5 ± 0.2[e]	2.0 ± 0.2[e]	1.6 ± 0.2[e]	1.3 ± 0.1[e]	1.2 ± 0.1[e]	2.5 ± 0.7[e]	1.3 ± 0.1[e]
E_m (% glutamate)	106 ± 6.0	111 ± 6.0	107 ± 6.0	123 ± 1.0	108 ± 3.0	111 ± 3.0	107 ± 2.0	105 ± 2.0

Dfd, degrees of freedom denominator; Dfn, degrees of freedom numerator; E_m, maximum system response; Log $\alpha\beta$ ($\alpha\beta$), modulator cooperativity; Log τ_A (τ_A), glutamate efficacy; Log τ_B (τ_B), modulator efficacy; n, transducer or binding slope; n.a., no agonist activity [log τ_B fixed to −100 (τ_B 0)]; pK_A (K_A), agonist affinity; pK_B (K_B), modulator affinity.
[a]Values derived by fitting previously reported experimental data (Sengmany et al., 2019).
[b]Values derived by fitting previously reported experimental data (Sengmany et al., 2017).
[c]The pK_A value was fixed to that determined in radioligand binding assays (Mutel et al., 2000).
[d]The log $\alpha\beta$ value was fixed to −100 due to complete inhibition of glutamate-mediated stimulation of Ca_i^{2+} mobilization, reflecting high negative cooperativity.
[e]An F test determined that data were fitted best when the transducer or binding slopes were different from unity. The F data used to test the hypothesis that n differed from 1 were the following: eq. 3 MPEP $P = 0.0003$, F [(Dfn, Dfd) 13.46 (1, 149)]; eq. 3 M-5MPEP $P = 0.0007$, F [(Dfn, Dfd) 11.96 (1, 126)]; eq. 3 VU-29 $P = 0.0015$, F [(Dfn, Dfd) 10.45 (1, 144)]; eq. 3 DPFE $P = 0.0062$, F [(Dfn, Dfd) 7.587 (1, 294)]; eq. 4 MPEP $P = 0.0002$, F [(Dfn, Dfd) 14.33 (1, 149)]; eq. 4 M-5MPEP $P < 0.0001$, F [(Dfn, Dfd) 22.26 (1, 126)]; eq. 4 VU-29 $P = 0.0003$, F [(Dfn, Dfd) 13.97 (1, 144)]; and eq. 4 DPFE $P < 0.0001$, F [(Dfn, Dfd) 24.13 (1, 294)].

Fig. 6. Allosteric modulation at the M_4 mAChR is fitted well by an operational model of allosterism with no cooperative agonist binding. Positive modulation of ACh-mediated guanosine 5′-*O*-(3-[^{35}S]thio)triphosphate ([^{35}S]GTPγS) binding by LY2033298 (ago-PAM) at the M_4 mAChR. Data were previously published (Leach et al., 2010) and are mean + S.D. from at least three independent experiments performed in duplicate. Curves through the data are the fits to the operational model of allosterism with cooperative agonist binding (eq. 4), where the equation was fitted best when n = 1 (i.e., no cooperative agonist binding). The parameters describing the fits are given in Table 6.

slope ranged from 1 to 2 the affinity of NAMs and PAMs estimated using the original operational model of agonism and allosterism fell within ~3-fold of the affinity simulated with the operational model of allosterism with cooperative agonist binding. Furthermore, only the affinity of the full NAM (where $\alpha\beta$ is assumed to approach zero) fell outside this 3-fold window once the agonist binding slope exceeded 2 (Fig. 7A). Similarly, when analyzed with the original operational model of agonism and allosterism, the $\alpha\beta$ values (0.1–10) were within a 3-fold range of simulated data when n_T ranged from 1 to 2. However, where the magnitude of cooperativity exceeded 10 for a PAM, or 0.1 for a NAM, the influence of cooperative agonist binding becomes more pronounced (Fig. 7B). These simulations confirm that the assignment of n to a transducer or binding slope would not be expected to greatly influence quantification of $mGlu_5$ allosteric modulation of glutamate for modulators with moderate cooperativity, which is consistent with our Ca_i^{2+} mobilization data.

Discussion

In the current study, we have assessed operational models of agonism and allosterism that account for receptors whose agonists bind multiple binding sites in a cooperative manner. The modified models accurately fit experimental data at an exemplar GPCR, the CaSR, which has high sensitivity for Ca_o^{2+} due to multiple Ca_o^{2+} binding sites that are linked in a positively cooperative manner. We show that agonist Hill slopes that differ from unity and remain unchanged by alterations in receptor expression levels or cellular coupling efficiencies (i.e., where τ_A differs) may be indicative of cooperative agonist binding. We demonstrate that if a steep Hill slope such as that observed at the CaSR is attributed to the transducer slope rather than to the agonist binding slope, the Black-Leff operational model of agonism underestimates agonist efficacy and overestimates agonist affinity. Extension to allosteric interactions shows the importance of accounting for cooperative agonist binding, since different models fitted to the same allosteric interaction data yield divergent modulator affinity and cooperativity estimates. For instance, the original operational model of agonism and allosterism estimates lower CaSR PAM and NAM cooperativity values and higher or lower

TABLE 6

Comparison of parameters describing M_4 mAChR allosteric interactions analyzed with different allosteric models

M_4 mAChR LY2033298 interactions with ACh in guanosine 5′-*O*-(3-[^{35}S]thio) triphosphate binding assays were analyzed with the original operational model of agonism and allosterism (eq. 3) or the operational model of allosterism with cooperative agonist binding (eq. 4) to determine agonist or modulator affinity, agonist or modulator efficacy, cooperativity, transducer or binding slopes, and maximum system response. Values obtained from fitting eqs. 3 and 4 to the data were identical; therefore, they are only presented in a single column.

Parameter	ACh vs. LY2033298 (eqs. 3 and 4)[a]
pK_A [K_A (μM)]	6.0 (1.0)[b]
pK_B [K_B (μM)]	5.9 ± 0.3 (1.3)
Log τ_A (τ_A)	0.9 ± 0.1 (7.9)
Log τ_B (τ_B)	0.5 ± 0.2 (3.2)
Log $\alpha\beta$ ($\alpha\beta$)	0.7 ± 0.3 (5.0)
n	1.0[c]
E_m (% ACh maximum)	112 ± 5.0

Dfd, degrees of freedom denominator; Dfn, degrees of freedom numerator; E_m, maximum system response; Log $\alpha\beta$ ($\alpha\beta$), cooperativity; Log τ_A (τ_A), agonist efficacy; Log τ_B (τ_A), modulator efficacy; n, transducer or binding slope; pK_A (K_A), agonist affinity; pK_B (K_B), modulator affinity.

[a]Data analyzed are from Leach et al. (2010).

[b]The pK_A value was fixed to that determined in radioligand binding assays (Leach et al., 2010).

[c]An F test determined that data were fitted best when the transducer or binding slopes were not different from unity. The F data used to test the hypothesis that n differed from 1 were the following: eq. 3 $P = 0.5766$, F [(Dfn, Dfd) 0.3129 (1, 172)]; and eq. 4 $P = 0.4541$, F [(Dfn, Dfd) 0.5629 (1, 172)].

affinity values, respectively. Data simulations support these findings and demonstrate that the impact of cooperative binding on estimates of modulator affinity and cooperativity is more pronounced as the magnitude of modulator cooperativity or cooperative agonist binding is increased. This was evidenced by our demonstration that for $mGlu_5$, where the glutamate Hill slope is ~1.8, differences in affinity and cooperativity are within the margin of experimental error (~3-fold range). Accordingly, for agonist-receptor concentration-response relationships with Hill slopes equal to unity, it does not matter whether the slope is governed by the transducer slope or the agonist binding slope.

The operational models of agonism and allosterism with cooperative agonist binding have important practical uses for analyzing data at receptors that possess multiple agonist binding sites. This is particularly true for the CaSR, but also for ion channels and other GPCRs where agonist binding coefficients differ from unity, such as GPR39, which binds at least two Zn^{2+} ions and responds to Zn^{2+} with a Hill slope of 2–3 (Storjohann et al., 2008; Sato et al., 2016). Similarly, cooperative binding can occur across a GPCR dimer, which may account for the steep Hill slope at $mGlu_5$ demonstrated in the present study. For instance, the $mGlu_2$ orthosteric agonist (1*S*,2*S*,5*R*,6*S*)-2-aminobicyclo[3.1.0]hexane-2,6-dicarboxylic acid (LY354740) stabilizes conformational rearrangements of a metabotropic glutamate receptor subtype 2 and 4 heterodimer ($mGlu_2$-$mGlu_4$) with a shallow Hill slope (Moreno Delgado et al., 2017), which is increased to unity when LY354740 is prevented from binding to the $mGlu_2$ or $mGlu_4$ orthosteric binding site in the dimer. In contrast, the glutamate E_{max} value is reduced when it can bind to only one of the orthosteric sites in the heterodimer (Moreno Delgado et al., 2017). These findings indicate negative (LY354740) and positive (glutamate) cooperativity across the dimer, respectively. Negative cooperative binding has also been demonstrated at several class A GPCRs dimers, including the 5-hydroxytryptamine$_{2A}$, A_3 adenosine, H_3 histamine, and D_2 dopamine receptors (Sinkins and Wells, 1993; Vivo et al., 2006; Brea et al., 2009; May et al., 2011). Accurate quantification of ligand affinity, efficacy, and cooperativity at such receptors using functional assays is critical, particularly where radioligand binding–based methods are not available. Indeed, there are no commercially available radioligands for the CaSR, thus pharmacological characterization, and indeed drug discovery at this receptor has generally relied upon functional measures of receptor activity to quantify drug actions. However, it must be noted that experimentally derived pharmacological data for agonists with steep Hill slopes will likely only be fitted to the cooperative agonist operational model and the operational model of allosterism with cooperative agonist binding when one of the binding or transducer slopes (n_B or n_T) is known and constrained as such. This was a key advantage of analyzing pharmacological data at the CaSR, where we showed experimentally that the transducer slope is 1.

Our findings have important implications for past and present drug discovery efforts at class C GPCRs and beyond. Establishing structure-activity relationship profiles that dictate drug affinity and cooperativity is essential for predicting drug efficacy in vivo. However, underestimates of cooperativity at class C GPCRs with cooperative agonist binding may explain previous observations that class C GPCR allosteric modulators have limited cooperativity when compared with their class A GPCR counterparts. For example, PAMs with $\alpha\beta$ values >100 have been reported for class A GPCRs (Leach et al., 2010; Abdul-Ridha et al., 2014), whereas for the CaSR potentiation is at most 5-fold for many modulators (Cook et al., 2015; Leach et al., 2016; Diepenhorst et al., 2018). Thus, for GPCRs with cooperative agonist binding, larger differences between modulator cooperativities were likely previously unappreciated. This is important because allosteric modulator

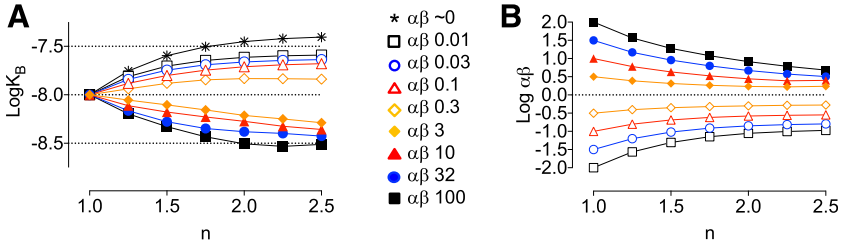

Fig. 7. Modulator affinity and cooperativity are influenced by assignment of the slope in the operational model of allosterism. Simulations demonstrating the influence of the agonist binding slope on the estimated modulator affinity and cooperativity when interaction data are analyzed using the original operational model of allosterism. Interaction data between an orthosteric agonist and a NAM or PAM were simulated with the operational model of allosterism with cooperative agonist binding. Orthosteric agonist affinity (1 μM), τ_A (10), and modulator affinity (10 nM) were held constant; different magnitudes of positive or negative cooperativity were examined alongside changes in the magnitude of cooperative agonist binding. The simulated data were analyzed with the original operational model of allosterism, and log K_B (A) or log $\alpha\beta$ (B) estimates were plotted against the agonist binding slope.

cooperativity can predict likely clinical efficacy or adverse effect liability. Inaccurate estimation of allosteric modulator affinity or cooperativity due to a failure to consider cooperative agonist binding likely also impacts interpretation of structure-function studies. If cooperativity values are narrowed, then more subtle effects of mutations on modulator cooperativity may have been missed.

In conclusion, we have validated a method for quantifying agonist and allosteric modulator actions at receptors possessing multiple agonist binding sites that interact in a cooperative manner. Our operational models of agonism and allosterism with cooperative agonist binding more accurately quantify the actions of both orthosteric and allosteric drugs acting at GPCRs with cooperative agonist binding and may be used for future drug discovery efforts at these important receptors.

Appendix

Cooperative agonist operational model

A model of signal transduction by a receptor with nB binding sites is displayed in the equilibrium:

$$(nB)A + R \overset{K_{A1}}{\Leftrightarrow} AR + (nB-1)A \overset{K_{A2}}{\Leftrightarrow} A_2R + (nB-2)A \overset{K_{A3}}{\Leftrightarrow} A_3R + (nB-3)A \Leftrightarrow \ldots \Leftrightarrow A_{nB}R \overset{K_E}{\rightarrow} E$$

Where K_E is the value of $A_{nB}R$ that elicits half the maximal system effect and agonist affinity for each site can be described by the equilibrium dissociation constants:

$$K_{A1} = \frac{[A][R]}{[AR]}, K_{A2} = \frac{[A][AR]}{[A_2R]}, K_{A3} = \frac{[A][A_2R]}{[A_3R]}, \text{etc}$$

We see that $K_{A1} \times K_{A2} \times K_{A3} \times \ldots \times K_{AnB} = \frac{[A]^{nB}[R]}{[A_{nB}R]} = {K_A}^{nB}$, where K_A is the geometric mean of the individual equilibrium dissociation constants.

For simplicity, the receptor is considered either empty (R) or fully occupied ($A_{nB}R$): $(nB)A + R \overset{{K_A}^{nB}}{\Leftrightarrow} A_{nB}R \overset{K_E}{\rightarrow} E$

$$ {K_A}^{nB} = \frac{[A]^{nB}[R]}{[A_{nB}R]}$$

The total receptor concentration can be expressed as:

$$[R_0] = [R] + [A_{nB}R]$$

where

$$[R] = \frac{{K_A}^{nB}[A_{nB}R]}{[A]^{nB}}$$

therefore

$$[R_0] = \frac{{K_A}^{nB}[A_{nB}R]}{[A]^{nB}} + [A_{nB}R]$$

$$[R_0] = [A_{nB}R]\left(\frac{{K_A}^{nB}}{[A]^{nB}} + 1\right)$$

$$[R_0] = [A_{nB}R]\ \left.\frac{{K_A}^{nB} + [A]^{nB}}{[A]^{nB}}\right)$$

Receptor occupancy is thus denoted:

$$[A_{nB}R] = \frac{[R_0][A]^{nB}}{{K_A}^{nB} + [A]^{nB}}$$

In accordance with the scheme of the operational model of agonism, the logistic function for the transduction of occupancy into response is: $E = \frac{E_m[A_{nB}R]^{nT}}{{K_E}^{nT} + [A_{nB}R]^{nT}}$ where nT is a logistic slope factor describing the transduction of agonist binding into a response (the transducer slope).

Using the previous expression of $[A_{nB}R]$ gives:

$$E = \frac{E_m\ \left.\frac{[R_0][A]^{nB}}{{K_A}^{nB} + [A]^{nB}}\right)^{nT}}{{K_E}^{n\mathrm{T}} + \left.\frac{[R_0][A]^{nB}}{{K_A}^{nB} + [A]^{nB}}\right)^{nT}}$$

Multiplying numerator and denominator by $({K_A}^{nB} + [A]^{nB})^{nT}$ gives:

$$E = \frac{E_m[R_0]^{nT}[A]^{nBnT}}{{K_E}^{nT}\left({K_A}^{nB} + [A]^{nB}\right)^{nT} + [R_0]^{nT}[A]^{nBnT}}$$

Dividing through by K_E and redefining $\frac{[R_0]}{K_E}$ as τ_A gives an operational model of agonism for a receptor with nB binding sites (Eq 2 in the main text):

$$E = \frac{E_m{\tau_A}^{nT}[A]^{nBnT}}{\left({K_A}^{nB} + [A]^{nB}\right)^{nT} + {\tau_A}^{nT}[A]^{nBnT}}$$

For use in Graphpad Prism or similar software, the above equation is described by the following notations, where n_T or n_B will likely need to be fixed to a known or theoretical value to fit real experimental data to this equation, and where a "Basal" response parameter is introduced to accommodate ligand-independent effects that deviate from zero:

KA = 10^LogKA
A = 10^X
tau = 10^Logtau

Part1 = (Em − Basal)*tau*(A^nB)
Part2 = tau*(A^nB) + (A^nB) + (KA^nB)
Y = Basal + (Part1^nT)/(Part2^nT)

Operational model of allosterism with cooperative agonist binding

In a ternary complex consisting of a receptor (lacking constitutive activity), an orthosteric agonist that binds nB binding sites, and an allosteric modulator, the stimulus-generating species are $A_{nB}R$, BR and $A_{nB}RB$. A model of ligand-receptor interactions in this ternary complex is displayed in the equilibrium:

$$(nB)A + R \overset{{K_A}^{nB}}{\Leftrightarrow} A_{nB}R;\quad B + R \overset{K_B}{\Leftrightarrow} BR \text{ and}$$

$$A_{nB}R + B \overset{\alpha}{\Leftrightarrow} A_{nB}RB$$

Where ${K_A}^{nB} = \frac{[A]^{nB}[R]}{[A_{nB}R]}$, $K_B = \frac{[B][R]}{[BR]}$, and $\frac{K_B}{\alpha} = \frac{[A_{nB}R][B]}{[A_{nB}RB]}$

From the latter expression we obtain:

$$\alpha = \frac{K_B[A_{nB}RB]}{[A_{nB}R][B]}$$

Assuming the pharmacological effect (E) is a function of the total stimulus (S_T) arising from the sum of the stimuli generated from each individual ligand-bound receptor species, then:

$$S_T = S_{A_{nB}R} + S_{BR} + S_{A_{nB}RB}$$

It is further assumed that the stimulus (S) generated from each individual ligand-bound receptor species is proportional to the product of the intrinsic efficacy of the ligand (ε) and the concentration of the ligand-bound receptor species, thus:

$$S_{A_{nB}R} = \varepsilon_{A_{nB}}[A_{nB}R]\ ;\ S_{RB} = \varepsilon_B[BR]\ ;\ S_{A_{nB}RB} = \varepsilon_{A_{nB}B}[A_{nB}RB]\ ;\ \text{and}$$
$$\varepsilon_{A_{nB}B} = \beta\varepsilon_{A_{nB}}$$

where $\varepsilon_{A_{nB}}$ denotes the intrinsic efficacy of the orthosteric agonist, ε_B denotes the intrinsic efficacy of the allosteric modulator, and β is a coupling factor that describes the effect of the allosteric modulator on the intrinsic efficacy of the orthosteric agonist when the two ligands are bound to the same receptor.

Thus, the effect (E) of an agonist in the presence of an allosteric modulator is processed through the following logistic equation

$$E = \frac{E_m {S_T}^{nT}}{{K_S}^{nT} + {S_T}^{nT}}$$

where E_m denotes the maximum possible response, K_S denotes a constant that governs the efficiency of stimulus-response coupling and nT denotes a logistic slope factor (the transducer slope).

If we consider the total receptor concentration:

$$[R_0] = [R] + [A_{nB}R] + [BR] + [A_{nB}RB]$$

where

$$[A_{nB}R] = \frac{[R_0][A]^{nB}}{[A]^{nB}\left(1 + \frac{\alpha[B]}{K_B}\right) + {K_A}^{nB}\left(1 + \frac{[B]}{K_B}\right)}$$

$$[BR] = \frac{[R_0][B]}{[B]\quad 1 + \frac{\alpha[A]^{nB}}{{K_A}^{nB}}\Big) + K_B\quad 1 + \frac{[A]^{nB}}{{K_A}^{nB}}\Big)} \text{ and}$$

$$[A_{nB}RB] = \frac{[R_0][A]^{nB}}{[A]^{nB}\left(1 + \frac{K_B}{\alpha[B]}\right) + {K_A}^{nB}\left(\frac{1}{\alpha} + \frac{K_B}{\alpha[B]}\right)};$$

substituting the above terms into $E = \frac{E_m {S_T}^{nT}}{{K_S}^{nT} + {S_T}^{nT}}$ gives the following operational model of allosterism at a receptor with nB orthosteric agonist binding sites (Eq 4 in the main text):

where

$$\tau_A = \frac{\varepsilon_{A_{nB}}[R_0]}{K_S}$$

and

$$\tau_B = \frac{\varepsilon_B[R_0]}{K_S}$$

For use in Graphpad Prism or similar software, the above equation is described by the following notations, where nT or nB will likely need to be fixed to a known or theoretical value to fit real experimental data to this equation:

KA = 10^LogKA
KA = 10^LogKB
tauA = 10^LogtauA
tauB = 10^LogtauB
A = (10^X)
alpha = 10^Logalpha
betta = 10^Logbeta
B = 10^LogAllo

Part1 = tauA*(A^nB)*(KB + alpha*betta*B) + tauB*B*(KA^nB)

Part2 = (A^nB)*KB + (KA^nB)*KB + B*(KA^nB) + alpha*(A^nB)*B

Stim = Part1/Part2

Y = Basal + ((Em − Basal)*(Stim^nT))/((Stim^nT) + (1^nT))

For the purposes of the current study, the model has been simplified further to enable analysis of data when the orthosteric agonist is a full agonist. Therefore, equation 4 in the manuscript reduces to:

$$E = \frac{E_m\left(\tau_A[A]^{nB}(K_B + \alpha\beta[B]) + \tau_B[B]{K_A}^{nB}\right)^{nT}}{{K_A}^{nBnT}(K_B + [B])^{nT} + \left(\tau_A[A]^{nB}(K_B + \alpha\beta[B]) + \tau_B[B]{K_A}^{nB}\right)^{nT}}$$

Dividing through by ${\tau_A}^{nT}$, and defining $[EC_{50}] = K_A/\tau_A$ yields the following expression:

$$E = \frac{E_m\left([A]^{nB}(K_B + \alpha\beta[B]) + \tau_B[B][EC_{50}]^{nB}\right)^{nT}}{[EC_{50}]^{nBnT}(K_B + [B])^{nT} + \left([A]^{nB}(K_B + \alpha\beta[B]) + \tau_B[B][EC_{50}]^{nB}\right)^{nT}}$$

Authorship Contributions

Participated in research design: Gregory, Christopoulos, Leach.
Conducted experiments: Diao.
Contributed new reagents or analytic tools: Giraldo, Christopoulos.
Performed data analysis: Diao, Gregory, Giraldo, Leach.

$$E = \frac{E_m\left(\tau_A[A]^{nB}(K_B + \alpha\beta[B]) + \tau_B[B][K_A]^{nB}\right)^{nT}}{\left([A]^{nB}K_B + {K_A}^{nB}K_B + {K_A}^{nB}[B] + \alpha[A]^{nB}[B]\right)^{nT} + \left(\tau_A[A]^{nB}(K_B + \alpha\beta[B]) + \tau_B[B]{K_A}^{nB}\right)^{nT}}$$

Wrote or contributed to the writing of the manuscript: Gregory, Giraldo, Christopoulos, Leach.

References

Abdul-Ridha A, Lane JR, Mistry SN, López L, Sexton PM, Scammells PJ, Christopoulos A, and Canals M (2014) Mechanistic insights into allosteric structure-function relationships at the M_1 muscarinic acetylcholine receptor. *J Biol Chem* **289**:33701–33711.

Aurelio L, Valant C, Flynn BL, Sexton PM, Christopoulos A, and Scammells PJ (2009) Allosteric modulators of the adenosine A_1 receptor: synthesis and pharmacological evaluation of 4-substituted 2-amino-3-benzoylthiophenes. *J Med Chem* **52**:4543–4547.

Black JW and Leff P (1983) Operational models of pharmacological agonism. *Proc R Soc Lond B Biol Sci* **220**:141–162.

Black JW, Leff P, Shankley NP, and Wood J (1985) An operational model of pharmacological agonism: the effect of E/[A] curve shape on agonist dissociation constant estimation. *Br J Pharmacol* **84**:561–571.

Brea J, Castro M, Giraldo J, López-Giménez JF, Padín JF, Quintián F, Cadavid MI, Vilaró MT, Mengod G, Berg KA, et al. (2009) Evidence for distinct antagonist-revealed functional states of 5-hydroxytryptamine$_{2A}$ receptor homodimers. *Mol Pharmacol* **75**:1380–1391.

Brown EM (1983) Four-parameter model of the sigmoidal relationship between parathyroid hormone release and extracellular calcium concentration in normal and abnormal parathyroid tissue. *J Clin Endocrinol Metab* **56**:572–581.

Christopoulos A (1998) Assessing the distribution of parameters in models of ligand-receptor interaction: to log or not to log. *Trends Pharmacol Sci* **19**:351–357.

Cook AE, Mistry SN, Gregory KJ, Furness SG, Sexton PM, Scammells PJ, Conigrave AD, Christopoulos A, and Leach K (2015) Biased allosteric modulation at the CaS receptor engendered by structurally diverse calcimimetics. *Br J Pharmacol* **172**: 185–200.

Davey AE, Leach K, Valant C, Conigrave AD, Sexton PM, and Christopoulos A (2012) Positive and negative allosteric modulators promote biased signaling at the calcium-sensing receptor. *Endocrinology* **153**:1232–1241.

Diepenhorst NA, Leach K, Keller AN, Rueda P, Cook AE, Pierce TL, Nowell C, Pastoureau P, Sabatini M, Summers RJ, et al. (2018) Divergent effects of strontium and calcium-sensing receptor positive allosteric modulators (calcimimetics) on human osteoclast activity. *Br J Pharmacol* **175**:4095–4108.

Ehlert FJ (1988) Estimation of the affinities of allosteric ligands using radioligand binding and pharmacological null methods. *Mol Pharmacol* **33**:187–194.

Geng Y, Mosyak L, Kurinov I, Zuo H, Sturchler E, Cheng TC, Subramanyam P, Brown AP, Brennan SC, Mun HC, et al. (2016) Structural mechanism of ligand activation in human calcium-sensing receptor. *eLife* **5**:e13662.

Giraldo J (2015) Operational models of allosteric modulation: caution is needed. *Trends Pharmacol Sci* **36**:1–2.

Huang Y, Zhou Y, Castiblanco A, Yang W, Brown EM, and Yang JJ (2009) Multiple Ca^{2+} binding sites in the extracellular domain of the Ca^{2+}-sensing receptor corresponding to cooperative Ca^{2+} response. *Biochemistry* **48**:388–398.

Keller AN, Kufareva I, Josephs TM, Diao J, Mai VT, Conigrave AD, Christopoulos A, Gregory KJ, and Leach K (2018) Identification of global and ligand-specific calcium sensing receptor activation mechanisms. *Mol Pharmacol* **93**: 619–630.

Kenakin TP (2012) Biased signalling and allosteric machines: new vistas and challenges for drug discovery. *Br J Pharmacol* **165**:1659–1669.

Leach K, Conigrave AD, Sexton PM, and Christopoulos A (2015) Towards tissue-specific pharmacology: insights from the calcium-sensing receptor as a paradigm for GPCR (patho)physiological bias. *Trends Pharmacol Sci* **36**:215–225.

Leach K, Davey AE, Felder CC, Sexton PM, and Christopoulos A (2011) The role of transmembrane domain 3 in the actions of orthosteric, allosteric, and atypical agonists of the M_4 muscarinic acetylcholine receptor. *Mol Pharmacol* **79**:855–865.

Leach K, Gregory KJ, Kufareva I, Khajehali E, Cook AE, Abagyan R, Conigrave AD, Sexton PM, and Christopoulos A (2016) Towards a structural understanding of allosteric drugs at the human calcium-sensing receptor. *Cell Res* **26**:574–592.

Leach K, Loiacono RE, Felder CC, McKinzie DL, Mogg A, Shaw DB, Sexton PM, and Christopoulos A (2010) Molecular mechanisms of action and in vivo validation of an M_4 muscarinic acetylcholine receptor allosteric modulator with potential antipsychotic properties. *Neuropsychopharmacology* **35**:855–869.

Leach K, Sexton PM, and Christopoulos A (2007) Allosteric GPCR modulators: taking advantage of permissive receptor pharmacology. *Trends Pharmacol Sci* **28**: 382–389.

May LT, Bridge LJ, Stoddart LA, Briddon SJ, and Hill SJ (2011) Allosteric interactions across native adenosine-A_3 receptor homodimers: quantification using single-cell ligand-binding kinetics. *FASEB J* **25**:3465–3476.

Moreno Delgado D, Møller TC, Ster J, Giraldo J, Maurel D, Rovira X, Scholler P, Zwier JM, Perroy J, Durroux T, et al. (2017) Pharmacological evidence for a metabotropic glutamate receptor heterodimer in neuronal cells. *eLife* **6**:e25233.

Mutel V, Ellis GJ, Adam G, Chaboz S, Nilly A, Messer J, Bleuel Z, Metzler V, Malherbe P, Schlaeger EJ, et al. (2000) Characterization of [^{3}H]quisqualate binding to recombinant rat metabotropic glutamate 1a and 5a receptors and to rat and human brain sections. *J Neurochem* **75**:2590–2601.

Sato S, Huang XP, Kroeze WK, and Roth BL (2016) Discovery and characterization of novel GPR39 agonists allosterically modulated by zinc. *Mol Pharmacol* **90**: 726–737.

Sengmany K and Gregory KJ (2016) Metabotropic glutamate receptor subtype 5: molecular pharmacology, allosteric modulation and stimulus bias. *Br J Pharmacol* **173**:3001–3017.

Sengmany K, Hellyer SD, Albold S, Wang T, Conn PJ, May LT, Christopoulos A, Leach K, and Gregory KJ (2019) Kinetic and system bias as drivers of metabotropic glutamate receptor 5 allosteric modulator pharmacology. *Neuropharmacology* **149**: 83–96.

Sengmany K, Singh J, Stewart GD, Conn PJ, Christopoulos A, and Gregory KJ (2017) Biased allosteric agonism and modulation of metabotropic glutamate receptor 5: implications for optimizing preclinical neuroscience drug discovery. *Neuropharmacology* **115**:60–72.

Sinkins WG and Wells JW (1993) G protein-linked receptors labeled by [3H]histamine in guinea pig cerebral cortex. II. Mechanistic basis for multiple states of affinity [corrected] [published correction appears in *Mol Pharmacol* (1993) **44**: 1278]. *Mol Pharmacol* **43**:583–594.

Stockton JM, Birdsall NJ, Burgen AS, and Hulme EC (1983) Modification of the binding properties of muscarinic receptors by gallamine. *Mol Pharmacol* **23**:551–557.

Storjohann L, Holst B, and Schwartz TW (2008) Molecular mechanism of Zn^{2+} agonism in the extracellular domain of GPR39. *FEBS Lett* **582**:2583–2588.

Vivo M, Lin H, and Strange PG (2006) Investigation of cooperativity in the binding of ligands to the D_2 dopamine receptor. *Mol Pharmacol* **69**:226–235.

Zhang C, Zhuo Y, Moniz HA, Wang S, Moremen KW, Prestegard JH, Brown EM, and Yang JJ (2014) Direct determination of multiple ligand interactions with the extracellular domain of the calcium-sensing receptor. *J Biol Chem* **289**:33529–33542.

Address correspondence to: Katie Leach, Drug Discovery Biology and Department of Pharmacology, Monash Institute of Pharmaceutical Sciences, Monash University, 399 Royal Parade, Parkville, Melbourne, VIC 3052, Australia. E-mail: katie.leach@monash.edu

1521-0111/93/6/619–630$35.00
MOLECULAR PHARMACOLOGY

https://doi.org/10.1124/mol.118.112086
Mol Pharmacol 93:619–630, June 2018

Identification of Global and Ligand-Specific Calcium Sensing Receptor Activation Mechanisms[S]

Andrew N. Keller, Irina Kufareva, Tracy M. Josephs, Jiayin Diao, Vyvyan T. Mai, Arthur D. Conigrave, Arthur Christopoulos, Karen J. Gregory, and Katie Leach

Drug Discovery Biology, Monash Institute of Pharmaceutical Sciences and Department of Pharmacology, Monash University, Parkville, Victoria, Australia (A.N.K., T.M.J., J.D., V.T.M., A.C., K.J.G., K.L.); Skaggs School of Pharmacy and Pharmaceutical Sciences, University of California, La Jolla, San Diego, California (I.K.); and School of Life and Environmental Sciences, Charles Perkins Centre (D17), University of Sydney, New South Wales, Australia (A.D.C.)

Received February 7, 2018; accepted April 6, 2018

ABSTRACT

Calcium sensing receptor (CaSR) positive allosteric modulators (PAMs) are therapeutically important. However, few are approved for clinical use, in part due to complexities in assessing allostery at a receptor where the endogenous agonist (extracellular calcium) is present in all biologic fluids. Such complexity impedes efforts to quantify and optimize allosteric drug parameters (affinity, cooperativity, and efficacy) that dictate PAM structure-activity relationships (SARs). Furthermore, an underappreciation of the structural mechanisms underlying CaSR activation hinders predictions of how PAM SAR relates to in vitro and in vivo activity. Herein, we combined site-directed mutagenesis and calcium mobilization assays with analytical pharmacology to compare modes of PAM binding, positive modulation, and agonism. We demonstrate that 3-(2-chlorophenyl)-*N*-((1*R*)-1-(3-methoxyphenyl)ethyl)-1-propanamine (NPS R568) binds to a 7 transmembrane domain (7TM) cavity common to class C G protein-coupled receptors and used by (α*R*)-(−)-α-methyl-*N*-[3-[3-[trifluoromethylphenyl]propyl]-1-napthalenemethanamine (cinacalcet) and 1-benzothiazol-2-yl-1-(2,4-dimethylphenyl)-ethanol (AC265347); however, there are subtle distinctions in the contribution of select residues to the binding and transmission of cooperativity by PAMs. Furthermore, we reveal some common activation mechanisms used by different CaSR activators, but also demonstrate some differential contributions of residues within the 7TM bundle and extracellular loops to the efficacy of the PAM-agonist, AC265347, versus cooperativity. Finally, we show that PAMS potentiate the affinity of divalent cations. Our results support the existence of both global and ligand-specific CaSR activation mechanisms and reveal that allosteric agonism is mediated in part via distinct mechanisms to positive modulation.

Introduction

The human calcium sensing receptor (CaSR) is a class C G protein-coupled receptor (GPCR) that negatively regulates parathyroid hormone secretion in response to serum extracellular calcium (Ca_o^{2+}) concentrations. As such, the small-molecule positive allosteric modulator (PAM), (α*R*)-(−)-α-methyl-*N*-[3-[3-[trifluoromethylphenyl]propyl]-1-napthalenemethanamine (cinacalcet), is approved for the treatment of secondary hyperparathyroidism, and some instances for the treatment of primary hyperparathyroidism (Nemeth and Goodman, 2016). Cinacalcet has also been used off-label to correct disorders caused by naturally occurring loss-of-function CaSR mutations (Mayr et al., 2016). Although various CaSR small-molecule PAM chemotypes have been discovered, cinacalcet remains the only one on the market. Failure to translate newer CaSR PAMs to the clinic may reflect complexities associated with detecting and quantifying in vitro allosteric modulator effects at class C GPCRs (Leach and Gregory, 2017), thus hampering structure-activity relationship (SAR) optimization efforts and predictions of in vivo drug efficacy, and impeding dissection of allosteric mechanisms of action. For instance, despite cinacalcet being the first clinically approved GPCR allosteric modulator to reach the market, surprisingly little is known about how cinacalcet and other PAMs mediate positive allosteric modulation and/or agonism at the CaSR. Understanding GPCR activation mechanisms can help guide SAR optimization of ligands with desired activity.

Structural studies of class A and B GPCRs indicate that during receptor activation a rotational and vertical movement of transmembrane (TM) 6 and TM7 relative to TM3 occurs,

K.L. and K.J.G. are Australian Research Council Future Fellowship recipients. A.C. is a Senior Principal Research Fellow of the Australian National Health and Medical Research Council.

This work was funded by the Australian National Health and Medical Research Council [Grants APP1026962 and APP1085143] and the National Institutes of Health National Institute of General Medical Sciences and National Institute of Allergy and Infectious Diseases [Grants GM117424 and AI118985, respectively].

https://doi.org/10.1124/mol.118.112086.

[S] This article has supplemental material available at molpharm.aspetjournals.org.

ABBREVIATIONS: AC265347, 1-benzothiazol-2-yl-1-(2,4-dimethylphenyl)-ethanol; ANOVA, analysis of variance; Ca_i^{2+}, intracellular calcium; Ca_o^{2+}, extracellular calcium; CaSR, calcium sensing receptor; cinacalcet, (α*R*)-(−)-α-methyl-*N*-[3-[3-[trifluoromethylphenyl]propyl]-1-napthalenemethanamine; ECL, extracellular loop; GPCR, G protein-coupled receptor; NPS R568, 3-(2-chlorophenyl)-*N*-((1*R*)-1-(3-methoxyphenyl)ethyl)-1-propanamine; PAM, positive allosteric modulator; SAR, structure-activity relationship; TM, transmembrane; 7TM, 7 transmembrane domain; VFT, Venus flytrap; WT, wild type.

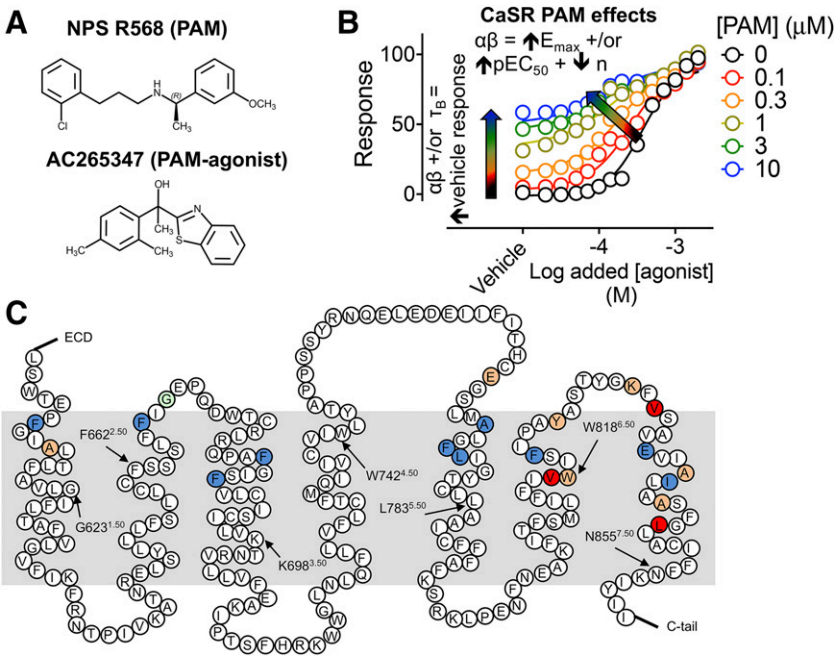

Fig. 1. Studying positive allosteric modulation at the CaSR. (A) Structures of the arylalkylamine PAM, NPS R568, and the PAM-agonist, AC265347, investigated in this study. (B) According to the operational model of allosterism, the CaSR PAM effects on orthosteric agonist signaling are governed by PAM affinity (K_B), binding and/or efficacy cooperativity between the PAM and the orthosteric agonist (α and β, respectively), and the efficacy of the PAM (τ_B); $\alpha\beta$ governs the magnitude of agonist potentiation, reflected by an increase in agonist E_{max} and/or potency, and enhanced vehicle-mediated signaling plus a reduction in the slope of the transducer function, n, if ambient orthosteric agonists are present in the buffer. If the PAM is also an agonist, τ_B will dictate PAM-mediated receptor signaling in the presence of vehicle. (C) Snake diagram of the primary CaSR 7TM domain and ECL sequence, indicating residues that were mutated in the current study. Mutations at residues previously shown to be important for the binding of the PAMs, cinacalcet, and/or AC265347, their cooperativity with Ca_o^{2+}, or both (Leach et al., 2016), are shown in blue, red, and orange, respectively. All engineered mutations were substituted with alanine, with the exception of A615$^{1.42}$, A772$^{5.39}$, A840$^{7.35}$, and A844$^{7.3}$, which were substituted with valine, and E837$^{7.32}$, which was mutated to aspartic acid and isoleucine. The residue highlighted in green indicates where a naturally occurring mutation alters the activity of some PAMs (Cook et al., 2015). Arrows point to the $\times$.50 conserved class C amino acid residues based on a modified Ballesteros-Weinstein numbering system (Doré et al., 2014).

resulting in conformational changes at the intracellular face of the receptor that promote transducer coupling (reviewed in de Graaf et al., 2017; Manglik and Kruse, 2017). For class C GPCRs, most endogenous agonists predominantly bind in the large extracellular Venus flytrap (VFT) domain, stabilizing activating conformational rearrangements that transmit through the 7 transmembrane domain (7TM) spanning regions and/or extracellular loops (ECLs) to the intracellular side of the receptor. Many synthetic molecules that target class C GPCRs bind to allosteric sites in the 7TM domain and/or ECL regions. Furthermore, for the CaSR, the 7TM and/or ECL domains also contain additional binding sites for endogenous agonists including polyamines and Ca_o^{2+} (Ray and Northup, 2002; Leach et al., 2016). However, the 7TM molecular mechanisms that underlie class C GPCR allosteric (and indeed orthosteric) activation are largely unknown. This is due to a complete lack of active-state class C GPCR 7TM structures, but also, in part, due to the difficulties in interpreting mutation-based structure-function studies to delineate residue contributions to the three key molecular properties that govern allosteric activity; ligand affinity, cooperativity, and efficacy.

In light of the difficulties associated with studying GPCR allosteric modulator effects, we developed pharmacological and analytical methods to robustly quantify allosteric modulation of GPCRs (Leach et al., 2007), and recently employed these methods to probe class C GPCR allostery (Gregory et al., 2012, 2013, 2014; Leach et al., 2016). We demonstrated unprecedented insights into class C GPCR drug actions by combining pharmacological, analytical, and detailed structure-function analyses. For instance, we identified a CaSR 7TM domain cavity that accommodates small-molecule CaSR PAMs and negative allosteric modulators, and showed that structurally diverse modulators bind to distinct regions in this cavity; the arylalkylamine PAM, cinacalcet, binds toward the top of the 7TM domain cavity, whereas the structurally distinct CaSR PAM-agonist, 1-benzothiazol-2-yl-1-(2,4-dimethylphenyl)-ethanol (AC265347), binds deeper in the pocket (Leach et al., 2016). Furthermore, we mapped residues that contribute to PAM potentiation of the CaSR's endogenous agonist, Ca_o^{2+}, revealing both shared and distinct activation mechanisms used by cinacalcet and AC265347 (Leach et al., 2016).

Given the importance of understanding the structural basis underlying ligand binding and activation mechanisms at class C GPCRs, the current study sought to build on our prior analysis of CaSR allostery by examining the structural basis of positive allosteric modulation mediated by the small-molecule PAM, 3-(2-chlorophenyl)-*N*-((1*R*)-1-(3-methoxyphenyl)ethyl)-1-propanamine (NPS R568). The binding of NPS R568 and other arylalkylamine PAMs is predicted to overlap with the cinacalcet binding site. Given that arylalkylamine PAMs display comparable in vitro pharmacology, we hypothesized that NPS R568 would demonstrate similar structure-function relationships to cinacalcet. We also hypothesized that the PAM-agonist, AC265347, mediates agonism via engagement of residues that transmit positive

modulation. Thus, we used mutagenesis to compare mechanisms of positive allosteric modulation and direct allosteric agonism mediated by NPS R568 and AC265347 (Fig. 1A). We identify both global and ligand-specific activation mechanisms at the CaSR, which could inform future drug discovery efforts seeking to rationally optimize the activity of CaSR activators and/or potentiators.

Materials and Methods

Materials. Dulbecco's modified Eagle's medium, blasticidin S HCl, and fetal bovine serum were obtained from Invitrogen (Carlsbad, CA), while hygromycin B was obtained from Roche (Mannheim, Germany). The Flp-In TREx human embryonic kidney 293 cells and Fluo-4 AM acetoxymethyl ester were purchased from Invitrogen. Quikchange mutagenesis kits were purchased from Agilent Technologies (Santa Clara, CA). NPS R568 was prepared as described previously (Davey et al., 2012). AC265347 and all other chemicals were from Sigma Aldrich (St Louis, MO).

Generation and Maintenance of Cell Lines Expressing Wild-Type (WT) and Mutant CaSRs. The generation of DNA and cells stably expressing c-myc-tagged WT and mutant human CaSRs in pcDNA5/frt/TO have been described previously (Davey et al., 2012; Leach et al., 2016). Cells were maintained in Dulbecco's modified Eagle's medium containing 5%–10% fetal bovine serum, 200 μg/ml hygromycin B, and 5 μg/ml blasticidin S HCl.

Intracellular Calcium (Ca_i^{2+}) Mobilization Assays. Cells were seeded in clear 96-well plates coated with poly-D-lysine (50 $\mu g/ml^{-1}$) at 80,000 cells/well and incubated overnight in the presence of 100 ng/ml^{-1} tetracycline. The following day, cells were washed with assay buffer (150 mM NaCl, 2.6 mM KCl, 1.18 mM $MgCl_2$, 10 mM D-Glucose, 10 mM HEPES, 0.1 mM $CaCl_2$, 0.5% bovine serum albumin, and 4 mM probenecid at pH 7.4) and loaded with Fluo-4 AM acetoxymethyl ester (1 μM in assay buffer) for 1 hour at 37°C. Cells were washed with assay buffer prior to the addition of fresh assay buffer. For interaction studies between Ca_o^{2+} and PAMs, modulators were coadded with Ca_o^{2+}. For assays in the absence of ambient divalent cations, cells were treated as described previously, except that the final assay buffer and the buffer used for washing and loading the cells did not contain $CaCl_2$ or $MgCl_2$.

For all studies, each well was treated with a single agonist and/or modulator concentration. The release of Ca_i^{2+} was measured at 37°C using Flexstation 1 or 3 (Molecular Devices, Sunnyvale, CA). Fluorescence was detected for 60 seconds at 485 nm excitation and 525 nm emission, and the peak Ca_i^{2+} mobilization response (approximately 12 seconds after agonist addition) was used for the subsequent determination of the agonist response. Relative peak fluorescence units were normalized to the fluorescence stimulated by 1 μM ionomycin to account for differences in cell number and loading efficiency.

Data Analysis. All nonlinear regression analyses were performed using GraphPad Prism 7 (GraphPad Software, San Diego, CA). Parametric measures of potency, affinity, and cooperativity were estimated as logarithms (Christopoulos, 1998). Interaction experiments between Ca_o^{2+} and allosteric modulators were fitted to an operational model of allosterism (Leach et al., 2007; Aurelio et al., 2009; Leach et al., 2010), which was modified to accommodate the presence of ambient agonist (Davey et al., 2012):

$$E = \frac{(E_{max} - \text{basal})\ [([A] + [A_e])\ (K_B + \alpha\beta[B])\ +\ \tau_B\ [B]\ [EC_{50}]]^n}{[EC_{50}]\ (K_B + [B])\ +\ [([A] + [A_e])\ (K_B\ +\ \alpha\beta\ [B])\ +\ \tau_B\ [B]\ [EC_{50}]]^n} \quad (1)$$

where $[A]$ denotes the concentration of exogenously added orthosteric agonist to stimulate the response; $[A_e]$ is the ambient orthosteric agonist concentration in the buffer; $[B]$ is the molar allosteric ligand concentration; K_B is the functional affinity of the allosteric ligand; τ_B denotes allosteric ligand intrinsic efficacy; α and β are the allosteric effects on orthosteric ligand binding affinity and efficacy, respectively (estimated as a composite $\alpha\beta$ value); E_{max} is the maximal possible system response; and n is the slope factor of the transducer function.

Concentration-response curves for Ca_o^{2+}, NPS R568, and AC265347 in the absence of ambient divalent cations were fitted to the following form of an operational model of agonism to obtain estimates of PAM affinity and efficacy:

$$E = \left(\frac{(E_{max} - \text{basal})\ \tau_B\ [B]}{(K_B + [B]) + \tau_B\ [B]}\right)^n \quad (2)$$

where all parameters are as described for eq. 1.

Statistics. An F test ($P < 0.001$) was used to determine whether eq. 1 best fit interaction data when NPS R568 and AC265347 were assumed to have no agonist efficacy at the WT and mutant CaSRs (i.e., whether the best-fit value for τ_B was equal to or differed from zero). Statistical differences between the Ca_o^{2+} pEC_{50}, or PAM pK_B and $\log\alpha\beta$ at the WT versus the mutant receptors were determined by one-way analysis of variance (ANOVA) with Dunnett's multiple comparisons post-test, where significance was defined as $P < 0.05$. Statistical differences between PAM pK_B at the WT and mutant receptors in the absence versus the presence of ambient divalent cations was determined by two-way ANOVA with Sidak's comparisons post-test, where significance was considered as $P < 0.05$.

Molecular Modeling and Docking Studies. A three-dimensional model of the CaSR 7TM domain was constructed by homology with $mGlu_5$ (PDB: 5CGD) (Christopher et al., 2015) using the ICM software package (Molsoft, San Diego, CA) (Abagyan and Totrov, 1994) as previously described (Leach et al., 2016). The 7TM helices in the model were additionally refined to accommodate irregularities such as nonconserved proline residues (e.g., $Pro682^{3.34}$) and a one-residue insertion in the extracellular part of TM5 ($Ile777^{5.44}$). Compound docking relied on the pharmacophore properties of the TM cavity as well as the results of earlier and present mutagenesis studies indicating that mutation of $Glu837^{7.32}$ abrogates activity of all arylalkylamines. A salt bridge is predicted to occur between the protonated arylalkylamine secondary amine and the $Glu837^{7.32}$ side chain (Petrel et al., 2003, 2004; Miedlich et al., 2004; Bu et al., 2008; Leach et al., 2016); therefore, the formation of this salt bridge was enforced in our docking studies by imposing a harmonic distance restraint between the corresponding atoms. The arylalkylamine docking proceeded by extensive conformational sampling of the ligands and the residue side chains lining the pocket in the internal coordinates in the presence of this distance restraint. All complexes were further refined by local minimization in the presence of distance restraints maintaining receptor secondary and tertiary structures, and inspected manually.

Results

Rationale for the Study. We have previously evaluated the effects of CaSR 7TM and ECL mutations on allosteric modulator activity using an interaction paradigm (Davey et al., 2012; Cook et al., 2015; Leach et al., 2016). Here, the effect of a CaSR PAM can manifest as: 1) modulation of the exogenously added agonist to stimulate the response, reflected by a change in the added agonist potency and/or E_{max}; 2) modulation of ambient agonist present in the buffer, reflected by an increase in the baseline response and/or a shallowing of the agonist concentration-response curve; and 3) direct PAM-mediated agonism, also reflected by an increase in the baseline response (Davey et al., 2012; Cook et al., 2015; Leach et al., 2016) (Fig. 1B). In this work, we have extended our analysis to account for ambient Ca_o^{2+} ions present in the assay buffer. Including the ambient Ca_o^{2+} concentration in the

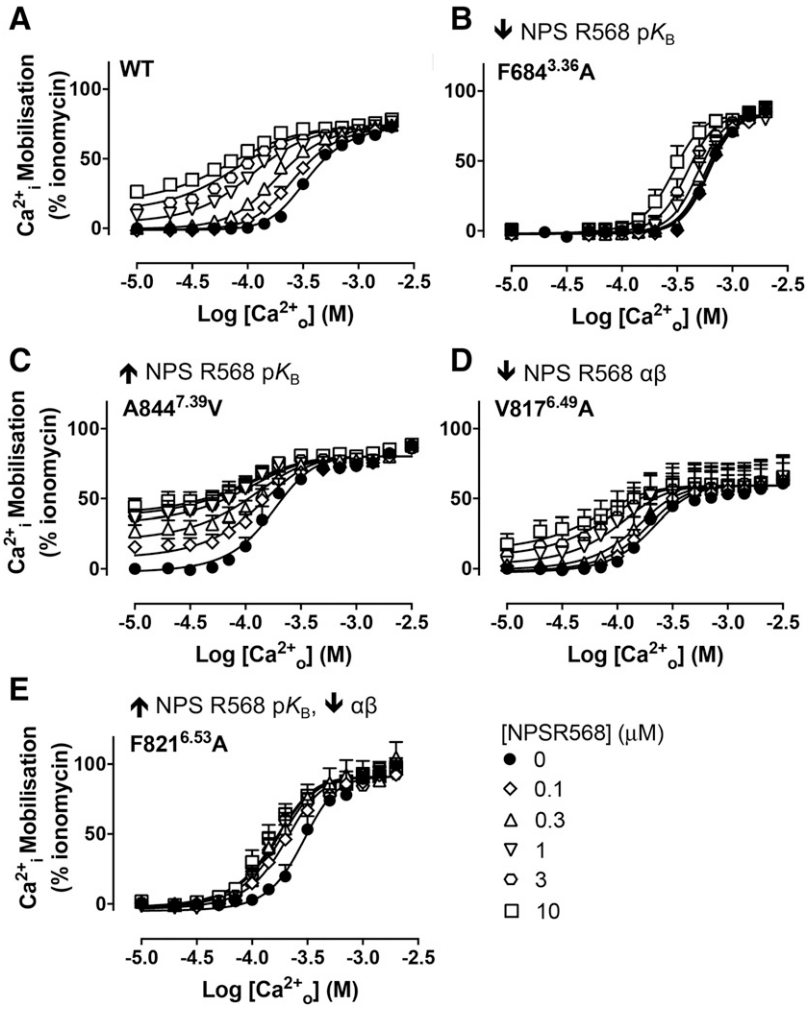

Fig. 2. 7TM mutations alter the activity of NPS R568 at the CaSR. Concentration-response curves to Ca_o^{2+} in the absence and presence of NPS R568 were determined in Ca_i^{2+} mobilization assays to identify mutations that altered NPS R568 activity (A–E). Representative mutants are shown that reduced NPS R568 affinity (F684$^{3.36}$A), increased NPS R568 affinity (A844$^{7.39}$V), reduced NPS R568 cooperativity (V817$^{6.49}$A), or increased NPS R568 affinity while decreasing cooperativity (F821$^{6.53}$A). Data are mean + S.E.M. pooled from at least four separate experiments performed in duplicate. Curves are the best fit of the data to eq. 1. Vehicle (buffer) is plotted as the smallest [Ca_o^{2+}] in accordance with the logarithmic scale.

operational model of allosterism allows delineation of PAM-mediated increases in the vehicle (buffer) response due to agonism versus potentiation of ambient Ca_o^{2+} (eq. 1). Accordingly, we are now able to quantify and delineate the effect of CaSR mutations on PAM affinity (pK_B), allosteric cooperativity with the orthosteric agonist ($\alpha\beta$), and allosteric agonism (τ_B).

Using this analytical paradigm, we examined two tool compounds; NPS R568 and AC265347. NPS R568 (Fig. 1A) was among the first identified CaSR PAMs (Nemeth et al., 1998) and a precursor to cinacalcet, which is an approved clinical treatment of human hyperparathyroidism. Both PAMs display similar in vitro pharmacology (Cook et al., 2015), despite subtle differences in their chemical structure; although NPS R568 and cinacalcet share a three carbon aliphatic chain linked to a secondary amine, they differ in their terminal aromatics: chlorophenyl and methoxyphenyl groups in NPS R568 were replaced with tri-fluoromethylphenyl and naphthyl groups in cinacalcet. With these differences in mind, we aimed to examine the SAR of NPS R568 in comparison with cinacalcet in more detail. Furthermore, whereas cinacalcet and NPS R568 exhibit little agonism, the chemically distinct CaSR PAM, AC265347, is both a PAM and an agonist (a PAM-agonist) (Cook et al., 2015). We were, therefore, interested in elucidating the different activation mechanisms used by these chemically and pharmacologically distinct CaSR activators. Of further interest, AC265347 exhibits biased CaSR modulation when compared with cinacalcet, presumably via stabilizing different active states (Davey et al., 2012; Leach et al., 2013, 2016; Cook et al., 2015).

Therefore, in this work, we used mutagenesis in combination with an operational model of allosterism that explicitly accommodates ambient agonist levels (eq. 1), to characterize important features of NPS R568 binding and positive cooperativity, and to directly probe AC265347 agonism. 7TM and ECL mutations were selected based on those known to alter the affinity and/or cooperativity of cinacalcet and/or AC265347 (Fig. 1C).

NPS R568 Binds to a Common 7TM Allosteric Binding Site. We first confirmed that NPS R568 bound within the same 7TM cavity used by other arylalkylamine modulators (Leach et al., 2016). We fitted NPS R568 interaction data at the WT and 7TM mutant receptors to an operational model of allosterism with ambient agonist to assess the impact of 7TM amino acid substitutions on NPS R568 affinity (pK_B). WT and representative mutants are shown in Fig. 2 that exemplify the different profiles observed. Similar to our previous observations with cinacalcet (Leach et al., 2016), F668$^{2.56}$A, F684$^{3.36}$A, F688$^{3.40}$A, E837$^{7.32}$I, and I841$^{7.36}$A mutations abolished NPS R568 activity or reduced

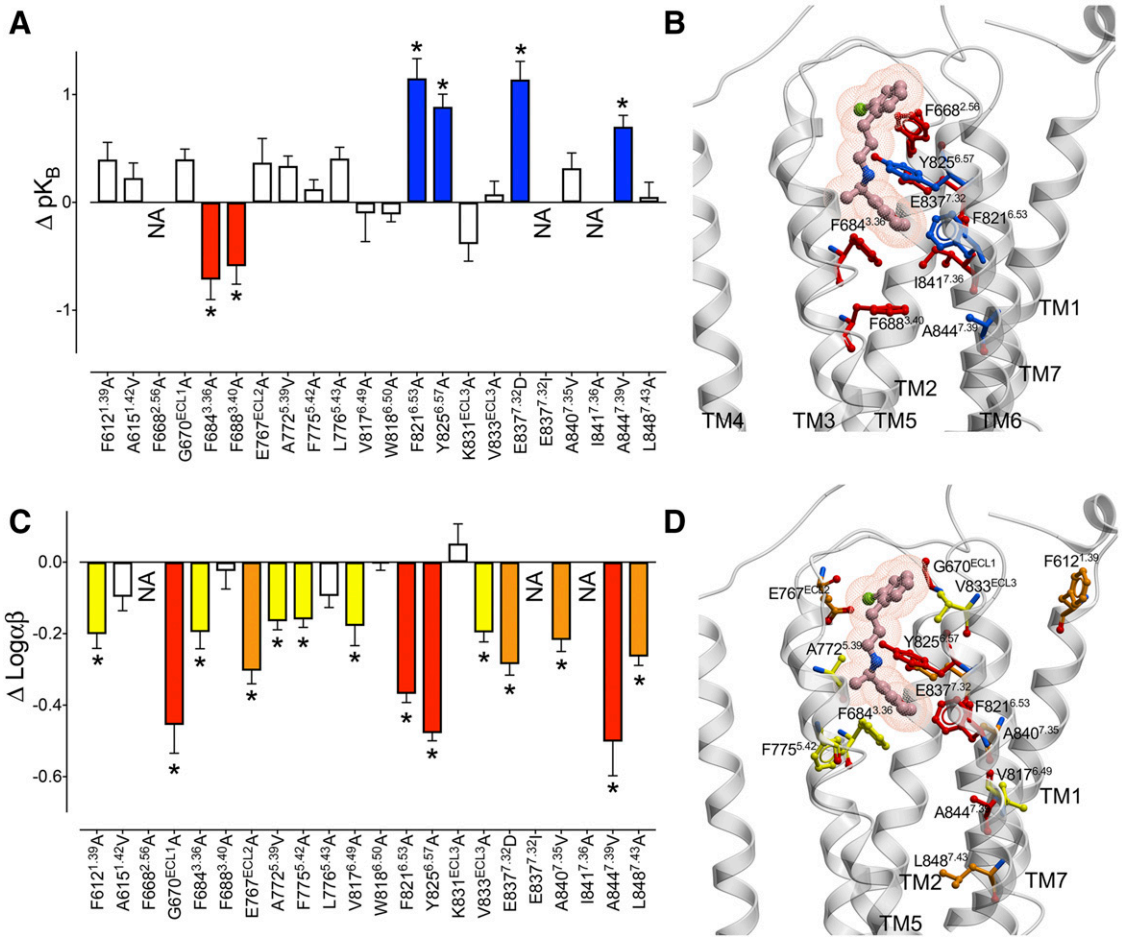

Fig. 3. 7TM and ECL mutations alter the affinity and cooperativity of NPS R568 at the CaSR. (A) Concentration-response curves to Ca_o^{2+} in the absence and presence of NPS R568 determined in Ca_i^{2+} mobilization assays were fitted to an operational model of allosterism (eq. 1) to determine the change in affinity (ΔpK_B) (A) and cooperativity ($\Delta \log\alpha\beta$) (C) of NPS R568 at the mutant CaSRs in comparison with the WT receptor. White bars represent no significant change in pK_B or $\log\alpha\beta$. Colored bars that sit above and below zero represent a significant increase or decrease in pK_B or $\log\alpha\beta$, respectively. A 1.5-fold or lower reduction in pK_B and/or $\log\alpha\beta$ is represented by yellow bars, a 1.6-fold to 2.5-fold reduction is represented by orange bars, and a greater than 2.5-fold reduction or increase is represented by red and blue bars, respectively. NA, negligible PAM activity. Data are the ΔpK_B or $\Delta\log\alpha\beta$ + S.E.M. calculated from WT and mutant pK_B or $\log\alpha\beta$ values and experiment numbers shown in Table 1; *denotes significant difference in comparison with WT ($P < 0.05$, one-way ANOVA with Dunnett's multiple comparisons post-test). Affinity (B) and cooperativity (D) residues are shown on a CaSR 7TM domain homology model (gray cartoon), along with the predicted NPS R568 pose from docking studies. Residue positions are shown as ball and stick, and colors correspond to the fold change in affinity or cooperativity shown in (A and C).

NPS R568 pK_B, whereas F821$^{6.53}$A, E837$^{7.32}$D, and A844$^{7.39}$V increased NPS R568 pK_B (Fig. 2; Fig. 3A; Supplemental Fig. 1; Table 1). Furthermore, although the magnitude of NPS R568 potentiation of Ca_o^{2+} potency at the Y825$^{6.57}$A mutant was reduced (Supplemental Fig. 1), a significant and maximal ~2-fold increase in Ca_o^{2+} potency was reached in the presence of 0.1 μM NPS R568, suggesting the PAM pK_B was increased. To confirm this finding, we performed interaction studies between AC265347 and NPS R568. We found that 0.1–10 μM NPS R568 caused a dextral translocation of the AC265347 concentration-response curve at the Y825$^{6.42}$A mutant, with no apparent decrease in AC265347 E_{max} (Supplemental Fig. 2); although limitations in AC265347 solubility prevented determination of complete AC265347 concentration-response curves in the presence of the higher NPS R568 concentrations. Nonetheless, these findings suggest that the interaction between NPS R568 and AC265347 is competitive, or an allosteric interaction governed by extremely high negative cooperativity. In support of a competitive or highly negatively cooperative interaction, when AC265347 and NPS R568 interactions at the Y825$^{6.42}$A mutant were fitted to a modified Hill/Gaddum/Schild equation (Motulsky and Christopoulos, 2004; Langmead et al., 2006), the Schild slope was not significantly different from unity. Under these circumstances, the concentration of NPS R568 that shifts the AC265347 EC_{50} 2-fold is equal to the NPS R568 pK_B; this analysis confirmed that the NPS R568 pK_B was increased by the Y825$^{6.57}$A mutation (Table 1). A similar increase in cinacalcet pK_B has been observed at this mutant (Leach et al., 2016). Our findings are consistent with NPS R568 binding in the 7TM cavity in a similar pose to cinacalcet, concordant with previous predictions that E837$^{7.32}$ forms a hydrogen bond with the core secondary amine in arylalkylamine modulators (Petrel et al., 2003, 2004; Miedlich et al., 2004; Bu et al., 2008; Leach et al., 2016). With this interaction, the terminal naphthyl (cinacalcet) or methoxyphenyl (NPS R568) moiety extends downward, π-stacking with F684$^{3.36}$ and forming hydrophobic interactions with F668$^{2.56}$, F688$^{3.40}$, and I841$^{7.36}$.

TABLE 1

Functional affinity (pK_B) and cooperativity ($\log\alpha\beta$) parameters for NPS R568 determined in Ca_i^{2+} mobilization assays using an interaction paradigm

Data are mean ± S.E.M. and 95% confidence interval from the indicated number of independent experiments (n).

	NPS R568		
	pK_B (95% CI)	$\log\alpha\beta$ (95% CI) ($\alpha\beta$)	n
WT	5.99 ± 0.05 (5.89–6.09)	0.55 ± 0.01 (0.52–0.58) (3.5)	17
F612$^{1.39}$A	6.39 ± 0.15 (6.03–6.75)	0.35 ± 0.04[a] (0.28–0.43) (2.2)	4
A615$^{1.42}$V	6.22 ± 0.13 (5.93–6.49)	0.45 ± 0.04 (0.38–0.53) (2.8)	6
F668$^{2.56}$A	<5	ND	4
G670^{ECL1}A	6.39 ± 0.08 (6.23–6.55)	0.09 ± 0.04[a] (−0.07–0.25) (1.2)	4
F684$^{3.36}$A	5.28 ± 0.18[a] (4.79–5.63)	0.35 ± 0.05[a] (0.28–0.51) (2.2)	4
F688$^{3.40}$A	5.40 ± 0.16[a] (5.00–5.73)	0.52 ± 0.05 (0.44–0.65) (3.3)	5
E767^{ECL2}A	6.36 ± 0.22 (5.93–6.77)	0.25 ± 0.03[a] (0.18–0.33) (1.8)	3
A772$^{5.39}$V	6.33 ± 0.08 (6.17–6.48)	0.38 ± 0.02[a] (0.35–0.42) (2.4)	4
F775$^{5.42}$A	6.11 ± 0.07 (5.95–6.27)	0.39 ± 0.02[a] (0.36–0.42) (2.5)	4
L776$^{5.43}$A	6.40 ± 0.09 (6.20–6.58)	0.46 ± 0.03 (0.40–0.51) (2.9)	4
V817$^{6.49}$A	5.89 ± 0.26 (5.29–6.38)	0.37 ± 0.05[a] (0.27–0.50) (2.3)	4
W818$^{6.50}$A	5.88 ± 0.05 (5.77–5.98)	0.55 ± 0.01 (0.52–0.58) (3.5)	5
F821$^{6.53}$A	7.14 ± 0.18[a] (6.80–7.58)	0.18 ± 0.02[a] (0.14–0.22) (1.5)	4
Y825$^{6.57}$A	6.88 ± 0.11[a,b] (6.65–7.11)	0.07 ± 0.02[a,c] (0.04–0.10) (1.2)	4
K831^{ECL3}A	5.60 ± 0.15 (5.26–5.91)	0.60 ± 0.05 (0.49–0.71) (4.0)	4
V833^{ECL3}A	6.07 ± 0.11 (5.77–6.33)	0.35 ± 0.02[a] (0.31–0.40) (2.2)	4
E837$^{7.32}$D	7.13 ± 0.16[a] (6.85–7.52)	0.26 ± 0.03[a] (0.22–0.32) (1.9)	4
E837$^{7.32}$I	<5	ND	7
A840$^{7.35}$V	6.31 ± 0.13 (6.05–6.56)	0.33 ± 0.03[a] (0.28–0.39) (2.1)	4
I841$^{7.36}$A	NA	NA	4
A844$^{7.39}$V	6.69 ± 0.09[a] (6.49–6.90)	0.05 ± 0.09[a] (−0.17–0.26) (1.1)	5
L848$^{7.43}$A	6.04 ± 0.13 (5.79–6.28)	0.29 ± 0.02[a] (0.25–0.32) (1.9)	4

CI, confidence interval; NA, negligible PAM activity; ND, not determined due to weak cooperativity or low affinity.
[a]significantly different to WT ($P < 0.05$, one-way ANOVA with Dunnett's multiple comparisons post-test).
[b]pK_B determined in interaction studies between AC265347 and NPS R568 ($n = 3$).
[c]pK_B was fixed to 6.88 determined in interaction studies between AC265347 and NPS R568.

There were, however, subtle differences in the effects of some mutations on NPS R568 pK_B when compared with cinacalcet. For instance, W818$^{6.50}$A decreased, whereas E767^{ECL2}A, A772$^{5.39}$V, or V833^{ECL3}A increased, cinacalcet pK_B (Leach et al., 2016); in contrast, these mutations had no significant effect on NPS R568 pK_B (Fig. 3A; Table 1). To better understand the differences in the pK_B effects of these mutations, we constructed a homology model of the CaSR 7TM domain based on the $mGlu_5$ 7TM structure (Christopher et al., 2015) and interrogated this model bound to NPS R568 in silico. Since the NPS R568 core consists of an arylalkylamine, whose secondary amine is predicted to interact directly with E837$^{7.32}$, the distance required for hydrogen bonding between this residue and the secondary amine of NPS R568 was maintained during the docking process. Unsurprisingly, this produced docking poses for NPS R568 that were consistent with previously published predictions for cinacalcet and other arylalkylamine-based modulators (Leach et al., 2016) (Fig. 3B).

Close inspection of docking poses for NPS R568 in the CaSR homology model explained the observed differences in mutational effects on cinacalcet versus NPS R568 pK_B. First, our predicted docking poses oriented the methoxyphenyl moiety of NPS R568 toward the hydrophobic-aromatic network that surrounds the napthyl group of cinacalcet (F684$^{3.36}$, F775$^{5.42}$, L776$^{5.43}$, W818$^{6.50}$, and I841$^{7.36}$), but crucially, the smaller and more hydrophilic NPS R568 moiety does not interact with W818$^{6.50}$ (Fig. 3B; Supplemental Fig. 3). This change in binding mechanism likely underpins why W818$^{6.50}$A does not influence NPS R568 pK_B. Second, the predicted NPS R568 pose places the chloro-phenyl group of NPS R568 in a position identical to the tri-fluoromethyl-phenyl group of cinacalcet, but the NPS R568 moiety occupies appreciably less chemical space. Indeed, the increase in cinacalcet pK_B observed at the E767^{ECL2}A and V833^{ECL3}A mutants is likely due to an increase in the volume of the top of the binding pocket, which is more favorable for cinacalcet but makes no difference to the binding of the smaller NPS R568 (Supplemental Fig. 3). Collectively, these data suggest that NPS R568 and cinacalcet bind to an overlapping binding site; however, due to key differences in their chemical topology, there are subtle distinctions in the contribution of select residues to the binding of the two PAMs.

Identification of Residues that Mediate Cooperativity between Ca_o^{2+} and NPS R568. By applying an operational model of allosterism to our data, we also revealed nine residues within the CaSR 7TM bundle that are involved in NPS R568 cooperativity ($\log\alpha\beta$) but not affinity (pK_B), with major contributions from ECL1 and 2 as well as TMs 6 and 7 (WT and representative mutants are shown in Fig. 2, quantification is shown in Fig. 3C). In contrast, five mutations influenced both affinity and cooperativity; F688$^{2.56}$A decreased pK_B and $\log\alpha\beta$, whereas F821$^{6.53}$A, E837$^{7.32}$D, Y825$^{6.42}$A, or A844$^{7.39}$V had differential effects on the two parameters (Fig. 3, A and C; Table 1). Thus, residues within the binding pocket differentially contribute to NPS R568 affinity versus cooperativity with Ca_o^{2+}.

Our previous structure-function analysis at the CaSR identified residues that contributed to the transmission of positive cooperativity between Ca_o^{2+} and cinacalcet (Leach et al., 2016). Comparisons between cooperativity determinants for cinacalcet and NPS R568 revealed key similarities and differences. Five mutations (E767^{ECL2}A, V817$^{6.49}$A, Y825$^{6.57}$A, A844$^{7.39}$V, and L848$^{7.43}$A) significantly reduced

TABLE 2
Efficacy (τ_B) of NPS R568 and AC265347 determined in Ca_i^{2+} mobilization assays using an interaction paradigm
Data are mean ± S.E.M. and 95% confidence intervals from the indicated number of independent experiments (n).

	NPS R568		AC265347	
	Logτ_B (95% CI) (τ_B)	n	Logτ_B (95% CI) (τ_B)	n
WT	ND	17	−0.22 ± 0.09 (−0.45 to −0.08) (0.6)	8
F612$^{1.39}$A	ND	4	0.12 ± 0.09[a] (−0.10 to 0.44) (1.3)	4
A615$^{1.42}$V	ND	6	0.04 ± 0.03 (−0.01 to 0.09) (1.1)	4
F668$^{2.56}$A	ND	4	ND	4
G670^{ECL1}A	−0.25 ± 0.06 (−0.41 to −0.15) (0.6)	4	−0.15 ± 0.09 (−0.39 to 0.02) (0.7)	4
F684$^{3.36}$A	ND	4	ND	5
F688$^{3.40}$A	ND	5	ND	4
E767^{ECL2}A	ND	3	0.05 ± 0.03 (−0.02 to 0.12) (1.1)	4
A772$^{5.39}$V	ND	4	ND	4
F775$^{5.42}$A	ND	4	−0.26 ± 0.07 (−0.48 to 0.14) (0.5)	7
L776$^{5.43}$A	ND	4	0.19 ± 0.12[a] (−0.11 to 0.32) (1.5)	6
V817$^{6.49}$A	ND	4	0.33 ± 0.04[a,b] (0.26–0.45) (2.1)	5
W818$^{6.50}$A	ND	5	ND	4
F821$^{6.53}$A	ND	4	ND	4
Y825$^{6.57}$A	ND	4	ND	4
K831^{ECL3}A	ND	4	−0.05 ± 0.03 (−0.10 to 0.00) (0.9)	5
V833^{ECL3}A	ND	4	ND	5
E837$^{7.32}$D	ND	4	0.09 ± 0.12 (−0.18 to 0.28) (1.2)	4
E837$^{7.32}$I	NA	7	NA	5
A840$^{7.35}$V	ND	4	ND	7
I841$^{7.36}$A	NA	4	ND	4
A844$^{7.39}$V	−0.22 ± 0.07 (−0.45 to −0.11) (0.6)	5	−0.12 ± 0.03 (−0.14 to −0.09) (0.8)	6
L848$^{7.43}$A	ND	4	−0.17 ± 0.07 (−0.35 to −0.07) (0.7)	4

CI, confidence interval; NA, negligible PAM activity; ND, not determined due to negligible efficacy.
[a]Significantly different from WT ($P < 0.05$, one-way ANOVA with Dunnett's multiple comparisons post-test).
[b]To account for a reduction in cell surface expression caused by V817$^{6.49}$A compared with the WT CaSR (Leach et al., 2016), logτ_B was normalized to determine what it would be if this mutant was expressed at the same level as the WT receptor (Gregory et al., 2010).

the cooperativity of both NPS R568 and cinacalcet, suggesting contributions to a common network that transmits positive cooperativity by structurally similar PAMs (Fig. 3, C and D). In contrast, six of the mutations that specifically reduce NPS R568 cooperativity with Ca_o^{2+} without impacting affinity (F612$^{1.39}$A, G670^{ECL1}A, A772$^{5.39}$V, F775$^{5.42}$A, V833^{ECL3}A, and A840$^{7.35}$V) did not influence cinacalcet cooperativity. Furthermore, A615$^{1.42}$V, W818$^{6.50}$A, and K831^{ECL3}A, which we previously reported to influence cinacalcet cooperativity, had no significant effect on the cooperativity between NPS R568 and Ca_o^{2+}, demonstrating that the contribution of these residues to the transmission of positive cooperativity is ligand specific. Collectively, our data reveal differences in the network of residues that transmit cooperativity mediated by structurally similar PAMs, indicating that distinct conformational states are favored by cinacalcet and NPS R568.

Identification of Global and Ligand-Specific Activation Mechanisms at the CaSR. Having identified the NPS R568 binding site and differentiated ligand-receptor interactions governing affinity and cooperativity, we next sought to compare activation mechanisms used by different CaSR activators. To do so, we first validated the ability of the operational model of allosterism with ambient agonist (eq. 1) to distinguish between PAMs (e.g., NPS R568) and PAM-agonists (e.g., AC265347). When applied to Ca_o^{2+} versus NPS R568 interaction data, we found that the operational model of allosterism with ambient agonist fit the data best when the PAM was presumed to have no efficacy (i.e., the best fit value for τ_B did not differ from zero, F test; $P < 0.001$) (Fig. 2A; Tables 1 and 2). This agreed with our previous study showing that cinacalcet, NPS R568, and other structurally related PAMs demonstrate negligible intrinsic agonism (Cook et al., 2015). In contrast, and also consistent with our previous study (Cook et al., 2015), the interaction between Ca_o^{2+} and the PAM-agonist AC265347 were fitted best when the model assumed AC265347 was an agonist (i.e., the best fit value for τ_B differed from zero, F test; $P < 0.001$) (Fig. 4A; Table 2). Importantly, reanalysis of these previously reported data with eq. 1 yielded similar estimates of AC265347 pK_B and log$\alpha\beta$ (Supplemental Table 1). Taken together, these findings demonstrate that our operational model of allosterism with ambient agonist can differentiate between two PAMs with different agonist activity. Therefore, we next assessed the impact of mutations on allosteric modulator efficacy, τ_B, independently of positive cooperativity.

Alanine substitution of F684$^{3.36}$ or F688$^{3.40}$ was previously found to reduce Ca_o^{2+} potency (Leach et al., 2016), and in the current study also abolished AC265347-mediated Ca_i^{2+} mobilization in the presence of vehicle (while positive cooperativity with Ca_o^{2+} was retained) (Fig. 4B; Supplemental Fig. 1; Tables 1 and 2). Using a tetracycline-inducible cell line, we titrated F684$^{3.36}$ and F688$^{3.40}$ receptor expression levels to establish the Ca_o^{2+} pEC_{50} under conditions where it should more closely reflect its affinity (i.e., in the absence of receptor reserve) (Supplemental Fig. 4). With reduced expression levels, Ca_o^{2+} pEC_{50} values at the F684$^{3.36}$A (2.90 ± 0.07) or F688$^{3.40}$A (2.95 ± 0.03) mutants were not significantly different from WT (3.06 ± 0.04), indicating that the reduction in Ca_o^{2+} potency at the mutants versus WT under high expression conditions was due to reduced Ca_o^{2+} efficacy, not affinity. In contrast, F612$^{1.39}$A, L776$^{5.43}$A, or V817$^{6.49}$A increased Ca_o^{2+} potency (Leach et al., 2016) and AC265347 efficacy (Table 2). The changes in Ca_o^{2+}

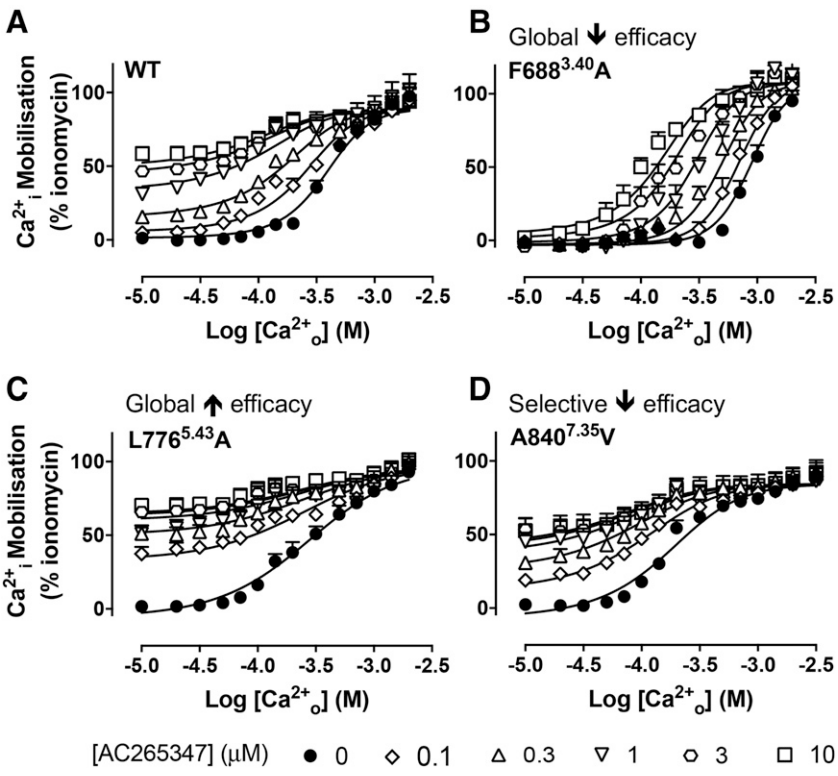

Fig. 4. 7TM domain mutations alter orthosteric and allosteric agonist activity at the CaSR. Concentration-response curves to Ca_o^{2+} determined in Ca_i^{2+} mobilization assays in the absence and presence of AC265347 (A–D) have been published previously (Leach et al., 2016), and were reanalyzed with an operational model of allosterism that considered ambient divalent cations to determine the effect of mutations on AC265347 efficacy (τ_B). WT and representative mutants are shown that caused a simultaneous reduction in Ca_o^{2+} potency and loss of AC265347 efficacy (F688$^{3.40}$A), a simultaneous increase in Ca_o^{2+} potency and gain in AC265347 efficacy (L776$^{5.43}$A), and a selective loss of AC265347 efficacy (A840$^{7.35}$V). Data are mean + S.E.M. pooled from at least four separate experiments performed in duplicate. Curves through the data points are the best fit of the data to eq. 1. Vehicle (buffer) is plotted as the smallest $[Ca_o^{2+}]$ in accordance with the logarithmic scale.

potency and AC265347 efficacy at the F684$^{3.36}$A, F688$^{3.40}$A, F612$^{1.39}$, L776$^{5.43}$, or V817$^{6.49}$A mutants under conditions where WT and mutant cell surface expression levels are comparable (Leach et al., 2016) suggests these residues are important for the transmission of agonism imparted by both Ca_o^{2+} and AC265347.

In contrast, W818$^{6.50}$A, F668$^{2.56}$A, A772$^{5.39}$V, F821$^{6.53}$A, Y825$^{6.57}$A, V833^{ECL3}A, A840$^{7.35}$V, or I841$^{7.36}$A did not reduce Ca_o^{2+} potency (several increased it), or with the exception of F668$^{2.56}$A did not reduce cell surface expression (Leach et al., 2016), but they all abolished AC265347 efficacy (Fig. 4D; Table 2). Qualitatively, AC265347 enhanced Ca_i^{2+} mobilization in the presence of vehicle alone at certain mutations (see, for example, Fig. 4D); however, our analysis is consistent with these baseline increases being attributable to positive modulation of ambient cations in the buffer rather than intrinsic AC265347 efficacy (Supplemental Table 1). Therefore, these eight residues are critical for mediating agonism of AC265347, but not Ca_o^{2+}.

Intriguingly, analysis of NPS R568 interactions with Ca_o^{2+} revealed two mutations (G670A^{ECL1}A and A844$^{7.39}$V) where there was a gain in allosteric agonism, as demonstrated by a significant increase in τ_B, but neither mutation enhanced AC265347 efficacy (Table 2). Combined with a comparison of mutations that influence Ca_o^{2+} potency (Supplemental Fig. 5) versus AC265347 efficacy (Fig. 5; Table 2), our findings indicate that some 7TM and ECL residues play a global role in agonism imparted by all classes of agonist (i.e., orthosteric and allosteric), whereas others contribute to ligand-specific receptor activation.

The finding that the G670A and A844V mutations significantly reduced NPS R568 cooperativity yet converted NPS R568 to a PAM-agonist was intriguing. Therefore, we next sought to compare the global and AC265347-specific activation residues with the AC265347 cooperativity networks previously established (Leach et al., 2016) to determine whether there were also distinctions between cooperativity versus agonism networks used by other PAMs. Two mutations (F612$^{1.39}$A and L776$^{5.43}$A) that increased AC265347 efficacy (Fig. 5, A and B) did not change positive cooperativity, whereas V817$^{6.49}$A increased AC265347 efficacy while decreasing cooperativity. In contrast, the loss in AC265347 efficacy at F668$^{2.56}$A was opposed by increases in cooperativity. Four mutations that decreased AC265347 cooperativity (A615$^{1.42}$V, E767^{ECL2}A, K831^{ECL3}A, and A844$^{7.39}$V) had no effect on AC265347 efficacy. Collectively, these data reveal differential contributions of residues within the 7TM bundle and ECLs to efficacy versus cooperativity.

CaSR PAMs Enhance the Affinity of Orthosteric Agonists. To confirm mutational effects on PAM efficacy predicted from our analysis of interaction data, we assessed the ability of NPS R568 or AC265347 to stimulate Ca_i^{2+} mobilization in the absence of ambient Ca_o^{2+} or Mg_o^{2+} at WT and select mutant receptors. We evaluated G670^{ECL1}A and A844$^{7.39}$V mutations, where NPS R568 was predicted to gain agonist activity, and A840$^{7.35}$V as a representative mutation that decreased AC265347 efficacy (Table 2). Furthermore, we evaluated E837$^{7.32}$D as a control, because this mutation had no effect on the efficacy of NPS R568 or AC265347. Where possible, we fit agonist concentration response data to an operational model of agonism (eq. 2) to determine agonist affinity and efficacy at WT and/or mutant CaSRs (Table 3).

In agreement with our previous evaluation of PAM agonism (Cook et al., 2015), up to 30 μM NPS R568 did not stimulate Ca_i^{2+} mobilization in the absence of ambient cations (Fig. 6A); due to limited solubility, it was not possible to test higher concentrations. Nonetheless, these findings confirm that NPS

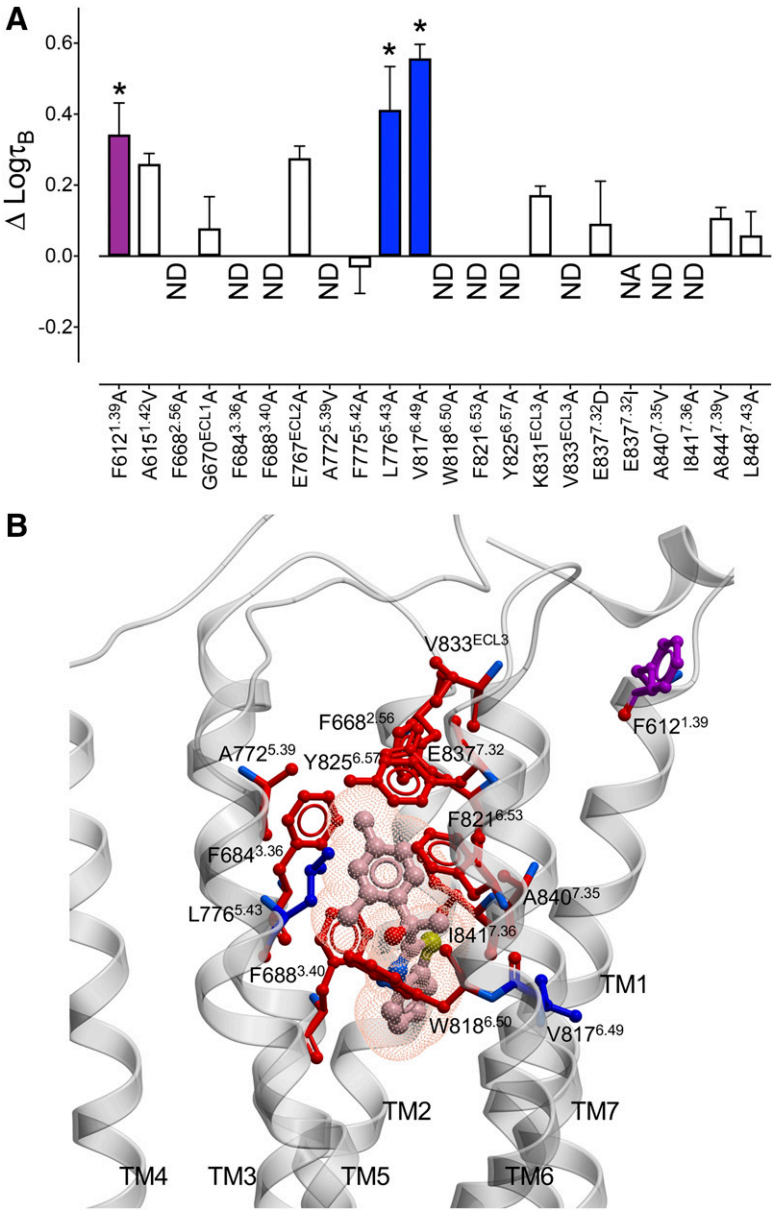

Fig. 5. 7TM and ECL mutations alter AC265347 efficacy at the CaSR. (A) Previously published concentration-response curves to Ca_o^{2+} in the absence and presence of AC265347 determined in Ca_i^{2+} mobilization assays (Leach et al., 2016) were reanalyzed with an operational model of allosterism that accounted for ambient divalent cations (eq. 1) to determine the change in AC265347 efficacy ($\Delta\tau_B$) at the mutant CaSRs in comparison with the WT receptor. White bars represent no significant change in τ_B. Colored bars that sit above zero represent an increase in τ_B. A significant 1.6–2.5-fold increase in τ_B is represented by the purple bar and a greater than 2.5-fold increase is represented by blue bars. ND, not determined due to negligible efficacy; NA, no PAM activity. Data are the $\Delta\tau_B$ + S.E.M. calculated from WT and mutant τ_B values and experiment numbers shown in Table 2; * demotes significant difference in comparison with WT ($P < 0.05$, one-way ANOVA with Dunnett's multiple comparisons post-test). Efficacy residues are shown on a CaSR 7TM domain homology model (B), along with the predicted AC265347 pose from docking studies. Blue and purple colors correspond to the fold change in efficacy shown in (A), whereas red corresponds to a complete loss in AC265347 efficacy.

R568 exhibits negligible agonism at the CaSR. In contrast to WT CaSR, NPS R568 stimulated concentration-dependent Ca_i^{2+} mobilization in the absence of ambient cations at $G670^{ECL1}A$ and $A844^{7.39}V$ (Fig. 6, B and C), suggestive of increased NPS R568 efficacy, as predicted by our operational model analysis that incorporated the presence of ambient cations (Table 2). However, the estimated NPS R568 pK_B at the $G670^{ECL2}A$ mutant was significantly lower in the absence of ambient cations (Table 3) than in their presence (Table 1) ($P < 0.05$, two-way ANOVA with Sidak's multiple comparisons). A similar trend toward a lower NPS R568 pK_B in the absence of ambient cations was also observed at the $A844^{7.39}V$ mutant, but this did not reach significance. At $E837^{7.32}D$ and $A840^{7.35}V$, NPS R568 exhibited negligible agonist activity, similar to WT CaSR and as predicted from our operational model of allosterism analysis.

In contrast to NPS R568, AC265347 stimulated relatively robust Ca_i^{2+} mobilization at the WT CaSR in the absence of ambient cations (Fig. 6A; Table 3), indicative of intrinsic agonism. AC265347 was also an agonist at the $G670^{ECL2}A$, $E837^{7.32}D$, and $A844^{7.39}V$ mutants in the absence of ambient cations, although there was a small but significant decrease in its efficacy at $A844^{7.39}V$ (Fig. 6; Table 3). Consistent with our operational model of allosterism analysis, AC265347 efficacy was reduced at the $A840^{7.35}V$ mutant.

Similar to NPS R568 at WT CaSR and $G670^{ECL2}A$, $A844^{7.39}V$, $E837^{7.32}D$, or $A840^{7.35}V$ mutants, AC265347 bound with lower affinity in the absence of ambient cations than in their presence ($P < 0.05$, two-way ANOVA with Sidak's multiple comparisons). The difference in affinities suggests that CaSR PAMs bind preferentially when an orthosteric agonist simultaneously occupies the receptor. Since cooperative allosteric effects on affinity are reciprocal (and, therefore, affect both agonist and modulator) (May et al., 2007), the elevated PAM affinity in the presence of ambient cations is expected if the PAM also enhances the

TABLE 3

Functional affinity (pK_B) and efficacy ($\log\tau_B$) parameters for NPS R568 and AC265347 determined in Ca_i^{2+} mobilization assays in the absence of ambient divalent cations

Data are mean ± S.E.M. and 95% confidence intervals from the indicated number of independent experiments (n).

	NPS R568			AC265347		
	pK_B (95% CI)	$\text{Log}\tau_B$ (95% CI) (τ_B)	n	pK_B (95% CI)	$\text{Log}\tau_B$ (95% CI) (τ_B)	n
WT	ND	ND	8	5.43 ± 0.10[a] (5.23–5.63)	0.05 ± 0.10 (0.01–0.11) (1.1)	8
$G670^{ECL1}A$	5.71 ± 0.18[a] (5.28–6.13)	−0.19 ± 0.04 (−0.27 to −0.11) (0.6)	7	6.13 ± 0.08[b] (5.96–6.31)	0.07 ± 0.03 (0.04–0.11) (1.2)	7
$E837^{7.32}D$	ND	ND	8	5.90 ± 0.14[a,b] (5.60–6.19)	−0.03 ± 0.03 (−0.10 to 0.03) (0.9)	8
$A840^{7.35}V$	ND	ND	7	ND	ND	7
$A844^{7.39}V$	6.48 ± 0.32 (5.78–7.21)	−0.27 ± 0.06 (−0.42 to −0.17) (0.5)	6	6.89 ± 0.20[b] (6.51–7.31)	−0.16 ± 0.04[b] (−0.25 to −0.09) (0.7)	6

CI, confidence interval; ND, not determined due to negligible efficacy and/or low affinity.
[a]Significantly lower than in the presence of ambient divalent cations ($P < 0.05$, two-way ANOVA with Sidak's comparisons post-test).
[b]Significantly different from WT ($P < 0.05$, one-way ANOVA with Dunnett's multiple comparisons post-test).

affinity of the ambient cations. Thus, NPS R568 and AC265347 likely act, at least in part, by potentiating the affinity of divalent cations. This could occur if the PAMs stabilized the closed form of the VFT via allosteric interactions between the 7TM and VFT domains.

Discussion

The current study has used a structure-function approach combined with analytical pharmacology to probe CaSR 7TM domain and ECL residues that contribute to receptor activation and positive allosteric modulation. Importantly, by incorporating the presence of ambient agonist into an operational model of allosterism, we were able to delineate the contribution of residues to PAM intrinsic efficacy (agonism) independently of positive cooperativity (potentiation of the orthosteric agonist) and affinity. We found both ligand-specific and global activation networks within the CaSR ECLs and 7TM bundle. The fact that mutations in these regions of the receptor have substantial effects on both orthosteric and allosteric ligands highlights the pivotal role that the 7TM domain and ECLs play in transmitting activating stimuli,

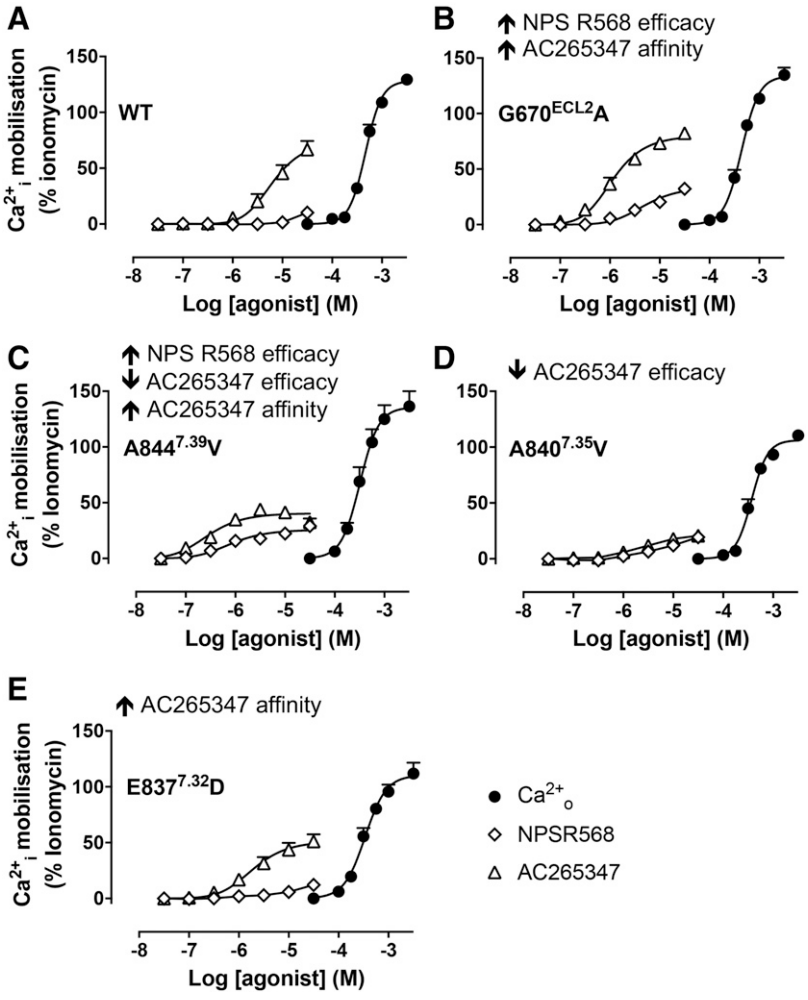

Fig. 6. CaSR PAMs bind with lower affinity in the absence vs. presence of ambient divalent cations, and exhibit differential efficacy at the 7TM domain and ECL mutants. Concentration-response curves to Ca_o^{2+}, NPS R568, and AC265347 were determined in Ca_i^{2+} mobilization assays in the absence of ambient divalent cations to evaluate PAM efficacy (A–E). Representative mutants were chosen based on their ability to provoke NPS R568 efficacy ($G670^{ECL2}A$ and $A844^{7.39}V$), reduce AC265347 efficacy ($A840^{7.35}V$), or have no effect on PAM efficacy ($E837^{7.32}D$). Data are mean + S.E.M. pooled from at least four separate experiments performed in duplicate. Curves are the best fit of the data to eq. 2. Vehicle (buffer) is plotted as the smallest [Ca_o^{2+}] in accordance with the logarithmic scale.

irrespective of the location of the ligand binding site. Importantly, our ability to delineate mutation effects on cooperativity and efficacy reveals that positive cooperativity appears to be mediated in part by residues that are distinct to those that transmit allosteric agonism. For instance, A615$^{1.42}$, E767^{ECL2}, and K831^{ECL3} all contributed to the transmission of AC265347 cooperativity yet played no role in AC265347 efficacy. Conversely, F612$^{1.39}$ and L776$^{5.43}$ constrained AC265347 efficacy but not positive cooperativity. In other instances, there were opposing contributions of residues to cooperativity versus efficacy, as was observed for G670^{ECL2} and A844$^{7.39}$; mutation of these residues decreased NPS R568 cooperativity yet converted NPS R568 to an agonist. Similarly, V817$^{6.49}$A increased AC265347 efficacy while decreasing cooperativity, where the opposite was true for F668$^{2.56}$A.

Using mutagenesis to dissect the contribution of 7TM and ECL residues to NPS R568 affinity, we confirm that NPS R568 binds to an extended cavity in the CaSR's 7TM domain, much like cinacalcet, with key interactions between F668$^{2.56}$, F684$^{3.36}$, F688$^{3.40}$, E837$^{7.32}$, and I841$^{7.36}$. We did, however, identify some subtle differences in the binding of NPS R568 and cinacalcet, likely attributed to their different terminal aromatic groups, permitting cinacalcet to occupy more space at the top and bottom of the binding pocket. Despite this, and the identification of a number of residues that differentially contribute to NPS R568 and cinacalcet cooperativity, these two PAMs from the arylalkylamine family are pharmacologically very similar (Cook et al., 2015). The differences in NPS R568 and cinacalcet SAR appear to be overcome by shared contributions of E767^{ECL2}, V817$^{6.49}$, Y825$^{6.57}$, A844$^{7.39}$, and L848$^{7.43}$ to their transmission of positive cooperativity. Importantly, E767^{ECL2}, V817$^{6.49}$, and A844$^{7.39}$ are also critical for positive cooperativity mediated by the structurally distinct PAM-agonist AC265347, suggesting that these residues may contribute to a global allosteric activation network. Furthermore, mutation of these residues also increases Ca_o^{2+} potency, suggesting a reduction in the energy barrier to transition to an active CaSR 7TM domain that mirrors the effects of PAMs. In fact, greater than 70% of the 7TM/ECL mutations studied herein increase Ca_o^{2+} potency (Leach et al., 2016), supporting the idea that substitution of residues in the allosteric binding cavity lowers the activation barrier for Ca_o^{2+}. Mutations that reduce Ca_o^{2+} potency (e.g., F684$^{3.36}$A, F688$^{3.40}$A, and E837$^{7.32}$I) were at residues critical to the binding of allosteric drugs. Collectively, the influence of these 7TM/ECL residues on both orthosteric agonist activity and small-molecule binding and agonism indicates that the 7TM allosteric binding site has evolutionary importance and raises the possibility that an endogenous allosteric modulator may act via this site.

With regards to mutational effects on agonism, it was of particular note that aside from L776$^{5.43}$ and V817$^{6.49}$, which were important for the efficacy of both Ca_o^{2+} and AC265347, the majority of residues differentially contributed to orthosteric versus allosteric efficacy. This was demonstrated by the opposing effect of many mutations, which increased Ca_o^{2+} potency yet decreased AC265347 efficacy. We cannot exclude the possibility that changes in Ca_o^{2+} potency were due to altered Ca_o^{2+} affinity, but we did show this was not the case for F684$^{3.36}$A and F688$^{3.40}$A mutations (Supplemental Fig. 4). With the exception of E837$^{7.32}$, which we postulate may bind Ca_o^{2+}, it is unlikely that mutation of other residues in this pocket significantly alter Ca_o^{2+} affinity, given that four key Ca_o^{2+} binding sites are located in the receptor's VFT domain (Geng et al., 2016). Thus, our data support the existence of global and ligand-specific activation mechanisms in the CaSR's 7TM and ECL regions.

Another key finding of this study is the demonstration that CaSR PAMs act by potentiating the affinity of Ca_o^{2+}. This is in contrast to other class C GPCR PAMs, which enhance orthosteric agonist-mediated efficacy but do not appear to potentiate their binding (Gregory et al., 2012). The significant loss in PAM affinity in the absence of ambient cations versus in their presence is reminiscent of the reciprocal interaction between Ca_o^{2+} and L-amino acids (Conigrave et al., 2000, 2004); structural studies suggest both ligands are bound to the CaSR's VFT domain to achieve a fully active receptor conformation (Geng et al., 2016; Zhang et al., 2016). However, unlike L-amino acids, our current and previous studies (Leach et al., 2016) demonstrate that small-molecule PAMs bind in an extended CaSR 7TM domain cavity.

Our findings have important implications for future drug discovery efforts at the CaSR. Cinacalcet use is restricted due to an adverse risk of hypocalcemia (Chonchol et al., 2009), in part caused by oversuppression of parathyroid hormone secretion along with stimulation of thyroid CaSRs and consequent calcitonin secretion, and/or suppression of Ca_o^{2+} reabsorption via activation of renal CaSRs (reviewed in Leach et al., 2014, 2015). There is consequently continued interest in developing CaSR activators with greater tissue selectivity. Indeed, weak (partial) agonists or PAMs would be expected to stimulate robust pharmacological responses only in tissues where strong stimulus-response coupling exists, such as high CaSR-expressing parathyroid cells. To date, no small-molecule CaSR agonists devoid of PAM activity have been identified, and there have been no reported efforts to examine the physiologic consequences of PAMs with different degrees of cooperativity. Furthermore, as demonstrated by AC265347, some PAMs also exhibit agonism, which may heighten adverse effects by further amplifying receptor signaling. A greater appreciation of the drivers of CaSR agonism versus allosteric potentiation may afford an opportunity to rationally tune in or tune out PAM and agonist activity.

In conclusion, the current study provides new insight into 7TM and ECL CaSR activation mechanisms. In the future, this information could facilitate rational structure-based design of novel CaSR activators whose pharmacological and consequent therapeutic properties could be optimized by fine-tuning their PAM and/or agonist activity.

Authorship Contributions

Participated in research design: Gregory, Leach.

Conducted experiments: Keller, Kufareva, Josephs, Diao, Mai, Gregory, Leach.

Performed data analysis: Gregory, Leach.

Wrote or contributed to the writing of the manuscript: Keller, Kufareva, Conigrave, Christopoulos, Gregory, Leach.

References

Abagyan R and Totrov M (1994) Biased probability Monte Carlo conformational searches and electrostatic calculations for peptides and proteins. *J Mol Biol* **235**: 983–1002.

Aurelio L, Valant C, Flynn BL, Sexton PM, Christopoulos A, and Scammells PJ (2009) Allosteric modulators of the adenosine A1 receptor: synthesis and pharmacological evaluation of 4-substituted 2-amino-3-benzoylthiophenes. *J Med Chem* **52**:4543–4547.

Bu L, Michino M, Wolf RM, and Brooks CL, III (2008) Improved model building and assessment of the calcium-sensing receptor transmembrane domain. *Proteins* **71**: 215–226.

Chonchol M, Locatelli F, Abboud HE, Charytan C, de Francisco AL, Jolly S, Kaplan M, Roger SD, Sarkar S, Albizem MB, et al. (2009) A randomized, double-blind, placebo-controlled study to assess the efficacy and safety of cinacalcet HCl in participants with CKD not receiving dialysis. *Am J Kidney Dis* **53**:197–207.

Christopher JA, Aves SJ, Bennett KA, Doré AS, Errey JC, Jazayeri A, Marshall FH, Okrasa K, Serrano-Vega MJ, Tehan BG, et al. (2015) Fragment and structure-based drug discovery for a class C GPCR: discovery of the $mGlu_5$ negative allosteric modulator HTL14242 (3-chloro-5-[6-(5-fluoropyridin-2-yl)pyrimidin-4-yl]-benzonitrile). *J Med Chem* **58**:6653–6664.

Christopoulos A (1998) Assessing the distribution of parameters in models of ligand-receptor interaction: to log or not to log. *Trends Pharmacol Sci* **19**:351–357.

Conigrave AD, Mun HC, Delbridge L, Quinn SJ, Wilkinson M, and Brown EM (2004) L-amino acids regulate parathyroid hormone secretion. *J Biol Chem* **279**: 38151–38159.

Conigrave AD, Quinn SJ, and Brown EM (2000) L-amino acid sensing by the extracellular Ca^{2+}-sensing receptor. *Proc Natl Acad Sci USA* **97**:4814–4819.

Cook AE, Mistry SN, Gregory KJ, Furness SG, Sexton PM, Scammells PJ, Conigrave AD, Christopoulos A, and Leach K (2015) Biased allosteric modulation at the CaS receptor engendered by structurally diverse calcimimetics. *Br J Pharmacol* **172**: 185–200.

Davey AE, Leach K, Valant C, Conigrave AD, Sexton PM, and Christopoulos A (2012) Positive and negative allosteric modulators promote biased signaling at the calcium-sensing receptor. *Endocrinology* **153**:1232–1241.

de Graaf C, Song G, Cao C, Zhao Q, Wang MW, Wu B, and Stevens RC (2017) Extending the structural view of class B GPCRs. *Trends Biochem Sci* **42**:946–960.

Doré AS, Okrasa K, Patel JC, Serrano-Vega M, Bennett K, Cooke RM, Errey JC, Jazayeri A, Khan S, Tehan B, et al. (2014) Structure of class C GPCR metabotropic glutamate receptor 5 transmembrane domain. *Nature* **511**:557–562.

Geng Y, Mosyak L, Kurinov I, Zuo H, Sturchler E, Cheng TC, Subramanyam P, Brown AP, Brennan SC, Mun HC, et al. (2016) Structural mechanism of ligand activation in human calcium-sensing receptor. *eLife* **5**:e13662.

Gregory KJ, Hall NE, Tobin AB, Sexton PM, and Christopoulos A (2010) Identification of orthosteric and allosteric site mutations in M_2 muscarinic acetylcholine receptors that contribute to ligand-selective signaling bias. *J Biol Chem* **285**: 7459–7474.

Gregory KJ, Nguyen ED, Malosh C, Mendenhall JL, Zic JZ, Bates BS, Noetzel MJ, Squire EF, Turner EM, Rook JM, et al. (2014) Identification of specific ligand-receptor interactions that govern binding and cooperativity of diverse modulators to a common metabotropic glutamate receptor 5 allosteric site. *ACS Chem Neurosci* **5**:282–295.

Gregory KJ, Nguyen ED, Reiff SD, Squire EF, Stauffer SR, Lindsley CW, Meiler J, and Conn PJ (2013) Probing the metabotropic glutamate receptor 5 ($mGlu_5$) positive allosteric modulator (PAM) binding pocket: discovery of point mutations that engender a "molecular switch" in PAM pharmacology. *Mol Pharmacol* **83**:991–1006.

Gregory KJ, Noetzel MJ, Rook JM, Vinson PN, Stauffer SR, Rodriguez AL, Emmitte KA, Zhou Y, Chun AC, Felts AS, et al. (2012) Investigating metabotropic glutamate receptor 5 allosteric modulator cooperativity, affinity, and agonism: enriching structure-function studies and structure-activity relationships. *Mol Pharmacol* **82**: 860–875.

Langmead CJ, Fry VA, Forbes IT, Branch CL, Christopoulos A, Wood MD, and Herdon HJ (2006) Probing the molecular mechanism of interaction between 4-*n*-butyl-1-[4-(2-methylphenyl)-4-oxo-1-butyl]-piperidine (AC-42) and the muscarinic M_1 receptor: direct pharmacological evidence that AC-42 is an allosteric agonist. *Mol Pharmacol* **69**:236–246.

Leach K, Conigrave AD, Sexton PM, and Christopoulos A (2015) Towards tissue-specific pharmacology: insights from the calcium-sensing receptor as a paradigm for GPCR (patho)physiological bias. *Trends Pharmacol Sci* **36**:215–225.

Leach K and Gregory KJ (2017) Molecular insights into allosteric modulation of class C G protein-coupled receptors. *Pharmacol Res* **116**:105–118.

Leach K, Gregory KJ, Kufareva I, Khajehali E, Cook AE, Abagyan R, Conigrave AD, Sexton PM, and Christopoulos A (2016) Towards a structural understanding of allosteric drugs at the human calcium-sensing receptor. *Cell Res* **26**:574–592.

Leach K, Loiacono RE, Felder CC, McKinzie DL, Mogg A, Shaw DB, Sexton PM, and Christopoulos A (2010) Molecular mechanisms of action and in vivo validation of an M4 muscarinic acetylcholine receptor allosteric modulator with potential antipsychotic properties. *Neuropsychopharmacology* **35**:855–869.

Leach K, Sexton PM, and Christopoulos A (2007) Allosteric GPCR modulators: taking advantage of permissive receptor pharmacology. *Trends Pharmacol Sci* **28**: 382–389.

Leach K, Sexton PM, Christopoulos A, and Conigrave AD (2014) Engendering biased signalling from the calcium-sensing receptor for the pharmacotherapy of diverse disorders. *Br J Pharmacol* **171**:1142–1155.

Leach K, Wen A, Cook AE, Sexton PM, Conigrave AD, and Christopoulos A (2013) Impact of clinically relevant mutations on the pharmacoregulation and signaling bias of the calcium-sensing receptor by positive and negative allosteric modulators. *Endocrinology* **154**:1105–1116.

Manglik A and Kruse AC (2017) Structural basis for G protein-coupled receptor activation. *Biochemistry* **56**:5628–5634.

May LT, Leach K, Sexton PM, and Christopoulos A (2007) Allosteric modulation of G protein-coupled receptors. *Annu Rev Pharmacol Toxicol* **47**:1–51.

Mayr B, Schnabel D, Dörr HG, and Schöfl C (2016) Genetics in endocrinology: gain and loss of function mutations of the calcium-sensing receptor and associated proteins: current treatment concepts. *Eur J Endocrinol* **174**:R189–R208.

Miedlich SU, Gama L, Seuwen K, Wolf RM, and Breitwieser GE (2004) Homology modeling of the transmembrane domain of the human calcium sensing receptor and localization of an allosteric binding site. *J Biol Chem* **279**:7254–7263.

Motulsky H and Christopoulos A (2004) *Fitting Models to Biological Data Using Linear and Nonlinear Regression. A Practical Guide to Curve Fitting*, Oxford University Press, New York.

Nemeth EF and Goodman WG (2016) Calcimimetic and calcilytic drugs: feats, flops, and futures. *Calcif Tissue Int* **98**:341–358.

Nemeth EF, Steffey ME, Hammerland LG, Hung BC, Van Wagenen BC, DelMar EG, and Balandrin MF (1998) Calcimimetics with potent and selective activity on the parathyroid calcium receptor. *Proc Natl Acad Sci USA* **95**:4040–4045.

Petrel C, Kessler A, Dauban P, Dodd RH, Rognan D, and Ruat M (2004) Positive and negative allosteric modulators of the Ca^{2+}-sensing receptor interact within overlapping but not identical binding sites in the transmembrane domain. *J Biol Chem* **279**:18990–18997.

Petrel C, Kessler A, Maslah F, Dauban P, Dodd RH, Rognan D, and Ruat M (2003) Modeling and mutagenesis of the binding site of Calhex 231, a novel negative allosteric modulator of the extracellular Ca^{2+}-sensing receptor. *J Biol Chem* **278**: 49487–49494.

Ray K and Northup J (2002) Evidence for distinct cation and calcimimetic compound (NPS 568) recognition domains in the transmembrane regions of the human Ca^{2+} receptor. *J Biol Chem* **277**:18908–18913.

Zhang C, Zhang T, Zou J, Miller CL, Gorkhali R, Yang JY, Schilmiller A, Wang S, Huang K, Brown EM, et al. (2016) Structural basis for regulation of human calcium-sensing receptor by magnesium ions and an unexpected tryptophan derivative co-agonist. *Sci Adv* **2**:e1600241.

Address correspondence to: Katie Leach, Drug Discovery Biology, Monash Institute of Pharmaceutical Sciences and Department of Pharmacology, 381 Royal Parade, Parkville, VIC, Australia 3052. E-mail: katie.leach@monash.edu or Karen Gregory, Drug Discovery Biology, Monash Institute of Pharmaceutical Sciences and Department of Pharmacology, 381 Royal Parade, Parkville, VIC, Australia 3052. E-mail: karen.gregory@monash.edu